APPRAISAL OF GEOPHYSICAL METHODS USED FOR GROUNDWATER EXPLORATION IN SOUTH AFRICA

Libuseng T. Kolobe

Submitted in fulfilment of the requirements for the degree

Magister Scientiae in Geohydrology

in the

Faculty of Natural and Agricultural Sciences

(Institute for Groundwater Studies)

at the

University of the Free State

Supervisor: Prof. FD Fourie

30 November 2023

DECLARATION

I, Libuseng KOLOBE, hereby declare that the dissertation hereby submitted by me to the Institute for Groundwater Studies in the Faculty of Natural and Agricultural Sciences at the University of the Free State, in fulfilment of the degree of Magister Scientiae, is my own independent work. It has not previously been submitted by me to any other institution of higher education. In addition, I declare that all sources cited have been acknowledged by means of a list of references.

Furthermore, I cede the dissertation's copyright and its contents in favour of the University of the Free State.

Libuseng KOLOBE

30 November 2023

ACKNOWLEDGEMENTS

I would hereby like to express my sincere gratitude to all who have motivated and helped me in the completion of this dissertation:

- Above all, our Mighty Heavenly Father God for His grace.
- My supervisor Prof. Francois Fourie, without your patient guidance and invaluable input this dissertation would not have been completed.
- The following consultants, that took time out of their busy schedules to locate and make available their reports: Aureon Geovation, GEOSS, GHT Consulting, Rock Hounds (Pty) Ltd, Cape Geophysics, and Umvoto Africa (Pty) Ltd.
- My fellow students, Ms Thoriso Lekoetje, Ms Likeleko Sehlabaka, and Mr Sibusiso Dumakude, your words of encouragement were appreciated beyond measure.
- My parents and sisters, who were understanding and supportive throughout the whole journey.
- And last but not least, my partner, Tanki Maema, for reigniting the fire when it was reduced to embers.

This work is based on the research funded in part by the National Research Foundation of South Africa (Grant Number: 130660)

TABLE OF CONTENTS

LIST OF FIGURES

LIST OF TABLES

LIST OF ABBREVIATIONS

BIC	Bushveld Igneous Complex
BIF	Banded Iron Formation
CZ	Critical Zone
EC	Electrical Conductivity
EM	Electromagnetic
ER	Electrical resistivity
ERT	Electrical Resistivity Tomography
FEM	Frequency Domain Electromagnetic
IP	Induced polarisation
LZ	Lower Zone
LGS	Lebowa Granite Suite
MRS	Magnetic Resonance Sounding
MT	Magnetotelluric
MZ	Main Zone
NMR	Nuclear Magnetic Resonance
NNMP	Namaqua-Natal Metamorphic Province
RLS	Rustenburg Layered Suite
SP	Spontaneous Potential
TCTA	Trans-Caledon Tunnel Authority
TDS	Total Dissolved Solids
TMG	Table Mountain Group
TP	Telluric Profiling
TEM	Time Domain Electromagnetic
VES	Vertical Electrical Sounding

LIST OF UNITS

A.ms	Ampere milliseconds
cm	centimetre
Ga	Billion years
g/cm³	grams per cubic centimetre
Hz	Hertz
kHz	kiloHertz
km	kilometre
L/h	litres per hour
L/s	litres per second
Ma	Million years
mbgl	metres below ground level
m/min	metres per minute
mg/l	milligrams per litre
mGals	milliGals
µs	microseconds
µS/cm	microsiemens per centimetre
mm	millimetre
mm/a	millimetres per annum
mS/m	millisiemens per metre
msec or ms	millisecond
mV	milliVolt
nT	nano Tesla
Ohm.m	Ohm metres
Ωm	Ohm metres

CHAPTER 1:
INTRODUCTION

1.1 GENERAL INTRODUCTION

Groundwater is a crucial resource that has been a means of survival for humans for many years, as seen in the tendency to settle near springs (Fitts, 2013). Interestingly, groundwater was extracted from dry mountain basins by Persians in what is now modern Iran (Fitts, 2013). Indeed, many methods have been developed over time to explore groundwater, as has been done with other resources of the Earth that are not readily visible.

According to Arefayne *et al*. (2016), groundwater exploration is "the investigation of underground formations to understand the hydrologic cycle, know the groundwater quality, and identify the nature, number, and type of aquifers". Numerous exploration methods are employed and are often used in conjunction with one another to ensure the most accurate estimation of groundwater potentiality in a given area.

These exploration methods may be direct or indirect (Balasubramanian, 2017), with surface methods often indirect. These include esoteric techniques, which are the most ancient, also known as water witching or dowsing. Here, operators using a forked stick or an egg (Balasubramanian, 2017) claim to be able to detect water underground, the accuracy of which is fairly unproven (Arefayne and Abdi, 2016). Geomorphological methods study the landforms in the area of interest to show where the groundwater is likely to occur (Balasubramanian, 2017). Features such as pediplains or valley flats often show good groundwater potential (Sedhuraman *et al*., 2014). The slope and drainage density are also particularly important features as there is more infiltration in gently sloping areas, and a higher drainage density indicates more runoff and, hence, less potential for recharge (Sedhuraman *et al*., 2014).

Other surface exploration methods may be geological in nature (Balasubramanian, 2017). Such methods first collect and analyse topographic maps, aerial photographs, geological maps, and core logs. This is then supplemented by geological field reconnaissance and evaluation of hydrological data on stream flows, springs, well yields, groundwater recharge levels, and water quality (Balasubramanian, 2017). Faults, joints, and lineaments are also noted, as these may form preferential flow paths for groundwater (Van Tonder *et al*., 2001).

The structure of the water-bearing strata can also give indications for groundwater occurrence (Balasubramanian, 2017). Contacts between permeable rock overlying impermeable strata along the sides of valleys are suitable locations for groundwater (Balasubramanian, 2017). Quartz veins and

dykes can be linear and form ridges (Nel, 2017). There, erosion-prone rock types may form depressions and are connected with structures ideal for water storage (Nel, 2017).

Geobotany, which is the study of how plants are related to the subsurface, can also be used in the exploration of groundwater (Odhiambo, 2016). This means observing any anomaly in the growth of vegetation or trees growing in a straight line can be an indicator of subsurface moisture changes (Nel, 2017). The presence of phreatophytes can also allude to the presence of groundwater (Nel, 2017). Halophytes and white efflorescence of salt on the ground may also be an indication of shallow brackish or saline groundwater (Balasubramanian, 2017). Playas and precipitation of salt are also good indicators of possible groundwater occurrence (Balasubramanian, 2017). Photogeology, which is the use of aerial photography to study geology, can also provide valuable information for targets of a groundwater exploration exercise (Mekel, 1988).

Another manner through which groundwater exploration can be conducted is through the use of geophysical methods. There are a variety of geophysical methods used in groundwater exploration employed for several reasons. However, the main objective of geophysical surveys in hydrogeology is to provide parameters for the creation of models essential for decision-making in groundwater exploration and protection (Mpofu *et al*., 2020).

Geophysical survey methods can be airborne, conducted on the surface, or even conducted down boreholes (Balasubramanian, 2017). These methods operate primarily by detecting anomalies or contrasts in the physical properties of the Earth (Balasubramanian, 2017). These properties include but are not limited to density, elasticity, magnetism, and electrical resistivity. Such anomalies indicate the potential zones which can be exploited for groundwater. The use of geophysics in groundwater exploration is very important as it removes the need to drill many boreholes before the target is reached (Mpofu *et al*., 2020). Geophysical tools are invaluable in groundwater exploration; therefore, this study will be primarily based on the use of geophysics for groundwater exploration in South Africa.

1.2 PROBLEM STATEMENT

Approximately a third of South African households lack access to basic water services (Mpofu *et al.*, 2020). With the unprecedented advent of the novel COVID-19 disease, the world was reminded of the importance of safe water – groundwater in many places – for human health (WHO, 2020).

Groundwater is a particularly important resource in predominantly semi-arid countries such as South Africa (Mvandaba *et al*., 2019). As the country faces growing water demands, the importance of groundwater is ever-increasing (Pietersen *et al*., 2011). Therefore, more groundwater exploration should be undertaken using methods based on sound science. Since geophysics has become

increasingly important in groundwater exploration programmes, an investigation into the methods that have been successfully applied in South Africa is warranted, with specific reference to the different lithologies in which exploration was done.

1.3 AIMS AND OBJECTIVES

This study aims to give an appraisal of the geophysical methods that have been successfully used for groundwater exploration in different geological settings in South Africa. To achieve this aim, the following objectives are identified:

- To establish which geophysical methods are commonly employed in South Africa in groundwater exploration programmes,
- To determine how the choice of geophysical method is influenced by the geology of the area under investigation,
- To establish which geological structures are typically targeted during geophysical exploration programmes in the various geological settings of South Africa,
- To identify the physical contrasts associated with the targeted geological structures in the different geological setting,
- To determine what geophysical responses are typically associated with these targeted geological structures, and,
- To make recommendations for the future use of geophysical methods for groundwater exploration in different geological environments in South Africa.

1.4 RESEARCH METHODOLOGY

This research project is a desktop study. To address the aims and objectives of this study, the following actions were taken:

- A review of international literature was conducted to gain insight into the geophysical methods used globally in groundwater studies and, more specifically, in groundwater exploration programmes. International case studies were included in this literature review.
- Literature was reviewed to understand the geological and hydrogeological conditions in the study area (South Africa). The literature was reviewed by subdividing the study area according to the major geological units (supergroups, complexes, and sequences) that occur within the country.

- Potential geological targets for groundwater exploration were identified within each of the major geological units and their subdivisions.
- The available published literature on geophysical groundwater exploration in South Africa was reviewed.
- Various hydrogeological consultants operating in South Africa were contacted and requested to provide examples (reports, extracts from reports) of case studies where geophysical methods were employed during groundwater exploration programmes (see **Appendix A**).
- The obtained publications and consultant reports were evaluated in terms of the geological settings of the studies, geological structures targeted during groundwater exploration, geophysical methods employed during exploration, the geophysical responses recorded across the targets, the drilling results (where available) of boreholes installed at the positions determined by the results of the geophysical surveys, and the aquifer (or borehole) yields (where available).
- All the obtained data and information were appraised to determine which geophysical methods have been successfully applied for groundwater exploration in the different geological settings of South Africa. The appraisal also considered the geological structures typically targeted in certain geological environments and the geophysical signatures that have been obtained across these targets.
- Based on the results of the study, recommendations were made for future geophysical groundwater exploration in the different geological environments in South Africa.

1.5 LIMITATIONS OF THE STUDY

The research is a desktop study and is limited by the availability of published documents and unpublished reports. Firstly, there is a dearth of publications relating to geophysical groundwater exploration in South Africa. This is a major limitation of the current study and a knowledge gap within South Africa that needs to be addressed. Secondly, it is challenging to obtain information on geophysical groundwater exploration from unpublished consultant reports. Consultants are often reluctant to share information for reasons of confidentiality and competition. They are also often unwilling to take the time to search their archives for specific reports. An additional limitation of the current study is that, to protect their reputations, consultants are more willing to share examples of successful geophysical groundwater exploration programmes than unsuccessful case studies. The knowledge that could potentially be gained from the unsuccessful groundwater exploration surveys is therefore lost to the study. Lastly, there is no control over the quality of work done by the

consultants, and their results and interpretations of the data have to be accepted as presented, and no alterations made.

1.6 STRUCTURE OF DISSERTATION

This dissertation comprises five chapters:

- **Chapter 1: Introduction**. This chapter provides a brief background to the study and sets up the need for, objectives of, and the methodology of the study.
- **Chapter 2: Literature Review**. Literature relating to the geophysical methods is summarised, and case studies of the use of geophysics for exploration in the international context are provided.
- **Chapter 3: Description of the Study Area**. South Africa is described in terms of its climate, socio-economic conditions, geology, general geohydrology and potential targets for geophysical groundwater explorations in the different regions of interest.
- **Chapter 4: Geophysical Groundwater Exploration in South Africa**. The different cases where geophysics was used in groundwater exploration within the context of South Africa are reviewed for the different regions of interest.
- **Chapter 5: Conclusions and Recommendations**. Conclusions are drawn based on the results of the current study, and recommendations are made for future geophysical groundwater exploration programmes in South Africa.

CHAPTER 2:
LITERATURE REVIEW

2.1 INTRODUCTION

In this chapter, the literature relevant to the application of geophysical methods to geohydrological studies will be reviewed. First, the geophysical methods commonly used in groundwater studies will be described. Then, examples of the application of the various geophysical methods for groundwater exploration will be provided in the form of several international case studies. Finally, a summary of lessons learnt from the international case studies is given at the end of the chapter.

2.2 GEOPHYSICAL METHODS COMMONLY USED IN GROUNDWATER INVESTIGATIONS

This section briefly summarises the most commonly used geophysical methods for groundwater prospecting. It is important to note that this list is not exhaustive and that there are many other methods not described in this section.

2.2.1 Gravimetric methods

Gravimetric methods are based on measuring changes in the gravitational field of the Earth due to variations in the densities of subsurface materials (Nel, 2017). These variations are then interpreted in terms of the local geological conditions. Figure 2.1 shows how a buried body might affect gravitational acceleration. Denser bodies in the subsurface may lead to measurable increases in the gravitational acceleration. In the context of hydrogeology, gravity methods are mainly used to investigate geological structures of interest in a survey area (Gabriel, 2009). For example, measuring changes in the gravitational field can help identify sinkholes or cavities in carbonate rocks when interpreted correctly (Nel, 2017).

Gravimetric methods measure the magnitude of gravitational acceleration using instruments called gravimeters (Gabriel, 2009). The gravity measurements are typically taken at regular station spacings along a traverse where the body is expected to occur. In addition to density contrasts in the subsurface, the magnitude of the gravitational acceleration of the Earth is dependent on latitude, elevation, topography, and Earth tides (displacements of the solid surface of the Earth due to the gravitational forces exerted by the Moon and the Sun). Gravity measurements need to be reduced (processed) to remove these latter factors to allow interpretation of the data in terms of only the density contrasts (Telford *et al*., 1990). Repeated readings are necessary at a base station to account for Earth tides and

instrument drift (Mariita, 2009), while accurate measurements of elevation and latitude are required at each survey station.

After the gravity data have been corrected appropriately, the resulting gravity values are called Bouguer anomalies. The regional (long-wavelength anomalies) may then be removed from the Bouguer anomalies to give residual gravity values (Gabriel, 2009). This can also be done digitally using a band-pass filter (Gabriel, 2009). This separation allows the effect of the anomalous body to be discerned (Figure 2.2) from the background variations in the gravitational field. The shapes and amplitudes of the residual gravity anomalies contain information on the positions, geometries, orientations and densities of the causative bodies. These parameters may be estimated through forward and inverse modelling, during which models of the causative bodies are obtained that give similar responses to the recorded anomalies.

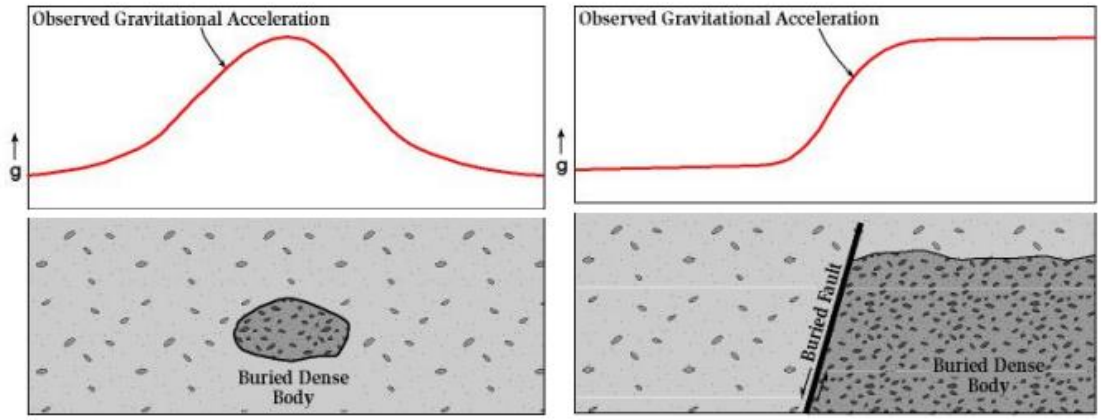

Figure 2.1: Illustration of the variation of gravitational acceleration due to buried bodies (Mariita, 2009).

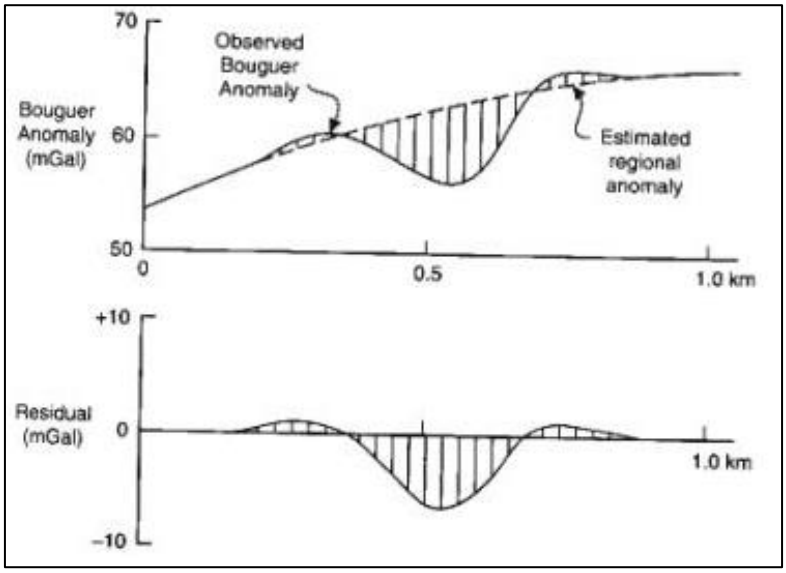

Figure 2.2: Removal of regional anomaly from Bouguer anomaly to yield residual values (Mariita, 2009).

Gravimetric methods are passive methods, making them better suited to operate in a highly populated setting than other geophysical methods that require the introduction of some form of energy (Mariita, 2009).

2.2.2 Seismic methods

Seismic methods exploit the elastic properties of the Earth (Rabbel, 2009). The technique consists of generating seismic waves and measuring the time it takes for the waves to travel from the source to an array of receivers called geophones. The shock waves can be generated by hammer blows for shallow investigations and vibrations for depths up to a kilometre (Rabbel, 2009). With knowledge of the travel times and velocities at which the waves travel, the recorded seismic arrivals are used to reconstruct the pathways along which energy travelled in the subsurface and to derive structural information (Telford *et al*., 1990). Apart from the travel times of the waves, the amplitudes and phases of the energy arriving at the geophones also contain information on the subsurface conditions.

Seismic methods generally measure the travel times of body waves (Rabbel, 2009). There are two types of body waves: S-waves (shear) and P-waves (compressional) (Rabbel, 2009). The velocity of P-waves (v_p) and S-waves (v_s) waves is dependent on the density of the subsurface (ρ), shear modulus (μ), and compressional modulus (k):

$$v_p = \sqrt{\frac{k + 4\mu/3}{\rho}} \qquad 1$$

$$v_s = \sqrt{\frac{\mu}{\rho}} \qquad 2$$

Different layers of the Earth have different propagation velocities, making the seismic method well-suited for mapping subsurface geology (Rabbel, 2009). When a pressure wave is incident on an interface between rocks of different acoustic impedances (velocity×density), some energy of the impinging wave is reflected back as P- and S-waves, while the remaining energy is transmitted into the underlying medium in the form of P- and S-waves (Reynolds, 1997). The directions of travel of the transmitted waves are changed upon entry into the new medium, and these waves are, therefore, referred to as refracted waves (Figure 2.3). The angle of incidence (i) is related to the angles of reflection (i, β_1) and refraction (r, β_2) through Snell's law:

$$\frac{sin\, i}{V_{P1}} = \frac{sin\, r}{V_{P2}} = \frac{sin\, \beta_1}{V_{S1}} = \frac{sin\, \beta_2}{V_{S2}} \qquad 3$$

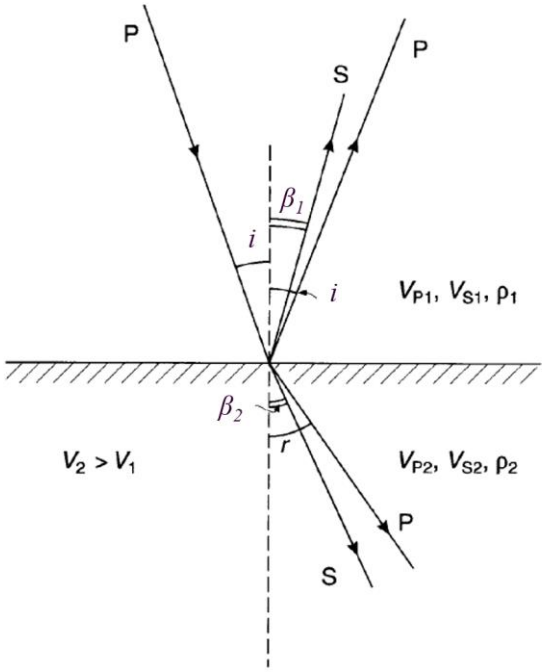

Figure 2.3: Reflection and transmission of seismic waves at an interface (adapted from Reynolds, 1997).

If the underlying layer has a higher seismic velocity than the overlying layer, the refracted wave will bend away from the normal (the dotted line perpendicular to the interface in Figure 2.3). When the angle of incidence reaches a particular value, known as the critical angle (i_c), the angle of refraction becomes 90^o and the refracted wave travels along the upper boundary of the lower medium, at the greater velocity of the lower medium (Reynolds, 1997). The material at the interface is then subject to oscillating stress from the passage of the refracted wave and in turn generates upward moving waves, known as head waves. The arrivals of the head waves may be measured at the array of geophones (Figure 2.4). Figure 2.5 shows the path of rays of interest for refraction and reflection surveys.

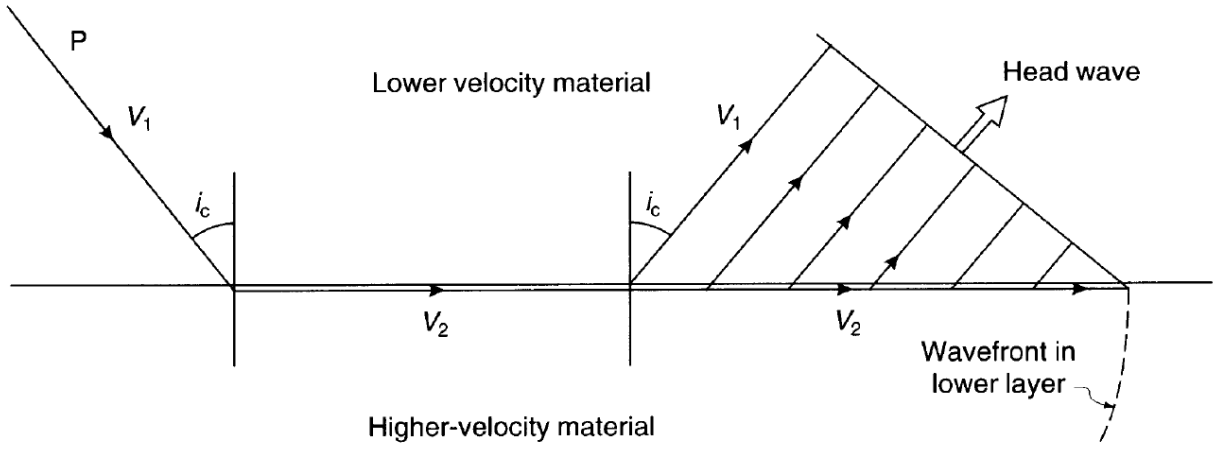

Figure 2.4: Critical refraction and the generation of head waves (Reynolds, 1997).

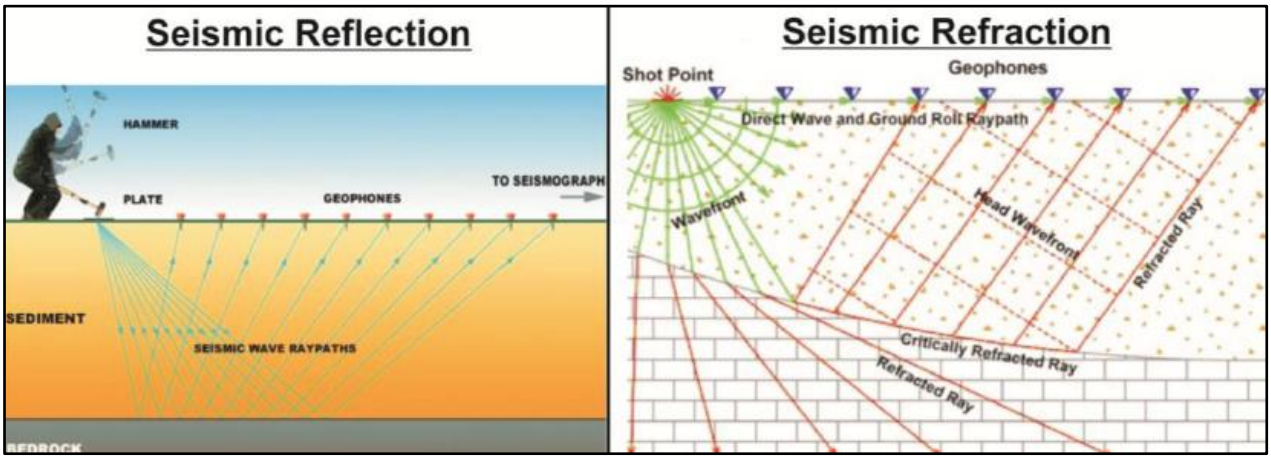

Figure 2.5: Seismic reflection compared with seismic refraction (Lourens, 2013).

Seismic surveys are typically used to indicate the presence of geological formations and their boundaries (Telford *et al*., 1990; Nel, 2017). As seismic methods can give quantitative information on the heterogeneity of the subsurface (Rabbel, 2009), they can indicate areas of deeper weathering, which are often considered targets in groundwater exploration (Nel, 2017). The P-wave velocity is furthermore dependent on the saturation and rock porosity, and seismic techniques could, therefore, potentially distinguish between saturated and dry rocks during groundwater exploration (Rabbel, 2009). However, the seismic method has a high cost of acquisition and interpretation in exchange for reliable information (Rabbel, 2009).

2.2.3 Electrical resistivity methods

Electrical resistivity methods are used to investigate the resistivities of subsurface materials. Resistivity surveys are particularly suitable for groundwater exploration because large changes in the resistivity are often associated with changes in the mineral and fluid content of the formation as well as the porosity and degree of water saturation (Balasubramanian, 2017).

In electrical resistivity methods, information on the subsurface resistivity distribution is obtained by injecting electrical current into the subsurface and by measuring the resulting distribution of electrical potential (Nel, 2017). In the standard setup, four electrodes are used: the current is injected into the surface through two current electrodes (A and B), while measurements of the electrical potential difference are taken at two potential electrodes (M and N) (Kirsch and Ernstson, 2009). If the assumption is made that the subsurface is homogenous, an apparent resistivity (ρ_a) can be calculated from the measured potential difference (∇V) and current (I):

$$\rho_a = K\frac{\nabla V}{I} \qquad 4$$

where K is the geometric factor given by:

$$K^{-1} = \frac{1}{2\pi}[AM^{-1} - AN^{-1} - BM^{-1} + BN^{-1}] \quad 5$$

where AM, AN, BM, and BN are the distances between the various electrodes. The calculated apparent resistivity is an averaged resistivity of all the subsurface materials through which current flow takes place (Kirsch and Ernstson, 2009). Since larger separations between the current electrodes lead to current flows at greater depths, the depth of investigation depends on the AB separation.

Different electrode arrays may be used during electrical resistivity surveys (Telford *et al*., 1990). Some common arrays are shown in Figure 2.6. These differ according to current and potential electrode placement.

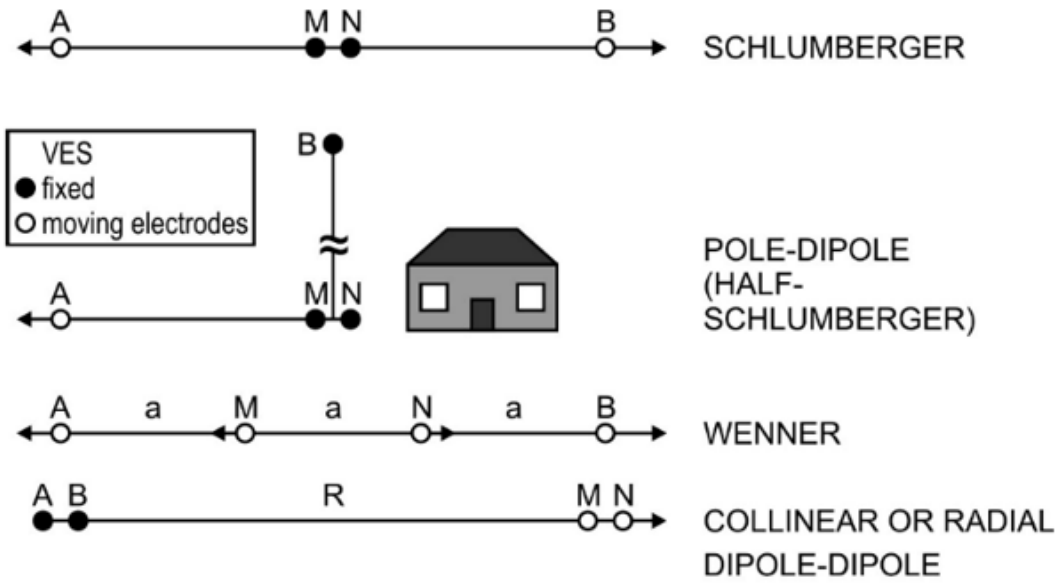

Figure 2.6: Common electrode arrays (modified from Kirsch and Ernstson, 2009).

Electrical resistivity surveys can be used to investigate both vertical and horizontal changes in the subsurface resistivities. *Vertical Electrical Sounding* (VES) involves the measurement of the apparent resistivities at a particular location (sounding centre) for increasing AB separations corresponding to larger depths of investigation (Telford *et al*., 1990). The apparent resistivities are plotted against the AB spacing to give a sounding curve (Figure 2.7).

In VES surveys, the subsurface is assumed to consist of horizontal or near-horizontal layers, each with its specific resistivity (Pozdnyakova *et al*., 2001). The recorded apparent resistivity data are then subjected to a mathematical process called inversion, during which models of the subsurface resistivity distribution are obtained.

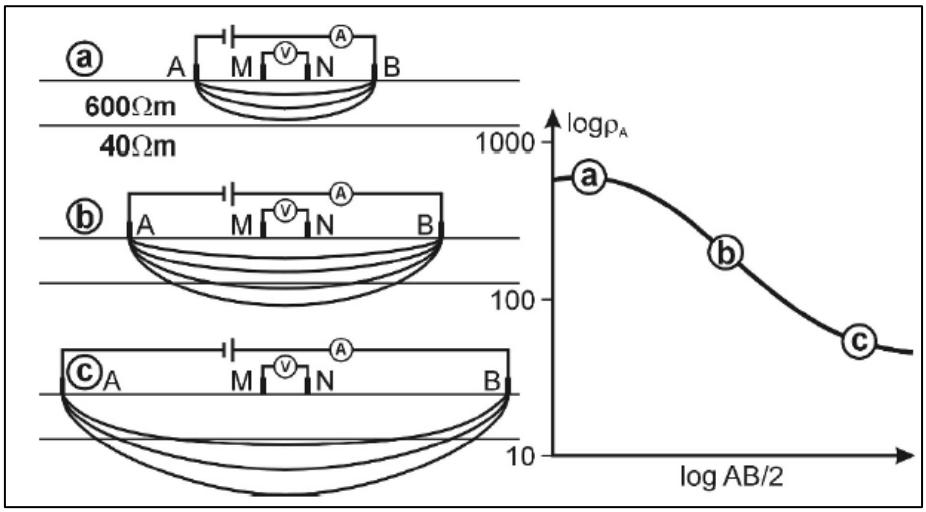

Figure 2.7: Measurements of apparent resistivity with increasing electrode spacing (left) and a sounding curve (right) compiled from the results (Kirsch and Ernstson, 2009).

On the other hand, *profiling* involves the measurement of the lateral changes in the resistivity distribution by moving the electrode array horizontally along the survey line while keeping the AB separation constant (Telford *et al*., 1990). This keeps the depth of investigation constant, allowing lateral changes in resistivity to be detected (Chandra, 2015). Figure 2.8 shows an example of profiling employing the dipole-dipole array.

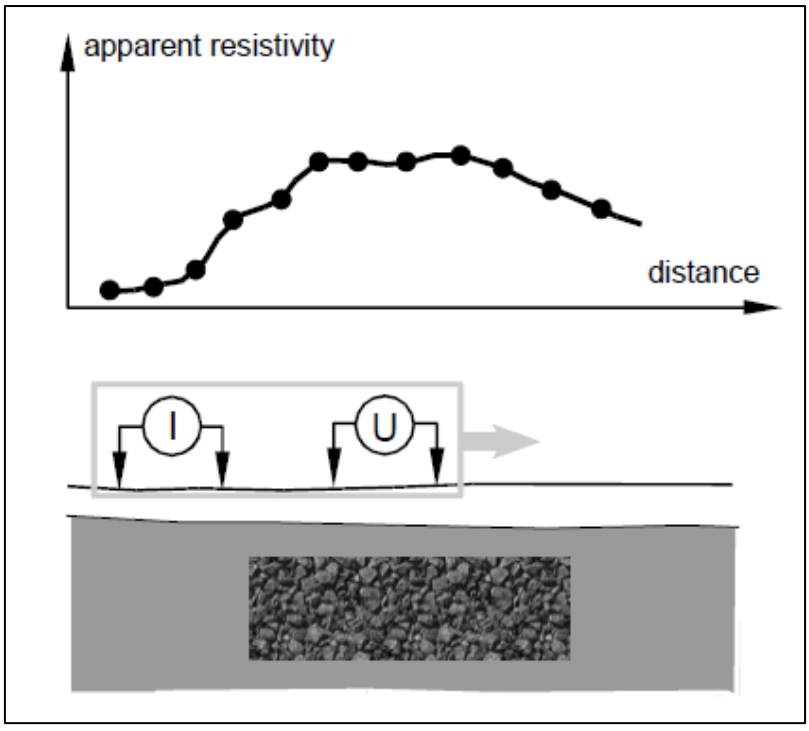

Figure 2.8: Resistivity Profiling using the dipole-dipole electrode configuration (Kirsch and Ernstson, 2009).

Electrical resistivity sounding and profiling can be combined to investigate more complex geology (Kirsch and Ernstson, 2009). However, this is very tedious, and to overcome this, lateral and vertical resistivity measurements are taken simultaneously in a technique called electrical resistivity

tomography (ERT) (Chandra, 2015; Patra *et al*., 2016). In ERT surveys, the number of electrodes is increased from four (as in VES) to 24, 48, 64, or more electrodes with a multicore cable connection and attached to an automatic switch (Patra *et al*., 2016). The system is controlled by a computer or multiprocessor-driven resistivity meter (Kirsch and Ernstson, 2009). According to the electrode array chosen, the current (C) and potential (P) electrodes are selected, and automatic measurement of the apparent resistivities is taken along the profile (Patra *et al*., 2016). This is done for multiple combinations and transmissions to allow measurement in the vertical and lateral directions (Patra *et al*., 2016). Figure 2.9 shows the arrangement made when taking measurements during an ERT survey. Observed data are presented as an apparent resistivity pseudo-section along the profile. These pseudo-sections are then subjected to inversion to obtain models of the resistivity of the subsurface (Figure 2.10) (Kirsch and Ernstson, 2009).

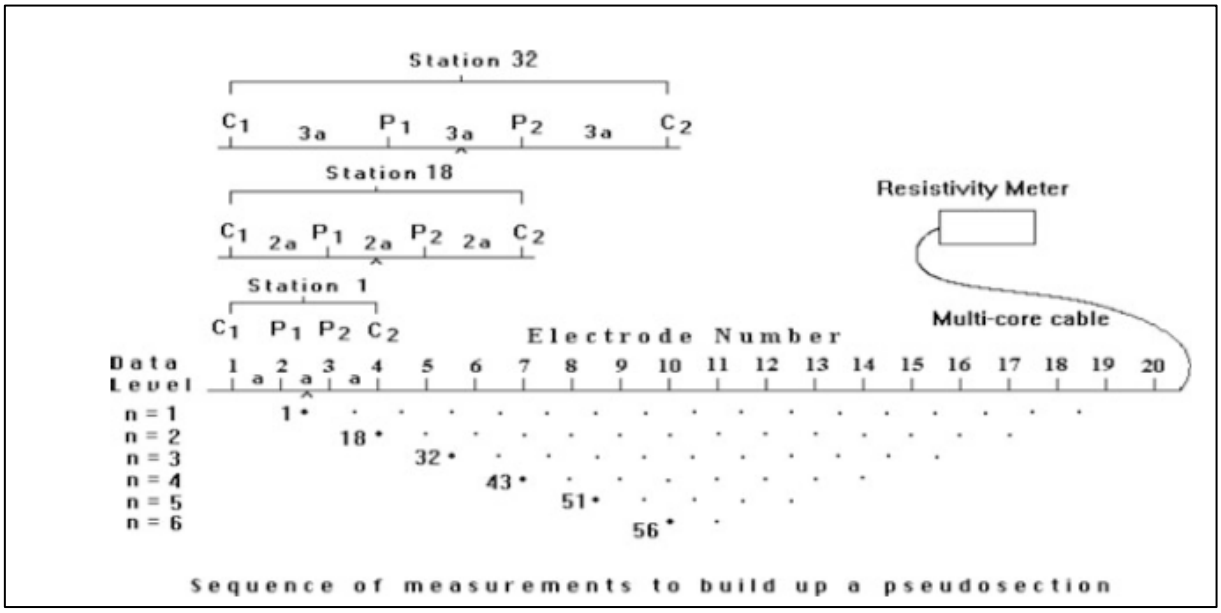

Figure 2.9: Sequence of measurement in a 2D ERT survey (Patra *et al*., 2016).

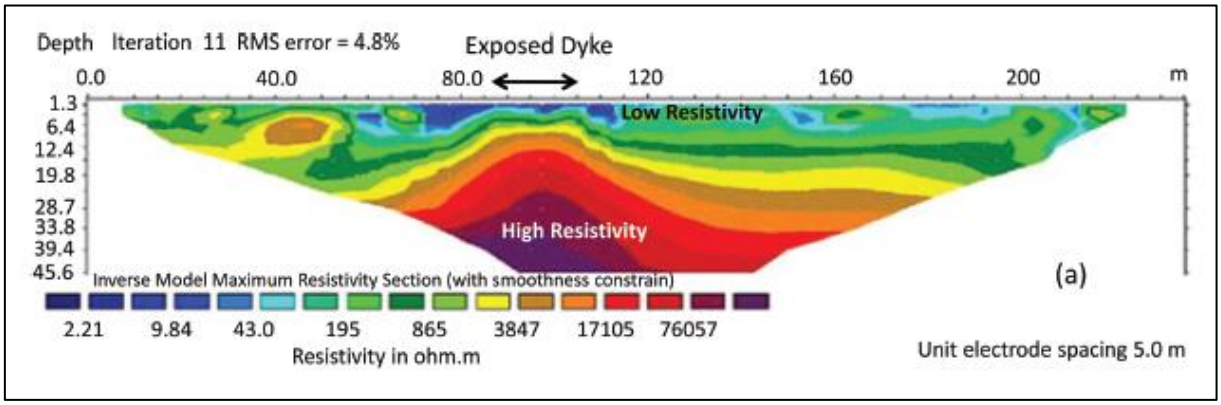

Figure 2.10: Inverse resistivity model for an ERT survey in a granitic terrain across an exposed dyke (Chandra, 2015).

2.2.4 Electromagnetic methods

Electromagnetic (EM) methods exploit the electrical conducting capabilities of different rock types (Nel, 2017). These can yield information on the water quality and the nature of the aquifer (Siemon, 2009). The principle of these methods is that continuous or transient electromagnetic waves are transmitted by a source to the subsurface, inducing a time-variable current in the ground, which in turn causes a time-variable secondary field which can be detected by a receiver (Telford *et al*., 1990; Siemon, 2009).

EM methods are based on the principle of electromagnetic induction. A conductor moving in a stationary magnetic field or a stationary conductor placed in a changing magnetic field can produce current flow through the conductor (Figure 2.11) (Jones, 2019). This is called Faraday's Law. Similarly, time-varying electrical current flow in one circuit can produce current flow in a second circuit, even when the two circuits are not in physical contact. This is known as inductive coupling.

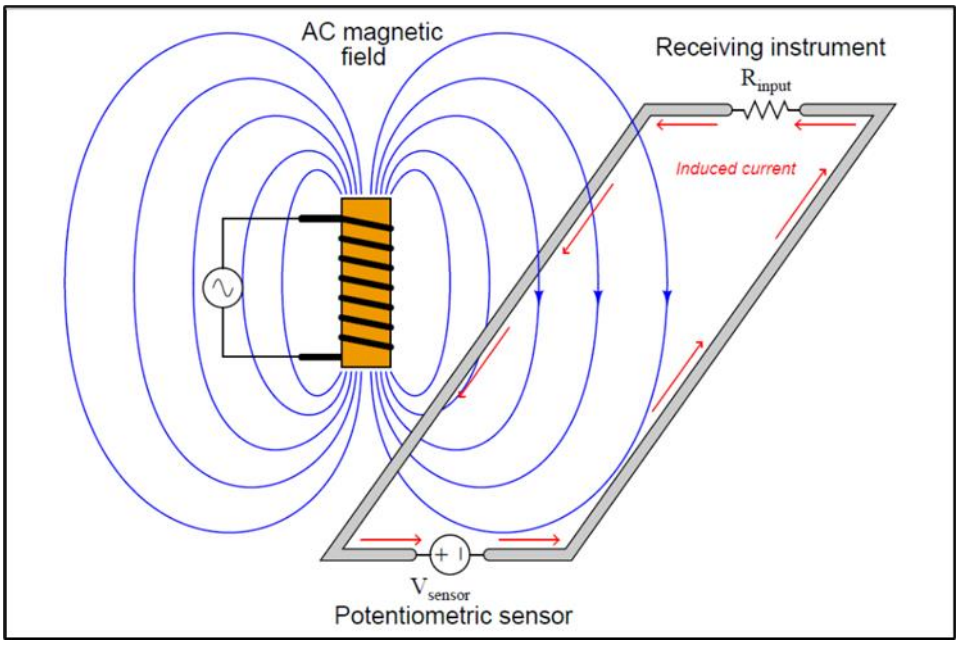

Figure 2.11: An illustration of electromagnetic induction. A time-varying magnetic field induces electrical current flow in a nearby circuit (Inductive Coupling Effects - Instrumentation Tools, n.d.).

The relationship between the magnetic and electric fields and their sources are described by Maxwell's equations, and they form the basis upon which EM methods operate (Fourie, n.d.). Four equations are included in Maxwell's equations. In differential form in a vacuum these equations are:

$$\nabla \times \mathbf{E} = -\frac{\partial \mathbf{B}}{\partial t} \qquad 6$$

$$\nabla \times \mathbf{B} = \mu_0 \left(\mathbf{J} + \frac{\partial \mathbf{D}}{\partial t} \right) \qquad 7$$

$$\nabla \cdot \mathbf{E} = \frac{\rho}{\varepsilon_0} \quad (8)$$

$$\nabla \cdot \mathbf{B} = 0 \quad (9)$$

where:

ε_0 = electric permittivity of free space

μ_0 = magnetic permeability of free space

ρ = electrical charge density

t = time

J = electrical current density

B = magnetic field

D = electrical displacement current

E = electric field

Equation 6 is Faraday's law, which states that "a time-varying field gives rise to a circulating electric field". Equation 7 is Ampere's law which states that "moving electric charges give rise to a circulating magnetic field". Equation 8 is Gauss's law stating that the divergence of an electric field at a specific location is proportional to the unbalanced electrical charge density at that position. Equation 9 states that magnetic monopoles do not exist; it is impossible to find an unbalanced magnetic pole.

In these equations, the del or nabla operator is a vector operator given by:

$$\nabla = \left(\frac{\partial}{\partial x}, \frac{\partial}{\partial y}, \frac{\partial}{\partial z}\right) \quad (10)$$

The general principle of the EM methods is illustrated in Figure 2.12. Time-varying electrical current in the transmitter causes a time-varying primary magnetic field. The changing flux of this magnetic field through a nearby conductor induces a time-varying emf (electromotive force) in the conductor, which causes eddy currents to flow (Keary *et al*., 2002). These eddy currents give rise to a secondary magnetic field, which can be measured at the surface at the receiver. For a transmitter using alternating current (AC), the secondary magnetic field is measured in the presence of the primary magnetic field.

EM methods can be applied either in the time domain (time-domain electromagnetics, TEM) or the frequency domain (frequency-domain electromagnetics, FEM) Christiansen *et al*. (2009). FEM methods operate by using a harmonic signal (AC) with a specific frequency and then measuring the phase shift between the secondary and primary magnetic fields. This phase shift contains information

on the conductivity of the conductive body. Since the secondary magnetic field is measured in the presence of the much larger primary field, very accurate measurements have to be taken to isolate the effects of the secondary magnetic field (Christiansen *et al*., 2009).

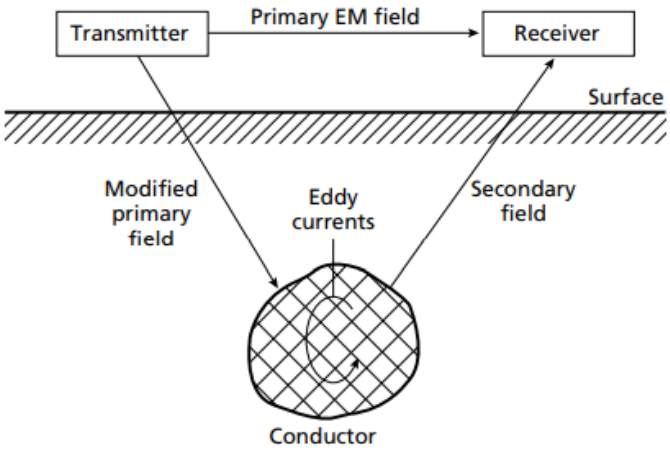

Figure 2.12: Principle of electromagnetic surveying (Kearey *et al*., 2002).

In TEM methods, the amplitude of the secondary magnetic field is measured as a function of time (Christiansen *et al*., 2009). A direct current is made to flow in the primary (source) loop and then terminated rapidly. Measurements of the decay rate of the secondary field can thus be taken in the absence of the primary field (Christiansen *et al*., 2009). The secondary current and magnetic field decay faster for poor conductors than for good conductors. Measurement of the decay rate thus allows insight into the conductivity of the subsurface conductors. Direct filtering of the surrounding noise (unwanted responses or interference caused by a variety of phenomena) is not possible with TEM methods, but this is alleviated by measuring the decaying transient signal in several gates (time channels) and stacking the values (Christiansen *et al*., 2009).

2.2.5 Magnetic methods

Magnetic methods measure the natural magnetic field of the Earth. Magnetic bodies occurring in the subsurface may become magnetised by the magnetic field of the Earth (Figure 2.13). This induced magnetism is superimposed on the Earth's magnetic field, causing local variations called magnetic anomalies in the total magnetic field (Ernstson, 2009). The shapes and amplitudes of the anomalies contain information on the positions, geometries, orientations and magnetic properties of the causative bodies. Magnetic methods can thus be used to detect the contacts between formations of differing magnetic properties, such as at faults (Ernstson, 2009; Nel, 2017).

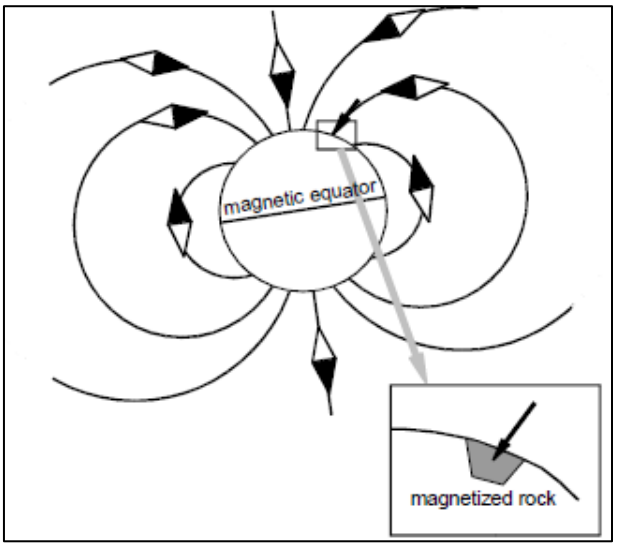

Figure 2.13: The magnetic field of the Earth and magnetisation of rocks (Ernstson, 2009).

Apart from induced magnetism, a body may also carry remanent magnetism, which is magnetism that the body acquired at its formation when the Earth's magnetic field had a different orientation to the current field. Both induced and remanent magnetism may thus contribute to the magnetic anomalies recorded during a survey (Ernstson, 2009). Figure 2.14 shows an example of the magnetic anomaly caused by a W-E striking magnetic body located in central Europe where the Earth's (inducing) magnetic field is 48 000 nT.

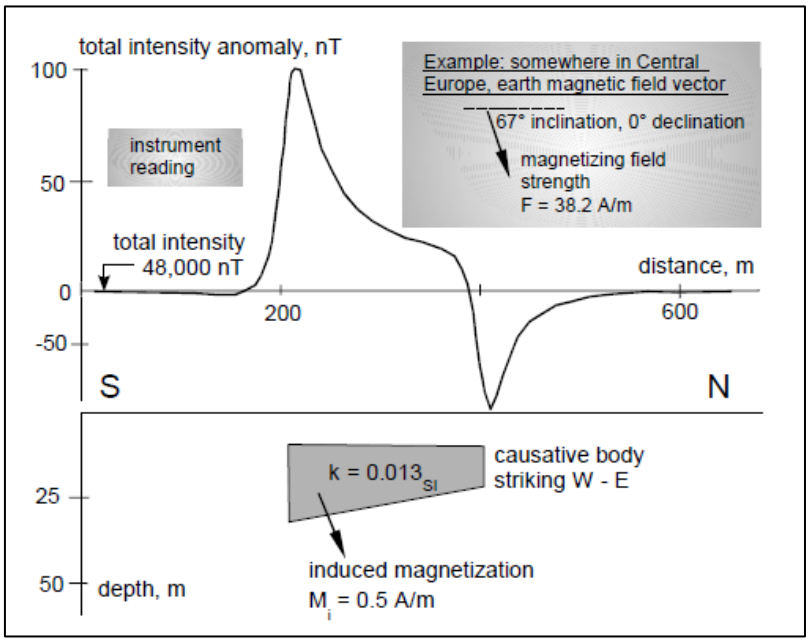

Figure 2.14: An illustration of the relationship between latitude, orientation, and magnetising field for a causative body (Ernstson, 2009).

In Figure 2.14, *k* refers to the magnetic susceptibility, which is a measure of how much a body will be magnetised. Both the orientation of the body and the strength and direction of the inducing field (Earth's field) affect the shape and amplitude of the resultant anomaly, as illustrated in Figure 2.15. In this figure, the same body of Figure 2.14 is shown for N-S and W-E strikes. Also shown is the

anomaly that would have been recorded across the body had it occurred at the magnetic equator, where the magnetic inclination is zero (Ernstson, 2009).

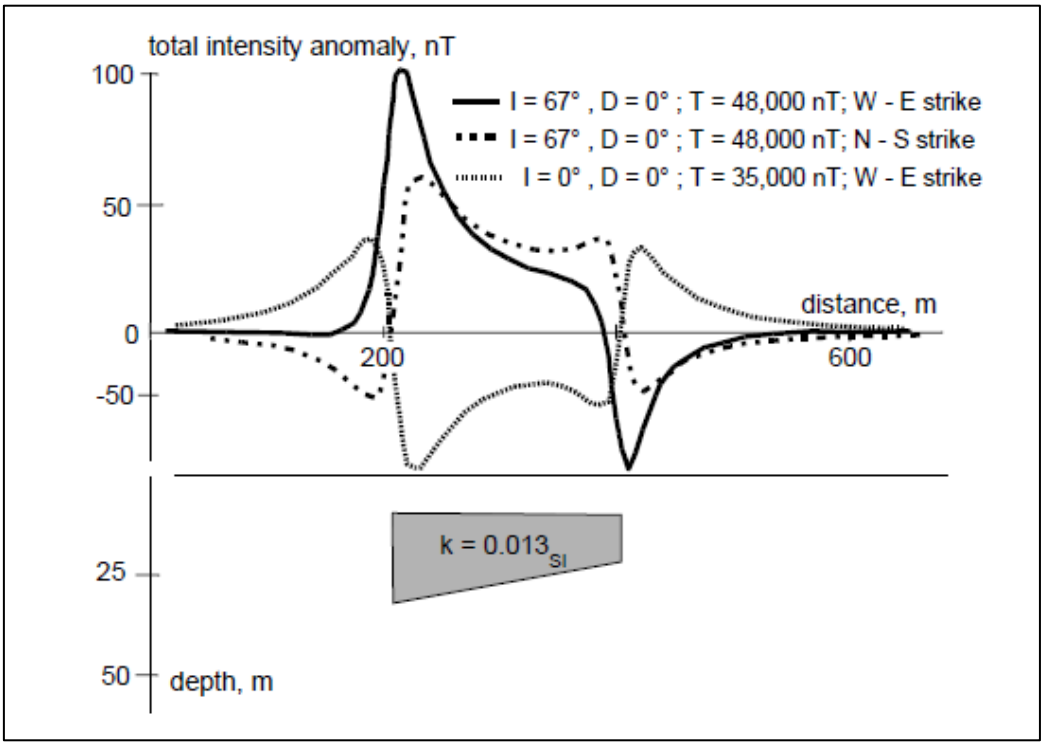

Figure 2.15: Total intensity anomalies calculated for a single causative body. T=48000nT is the total field intensity in the undisturbed field in central European latitudes (Ernstson, 2009).

During magnetic surveys, the magnetic field of the Earth is measured using instruments called magnetometers. Magnetic surveys are typically conducted along profile lines orthogonal to the strike of the body with an appropriate station spacing (Ernstson, 2009). Repeated base station readings need to be made to account for different ionospheric processes that cause diurnal variations in the Earth's magnetic field and thus affect the readings taken during a survey (Ernstson, 2009). Care must be taken to ensure sufficient distances from sources of noise, such as metal poles and cars, during the survey. Magnetic data are also often filtered to remove effects from regional anomalies to aid in interpretation (Ernstson, 2009).

2.2.6 Magnetotelluric methods

There are large-scale, low-frequency magnetic fields that exist in and around the Earth that are called magnetotelluric fields (Kearey *et al.*, 2002). These fields induce electric currents called telluric currents in the Earth (Kearey *et al.*, 2002; Chave and Jones, 2012). The magnetotelluric fields may be the result of fluctuations in the magnetic field of the Earth caused at frequencies <10 Hz by the interaction of plasma and the ionosphere and at frequencies >10 Hz by global lightning activity (Chave and Jones, 2012).

The magnetotelluric method is a passive electromagnetic method, which means that it makes use of a natural source of energy for measurements (Chave and Jones, 2012). When using the magnetotelluric method, both the magnetic and electric fields are measured (Kearey *et al.*, 2002). The magnetic field is measured by its inductive effect on a receiver coil or by using a fluxgate magnetometer. Three components (*x*, *y* and *z*) of the magnetic field are typically measured while the two horizontal components (*x* and *y*) of the electric field are measured at each station (Figure 2.16). The latter are measured using grounded electrode pairs.

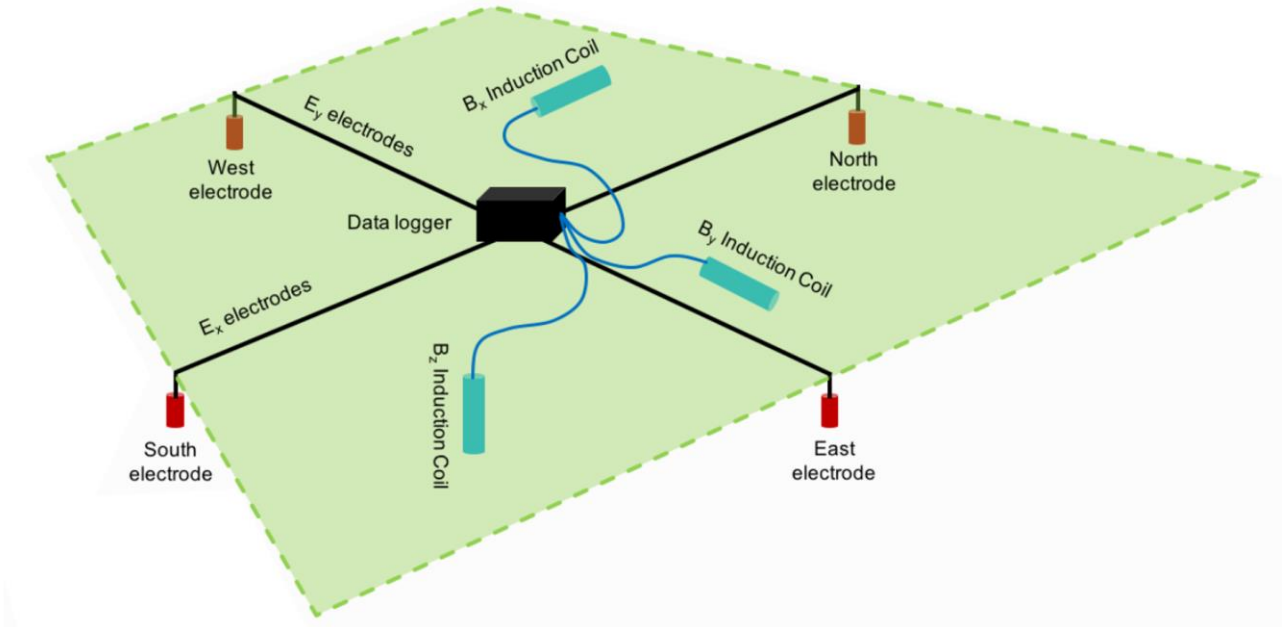

Figure 2.16: Components of the electric and magnetic field typically measured during a magnetotelluric survey (https://resistics.io/tutorial.html).

The relation of the orthogonal components of the horizontal electric and magnetic field is described by the impedance tensor **Z**:

$$\begin{pmatrix} E_x \\ E_y \end{pmatrix} = \begin{pmatrix} Z_{xx} & Z_{xy} \\ Z_{yx} & Z_{yy} \end{pmatrix} \begin{pmatrix} H_x \\ H_y \end{pmatrix} \qquad 11$$

If the subsurface is assumed to be homogeneous, the impedance is independent of the polarisation of the incident field and is related to the subsurface resistivity and frequency of the electromagnetic field. This principle can be used to define an apparent resistivity for the subsurface as a function of frequency:

$$\rho_a = \frac{1}{5f}\left|\frac{E}{H}\right| \qquad 12$$

The frequency of the magnetotelluric field and the subsurface resistivity determine the depth to which the field penetrates (Kearey *et al.*, 2002). Using varying frequency, apparent resistivity at different

depths can be found, giving results analogous to those of vertical electrical sounding (Kearey *et al*., 2002). The magnetotelluric method can be used to provide high-resolution information about lateral and horizontal variations of the subsurface conductivity by using available master curves or using computer software to map results (Kearey *et al*., 2002; Chave and Jones, 2012).

The magnetotelluric method can give information at very shallow depths or great depths from near surface to beyond 410 km; however, like other geophysical methods, it cannot be used in noisy areas (Chave and Jones, 2012). At high frequency, the audio frequency magnetotelluric method has been used to map groundwater in the range of 250-2000 m (Chave and Jones, 2012).

2.2.7 Nuclear magnetic resonance methods

The nuclear magnetic resonance (NMR) method is unique in that it measures the water content of the subsurface directly, unlike the other techniques discussed so far (Chandra, 2015). It allows for groundwater to be quantified to a depth of about 100 m (Chandra, 2015).

Water molecules contain hydrogen atoms with one proton. The spin of hydrogen protons around their nuclei is the physical property used in NMR methods (Yaramanci and Hertrich, 2009). The spin is the possession of angular momentum without physical rotation and an associated magnetic moment (Yaramanci and Hertrich, 2009). The protons are, therefore, regarded as spinning magnetic dipoles with their axes parallel to the axis of spin (Chandra, 2015). In the existence of an ambient static magnetic field, the magnetic dipole aligns itself with the field and precess at a rate dependent on that field's magnitude at that point (Chandra, 2015). This frequency is called the Larmor frequency ω_0 and is related to the static field by what is called the gyromagnetic ratio γ_p (Chandra, 2015):

$$\omega_0 = 2\pi f_0 = \gamma_p |\mathbf{B_0}| \qquad 13$$

where $\gamma_p$is the gyromagnetic ratio of a proton, and $\mathbf{B_0}$ is a static magnetic field. The gyromagnetic ratio is unique for each type of nucleus; thus, the Larmor frequency can be used to investigate unique nuclei (Chandra, 2015).

The precession axis of the protons can be antiparallel or parallel to the direction of the static magnetic field (Chandra, 2015). The low energy state is associated with parallel layout, and the high energy state with the antiparallel. A slightly larger number of protons with a low energy state than those with a high energy state results in a net magnetisation in the direction of the ambient static magnetic field (Chandra, 2015).

When an external oscillating magnetic field at the Larmor frequency is applied, its component orthogonal to the static field generates torque and alters the spin axes of the protons (Chandra, 2015). When the oscillating field is turned off, the protons produce a relaxation magnetic field at the Larmor

frequency and equilibrate by realigning with the static field (Chandra, 2015). The response from the protons as they precess back to the static field is measured. The amplitude of the recorded signal is proportional to the number of hydrogen atoms present, and the water content can thus be assessed (Chandra, 2015). Figure 2.17 illustrates the principle of magnetic resonance with stages of rest, excitation, and relaxation, respectively.

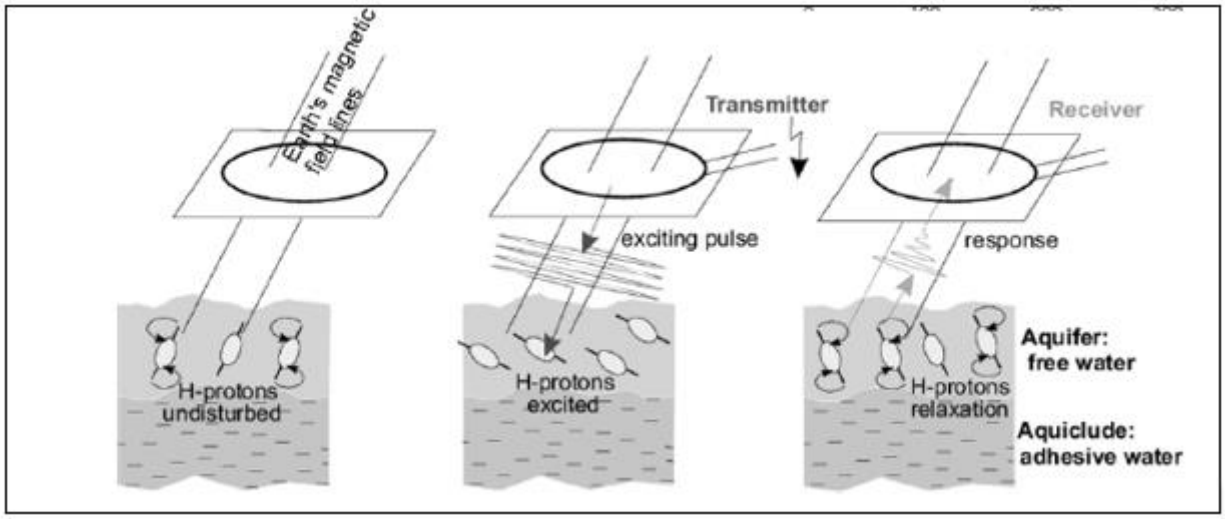

Figure 2.17: The principle of magnetic resonance. Modified from (Yaramanci and Hertrich, 2009).

Magnetic resonance sounding (MRS) is based on this principle. First, the magnetic field intensity of the Earth (the static field) is measured with a magnetometer (Chandra, 2015). Then, the instrument passes an excitation current at the Larmor frequency for a few milliseconds through a transmitter loop placed on the ground before the current is quickly terminated. The same loop then records the relaxation signal (Chandra, 2015). To measure at different depths, the pulse moment (product of the intensity of loop current at Larmor and pulse duration) is varied (Chandra, 2015).

According to Chandra (2015), the method has mostly been applied to sedimentary basins to estimate the vertical water content distribution but has also been used in hard-rock aquifers to determine the water content in fractured and weathered zones. NMR has also been used in borehole logging to estimate porosity by finding the amount of fluid in the formation (Kearey *et al*., 2002).

2.2.8 Geophysical borehole logging

The continuous depth-wise measurement of the physical properties of formations around the borehole is known as geophysical logging (Chandra, 2016). These techniques provide information such as fractured zones crossed by the borehole, the thickness of the aquifer, and the detection of bed boundaries or saline water-bearing zones (Patra *et al*., 2016; Chandra, 2016). Logs are usually taken as soon as the borehole is drilled by means of a sensor lowered into the borehole. The log is then

taken when the sensor (called a sonde) is drawn up back to the source at a uniform speed, and the data is transmitted and recorded (Figure 2.18). The data collected is often compared to the geological log taken during drilling.

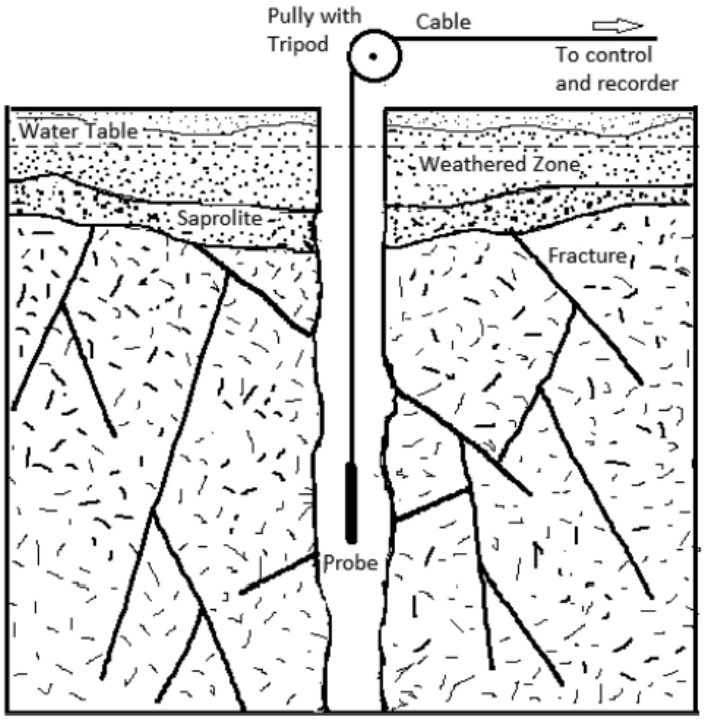

Figure 2.18: Illustration of geophysical logging (Chandra, 2016).

Like other geophysical methods, the logging techniques may be passive or active. These techniques can provide invaluable information about the hydrogeology of the locale, which can be used to drill new boreholes in nearby sites (Balsubramanian, 2017). Table 2.1 summarises some common geophysical logging techniques and their applications.

Table 2.1: Summary of geophysical logging techniques (Chandra, 2016; Patra *et al.*,2016)

Logging technique	Parameter measured	Use	Unit
Spontaneous potential / Self-potential (SP)	Natural potential of electrochemical origin due to different electrical conductivities of borehole and formation fluid	Detect bed boundaries, porous and permeable zones, formation water resistivity	mV
Single point resistance (SPR)	Formation resistance	Detect resistive porous and permeable freshwater zones like fractures	Ohm
Resistivity	Potential difference between potential electrodes measured to give resistivity variations with depth	Detect bed boundaries, fracture zones	Ohm.m
Induction logging	Electrical conductivities of formation	Contaminant detection, monitoring	mS/m
Fluid conductivity	Electrical conductivities of borehole fluid	Water quality, locate trnsmissive zones	µS/cm
Temperature	Depthwise change in borehole fluid temperature	Provide information on source and movement of water	^{o}C
Natural gamma radioactivity	Total gamma radiations emanating from formations in the immediate vicinity of the borehole that interact with the probe	Identifies lithological units; moslty clay and shale	Counts per second
Gamma-gamma ray/density log	Intensity of scattered gamma rays which is dependent on formation density	Estimate porosity, determine lithology	g/cm^3
Neutron	Records response due to nuetron-capture gamma rays, depends on formation hydrogen content	Estimate porosity, determine lithology	Counts per second
Caliper	Depthwise variation in borehole diameter	Determine borehole volume, locate fractures, determine depth of parting or collapse, etc	cm

Table 2.1 (continued): Summary of geophysical logging techniques (Chandra, 2016; Patra *et al.*,2016)

Logging technique	Parameter measured	Use	Unit
Flow meter	Groundwater flow rates with depth	Determine yield contribution of individual fractured zones with depth, directions of flow, vertical variation in hydraulic conductivity	m/min
Acoustic/Sonic	Measures depthwise travel time of sonic waves through formations	Determine porosity, fracture zones and lithology	μs
Borehole televiewer (optical)	Obtains images of the walls of dry or clear water filled borehole	To locate the voids, joints, fractures, alteration, bedding planes, change in lithology, ruptures, perforations and corrosion in the casing of cased wells	
Borehole radar (BHR)	Transmits impulsive radar waves and measures their response to subsurface materials	Delineate fracture zones, their radial extent beyond the borehole and their orientation	
Nuclear magnetic resonance (NMR)	Relaxation time of hydrogen protons after exposure to an exciting signal	Water content, can distinguish free and clay bound water	ms

2.2.9 New and unconventional methods

In recent years, several new and unconventional geophysical technologies for groundwater exploration have been introduced to the market. These systems are usually much more affordable than conventional geophysical equipment and are typically very user-friendly. For these reasons, these systems have become very popular among geologists and hydrogeologists who often do not have formal training in geophysics.

In particular, systems that measure the natural variation in the Earth's electrical field have become popular in South Africa (Gomo, 2023). Two examples of such systems are the ADMT groundwater detectors and PQWT groundwater detectors (Figure 2.19). These systems appear to operate similarly, involving the measurement of the electrical potential difference between two grounded electrodes at several frequencies (Figure 2.20). The systems, therefore, appear to measure the effects of telluric currents in the subsurface. The frequencies used during measurement are then converted to depths of investigation, probably by using the simplified formula for the skin depth (δ) of an EM wave penetrating a conductive medium: $\delta = 503.5\sqrt{\rho/f}$, where ρ is the resistivity of the medium and f is the frequency at which the measurement is taken. The recorded data are then displayed as pseudo-sections of potential difference against estimated depth of investigation (Figure 2.21). Although not labelled in these pseudo-sections, the horizontal axis represents the station number along the measurement line, while the vertical axis gives the estimated depth of investigation. The amplitude of the signal is probably measured in millivolt (mV).

Figure 2.19: ADMT 300SX (left, centre) (Aidu Energy Technology, 2023), PQWT- S500 500M (right) (PQWT, n.d.).

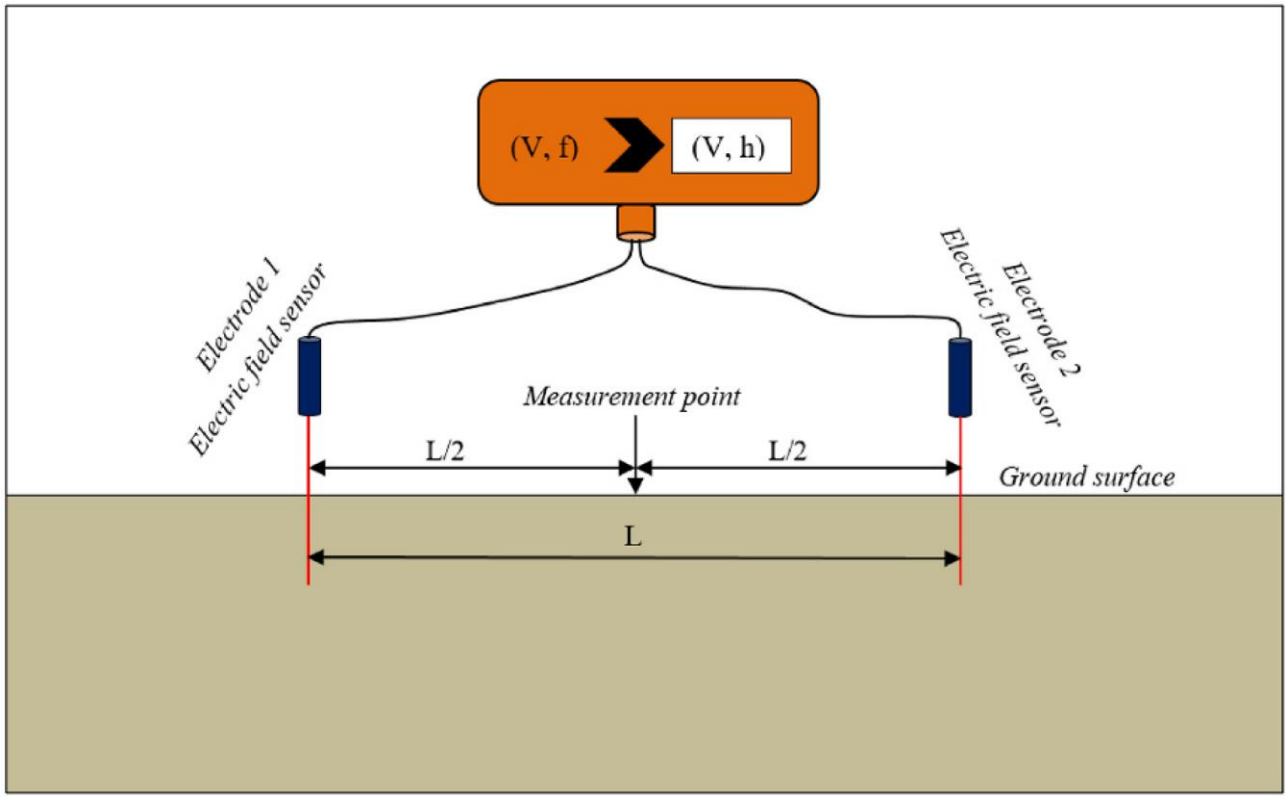

Figure 2.20: Illustration of the typical groundwater detector placement in the field (Gomo, 2023).

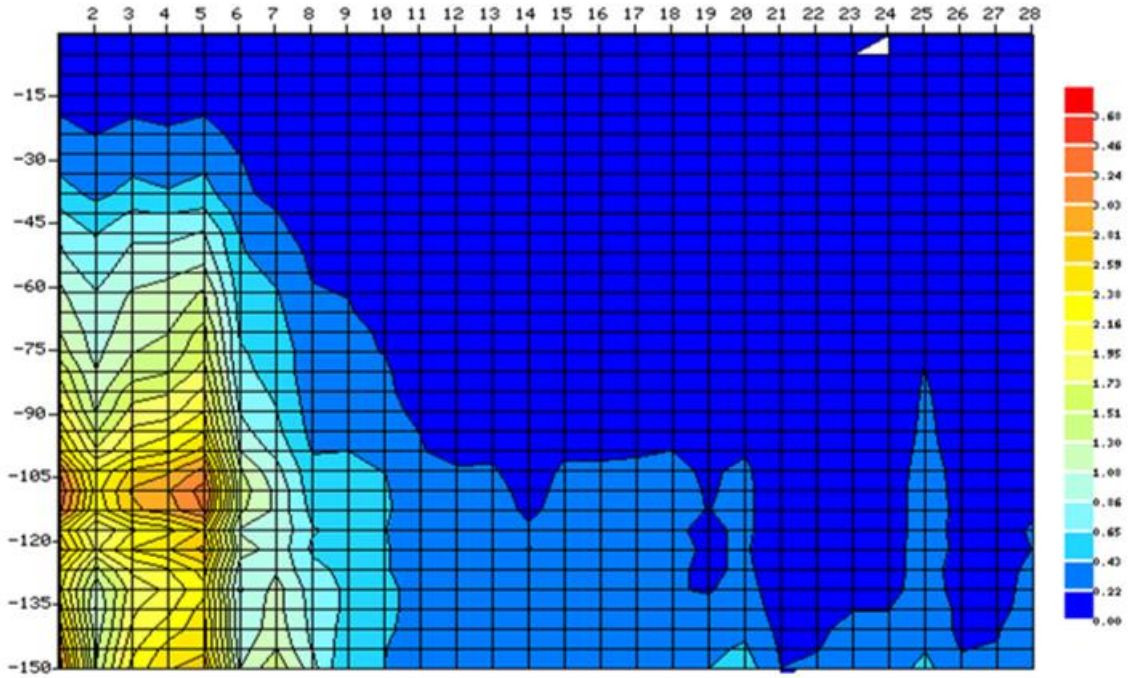

Figure 2.21: Example of a pseudo-section obtained with the PQWT groundwater detector.

Although these systems have become popular, several concerns exist about the assumptions on which they are based:

- For the conversion of frequency to depth, it is assumed that the subsurface is homogeneous in terms of its resistivity to allow calculation of the skin depth. It is not known what value is

assumed by the system for the subsurface resistivity, but large errors in the estimated skin depth can be expected for an inhomogeneous subsurface.

- The skin depth is a parameter that allows insight into the depth of penetration of an EM wave into a conductive (or resistive) medium. It corresponds to the depth at which the amplitude of the wave decreases by a factor 1/*e* (or 37%) due to attenuation. The skin depth does not in itself equate to the depth of investigation.
- The pseudo-sections obtained with the PQWT system are not subjected to inversion. This means that no models of the subsurface are calculated from the pseudo-sections. The raw data (measured potential differences) are directly interpreted in terms of changes in the subsurface properties at particular horizontal positions and at the estimated depths.

There are also concerns about the repeatability of the results obtained with the groundwater detectors. Figure 2.22 shows the results of two surveys with the PQWT system conducted on the same line, but six months apart, in an area with a sandstone recumbent fold overlying shale. The investigation depth was 300 m and stations were 5 m apart. The two data sets yielded very different results. Rock Hounds (n.d.) suggested that looking at colours in the obtained pseudo-sections is an unreliable way of discerning differences in the subsurface. Rock Hounds (n.d.) further proposed that the results obtained are dependent on telluric currents which are not constant, therefore results for a single site can vary on repeated surveys. This unrepeatability of results raises questions about the reliability of the results obtained with these unconventional systems.

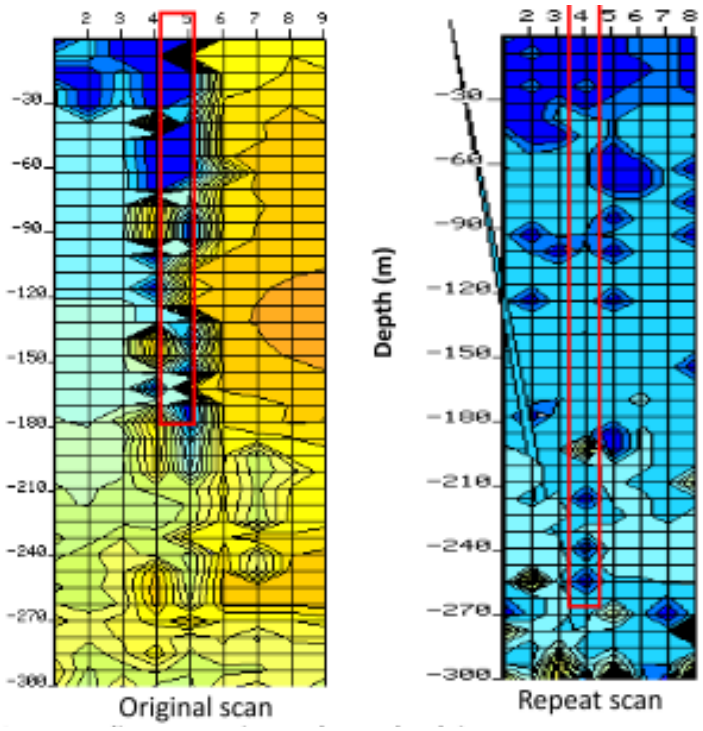

Figure 2.22 Two surveys on the same line conducted six months apart (Rock Hounds, n.d.)

2.3 GEOPHYSICAL METHODS FOR GROUNDWATER EXPLORATION

Geophysical surveys are important because they remove ambiguity in placing boreholes and can, in the long run, reduce the costs of drilling boreholes "blindly". Different methods, however, have different applications depending on the setting. The geophysical investigation chosen through a single or combination of methods is dependent on the individual programme aims, local geology, infrastructure, available equipment, interpretational software, expertise, and other site-specific demands so that the desired outcomes can be achieved (Chandra, 2015). Table 2.2 gives a summary of some geophysical methods and their limitations.

Table 2.2: Geophysical methods used for groundwater exploration (Kirsch, 2006; Moore, 2011; Chandra, 2015; Milloy *et al*., 2015).

Method	Major use in groundwater investigations	Limitations
Electrical resistivity	Characterise material as consolidated rock or clay, silt, or sand. Weathered zone aquifer thickness. Water quality, fracture demarcation, bedrock topography, mapping contaminant plumes, locating abandoned wells.	Non-uniqueness due to equivalence, poor resolution of thin targets due to transition and layer suppression, need for a large area for deeper investigation, and highly conductive or resistive overburden.
Frequency domain controlled-source electromagnetic	Fractured zone demarcation	Highly conductive overburden, thin targets, equivalence.
VLF electromagnetic	Fractured zone, top layer resistivity	Fractured zone orientation, highly conductive overburden.
Time-domain electromagnetic	Conductive layers	Difficult to discriminate resistivity of resistive layers. Anthropogenic noise and high overburden conductivity for airborne TEM.
Seismic refraction and reflection	Weathered zone thickness, fractured zone and orientation, dry and saturated fractures, buried channels	Low-velocity layer underneath high-velocity layer in the case of refraction, energy source.
Self-potential	Direction of groundwater flow, seepage	Influence of other electrical potentials.
Magnetic	Delineation of basic dykes, lithological contacts, faults, bedrock topography	Influence of other magnetic bodies, magnetic contrast and non-uniqueness.
Nuclear magnetic resonance Magnetic resonance sounding	Water content	Low volume of water in fractures compared to large volume of rock in hard rocks. May not have a high enough signal to overcome noise.

2.4 INTERNATIONAL CASE STUDIES OF GEOPHYSICAL GROUNDWATER EXPLORATION

Geophysical groundwater exploration has been conducted extensively internationally. In this section, a summary of a few recent publications where geophysics was used for this purpose is given. Geophysical methods often reinforce one another. Thus, the reader will find that a study may be classified under a specific method even though different types of geophysics were used in that study.

Where this is the case, more emphasis is placed on the geophysical method under which the case study is classified.

2.4.1 Groundwater exploration using gravimetric methods

2.4.1.1 Case study 1: Plaine du Nord, Haiti

A study was conducted in the Plaine du Nord alluvial aquifer near Cap Haitien in the Republic of Haiti. The aim of the study was to determine the groundwater potential and the thickness of the western part of the aquifer. Due to the constrained budget for the study, the gravity method and the hybrid source audio-magnetotelluric (HSAMT) methods were employed (Miner *et al.*, 2022). The gravity method allows the mapping of density anomalies in the subsurface, assisting in interpreting the depth to the bedrock or the aquifer thickness. The HSAMT is able to characterise subsurface resistivity to give an understanding of the hydrogeologic conditions (Miner *et al.*, 2022).

The study area is approximately 270 km^2, and there was limited knowledge of the aquifer stratigraphy due to a lack of drilling records or use of geophysics in the area. Several faults exist along the boundaries of the aquifer and beneath the basin fill. Seventy-five HSAMT soundings and 50 gravity readings were taken and modelled into eight 2D resistivity lines and six 2D gravity lines (Miner *et al.*, 2022). Figure 2.23 shows the location of the survey lines used in this study.

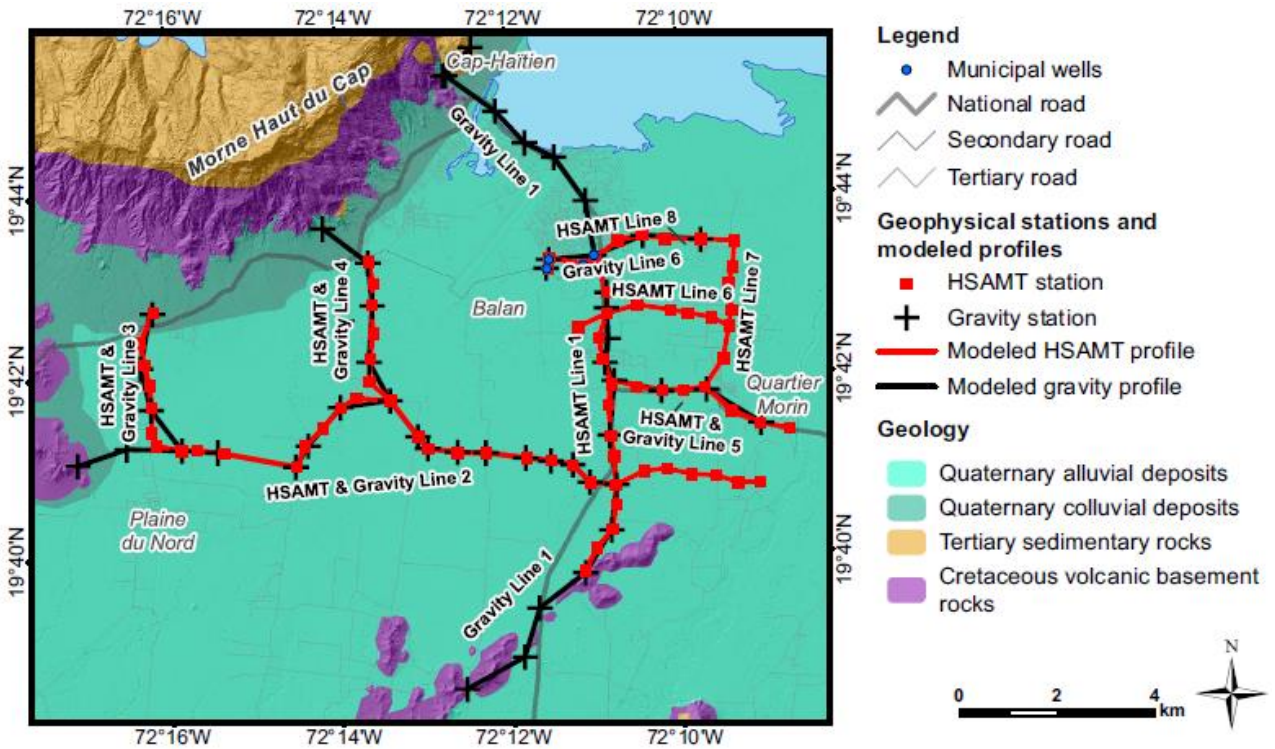

Figure 2.23 Geophysical traverses (Miner *et al.*, 2022).

Borehole data were used to calibrate the HSAMT and gravity results, but data limitations caused uncertainties with depths below the extent of known boreholes. The HSAMT field data consists of

sounding curves that are logarithmic plots of apparent resistivity against frequency. Higher frequencies and low resistivities correspond to shallower depths of investigation. A broadband instrument- Geometrics Inc. Stratagem EH4 HSAMT- was used to record the data for the 10 Hz-1 kHz, 500 Hz-3 kHz, and 750 Hz-92 kHz. Each sounding had 15 m electric dipoles, and magnetic sensors were orientated such that each E_x and H_x were orientated parallel to the assumed geoelectric strike, while E_y and H_y were orientated perpendicular (Miner *et al*., 2022). For the project, 2D depth sections were modelled in the scalar transverse electric mode along profiles using the Geometrics Electromagnetic Array Profile and the Schlumberger WGlink software (Miner *et al*., 2022).

Gravity data were recorded using the LaCoste and Romber Model G gravity meter. Measurements at a base station were taken at intervals of less than 8 hours. Gravity data were processed using the Geotools Corporation's Grav Master computer program following the standard corrections. The Bouguer slab density was set at 2.67 g/cm^3 to process the data, a standard value for the Caribbean. Gravity data were then modelled using the Interpex Ltd. IX2D-GM program (Miner *et al*., 2022). The acquired data was important in determining the sediment thickness and positions of any present faults, which have a bearing on groundwater occurrence. The modelled HSAMT and gravity results are shown in Figure 2.24 and Figure 2.25, respectively.

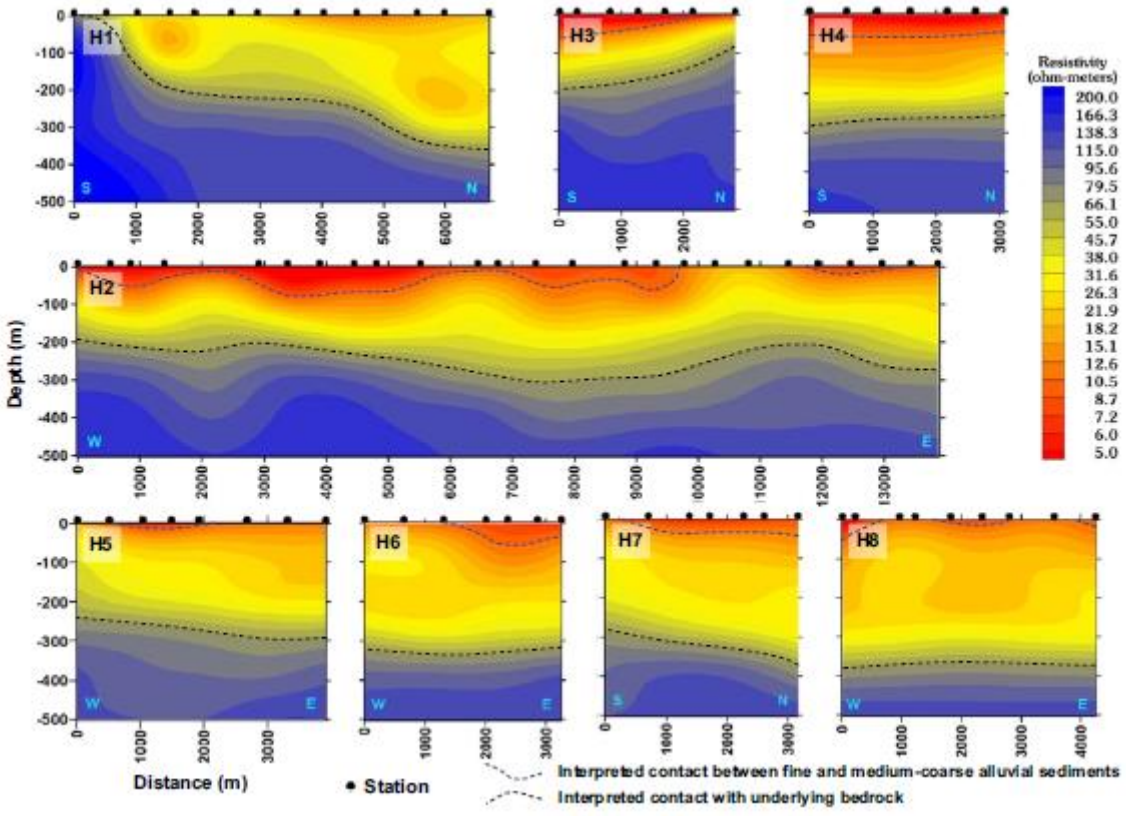

Figure 2.24: Modelled HSAMT lines (Miner *et al*., 2022).

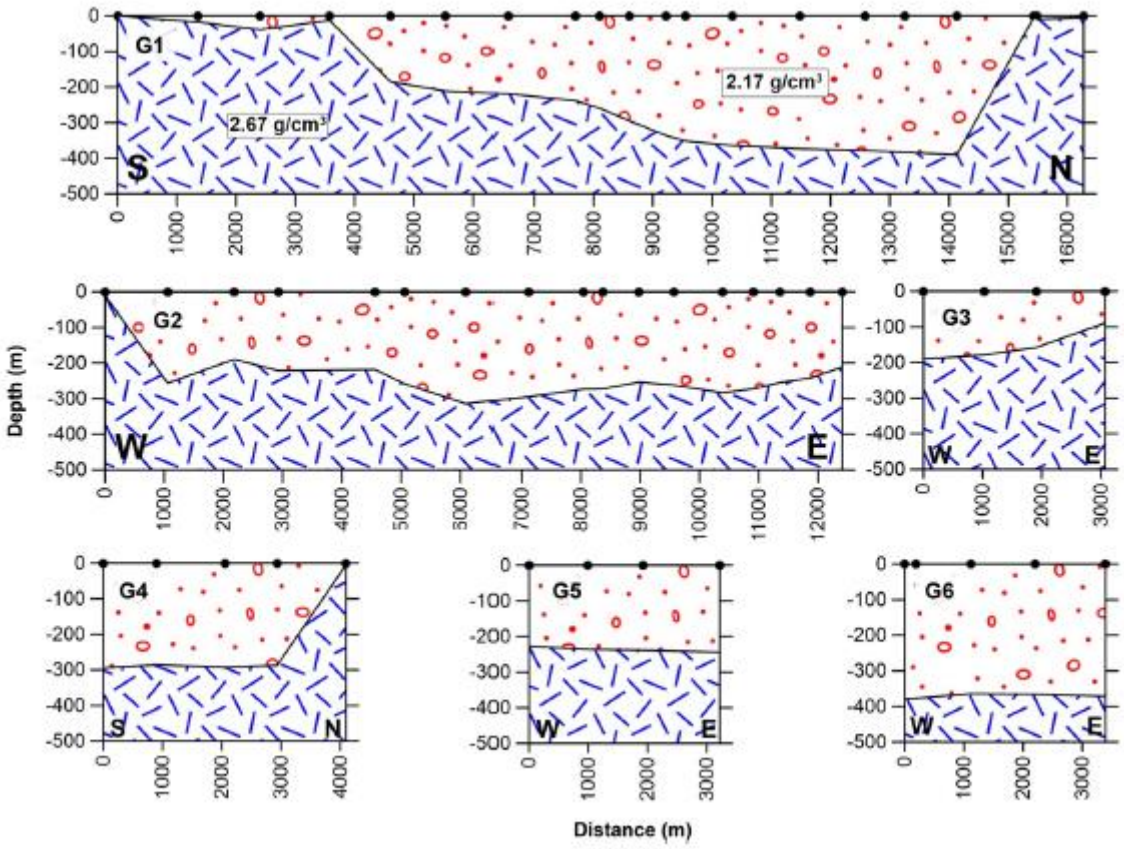

Figure 2.25: Modelled sediment thickness. Lines used 2.17 g/cm^3 and 2.67 g/cm^3 densities for basin fill and basement, respectively (Miner *et al*., 2022).

The models obtained from the two data sets showed good correlation, although some deviation was likely due to other lithologies apart from bedrock or alluvium used in the gravity model. The overall results supported the estimations of the aquifer thickness and other characteristics and will support exploratory drilling. The authors cautioned that the data must be adjusted accordingly as new borehole data become available (Miner *et al*., 2022).

2.4.1.2 Case study 2: Gongola basin, Nigeria

Epuh *et al.* (2020) conducted a study to evaluate the adequacy and accuracy of lineaments extracted from remotely sensed data as compared to reference datasets created through gravity methods. Lineaments are typically indicative of zones of high groundwater potential, as they may be the result of structural features such as joints, faults or folds. Gravity anomalies taken from the horizontal derivative are typically able to reflect lineaments quite well, and the process of extraction is well established. This study thus aimed to evaluate the adequacy of lineaments extracted from remote sensing data. The integration of the two datasets was also tested to see their usefulness in groundwater exploration. The area of interest was the western sector of the Gongola Basin within the Bauche and Gombe states of Nigeria. A total of 1813 gravity observations were acquired from a previous study

which used the La Coste Model G No. 572 gravimeter, while the Landsat 8 imagery for the area was used for the satellite approach.

Gravity methods can usually only detect lateral changes in density between sediment and basement because the difference in density between two sedimentary layers is not sufficient. Using a truncated horizontal-plate model, the lineaments from the gravity data were highlighted by several steps, including locating density boundaries from the gravity data, estimating horizontal gradients, identifying the lineaments, connecting the lineaments to form faults, and producing the lineament maps.

The resulting lineament density maps are shown in Figure 2.26, with a) showing the lineament density map generated from the gravity data and b) showing lineament density derived from remotely sensed data. The lineament density map derived from the remotely sensed data was similar to that taken from the gravity data, although the former showed greater lineament density in the southwest. Lineament intersections on the maps (likely fracture zones) show areas where there is increased groundwater potential, with orientation giving insight into groundwater flow direction. The study found that satellite-derived lineaments are useful in aiding geophysical exploration (Epuh *et al.*, 2020).

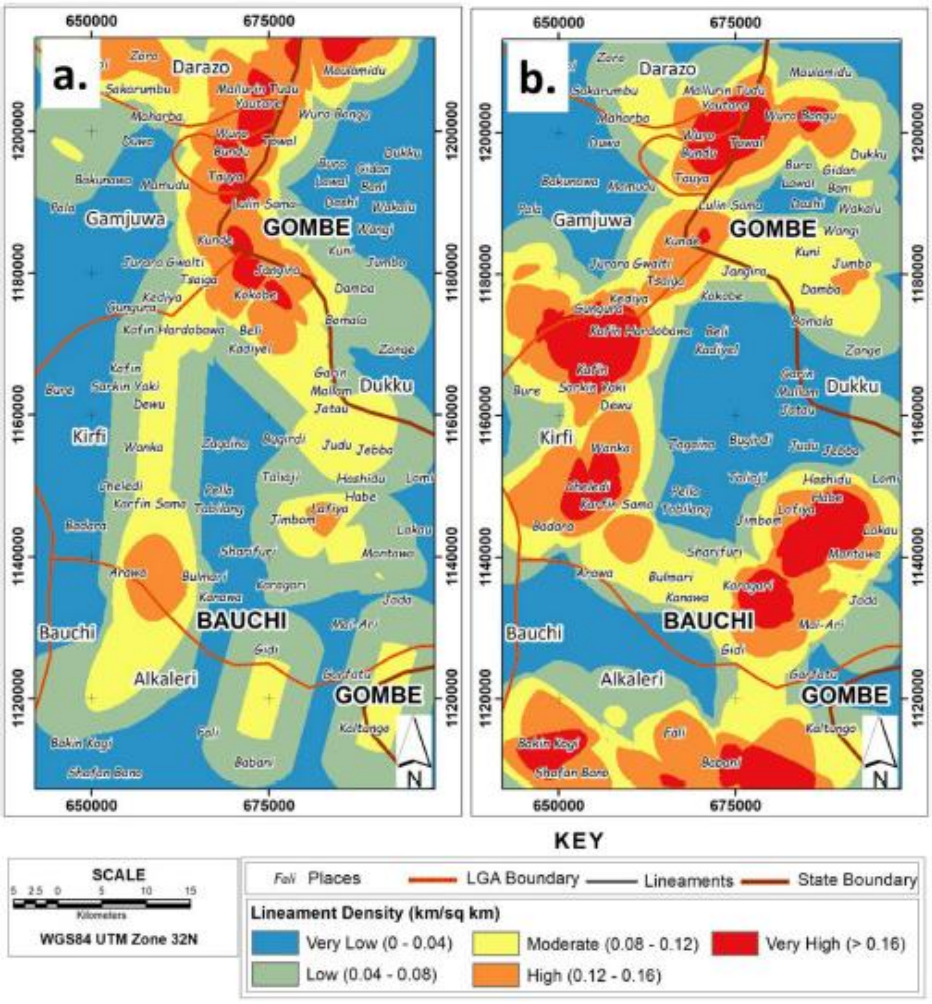

Figure 2.26: Lineaments density maps: a) gravity b) Landsat (Epuh *et al.*, 2020).

2.4.2 Groundwater exploration using seismic methods

2.4.2.1 Case study 1: Selangor and Pahang, Malaysia

Seismic refraction and 2D resistivity imaging were conducted in Kalumpang, Hulu Selangor and Simpai Pahang, Malaysia, to characterise the subsurface and determine groundwater location (Musa *et al.*, 2017). The study area has a Quaternary alluvial sediment cover consisting of clays and sands, with a basement of metasedimentary rocks in Kalumpang and conglomerates, shales and sandstones in Simpai. Three resistivity surveys were conducted in the area, with seismic refraction conducted along the same lines.

The ABEM Lund Imaging System was used to conduct the resistivity survey with the electrodes arranged in the Pole-Dipole array. Four imaging cables were used, with outer cables having an electrode spacing of 10 m and inner cables having a 5 m spacing. The acquired apparent resistivity data were inverted in the Res2DInv software to model the subsurface resistivity. Figure 2.27 shows the modelled resistivity for one of the lines at Simpai. It shows a low conductivity layer overlying an entity of low resistivity at a depth of about 20 m, which, according to Musa *et al.* (2017), might be a possible fault.

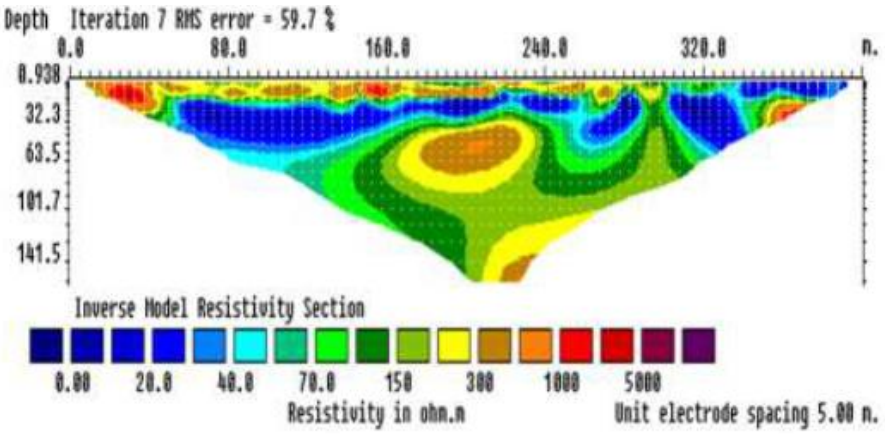

Figure 2.27: Simpai, Pahang resistivity section (Musa *et al.*, 2017).

The seismic data were acquired using the 24-channel ABEM terraloc MK8 seismograph. A 40 kg weight drop (P-wave energy source) propagated the seismic waves through the ground while striking a steel plate. There were 24 geophones with an interspacing of 5 m, and the entire spread covered 115 m, which allowed for an investigation depth of about 10 m. Field data were processed using the Ixseg2segy (a filter), Firstpicks and Gremix15 (to pick first arrivals) software packages (Musa *et al.*, 2017). The seismic refraction survey was able to resolve three separate velocity layers (V1, V2, and V3), which correspond with alluvial material, the weathered zone and the bedrock.

Figure 2.28 shows the depth-velocity and depth sections at Simpai. A sudden increase in velocity for the third layer to 3000-6000 m/s from 1600-3000 m/s indicates an increase in saturation and is seen

in the depth profile. This implies the presence of a fracture. This result was in agreement with the resistivity result.

The resistivity and seismic methods successfully provided reliable data for borehole siting. It was noted that saturated layer velocities need to be significantly higher than the overlying layer velocities for the seismic refraction to successfully determine the depth to the water table. The study was also able to show that the accuracy of depth determinations from resistivity is significantly improved when used in conjunction with seismic methods (Musa *et al.*,2017).

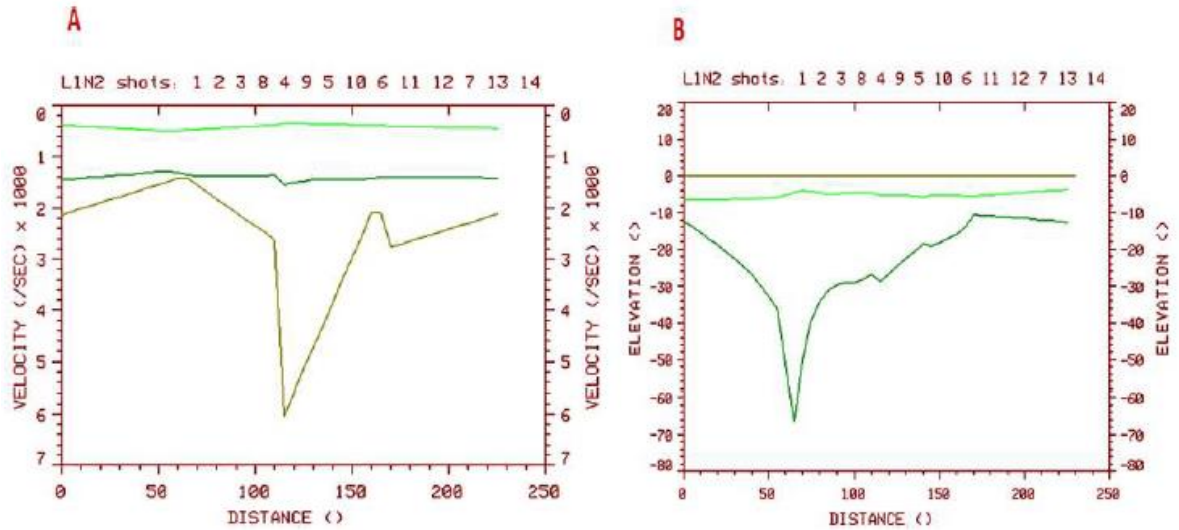

Figure 2.28: Simpai, Pahang A) Depth-velocity B) Depth section (Musa *et al.*, 2017)

2.4.2.2 Case study 2: Łódź Trough, Poland

Maćkowski *et al.* (2019) conducted a study in Poland using archival seismic reflection data to determine geothermal aquifer geometry, geological structures and recharge zones of the geothermal reservoir. The Łódź Trough is a graben located in the central part of the Polish Lowlands. Lithologies that are encountered include gaizes, limestones, sandstones, claystones, and mudstones (Maćkowski *et al.*, 2019).

The seismic survey data used were collected from the 1970s to 1990s (Maćkowski *et al.*, 2019). The oldest data were recorded with 24-channel end-on spread with seismic waves generated by dynamite explosions with shot spacing of 100 m and 50 m geophone spacing. Later projects increased the channels to 48 and reduced shot spacing to 50 m. In the 1990s, 240 channels were used with a split spread and regular grid of profiles. Shot spacing was 50 m, geophone spacing 25 m and the fold was 60. The seismic data were generated using vibrators with a frequency of 8-80 Hz (Maćkowski *et al.*, 2019). The newer data had better resolution and better imaging quality than that of the 1970s, which had a high signal to noise ratio due to low noise and poor processing methods.

The old seismic data were reprocessed to improve resolution and geological interpretation conducted. The stratigraphic identification of the seismic reflection data in time sections was based on interpretations of stratigraphy from well logs, checkshot data and synthetic seismograms that were correlated at the borehole site. Figure 2.29 shows the correlation between the synthetic seismogram and the true seismic section. Codes refer to different seismic horizons that can be identified based on the local geology. Time depth conversion of the seismic data was later conducted.

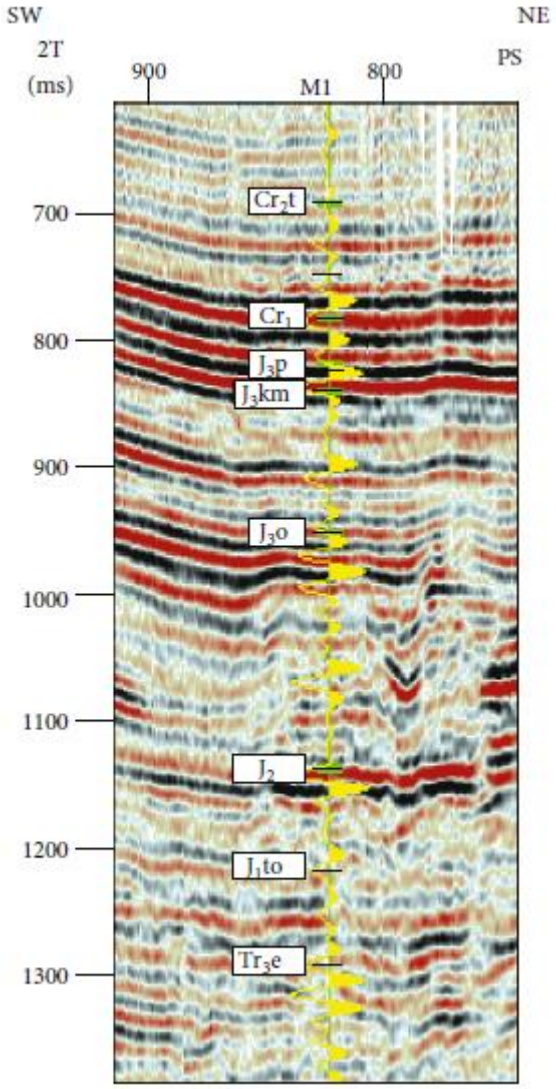

Figure 2.29: Synthetic seismogram (yellow trace) correlated with true seismic section (black and red) for a borehole (M1) (Maćkowski *et al.*, 2019).

The result of the structural interpretation of the seismic depth section is presented in Figure 2.30, where F2, Z1 and M1 are wells with the extent up to the red line. The study revealed the precise graben geometry and the presence of structures such as faults that may influence the recharge and quality of the geothermal reservoir.

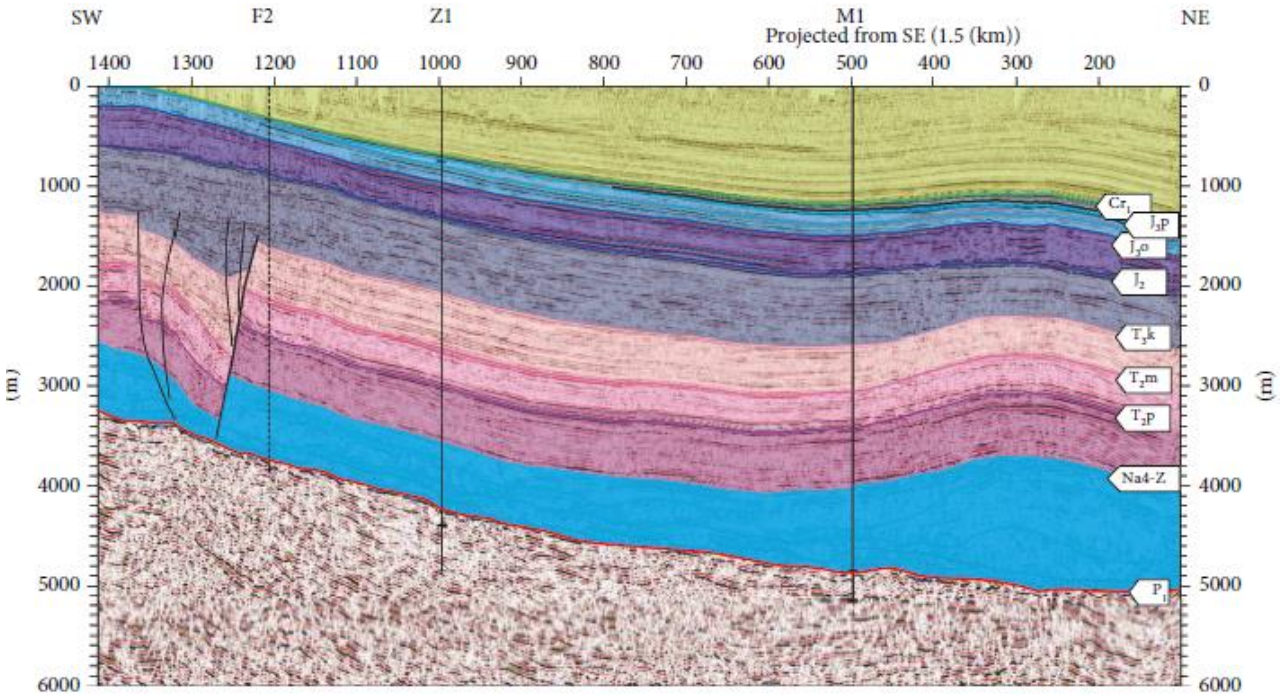

Figure 2.30: Result of structural interpretation of seismic data in the vicinity of wells Modified from Maćkowski *et al.* (2019).

2.4.3 Groundwater exploration using resistivity methods

2.4.3.1 Case study 1: Ndokwa, Delta State, Nigeria

In Ndokwa, Delta State, Nigeria, spontaneous potential (SP) borehole logging and vertical electrical sounding (VES) were undertaken to assess the geology as well as the condition of the groundwater to identify structures and formations suitable for groundwater development (Anomohanran *et al.*, 2017). SP borehole logging is used to determine chemical contrasts between adjacent rocks and the formation water (Anomohanran *et al*., 2017). Figure 2.31 shows the study area with the VES survey points indicated. The site is underlain primarily by sand with approximately 5% clay. The package is overlain by Quaternary deposits comprising mainly coastal plain sands and deltaic plain deposits overlain by coastal alluvium and freshwater swamp. The sandy zone is the main water-bearing formation in the area (Anomohanran *et al*., 2017).

A well was drilled, and a lithological log taken from the rock cuttings. An SP and resistivity log was conducted to obtain information on the lithology, total dissolved solids (TDS) and electrical conductivity of the water in the formation, with the probe used connected to a Terrameter. For the VES, measurements were taken at 30 sounding centres using the Schlumberger configuration. Interpretation of the sounding data revealed the aquifer makeup (Anomohanran *et al*., 2017). The ABEM Terammeter SAS 1000/4000 was used with current electrode spacing kept between 100 m and 150 m (Anomohanran *et al*., 2017). The apparent resistivity from VES was plotted against half the electrode spacing, an example of which is shown in Figure 2.32. Four geoelectric layers could be

discerned for the sounding, which held true for the other soundings conducted in the area. Thickness and resistivity values from curve matching were input into the WIN Resist software to compute the thickness and true resistivity of the layers and to create a geoelectric section for the area (Anomohanran *et al*., 2017). A generalised geoelectric section for the entire area is shown in Figure 2.32.

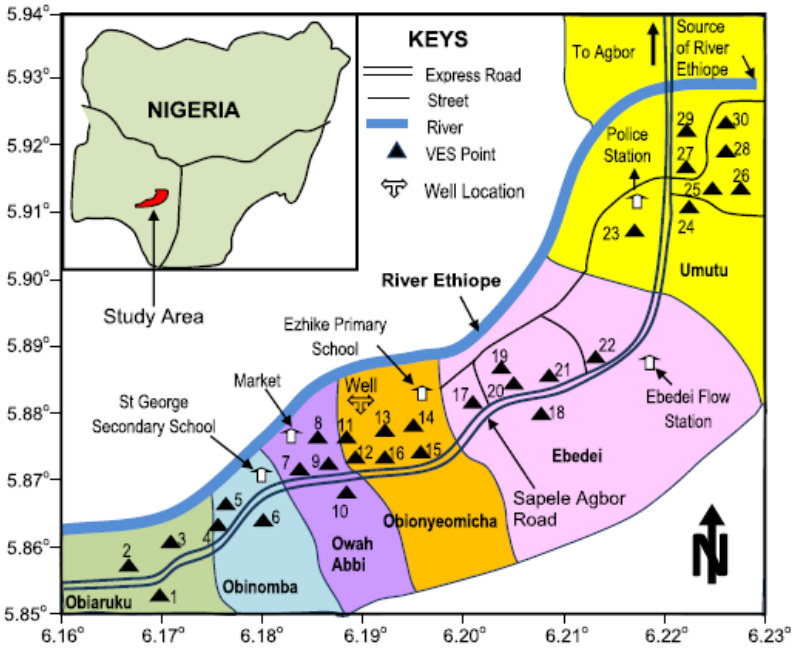

Figure 2.31: Map of the study area in Ndokwa, Nigeria (Anomohanran *et al*., 2017)

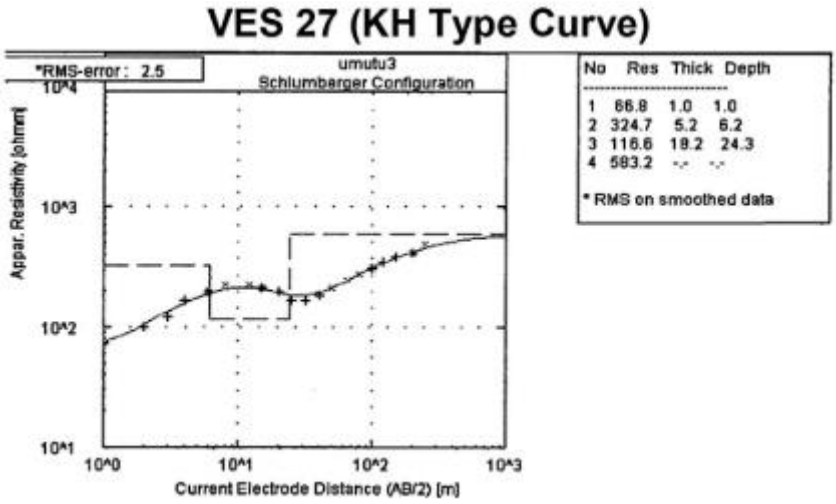

Figure 2.32: Example of VES curve from Umutu (Anomohanran *et al*., 2017)

The lithology, revealed from drill cuttings, showed that the topmost layer was lateritic soil underlain by sand and clay, while the aquifer in the region was found to be the fourth layer with a depth of 17.8-38.8 m across the area (Figure 2.33) (Anomohanran *et al*., 2017). The results from both the SP log

and VES agreed with the lithological log obtained from the rock cuttings, showing the reliability of geophysical techniques (Anomohanran *et al*., 2017).

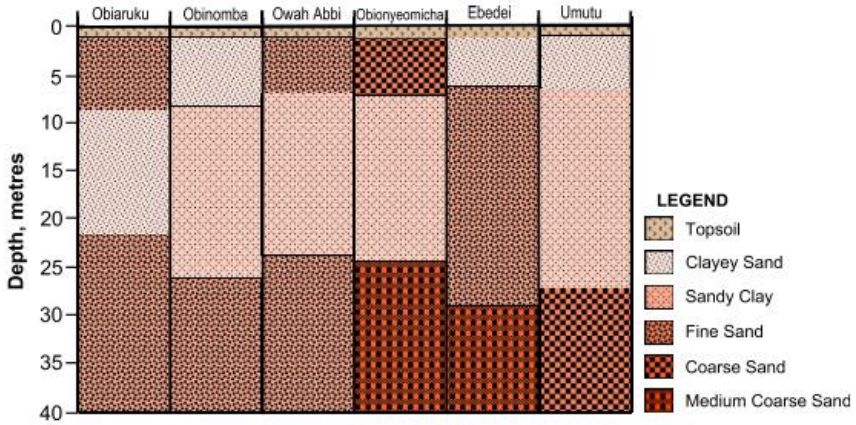

Figure 2.33: Generalised lithological overview of the study area (Anomohanran *et al.*, 2017)

2.4.3.2 Case study 2: Kanthan, Perak, Malaysia

A study was conducted in a cement quarry in Gunung Kanthan Chemor Perak, Malaysia (Lee *et al*., 2021). The site is underlain by limestone bedrock, which is subject to fracturing, faulting, and folding (Lee *et al*., 2021). Using a single geophysical method in a hard rock environment can lead to partial information on the subsurface, so an integrated approach was used (Lee *et al*., 2021). A variety of different arrays are available for 2D ERT surveys, with a single array often being used for a project (Lee *et al*., 2021). However, each array has its advantages and disadvantages, and ambiguities can be encountered in results obtained for different arrays used in a single area.

Recognising that the 2D ERT has low to moderate resolution, Lee *et al*. (2021) aimed to improve the resolution issue of this method by using data levels synthesisation (DLS) to merge different arrays for a high-resolution image (Lee *et al*., 2021). The DLS method combines data levels from two different optimised arrays to create a single resistivity image to attain high-resolution 2D ERT and address uncertainties in individual ERT results interpretation (Lee *et al*., 2021). Other aims of the project were to explore potential hard rock aquifers in Kanthan and to prove that DLS is effective in improving the resolution of the 2D ERT.

A simple fault and cavity model (Figure 2.34) with fixed dimensions was created using RES2MOD software. Then, apparent resistivity data were input into the RESDINV program to create an inversed model for the Wenner-Schlumberger (W-S), dipole-dipole (D-D), and pole-dipole (P-D) arrays (Lee *et al*., 2021). The W-S array inverse model (Figure 2.35a) reflected the shape of the initial theoretical model well but distorted the dimensions and shifted the position of the fault in the model. The D-D array (Figure 2.35b), on the other hand, showed the vertical fault and boundary accurately, but boundary sizes were not equal. In contrast, the P-D array (Figure 2.35c) showed the cavity well but

failed to show the position of the fault clearly. The different arrays were combined using DLS to find the combination with the best resolution in the vertical and horizontal direction, which was the W-S array + D-D array (Lee *et al*., 2021). The study found that these arrays enhance the anomaly's shape, horizontal location, and depth (Lee *et al*., 2021). This was then applied practically by conducting a ground geophysical survey with targets chosen from lineaments mapped from satellite imagery. Each array was executed one after the other along the same profile to give two sets of the 2D ERT data which were synthesised at a later stage (Lee *et al*., 2021). The ERT survey was performed along two lines with the ABEM Lund Imaging System.

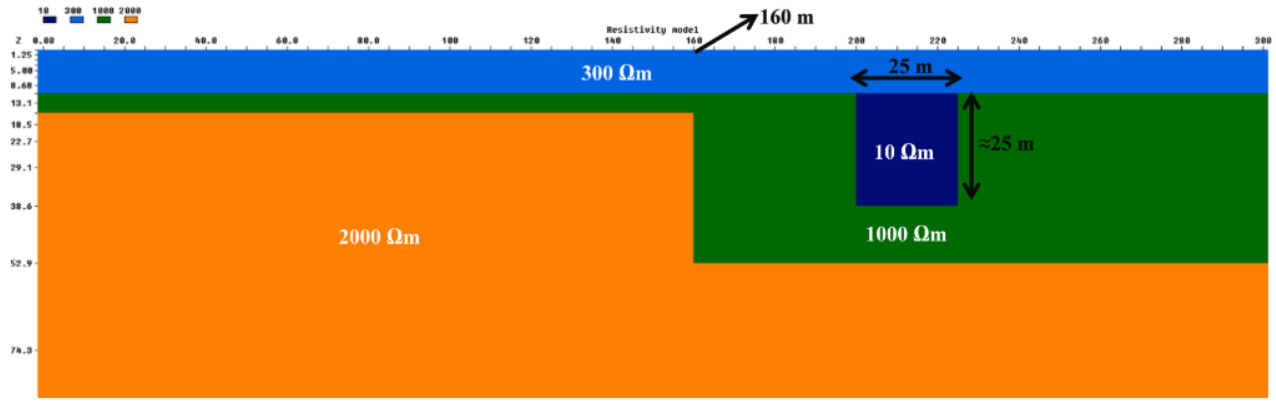

Figure 2.34: Simple cavity and fault model (Lee *et al*., 2021)

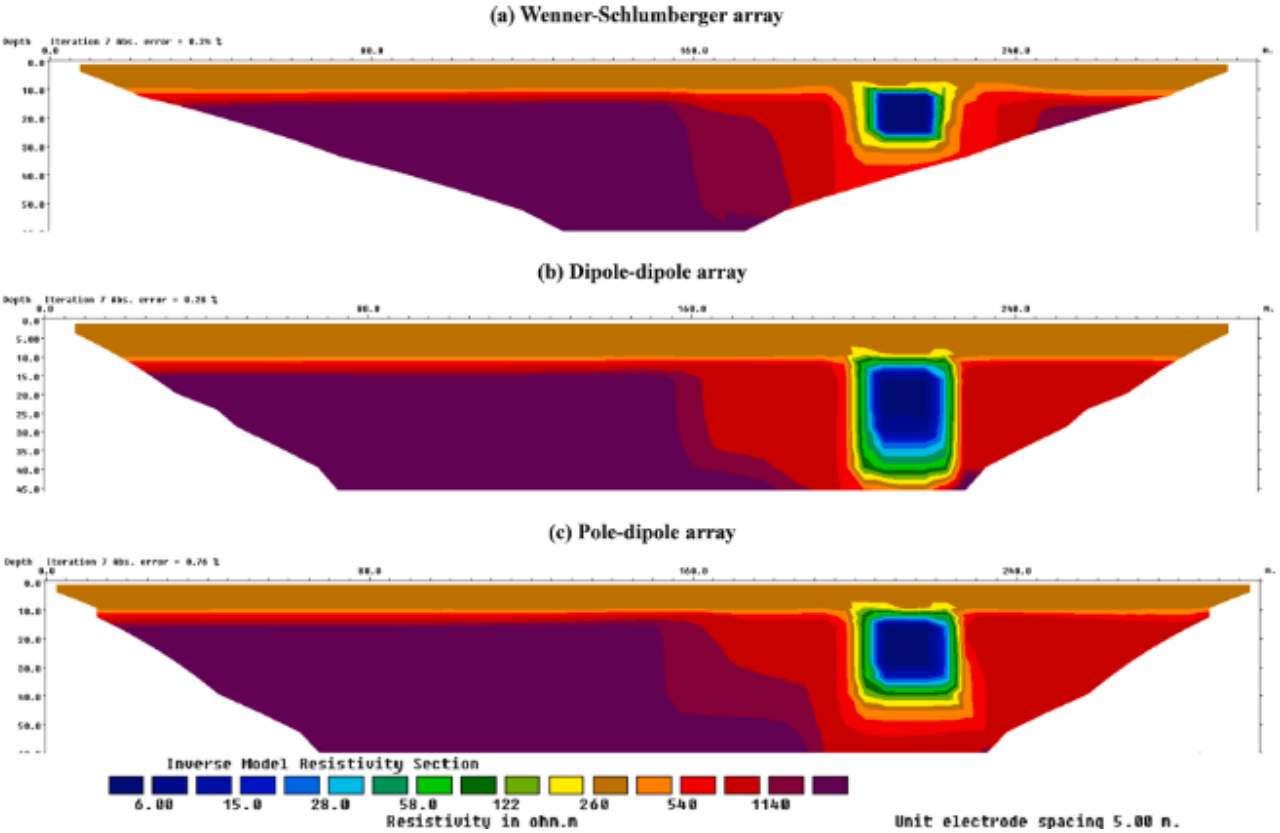

Figure 2.35: Simple cavity and fault inversion model for a)Wenner-Schlumberger b) Dipole-dipole, and c) Pole-dipole arays (Lee *et al*., 2021)

To supplement the ERT surveys, seismic refraction was undertaken on the same traverses to further understand the layering and depth of the various rock units and delineate the rock interfaces of the study area (Lee *et al*., 2021). The seismic survey used an ABEM Terraloc MK-8 seismograph (Lee *et al*., 2021). The results of the surveys were interpreted, and water wells were drilled at sites that corresponded with significant discontinuities in the ERT and seismic surveys (Lee *et al*., 2021).

Figure 2.36 shows the result of the DLS of one of the 2D ERT surveys with the seismic depth profile, the positions of discontinuities, and a drilling log indicated. The discontinuities were prominent vertical boundaries between the high resistivity zones and a decrease in p-waves velocity corresponding to locations of highly fractured rock. These were interpreted as shear and fracture zones. The borehole was drilled in the identified fracture zones and had a blow yield of 1000 L/s (Lee *et al*., 2021). The drilling logs were then used to verify the seismic and ERT results (Lee *et al*., 2021). The study showed that although the DLS method is time-consuming, it successfully decreased ambiguity in ERT data interpretation and aided in locating areas with high groundwater potential (Lee *et al.*, 2021).

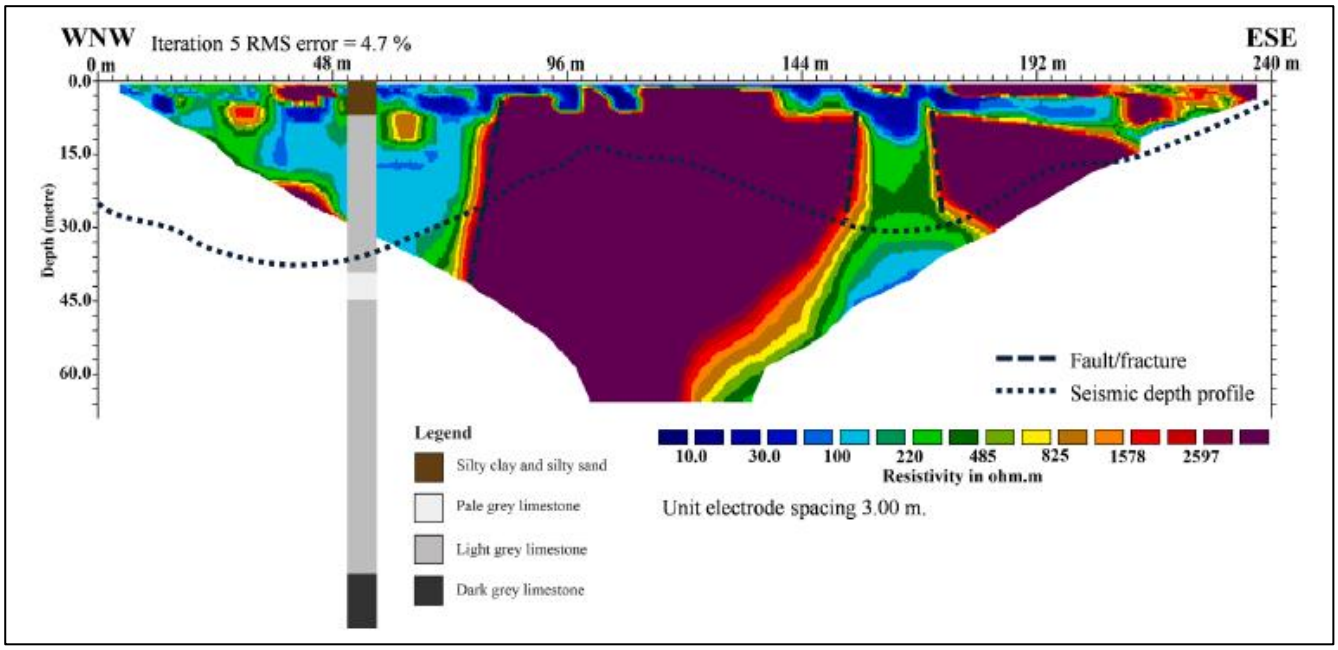

Figure 2.36: Integration of a drilling log with a seismic refraction depth profile and an ERT image created using the DLS method (Lee *et al*. 2021)

2.4.4 Groundwater exploration using electromagnetic methods

2.4.4.1 Case study 1: South Sinai, Egypt

In the arid South Sinai province in Egypt, Basheer and Alezabawy (2020) conducted a study to find the distribution and the quality of groundwater in an area known as Wadi (valley) Barqa (Basheer and Alezabawy, 2020). The steps followed in the study are summarised in Figure 2.37. They created a Digital Elevation Model (DEM) of the study area to delineate areas conducive for infiltration,

followed by geophysical investigations using the Time Domain (transient) Electromagnetic sounding (TDEM) and VES (Basheer and Alezabawy, 2020)

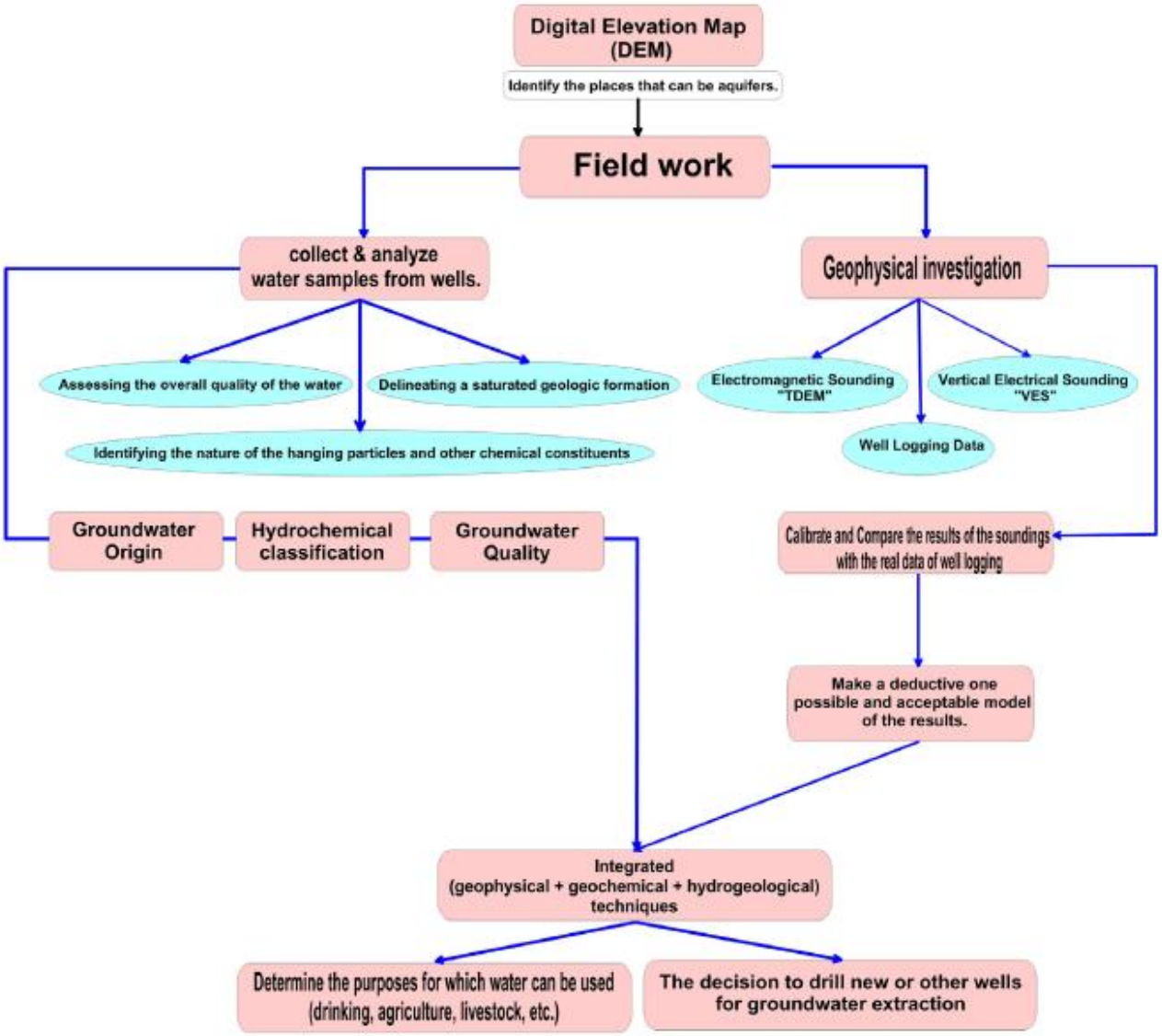

Figure 2.37: Steps carried out in the investigation of the study area (Basheer and Alezabawy, 2020).

The survey lines were placed close to known drilled wells so that an acceptable model of the results could be made (Basheer and Alezabawy, 2020), noting that the aquifer in the area of study is a Nubian sandstone aquifer (Basheer and Alezabawy, 2020). The VES was conducted in the Schlumberger array with AB/2 between 1-1000m. The data were collected by the direct current resistivity meter known as the Sycal Pro instrument 1996. Twenty-one VESs were conducted (Basheer and Alezabawy, 2020). The TEM survey was conducted with the AIE-2 TDEM 2004 instrument, which has a copper cable loop with dimensions of 50×50 m. The device has both the transmitter and receiver in the same unit. The current was switched on for 0.23–0.37 msec (Basheer and Alezabawy, 2020). Measurements were repeated at each station so that the best result was chosen for the TEM

measurements. 21 TEM stations in locations similar to those of the VES were used (Basheer and Alezabawy, 2020).

VES results were analysed using Zohdy (1989), whose results were used as input to the IPI2Win Program version 3.0.1 (2003). The ZONDTEM1D 2016 was used to analyse and interpret the TEM data (Basheer and Alezabawy, 2020). Eleven groundwater samples were analysed for their geochemical makeup. Figure 2.38 shows the 1D model inversion example for a single VES station, TEM station, lithological design for a single well and well logging chart (resistivity and gamma rays).

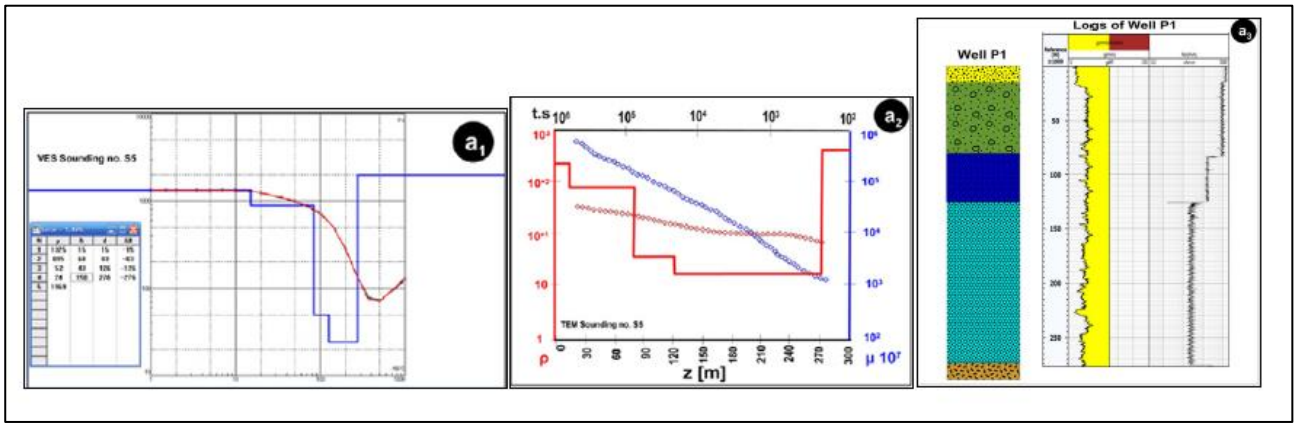

Figure 2.38: a_1) 1D inversion model of a single VES station, a_2) 1D inversion model of a TEM station and a_3) well logging charts and lithological design of a single well. Modified from (Basheer and Alezabawy, 2020).

The geoelectrical parameters obtained from the survey found that the study area consists of five distinct geoelectrical layers, which were in line with well logs (Figure 2.38) (Basheer and Alezabawy, 2020). Two aquifers were identified in the region, which were both Nubian sandstone aquifers. Their study recommended that DEM be performed before geophysics is conducted, followed by electrical resistivity imaging and TEM soundings before drilling boreholes in the valley lowlands (Basheer and Alezabawy, 2020).

2.4.4.2 Case study 2: San Diego, USA

In semi-arid San Diego, United States of America, a study was conducted to identify fresh submarine groundwater in the offshore section of the coastal San Diego Formation (SDF) aquifer (King *et al.*, 2022). The study aimed to characterise and map pore fluids within the offshore aquifer using controlled-source electromagnetic methods (CSEM) to improve understanding of the onshore part of the aquifer. The SDF aquifer is heavily faulted and may lock pockets of freshwater offshore. The electromagnetic system used in the study is illustrated in Figure 2.39. It consists of a transmitter that generates an electric dipole, four receivers called porpoises and a dorsal device that collects water conductivity and water depth data. These are towed on the water by a rope. The receiver spacing was 100 m, and the maximum source-receiver spacing 400 m (King *et al.*, 2022)..

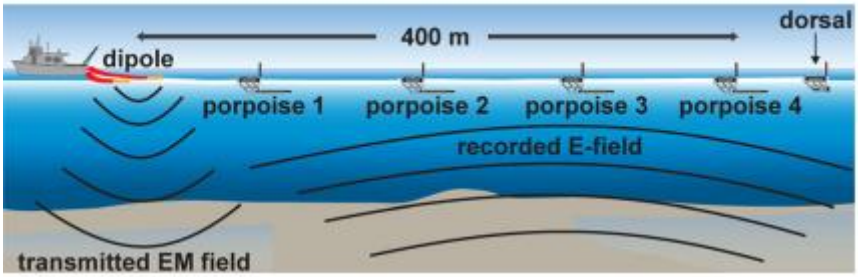

Figure 2.39: Illustration of the CSEM array used in the San Diego survey (King *et al.*, 2022).

Amplitude and phases of the CSEM response functions were extracted from the raw time series data. The modelling software used in the study was the 2D MARE2DEM, and the data were manually examined for any obvious outliers before being included in the inversion. Sea water was also made a fixed parameter in the starting models using data collected from the dorsal device. The results of the survey revealed that at depths of 50-80 m, some resistive anomalies are separated by down-dropped blocks of the Silver Strand fault zone, as shown in Figure 2.40. The anomalies with resistivity > 10 Ωm (indicated by warm colours in Figure 2.40) correspond with fresh to slightly saline pore fluids. U-shaped features (paleochannels), referred to as EPC and WPC, are related to parts of the SDF which are conductive (King *et al.*, 2022).

The CSEM was able to identify areas within the SDF submarine aquifer with substantial volumes of fresh-slightly saline pore fluids. King *et al.*, (2022) showed that CSEM methods have the potential of mapping the extent of coastal aquifers in diverse geological settings.

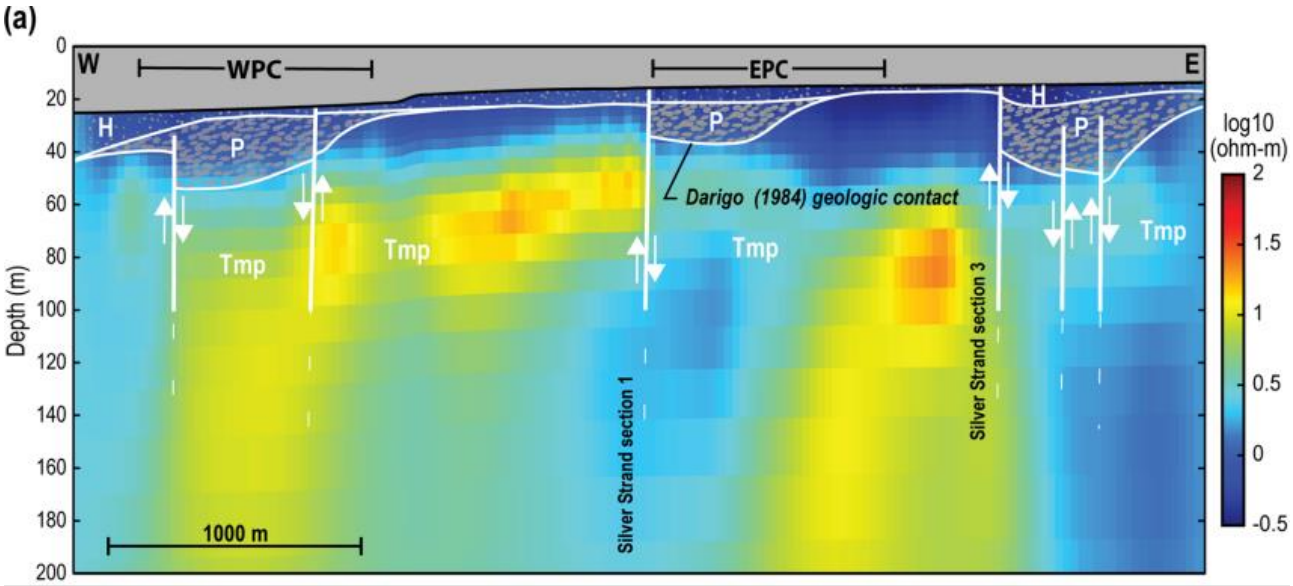

Figure 2.40: Plot of 2D vertical resistivity data from one line of data from the third receiver in the array. White labels refer to different lithologies of the SDF. Modified from (King *et al.*, 2022).

2.4.5 Groundwater exploration using magnetic methods

2.4.5.1 Case study 1: Perambalur, India

Muthamilselvan (2021) conducted a study in the Perambalur district of Tamil Nadu, India, to explore groundwater potential and identify suitable locations for open wells and boreholes on the site. The site is covered by alluvium and underlain by weathered granites and fresh granite. The magnetic method was chosen for the study, with the magnetic survey undertaken using a proton precession magnetometer. Eighty-four data recordings were done from six 140 m long traverses, with line separation of 20 m while station spacing was 10 m (Muthamilselvan, 2021). The magnetic data were processed, and the total magnetic intensity (TMI) maps, the analytical signal (AS) and reduction to the equator (RTE) were prepared.

A directional cosine filter (DCF) was then applied to the TMI map to enhance structural elements. Structures such as faults and fractures, which trend primarily NW-SE, were identified in the TMI and RTE maps and could be seen in the AS and DCF maps. The regional and residual anomaly maps were also generated using Gaussian regional/residual filters. Figure 2.41-Figure 2.43 show the various maps with the magnetic breaks (black dashed lines), which were interpreted as faults and fractures shown (Muthamilselvan, 2021).

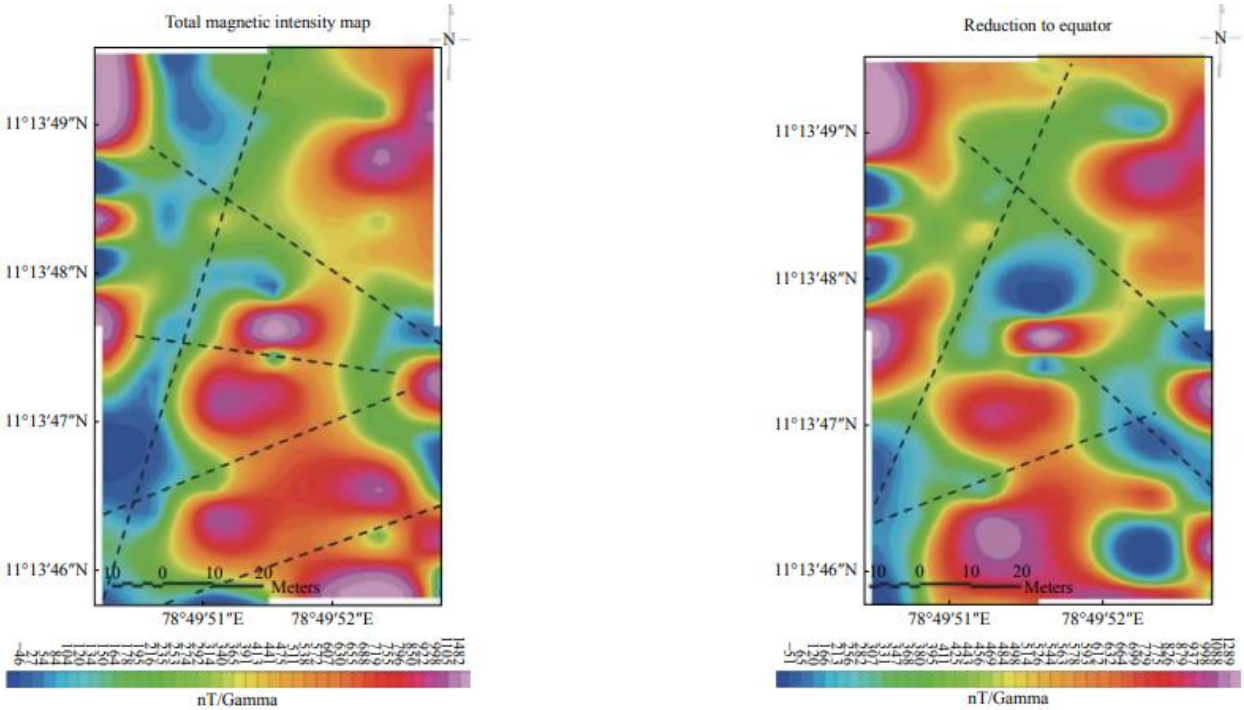

Figure 2.41: TMI (left) RTE (right), magnetic breaks (Muthamilselvan, 2021).

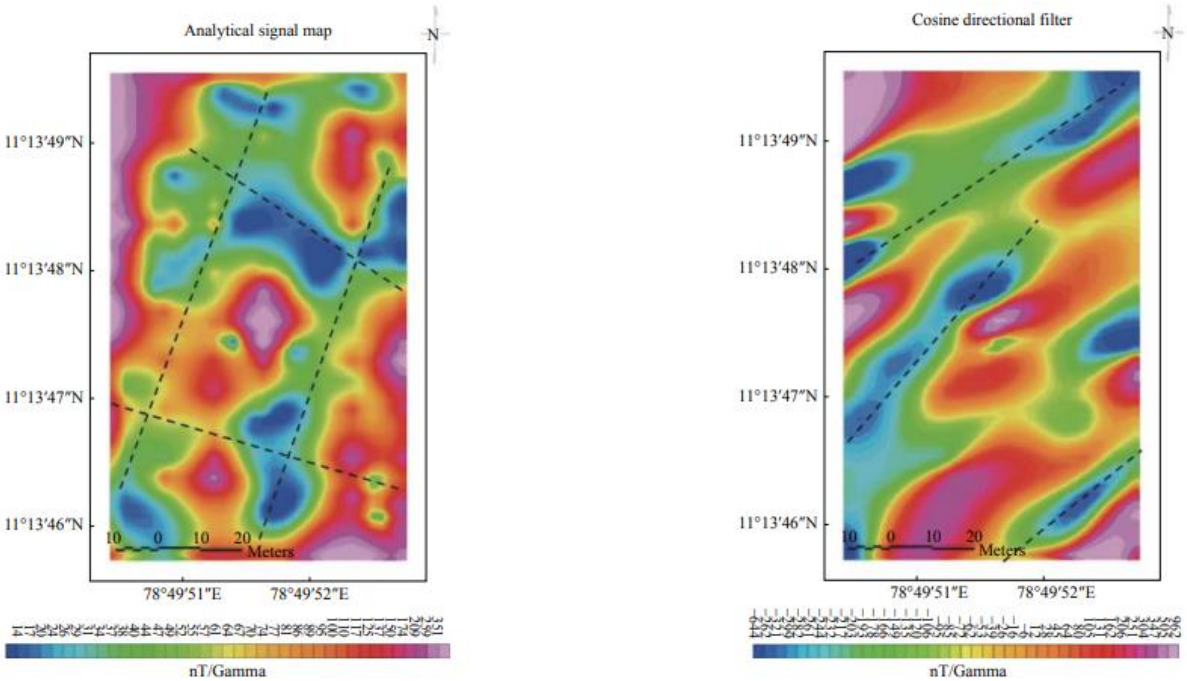

Figure 2.42: AS (left), DCF (right) magnetic breaks (Muthamilselvan, 2021).

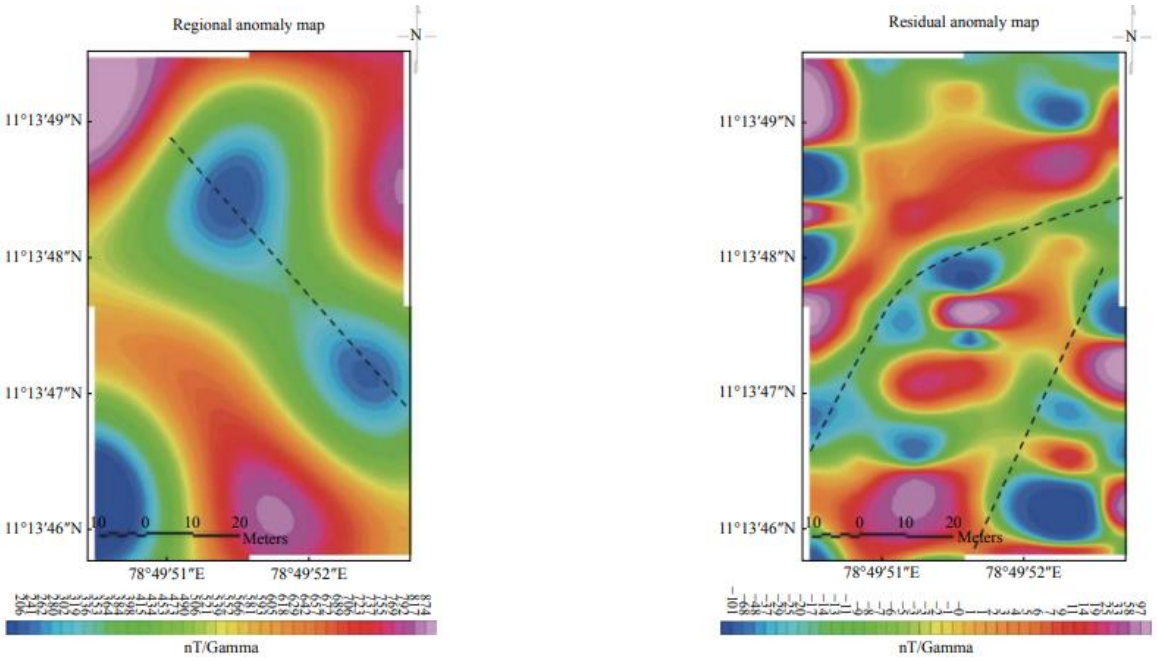

Figure 2.43: Regional anomaly (left), Residual anomaly (right) (Muthamilselvan, 2021).

Muthamilselvan (2021) also individually studied the magnetic profile lines, which gave insight into an observed structurally weak zone in all the lines. Finally, a radially averaged power spectrum allowed for the residual and regional depth to be estimated, while the Euler deconvolution method helped estimate the basement depth and structural deformations. The result of the study was an understanding of the subsurface structure and selection of suitable borehole sites, which were areas of interpreted fracture zones.

2.4.5.2 Case study 2: South Guangdong, China

Hasan *et al.* (2021) conducted a study in Dakengou, South Guangdong, China, to exploit the groundwater resources in that hard rock terrain. Acidic volcanic rocks are dominant throughout the study area, with occurrences of magmatic and granitic rocks. The province is located within a fold system, and faults are encountered. Generally, the subsurface lithology can be divided into the upper topsoil cover, highly weathered rock, partly weathered rock and unweathered basement (Hasan *et al.*, 2021). A joint geophysical prospecting approach was employed in the study, which used ERT, magnetic, and a joint profile method (JPM). Figure 2.44 shows the profile lines for the ERT, magnetic and JPM surveys, with borehole and pump test locations indicated.

The JPM survey acquired joint measurements of spontaneous potential (SP), electrical resistivity (ER), and induced polarisation (IP). IP measures chargeability, which is dependent on grain size, mineral type, electrolyte properties in pore space, contact between fluid and surface, and the internal surface to volume ratio. IP, in conjunction with ERT, can, therefore, differentiate between water content and clay. The JPM measurements were taken in the pole-dipole array using a multifunctional electric device called the WDJD-4 from the Chongqing Pentium Research Center, China. There were two traverses 390 m long, with 40 electrodes and a spacing of 10 m (Hasan *et al.*, 2021). The depths of investigation were 90 m and 180 m (Hasan *et al.*, 2021). Four ERT profiles were performed using the ABEM Lund Imaging System with a multi-electrode acquisition system of 56 electrodes. The pole-dipole array was used with a constant electrode separation of 5 m. The MAP60 (Garmin, USA) GPS devices were used to obtain electrode positions. RES2DINV was used to invert the apparent resistivity data.

Two proton precession magnetometers (Geometrics 856) with a 0.1 nT accuracy and a sampling rate of 3 s were used during the survey. One magnetometer was the base station, and the other measured total magnetic susceptibility. Diurnal corrections were made after one minute. There were 79 magnetic stations with a 5 m station spacing and profile length of 390 m. The magnetic anomaly was also modelled along the profile to acquire more information. 2D forward modelling of the magnetic data was conducted using the IX2D software to elucidate information on the subsurface weathered or fractured zones for groundwater investigation (Hasan *et al.*, 2021). A contour map of the total magnetic anomaly is shown in Figure 2.45. Magnetic intensity varies from -48-12 nT along the surveyed area. Areas with high magnetic intensity correspond with unweathered bedrock, while low magnetic intensities are areas with weathered and fractured rock. To delineate the discrete subsurface units forward modelling of the magnetic data was conducted.

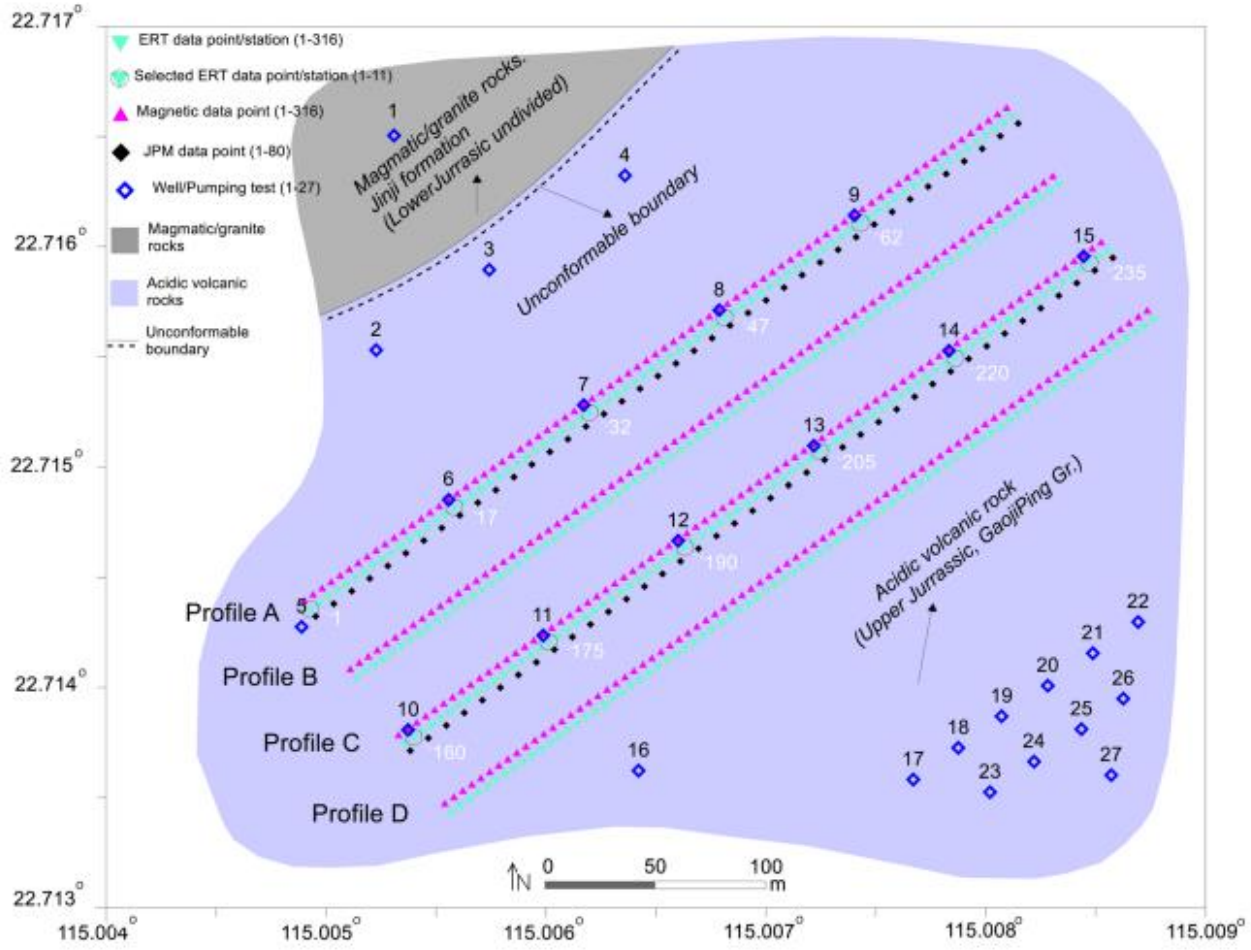

Figure 2.44: Locations of the geophysical surveys and boreholes at the South Guangdong site (Hasan *et al.*, 2021).

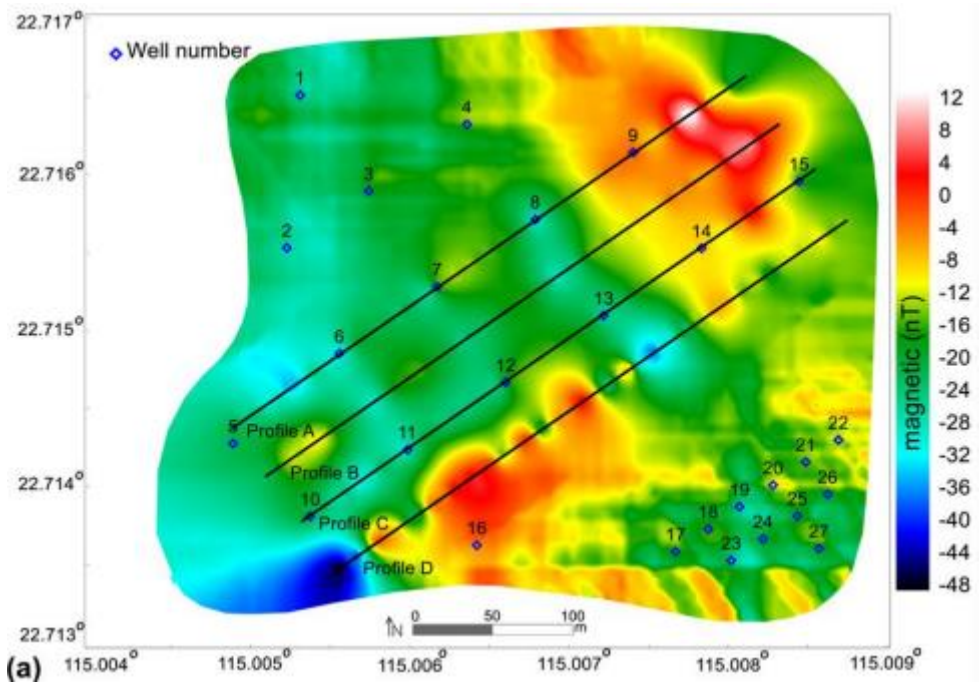

Figure 2.45: Contour map of total magnetic anomaly in the study area. Modified from (Hasan *et al.*, 2021).

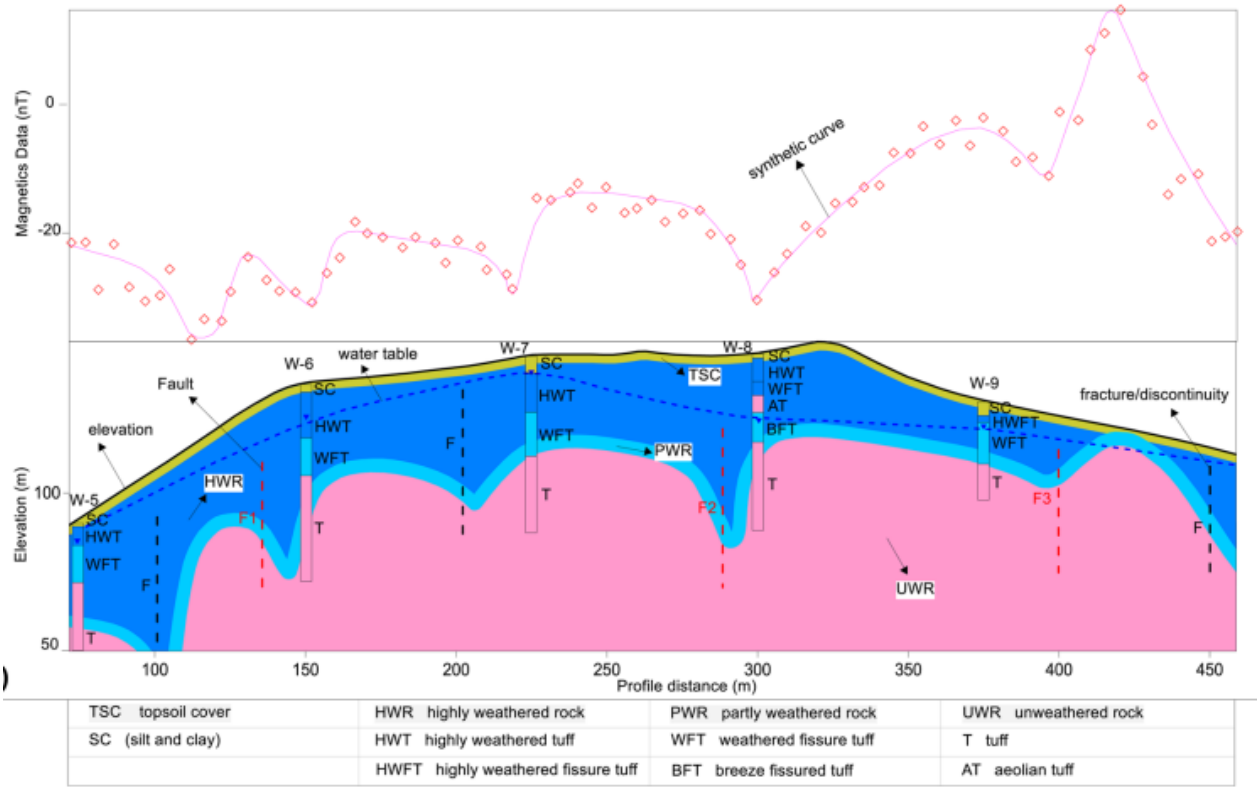

Figure 2.46: Interpreted 2D magnetic model along profile A (modified from (Hasan *et al.*, 2021).

An interpreted 2D magnetic model along profile A is presented in Figure 2.46. The joint ERT and magnetic data were able to reveal three faults in the area to a depth of about 50 m, while the JPM profiles traced the faults to depths of 90 and 180 m (Hasan *et al.*, 2021). Borehole data also informed the construction of the models made in the study. Physiochemical and XRD analyses were also conducted in conjunction with the geophysics. The joint prospecting removed ambiguity in the interpretation of the various data and gave a more detailed view of the subsurface geology. According to Hasan *et al.* (2021), this approach can assess any hard rock site with 90% confidence.

2.4.6 Groundwater exploration using magnetotelluric methods

2.4.6.1 Case study 1: El Sheikh Marzouq area, Farafra oasis, Egypt

In El Sheikh Marzouq, Farafra Oasis, Egypt, integrated geophysical methods were used for groundwater exploration as part of a government development project (Abdel Zaher *et al.*, 2021). Various geophysical methods were employed to deduce the shape, depth, and structure of aquifers in this area dominated by sandstone. These methods were audio magnetotelluric (AMT), control source magnetotelluric (CSAMT), very low frequency (VLF), TEM and VES methods (Abdel Zaher *et al.*, 2021).

All the measurements were conducted along the same profile lines (with the exception of VLF) to correlate the different measurements taken, and the survey locations are shown in Figure 2.47 (Abdel

Zaher *et al*., 2021). The VES were undertaken at nine points in the Schlumberger array using the Sycal R2 resistivity meter, and 1D models were applied to the resistivity data using IPI2Win software (Abdel Zaher *et al*., 2021). TEM measurements were taken at the same location as the VES at different time windows. TEM measurements were made using the SIROTEM-MK3 conductivity meter (transmitter and receiver are in the same loop), and the data were processed and modelled with the TEMIX XL V4 and ZONDTEM1D programs (Abdel Zaher *et al*., 2021). An example of the modelled result for the VES and TEM is shown in Figure 2.47.

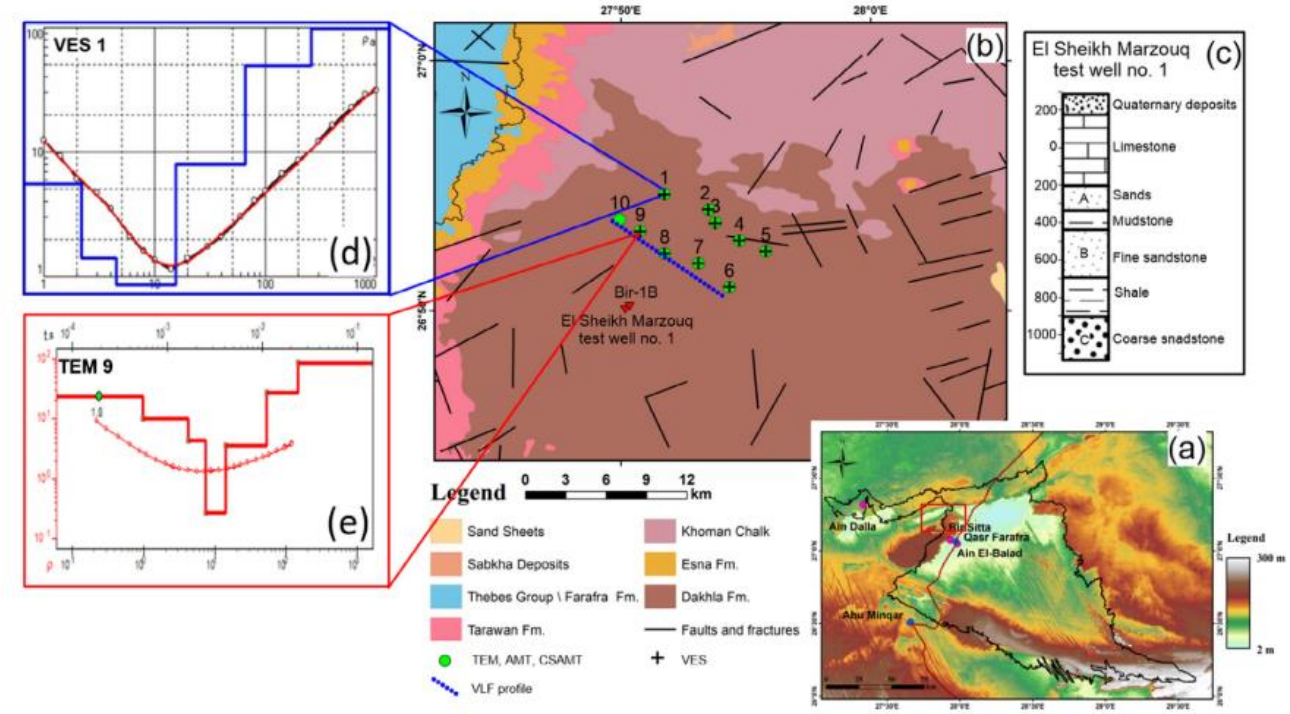

Figure 2.47: a) DEM of Farafra Oasis b) geological map of the study area c) Stratigraphy of test well 1 d) observed and modelled VES data at different apparent resistivities for site 01 e) TEM resistivity curve and modelled results for site 09 (Abdel Zaher *et al*., 2021).

The MT survey was conducted using the Stratagem instrument, with data for the 10 AMT and CSAMT sites covering a period of 0.00001 s to 1 s (Abdel Zaher *et al*., 2021). Low-frequency magnetotelluric waves were measured using AMT only (0.1 Hz-1 kHz), and then the same measurement was repeated using the CSAMT. For the CSAMT, a grounded dipole transmitter creates an unpolarised electromagnetic field as a source (1-70 kHz). The data sets of CSMAT and AMT were then collated into a single set (Abdel Zaher *et al*., 2021). A dimensionality analysis was conducted on the MT data, which was 2D inverted. The final 2D models for profiles 1 and 2 are shown in Figure 2.48. These reach a depth of 1000 m and show that most of the investigated area is underlain by conductive media with restivities of 1-100 Ωm. Shallower parts have low resistivities < 10 Ωm. Faults can be seen in the MT inversion models with the letters A (shallow zone), B (middle zone, 400 m to

700 m), and C (deep zone, 900 m) referring to identified aquifer zones in the Nubian sandstone (Abdel Zaher *et al*., 2021).

Eighty remote radio transmitters were observed using a T-VLF instrument along an 8 km profile, with 100 m spacing between stations (Abdel Zaher *et al*., 2021). A Fraser filter was applied to the VLF data to enhance horizontal anomalies within the site, while a Karous-Hjelt (k-H) filter gave a pseudo-section of current density anomalies and showed locations of features such as fracture zones or conductors (Abdel Zaher *et al*., 2021).

The TEM and VES data elucidated the apparent resistivity of the subsurface. They showed four geoelectric units with variable conductivity, while the MT showed three distinct units and the depths to those units (Abdel Zaher *et al*., 2021). However, the four units shown in the TEM and VES data correspond with the topmost zone (A) in the Nubian aquifer, while MT methods detected all three zones present in the aquifer (Abdel Zaher *et al.*, 2021). The VES and TEM sections indicated faults. The VLF data also aided significantly in detecting the faults in the Nubian aquifer system of the area (Abdel Zaher *et al*., 2021). The study maximised the use of various geophysical techniques to successfully find the nature of the aquifer. Where one method came short, another made up for this shortfall (Abdel Zaher *et al*., 2021).

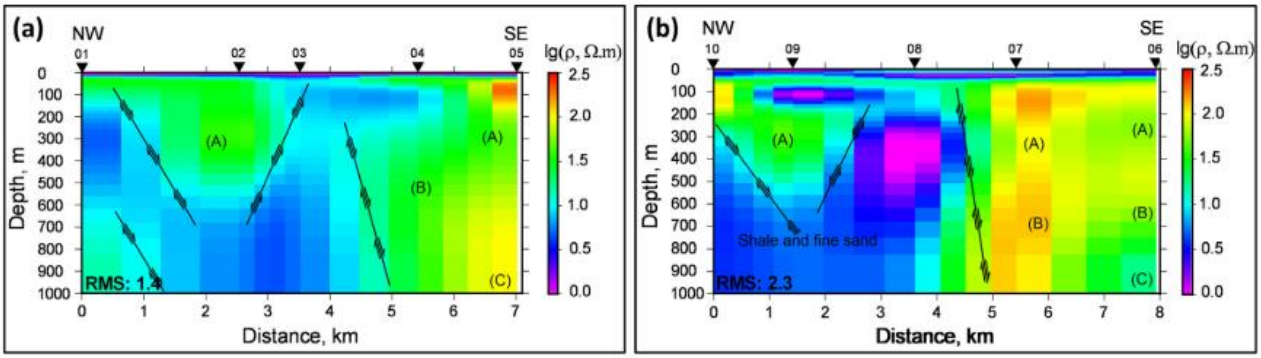

Figure 2.48: 2D inversion models along profiles 1 and 2, respectively. Interpreted Faults are solid lines; letters are aquifer layers (Abdel Zaher *et al*., 2021).

2.4.6.2 Case study 2: Mankessim, Ghana

Agyemang (2022) conducted a study to search for suitable drilling positions Mankessim, Ghana, using the magnetotelluric method. The study area is underlain by the Precambrian Birimian and Tarkwaian Formations. These are sedimentary and metamorphosed rocks that have folding and faulting. Three traverses, A (50 m), B (50 m), and C (100 m) were conducted 25 m from one another. Data were taken using the GMS-06 Metronix Inc multichannel geophysical measurement system at

5 m station spacing. The field data were then inverted using the Mapros (for Edi file) and ZondMT2D (for subsurface resistivity model) software at frequencies of 32-288 Hz (Agyemang, 2021).

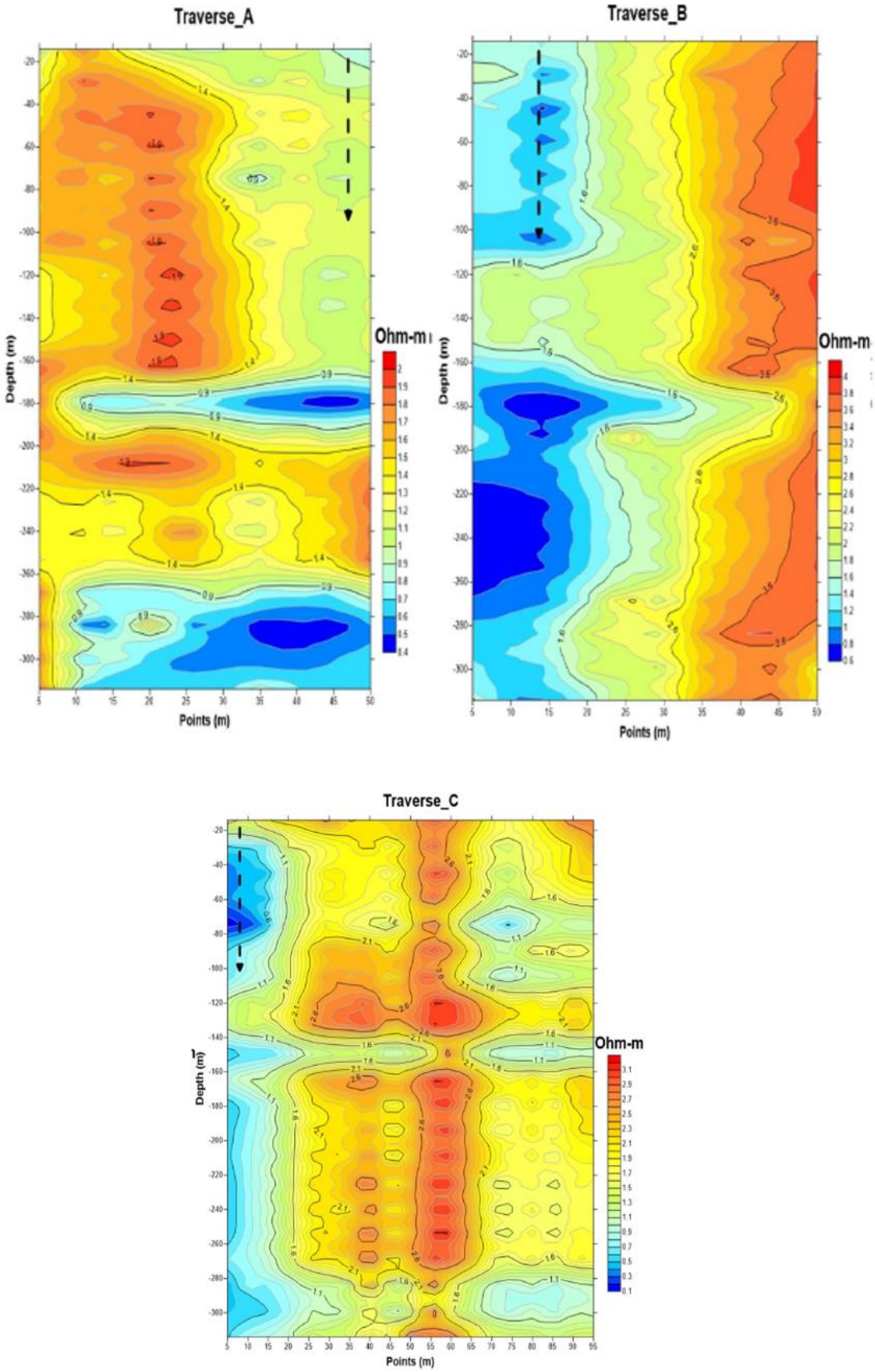

Figure 2.49: 2D apparent resistivity pseudo-sections for traverses A, B, and C (Agyemang, 2021).

Following the removal of noise from the E and H data, the MT time series data were transformed to apparent resistivity and phase amplitude using the Fast Fourier Transform technique (Agyemang, 2021). The generated 2D MT models (Figure 2.49) showed the conductive subsurface with resistivity values of 0.1-4.0 Ωm. The general low resistivity was accounted for by the high clay content of the Birimian rocks. At depths of 170–190 m and 260 m-below, 20–120 m and 160 m-below, and 20–120 m and 140 m-below (for profiles A, B, and C, respectively) are areas of the lowest resistivity (which implies the presence of a localized conductive anomaly). This anomalous area is at the end of profile A and the beginning of profiles B and C and was interpreted as a fractured zone. A low resistivity anomaly at a depth of 20-300 m was determined to be a contact (Agyemang, 2021). Agyemang (2021) successfully applied the MT method to characterise the subsurface and was able to identify the areas with the greatest groundwater potential at the site.

2.4.7 Groundwater exploration using nuclear magnetic resonance methods

2.4.7.1 Case study 1: Oddar Meanchey, Cambodia

A study was conducted to map groundwater reserves in Along Veng and Trapeang Prasa districts in the east of Oddar Meanchey province, Cambodia (Valois *et al*., 2018). Lithologies encountered in the study area include sandstones, siltstones, conglomerates, and limestones with some volcanic rocks. A cover of sand, silt and clay is found in the area. There is no evidence of tectonic faulting in the area, and beds are gently dipping; however, an E–NE to W–SW oriented anticline may have affected geological units south of the study area (Valois *et al.*, 2018).

The study conducted between 2009-2014 used statistical analysis of a database with 55 wells and lithologs, 66 combined TEM and magnetic resonance soundings (MRS), and a total of 612 TEM soundings (Valois *et al.*, 2018). The TEM soundings used a FAST 48HPC in a coincident-loop configuration with the same loop acting as the transmitter (Tx) and receiver (Rx). The loop size (either 25 m, 50 m, or 100 m) was adapted based on local obstacles such as trees or houses. AarhusInv software was used to invert the TEM data, which was eventually used to create a 3D resistivity model of the subsurface (Valois *et al.*, 2018).

The MRSs were conducted with a coincident loop, with the same loop as both transmitter and receiver. Loop side sizes, which depended on the presence of obstacles, ranged from 50 m with two loop turns to 100 m with one loop turn (Valois *et al.*, 2018). 10-16 pulse moments ranging from 10-7000 A.ms were used in the study. (Valois *et al.*, 2018) The instrument employed was the Numis^{plus} from Iris, and the total depth of investigation was 50-80 mbgl. Specific yield (S_y) determined from MRS decay time (T_2^*) were used to determine the groundwater reserves (Valois *et al.*, 2018). Some representative MRS results are shown in Figure 2.50. The raw and calculated data are in Figure 2.50a, while the corresponding model is in Figure 2.50b. A water content of about 1.1% produced a response

of 40 nV (Valois *et al.*, 2018). With the addition of information obtained from available lithologs, specific yield and resistivity of each layer observed could be determined.

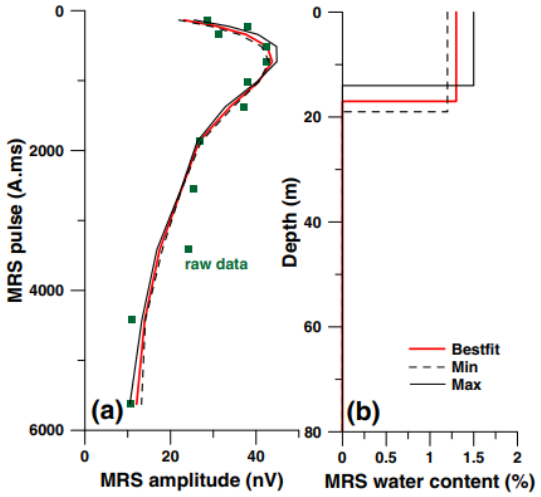

Figure 2.50: Select MRS results: a) Raw and calculated data b) models used to calculate T_2^* of 180 ms (Valois *et al.*, 2018).

The study found no link between restivity and geology due to issues of equivalence in different layers. However, the MRS S_y with TEM resistivity was able to identify four resistivity and elevation classes with unique S_y properties. According to Valois *et al.* (2018), the approach used in this study can increase the probability of drilling a successful borehole to 95%; the remaining uncertainty may be due to weak MRS signals. Groundwater reserve maps were also produced from the data obtained in the study, and the overall understanding of the hydrogeology of Along Veng and Trapeang Pasat was raised.

2.4.7.2 Case study 2: Maqu County, China

Conventional surface nuclear magnetic resonance (SNMR) is plagued by low signal-to-noise ratios. To improve this ratio, Pan *et al.* (2021) designed an optimum pulse sequence based on the correspondence between the pulse moment strength and its best detection depth. It was found that a specific pulse moment (defined as the optimum) can energize an aquifer of a certain depth to its best state; thus, this relationship can be exploited to achieve focused excitation of the target formation or aquifer (Pan *et al.*, 2021). Field experiments to test the efficacy of the optimum pulse moment were conducted in Maqu County, China. Fine sand, gravel and mudstone are found in the area which is crossed by a river.

An ERT and an SNMR survey were conducted in the area with RES2DINV software used to invert the ERT data. From the modelled resistivity (Figure 2.51 a), three layers can be discerned, with the low resistivity layer between 20 m and 60 m likely having free groundwater (Pan *et al.*, 2021). For the SNMR test, the NUMIS^{poly} with square loops of 150 m sides was used. Sixteen traditional pulses

were conducted whose inversion results are shown in Figure 2.51 b) and c). Forty pulse moments between 59-8300 A.ms were used to acquire the 12 optimum pulses. A red curve in Figure 2.52b illustrates the inversion result of the optimum pulse sequence, with the conventional result in Figure 2.52a, and the blue curve of the 40 conventional pulses is shown for reference (Pan *et al.*, 2021). The distribution depth range of the aquifer at 5-50 m (greatest water content) was in agreement with the ERT result. The decay time of the SNMR signal was also used to study pore characteristics. In general, this study found that the low signal-to-noise ratio in traditional SNMR measurement can be improved by using optimum pulse sequences. However, the approximate depth to the aquifer must be known, which is not useful in an area where the hydrogeology is unknown.

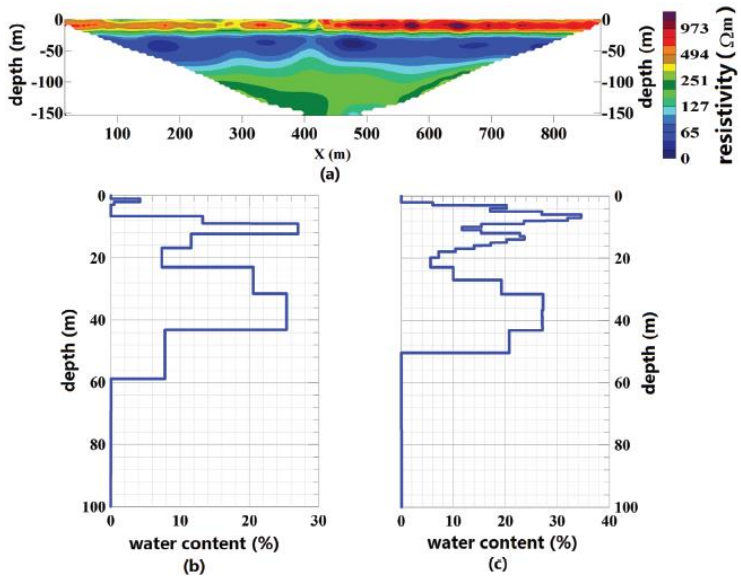

Figure 2.51: a) Modelled resistivity b) and c) show SNMR inversion result of tests 1 and 2, respectively (Pan *et al*., 2021).

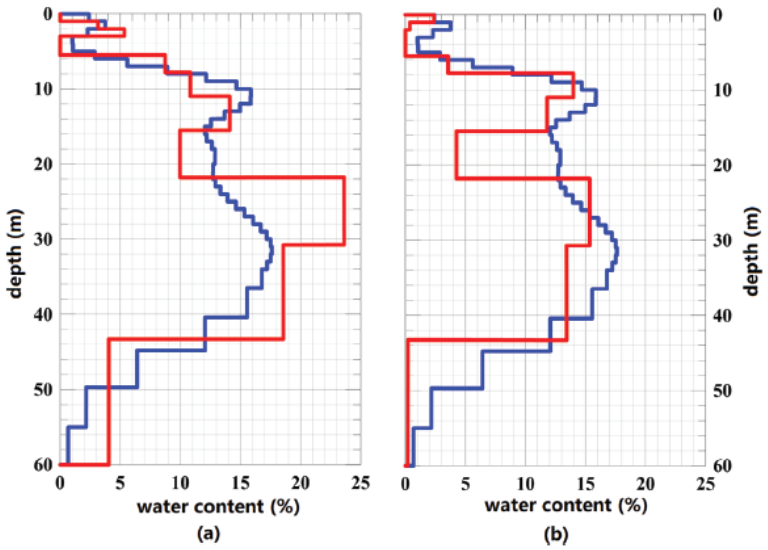

Figure 2.52: Inversion results of water stimulated with different pulses. Red line in a) inversion from 12 traditional pluses while in b) is inversion from the optimum pulse. The blue line in both shows the result from the conventional exponential growth of 40 pulse moments (Pan *et al.*, 2021).

2.4.8 Groundwater exploration using geophysical borehole logging techniques

2.4.8.1 Case study 1: Agbor, Nigeria

Anomohanran *et al.* (2021) conducted a study in Agbor, Nigeria, to identify suitable sites for groundwater development, aquifer depth, and overall hydraulic characteristics of the aquifer. The study area is situated in the Niger delta sedimentary basin. Twenty vertical electrical soundings were conducted in the Schlumberger array. Potential electrode spacing was 1 m, while current electrode spacing was 2 m (Anomohanran *et al.*, 2021).

A 60 m well was drilled in the area where spontaneous potential and electrical resistivity logging were conducted using a calibrated cable connected to an SAS 1000 Terrameter. The probe was lowered into the well at 4 m intervals (Anomohanran *et al.*, 2021). Figure 2.53 shows the resistivity, SP, and lithological log for the borehole drilled onsite. The geophysical logs are in agreement with the observed lithologs, with observed changes in lithology correlating to changes in the SP and resistivity logs. The resistivity log shows a decrease in resistivity up to 20 m thereafter the resistivity steadily increases, reflecting the observed lithology (Anomohanran *et al.*, 2021). The SP log shows an increase in spontaneous potential down the borehole which implies an increase in formation water content.

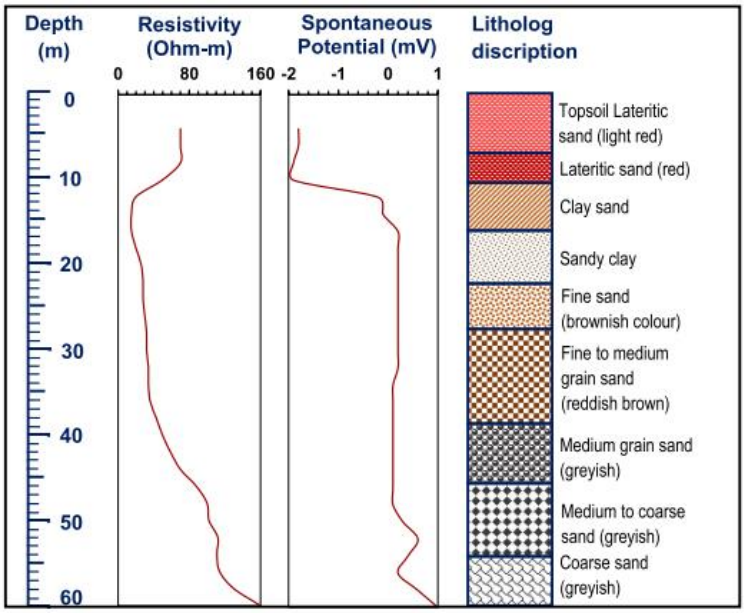

Figure 2.53: Borehole logs (Anomohanran *et al.*, 2021).

A pumptest was later conducted to determine the hydraulic parameters of the study area aquifer. From the VES and geophysical logging it was found that the aquifer depth was between 20-82 m, with determination of TDS and electrical conductivity confirming that the groundwater source is fit for domestic purposes (Anomohanran *et al.*, 2021).

2.4.8.2 Case study 2: Southwest Bani Sweif and West Asyoute, Egypt

The groundwater potential, lithology, hydraulic properties and petrophysical properties of an aquifer in the region between southwest Bani Sweif and West Asyoute in Egypt were determined (Metwally *et al.*, 2023). The aquifer in the region is a limestone aquifer. Several faults are found throughout the region, which have an influence on the aquifers present. Sixteen borehole logs were conducted in the area, and the available data were from:

- Density (porosity)
- neutron (for porosity)
- gamma ray (for shale volume)
- resistivity (lithology)
- calliper log (borehole diameter)
- sonic (lithology), and
- spontaneous potential logs

The data collected from the various available geophysical logs were used to calculate parameters that characterise the aquifer. Pumping tests were also conducted in the area. The combination of these techniques was able to determine, amongst others, the porosity, permeability, shale volume, depth to the water table, hydraulic conductivity and lithology of the aquifer in the area and give recommendations on sustainable yield (Metwally *et al.*, 2023).

2.4.9 Discussion

The case studies summarised in the previous section clearly indicate that the various geophysical methods are an essential feature of any groundwater exploration exercise. The geophysics provides necessary information to determine areas with the greatest groundwater potential. This increases the success in borehole siting because various physical properties of the earth are analysed, and the observed results are interpreted based on the known or expected geology of the area. In most areas, features that were of interest were faults and fracture zones, contacts and weathered zones, which are seen as anomalous zones or discontinuities in the observed results. Clayey formations and fresh bedrock were often avoided due to low potential.

Most studies used multiple geophysical methods to reduce issues of ambiguity that may be encountered during the interpretation of results. For example, different layers with similar apparent resistivities may be suppressed in a resistivity survey but could be clearly detected by other means such as a seismic survey. This shows the importance of using geophysical methods that detect

different physical contrasts. Methods are also chosen based on the geology to be expected on site. For example, magnetic methods would not be appropriate for use in areas where the majority of the encountered geology is magnetic, as no contrast would be discernible or electromagnetic methods in an area crossed by power lines or electric fences, as these are significant sources of noise. The geophysical methods also increase the understanding of the aquifers because they can detect the depth to different formations, be used to calculate a variety of hydrogeological parameters, such as porosity, water quality and even water content, and can determine the presence of secondary features such as faults in the subsurface. The variety of geophysical methods (with the vast array of technologies used to conduct surveys and interpret results) are invaluable tools in characterising a subsurface. Without the use of geophysics, it would have proven difficult to characterise the subsurface without direct observation.

CHAPTER 3:
DESCRIPTION OF THE STUDY AREA: SOUTH AFRICA

3.1 INTRODUCTION

As its name indicates, South Africa is Africa's southernmost country. The country, whose area is 1,219,912 km^2 (Schluter, 2008) with a coastline that is about 2800 km long (Alexander, 2018), is located between the latitudes 22°S to 35°S and longitudes 17°E to 33°E. The country is split into nine provinces and shares borders with six countries; Lesotho (which is entirely landlocked by the country), eSwatini, Mozambique, Zimbabwe, Botswana, and Namibia.

On the country's west coast lies the Atlantic Ocean, and on the east coast, the Indian Ocean. The country possesses a prominent feature called the great escarpment, which extends for hundreds of kilometres in the interior of southern Africa (Grab and Knight, 2015a). It separates the interior plateau from the coastal lowlands and fold mountains on the fringe of the country (Grab and Knight, 2015a). The great escarpment is illustrated in the map of South Africa in Figure 3.1.

Figure 3.1: South Africa with its neighbouring countries and its provinces. The location of the Great Escarpment is also demonstrated (Grab, 2015).

There are four distinct zones into which the country can be divided: the western plateau slopes, the Cape Fold Belt, eastern plateau slopes and the interior plateau slopes (World Bank Climate Change Knowledge Portal, 2021). The interior plateau at 1200 m above sea level lies in the area between the

Kalahari in the west, the Karoo in the south, and the eastern grasslands (World Bank Climate Change Knowledge Portal, 2021). The great escarpment creates a topographic, geomorphic, and climatic boundary with the result that neighbouring areas can differ significantly from one another (Grab and Knight, 2015a).

In this chapter, the country will be described in terms of its climate, socio-economic conditions, geology and geohydrology. The typical structures or features targeted during geophysical exploration in selected environments will also be described.

3.2 CLIMATIC CONDITIONS

Climatic conditions in South Africa vary significantly from the eastern to the country's western reaches (Alexander, 2018). It experiences a warm subtropical climate in the northeast, wet, cool conditions in the Drakensberg region, a Mediterranean climate in the southwest, and warm, dry desert conditions in its central and western regions (World Bank Climate Change Knowledge Portal, 2021). The climatic conditions are influenced by the warm Agulhas current that flows on the east coast and the cold Benguela current on the western coast of the country (Alexander, 2018).

South Africa has a mean rainfall of 465 mm/a that varies drastically and is categorised as a semi-arid to arid country (DWS, 2018). This average is below the world average rainfall, which is 786 mm/a (Wright *et al*., 2021). The majority of the country experiences summer rainfall from December to February, except for the Western Cape, with its Mediterranean climate, which receives winter rainfall between June and August (World Bank Climate Change Knowledge Portal, 2021).

The highest rainfall occurs in the east, in Mpumalanga and KwaZulu Natal, which receive year-round rainfall. Conditions progressively become drier westward into the interior, on the interior Karoo plateau with desert conditions in the Northwestern region of the country (Alexander, 2018). Average temperatures in the country vary from 15°C-36°C in the summer months and -2°C-26°C during winter (World Bank Climate Change Knowledge Portal, 2021). The climate and topography of South Africa are illustrated in Figure 3.2. The temperatures and climate of South Africa can be characterised in a Koppen Geiger map as shown in Figure 3.3, where the letters each describe a certain aspect; the first describes the main climate, the second precipitation, and the third temperature characteristics. A – equatorial, B – arid, C – warm temperate. S – steppe, W-desert, w-winter dry, s-summer dry, f – fully humid. a- hot summer, b-war summer, k-cold arid, h – hot arid (Lennard, 2019).

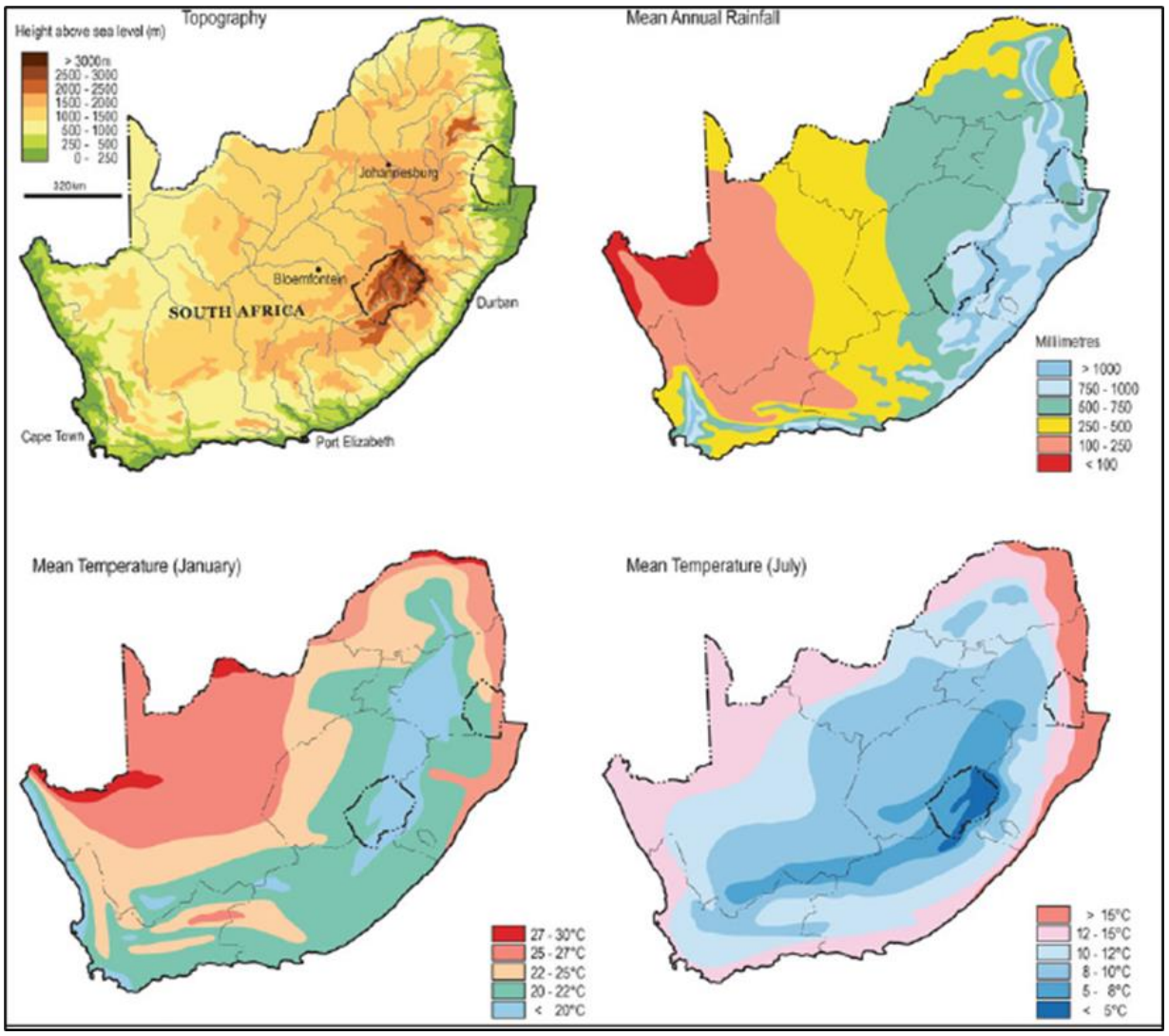

Figure 3.2: South Africa's climate and topography (Grab and Knight, 2015b).

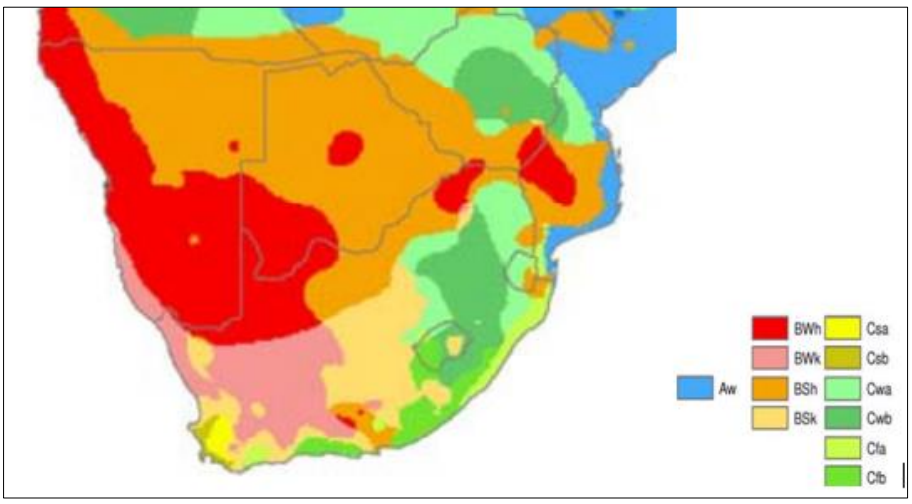

Figure 3.3: Koppen-Geiger climate zone across South Africa and its neighbouring countries modified from (Peel, Finlayson and MacMahon, 2007).

3.3 SOCIO-ECONOMIC CONDITIONS

South Africa had an estimated population of 60.6 million in mid-2022 (Stats SA, 2023b). Gauteng province is the most populated, with a share of the population of 24.3%, 20% for KwaZulu Natal, 12% for the Western Cape, 11.6% in Eastern Cape, 10.6% in Limpopo, 8.3% in Mpumalanga, 6.1% in the North West, 4.8% for the Free State, while the least populous province is the Northern Cape province, with a share of 2.2%. (Stats SA, 2023b). The number of households in South Africa in 2022 was 18.5 million (Stats SA, 2023a).

According to Stats SA (2023a), the number of households with access to piped drinking water inside their dwelling in 2022 was 46.6%. 2.3% of households had a borehole on site, 1.1% used a borehole outside of the yard, and 3% received their water from wells, springs, stagnant water pools, dams, and rivers. Groundwater was used as the main water source in 22% of towns, while a further 34% used it in combination with surface water sources (DWS, 2016), with its use of increasing importance due to water scarcity in South Africa.

3.4 THE GEOLOGY OF SOUTH AFRICA

South African geology is old and variable, spanning more than three billion years of the history of the Earth (McCarthy and Rubigde, 2005). There are large sections of the country underlain by Precambrian rocks, some of which are Archean age, such as the rocks of the Barberton. The country's geology is extensive, and a selection of some features of the South African geology will be discussed in the following sections. The geology is described from youngest to oldest consolidated deposits of the selected areas, and then at the end of the section, a description of selected unconsolidated deposits is provided. Figure 3.4 shows the generalised geology map of South Africa. It is important to describe the geology of the country as informs the geohydrological characteristics of different locales and the recorded geophysical responses observed. Its understanding is needed for the correct interpretation of geophysical data.

3.4.1 The Karoo Supergroup

The Karoo Supergroup rocks were deposited between 150-320 Ma years ago (Johnson *et al.,* 2006). The are other basins similarly aged to the main Karoo Basin across south-central Africa, which were also deposited on the ancient supercontinent Gondwana; these are shown in Figure 3.5. For this paper, only the main Karoo Basin will be discussed.

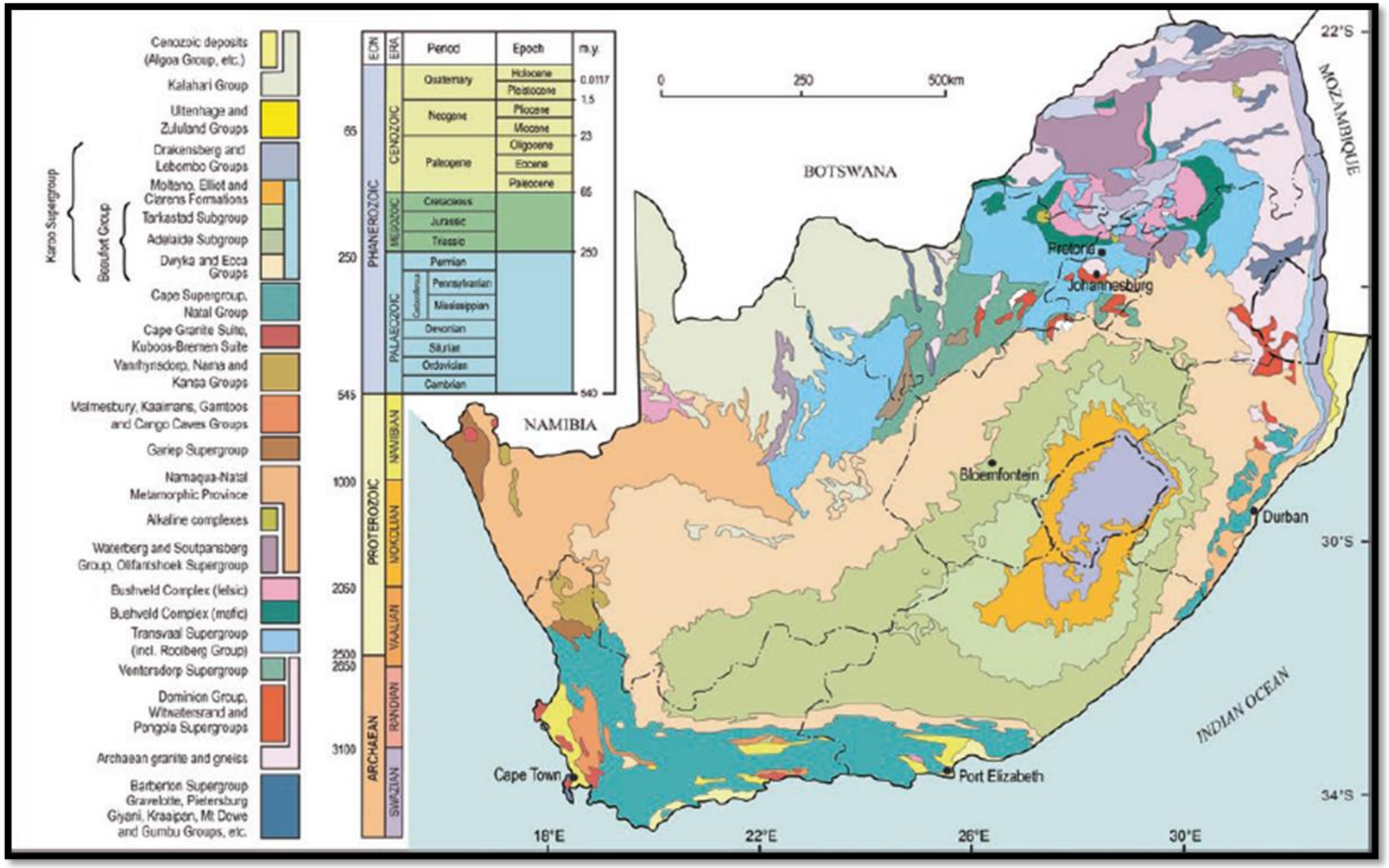

Figure 3.4: Generalised geology of South Africa (Johnson *et al*., (2016) in (Knight, 2019)).

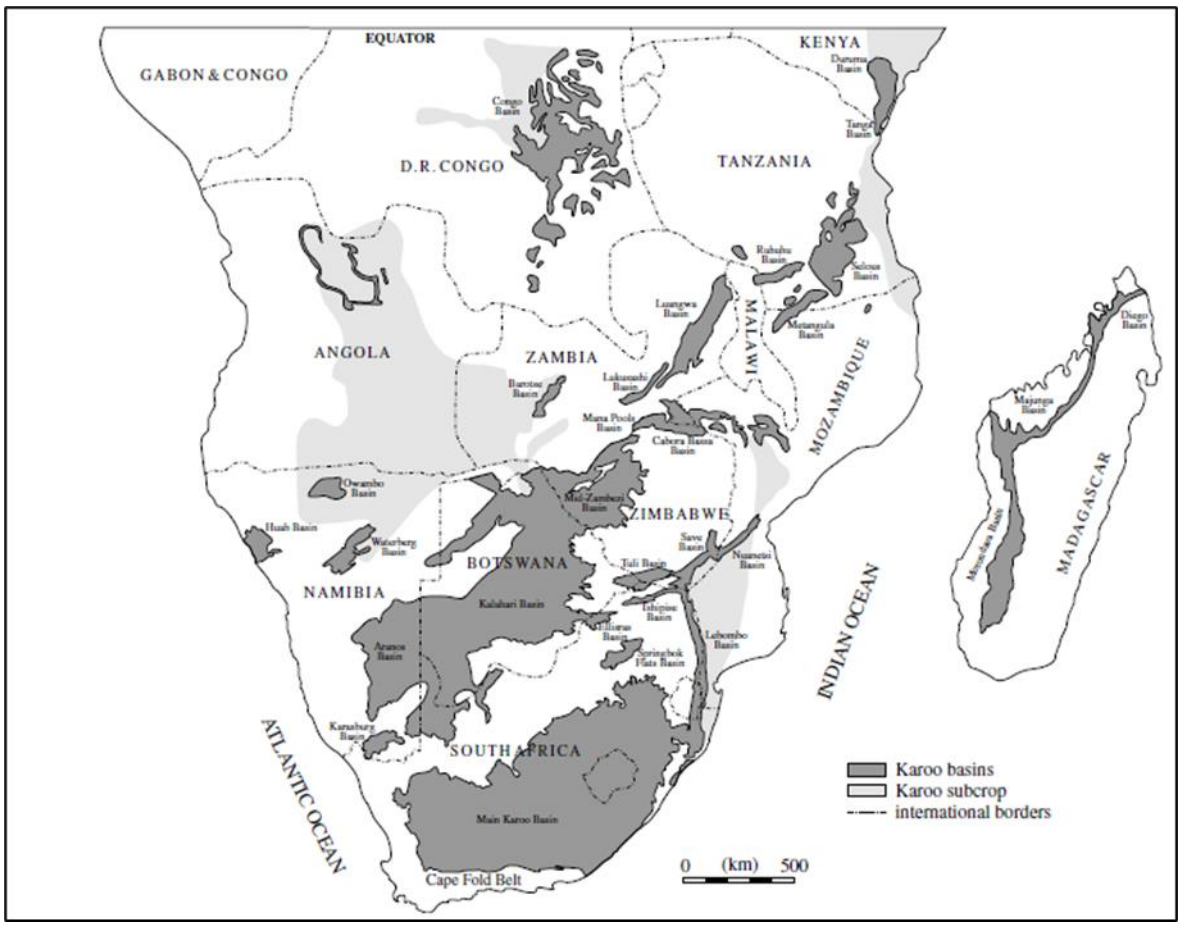

Figure 3.5: South-central African Karoo Basins (Catuneanu *et al*., 2005).

Approximately two-thirds of South Africa is underlain by the main Karoo Basin, which is up to 12 km thick (Rubigde and Hancox, 2002). The sediments of the Karoo were deposited under the controls of climate and tectonism (Catuneanu *et al*., 2005). The main Karoo basin forms part of a retro-arc foreland basin (Johnson *et al*., 2006), which is bound by a fold belt in its southern margin, the Indian Ocean in the southeastern margin, and a cratonic basement in the west to the northeast (Woodford and Chevallier, 2002; Johnson *et al*., 2006; Lourens, 2013).

The main tectonic regime during the Karoo sedimentation was variable, changing from flexural dominated in the southern margin of Gondwana to extensional in its northern margin (Catuneanu *et al*., 2005). Climatic conditions also influenced deposition, with a shift from glacial to semi-arid from the Permian to the Carboniferous and eventually hot climate during the remaining period of its deposition (Catuneanu *et al*., 2005). The main Karoo basin is divided into the; Dwyka, Ecca, Beaufort, Stormberg, and Drakensberg Groups (Catuneanu *et al*., 2005). An illustration of the areal distribution of the Karoo lithostratigraphic units is shown in Figure 3.6. A cross-section across the Karoo is shown in Figure 3.7, while the generalised lithostratigraphy of the Karoo Supergroup is shown in Figure 3.8.

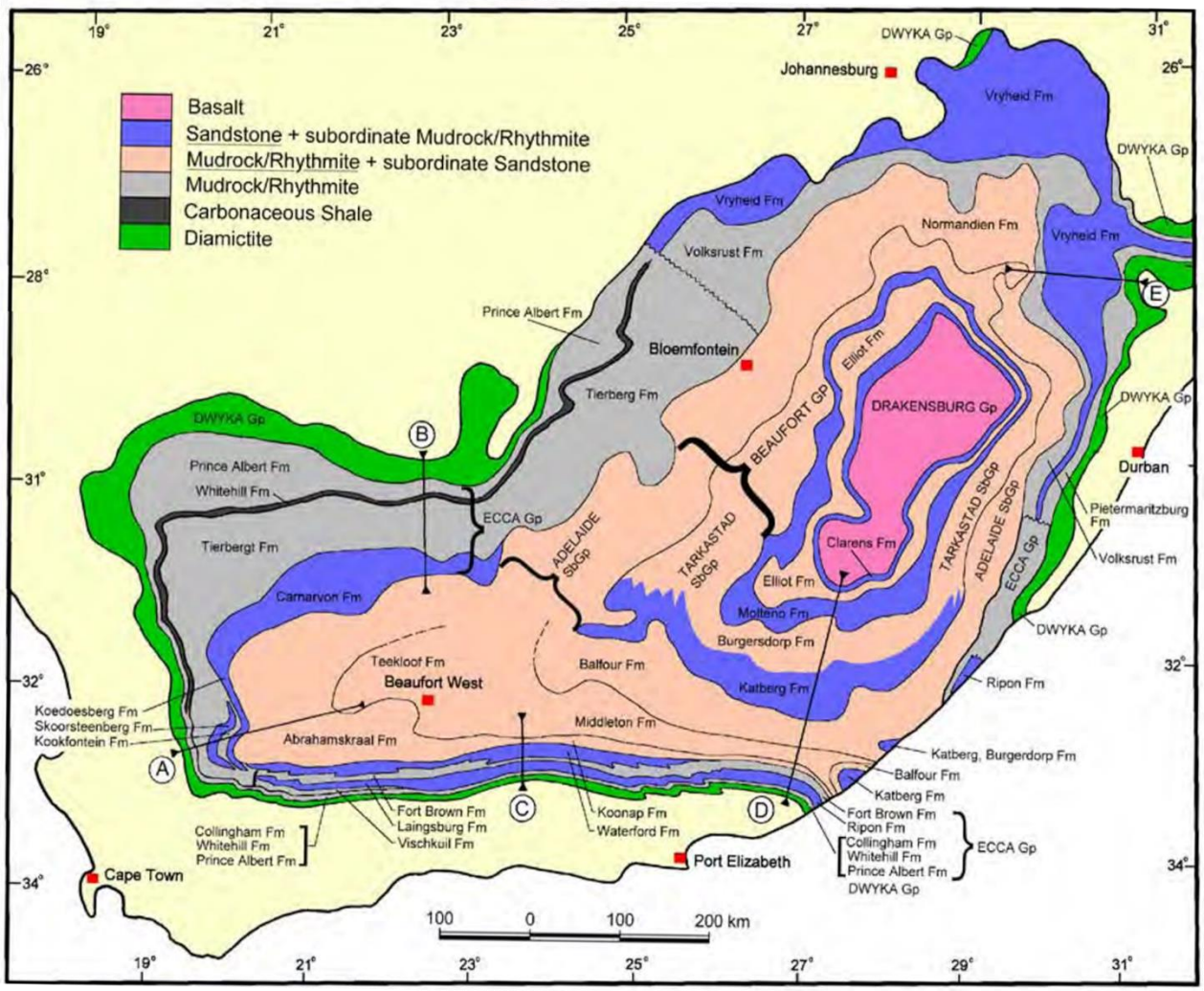

Figure 3.6: The areal distribution of the main Karoo basin lithostratigraphic units (modified from Johnson *et al* (1997) in Woodford and Chevallier (2002)).

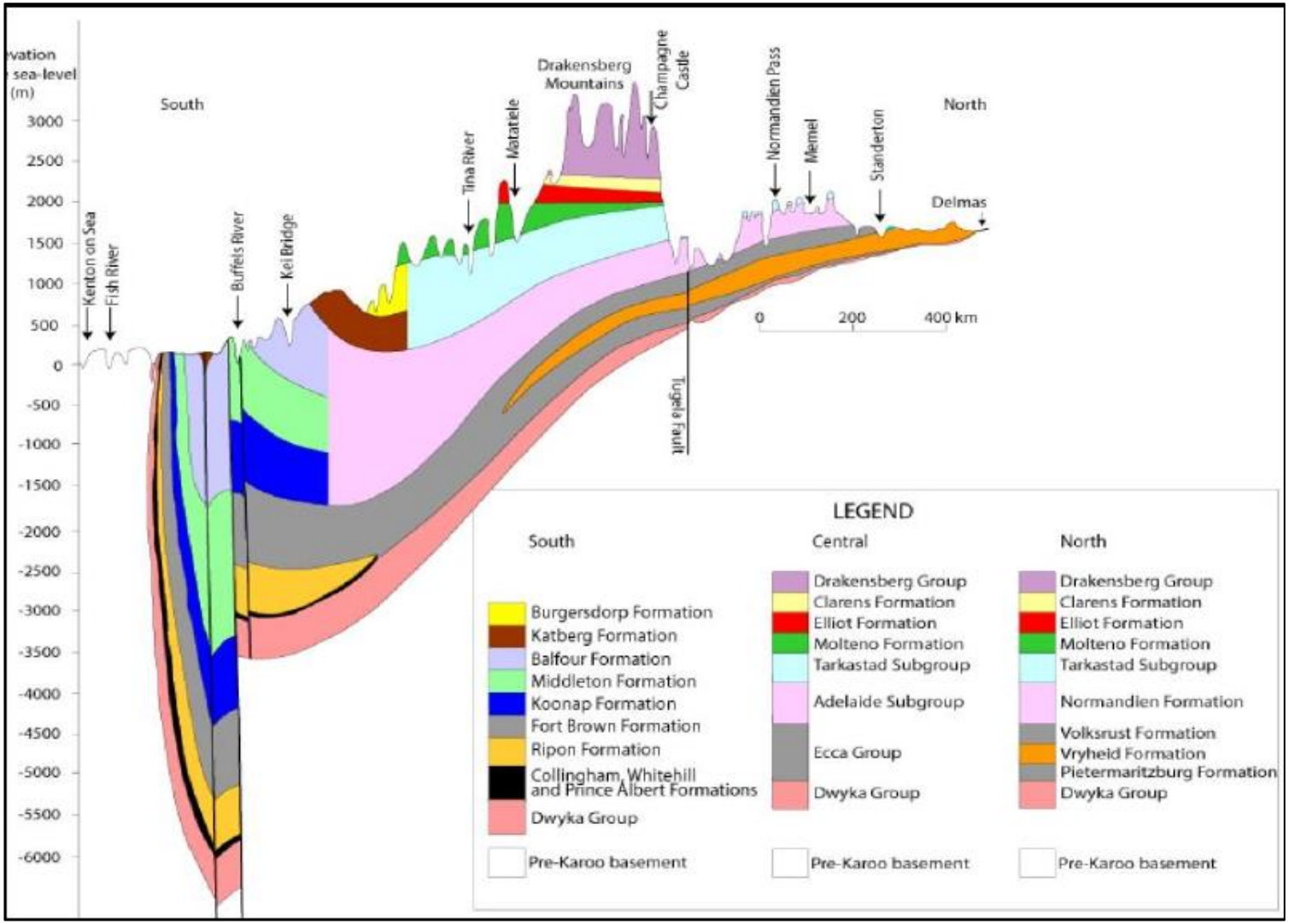

Figure 3.7: Cross-section through the main Karoo Basin (Lourens, 2013).

3.4.1.1 The Dwyka Group

It was between the late Carboniferous to early Permian that the Dwyka was deposited by glacial action (Woodford and Chevallier, 2002) over Precambrian granite in the north and the Cape Supergroup rocks in the south (Botha *et al*., 1998). The rocks are mainly diamictites that are predominantly massive and have limited jointing but may be stratified elsewhere. Conglomerate, rhythmite, sandstone, and mudrock are in subordinate amounts (Woodford and Chevallier, 2002).

The Dwyka is such that it can be divided into a northern facies, deposited in deep paleovalleys excavated by glaciers, and a southern platform facies, deposited in glaciomarine conditions on a sea bed (Botha *et al*., 1998; Woodford and Chevallier, 2002). Rapid thickness changes are common in the northern facies, with up to 200 m change in thickness over short distances. The northern facies has varying lithology, ~20% massive diamictite, and high mudrock content at about 40% (Woodford and Chevallier, 2002; Lourens, 2013). The southern facies, on the other hand, has a regular increase in thickness from about 100-800 m towards the south and regular lithology. It has a low mudrock content of about 8% and a high massive diamictite content of about 70% (Johnson *et al*., 1997).

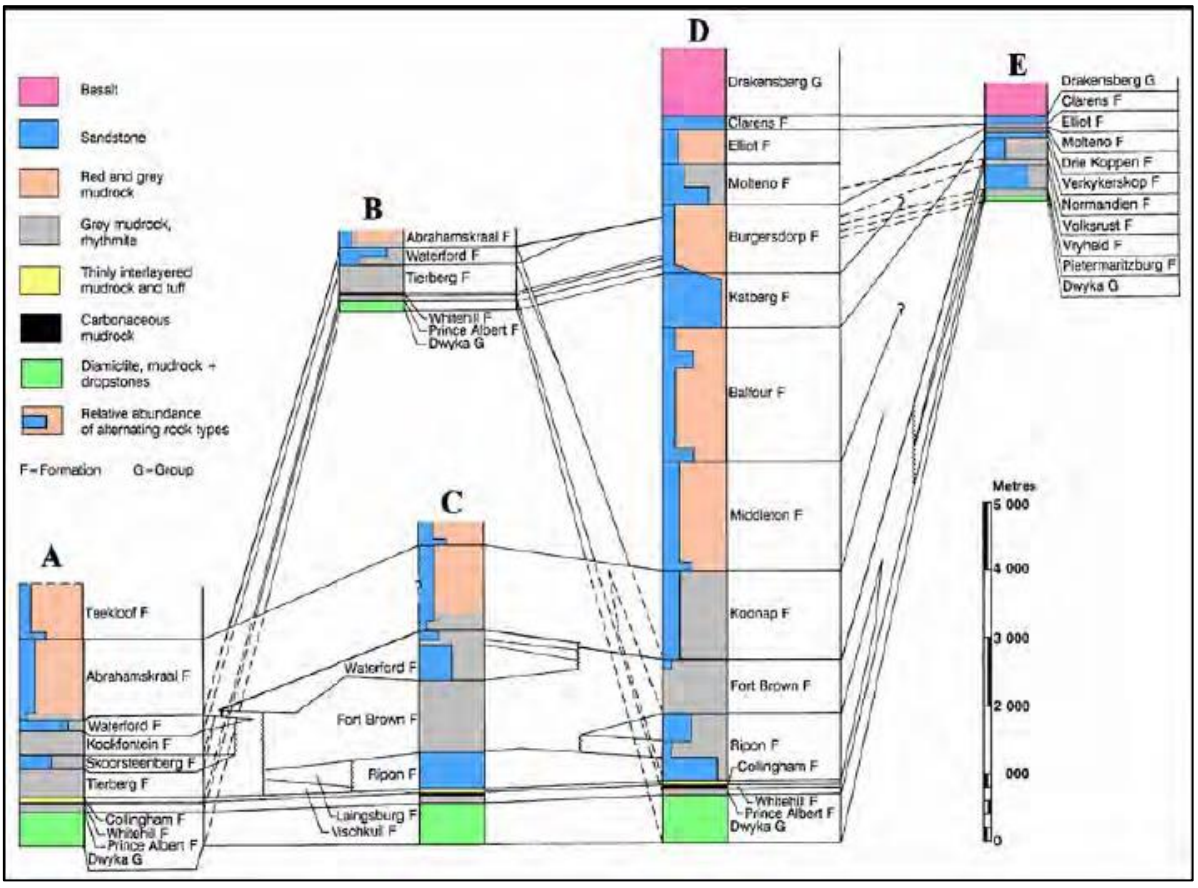

Figure 3.8: Generalised lithology and stratigraphy of the Main Karoo Basin modified from (Johnson *et al*., 1997).

The Dwyka diamictite comprises individual clasts of basement rock that are angular to rounded up to 3 m in diameter, embedded in a matrix of silt and clay (Woodford and Chevallier, 2002). The

conglomerate facies, according to Johnson *et al.* (2006), varies from boulder layers with single beds to pebble and granule conglomerates that are poorly sorted. The sandstone facies is composed of immature sandstones that are very fine-medium-grained, have trough cross-bedding and are massive-ripple laminated (Johnson *et al.,* 2006). The mudrock facies comprise dark and usually carbonaceous mudstone, shale, or rhythmites (Johnson *et al*., 1996).

3.4.1.2 The Ecca Group

The Ecca is Permian age and comprises 16 formations that show the lateral facies change of the group (Johnson *et al.,* 2006; Woodford and Chevallier, 2002). Apart from the Whitehill and Prince Albert Formations, separate formations within the group can be divided into three geographical areas; western + northwestern, northeastern, and southern areas (Woodford and Chevallier, 2002).

Basal formations in the south, west, and north-west:

Prince Albert Formation: At the bottom of the Ecca and restricted to the Karoo's southwestern section (Johnson *et al*., 1997). The formation thins or pinches out into the basement rocks towards the northeast or merges the Pietermaritzburg or Vryheid Formations. Its thickness is variable along the southern and western outcrop belts (40 m-150 m), but data from boreholes suggest a maximum thickness of 300 m. Southern and northern facies may be recognised in this formation (Johnson *et al*., 1997). A marked shift from the Dwyka below, grey, silty shale and greyish to olive-green, micaceous shale exists (Johnson *et al.,* 1997). There is also fine to medium-grained feldspathic arenite, wacke, and dark grey to black carbonaceous shale. Dark-grey, pyrite-bearing, splintery shale, siltstone, with dark-coloured chert and phosphatic nodules and lenses characterise the southern facies (Johnson *et al*., 2006).

Whitehill Formation: It lies on top of the Prince Albert Formation and coincides with its location (Johnson *et al*., 1997). On the divide between the two, there is often a gradational change (Branch *et al*., 2007). It is composed of black carbonaceous shale with irregular chert lenses and pyritic stringers seldom over 20 mm thick (Branch *et al.,* 2007). The formation is generally massive and appears white at the surface because of pyrite weathering to gypsum (Branch *et al.,* 2007). The formation thickness is variable between 10 m and 80 m (Johnson *et al.,* 2006).

Southern formations above the Whitehill Formation

Collingham Formation: This formation only outcrops in the western and southern margins of the Karoo Basin (Johnson *et al*., 1997). 30 m-70 m thick, this formation comprises very thin beds of softer yellowish tuff and thin, continuous beds of hard, dark-grey, siliceous mudrock alternating rhythmically (Johnson *et al*., 1997). A distinct layer of chert 0.2 m-0.6 m thick, called the Matjiesfontein Chert Bed, is found at the bottom of the formation, while subordinate siltstone and

sandstone units are found in the upper sections within the western part of the area (Johnson *et al*., 1997).

Vischkuil Formation: In the basin's southwestern part, it is underlain by the Collingham Formation. It is predominantly argillaceous but becomes increasingly arenaceous in the east and has a gradational contact with the Ripon Formation (Johnson *et al*., 2006; Lourens, 2013). It is between 200 m and 400 m thick (Johnson *et al*., 2006). This formation comprises dark shale that alternates with minor fine-grained sandstone, siltstone, and subordinate yellowish tuff layers (Johnson *et al*., 1997). The shale units lack structure or are thinly laminated and show sharp upper contacts and sharp to gradational lower contacts (Johnson *et al*., 1997).

Greywacke beds are 0.3 m-1.5 m thick and are fine-grained with various primary structures (Johnson *et al*., 1997). Thicker sandstone beds are mostly massive or planar laminated, while thinner, very fine-grained sandstones lower in the formation have a cross-laminated and/or planar laminated zone (5-18 cm). These are followed by a structureless zone containing pseudo-nodules and an upper structureless zone that grades into the overlying shales (Johnson *et al*., 1997). There are sporadic occurrences of 1-20 cm thick yellowish-green to khaki-green tuff layers throughout the formation (Johnson *et al*., 1997).

Laingsburg Formation: A gradational contact exists between this Formation and the underlying Vischkuil Formation. It is ~400 m thick and consists of four sandstone-rich layers with shale units in between but thins out toward the west and north (Woodford and Chevallier, 2002). The fine to medium-grained sandstones are massive with sharp lower and upper contacts. Siltstone and shale units are planar, limited and occasionally have lenticular calcareous concretions and coalified plant fragments (Woodford and Chevallier, 2002).

Ripon Formation: 600-700 m thick but is 1000 m thick in its eastern outcrop area. It consists of medium grey lithofeldspathic sandstones that are medium to fine-grained and poorly sorted, that alternate with dark grey fine-grained clastic rhythmite and mudrock units (Johnson *et al*., 1997). It is the Laingsburg Formation equivalent in the west (Tankard *et al*., 1982).

Fort Brown Formation: This formation is characterised by mudrock and rhythmite with some small intercalations of sandstone and generally shows an upwards coarsening trend (Johnson *et al*., 1997). The average thickness of the formation is about 1000 m. The individual layers of silt and sand or silt and clay that comprise the rhythmite are of similar thickness, although sand displays an increase in thickness upwards in the sequence (Johnson *et al*., 1997).

Waterford Formation: The arenaceous formation is confined to the southern outcrop area and underlain by the Fort Brown Formation (Johnson *et al*., 1997). Alternating layers of medium grey lithofeldspathic sandstones and medium-dark grey mudrock or clastic rhythmite units comprise the

formation (Johnson *et al*., 1997). The upper part of the formation, the Britskraal Shale Member, is 100 m thick, while the formation thickness fluctuates between 200 m and 800 m. Ball and pillow and other associated structures are typical of the Waterford Formation (Johnson *et al*., 1997).

Western and northwestern formations above the Whitehill Formation

Tierberg Formation: It is a mostly argillaceous formation of 700 m in the western margin but thins to about 350 m in the northeastern section of the basin (Woodford and Chevallier, 2002). There is a sharp contact between it and the Whitehill or Collingham formations. Where the Waterford formation is present, it grades upwards into it or into the Adelaide Subgroup of the Beaufort in its absence (Johnson *et al*., 2006). It comprises mostly well laminated bluish grey to almost black shale, which is carbonaceous and pyrite rich (Johnson *et al*., 1997).

In lower parts of the sequence, there are yellowish tuff beds up to 10 cm thick, calcareous concretions occur near the top of the formation, while clastic rhythmites are common at different depths in the formation (Woodford and Chevallier, 2002). Upwards coarsening sequences are found at the top of the sequence and comprise 2-10 cm thick mudstones, siltstones, and very fine-grained sandstones (Woodford and Chevallier, 2002). Clay pellet conglomerate also occurs (Woodford and Chevallier, 2002).

Skoosteenberg Formation: It is in the southwestern section of the basin and is an arenaceous flat-lying lens-shaped formation. Its greatest thickness is 200 m and consists of five sandstone-rich units with a maximum thickness of 65 m, separated by shale units (Johnson *et al*., 1997). Massive bedding, rip-up clasts, and dewatering structures are common (Johnson *et al*., 1997).

Kookfontein Formation: consists of approximately 400 m thickness of siltstone shale and fine-grained sandstones (Woodford and Chevallier, 2002). Horizontally laminated dark-grey shales alternating with rhythmically interbedded shales and siltstones, which create minor upward thickening cycles, are characteristic of the lower reaches of the formation (Johnson *et al*., 1997). Cycles are thickest at the top of the sequence at about 15 m thick and comprise siltstone alternating with thin sandstone beds and are capped by thick sandstone in some places (Woodford and Chevallier, 2002). The Kookfontein is laterally equivalent to the upper section of the Tierberg Formation (Woodford and Chevallier, 2002).

Waterford Formation of the western zone: Outcrops along the western edge of the basin. It is underlain by the Kookfontein and Tiersberg formations with a gradational contact and has a sharp contact with the Abrahamskraal Formation above it (Woodford and Chevallier, 2002). It is 130 m thick and comprises fine- to medium-grained sandstone, rhythmite, shale, and siltstone (Woodford and Chevallier, 2002)

Waterford Formation of the northwestern zone: This formation in the northwestern zone is 250 m thick and consists of fine- to very fine-grained tabular sandstones with maximum thicknesses of 8 m, siltstone, shale, and rhythmite (Woodford and Chevallier, 2002).

Northeastern Formations

Pietermaritzburg Formation: It consists of bluish-grey silty mudrock that outcrops along the north-eastern section of the basin (Johnson *et al*., 2006). The shales and mudstones are interlayered with fine-grained sandstones. Its greatest thickness is 400 m in the southeast and thinning to under 100 m in the northern direction (Johnson *et al*., 2006). There is mostly a sharp contact between it and the Dwyka Group below it (Johnson *et al*., 2006).

Vryheid Formation: This formation has a wedge-like shape, thinning in the north, south, and west from a maximum thickness of 500 m. It comprises siltstone, mudstone, rhythmite, and fine to medium-grained sandstones (Woodford and Chevallier, 2002). Coal seams also occur within this formation. The pre-Karoo topography near the northwestern and basin's northern edge, where this formation lies over pre-Karoo rocks, or Dwyka tillite, is the reason for the distinct difference in thickness (Woodford and Chevallier, 2002). For most of the northeastern zone, it is underlain by the Pietermaritzburg Formation (Johnson *et al*., 1997).

Volksrust Formation: This is an argillaceous formation that comprises grey to black, silty shale with thin siltstone or sandstone beds and bioturbated lenses, especially towards its upper and lower boundaries (Woodford and Chevallier, 2002). It is up to 380 m thick, thinning to 280 m in the east (Woodford and Chevallier, 2002).

3.4.1.3 The Beaufort Group

This group of rocks is of Permo-Triassic age and was deposited by fluvial processes (Catuneanu *et al*., 2005). The Beaufort covers about 200,000 km^2 of land in South Africa and attains a maximum cumulative depth of 7000 m but thins out rapidly toward the north (Catuneanu *et al*., 2005). Siltstones and mudstones with subordinate lenticular and tabular sandstones are typical features of Beaufort Group strata (Catuneanu *et al*., 2005). The group is separated into the Adelaide and Tarkastad Subgroups.

Adelaide Subgroup

Deposited in the late Permian, this assemblage consists of the Koonap, Middleton, and Balfour Formations in the southeastern (proximal) section of the basin and the Nomarndien Formation in the northeastern (distal) part (Johnson *et al*., 1997; Woodford and Chevallier, 2002). The Koonap and Middleton formations form an upwards fining sequence (Catuneanu *et al*., 1998). Greenish silty

mudstones and sandstones characterise the former, while maroon and greenish-grey sandstones are typical for the latter (Catuneanu *et al*., 1998).

In the western zone of the basin, the Abrahamskraal and Teekloof formations are approximated equivalents of the Koonap and Middleton Formations and have maximum thicknesses of 2500 m and 100 m, respectively (Johnson *et al*., 1997). The Koonap and Middleton Formations have maximum thicknesses of 1300 m and 1600 m, respectively (Johnson *et al*., 1997).

The Balfour Formation constitutes an upwards fining sequence and consists of yellowish and bluish-greenish-grey sandstones interbedded with dark mudstones (Catuneanu *et al*., 1998). This formation is up to 2000 m thick (Catuneanu *et al*., 2005). The Normandien Formation comprises interbedded mudstones and sandstones, and it correlates with the top of the Balfour Formation, being of similar age (Catuneanu *et al*., 1998).

Tarkastad Subgroup

This early Triassic subgroup contains a larger volume of sandstones and red mudstones than the Adelaide Formation (Woodford and Chevallier, 2002). The subgroup unconformably overlies the Balfour Formation, and it is up to 2000 m thick in the south but thins to 800 m in the middle outcrop area and 150 m in the far north (Johnson *et al*., 1997). It is divided into the Katberg and Burgersdorp Formations in the southern margin and the Verkykerskop and Driekoppen Formations (in Natal, referred to as the Belmont and Otterburn Formations, respectively) in the northern facies of the subgroup (Catuneanu *et al*., 1998).

The Katberg Formation comprises thick, light olive-grey, coarse-grained sandstones with trough cross-bedding and horizontal bedding (Catuneanu *et al*., 1998). The Verkykeskop Formation in the northern facies consists of thin, laterally extensive sandstones that are fine to medium-grained and cross-bedded (Catuneanu *et al*., 1998). Thick, upward fining units of olive-grey fine to medium-grained sandstones that underlie red-maroon mudstones are characteristic of the Burgerdorp Formation. It overlies the Katberg Formation conformably and lacks a significant lateral extent (Catuneanu *et al*., 1998). In the northern facies, the thin fine-grained, horizontally bedded sandstones topped by thick, massive to diffusively laminated siltstones and mudstones comprise the Driekoppen Formation (Catuneanu *et al*., 1998).

3.4.1.4 The Stormberg Group

This Group is about 1200 m thick in the main Karoo Basin and is split into the Molteno, Clarens, and Elliot Formations (Catuneanu *et al*., 2005). Unlike the other previously discussed groups, this one is present only in the distal section of the Karoo basin (see Figure 3.9).

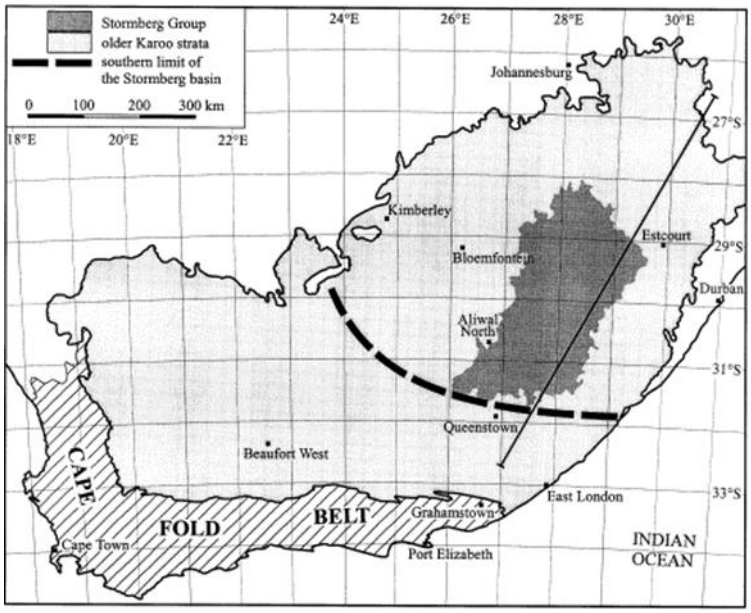

Figure 3.9: An illustration of the distribution of the Stormberg Group on and beneath the surface. (Catuneanu, Hancox and Rubidge, 1998).

The formations are discussed in the following section.

Molteno Formation

This formation is late Triassic in age (Johnson *et al*., 1997). Its maximum thickness is about 600 m in the southern outcrop area (Woodford and Chevallier, 2002). It consists of alternating sheets of tabular, medium to coarse-grained sandstones that "glitter" due to quartz overgrowth (Woodford and Chevallier, 2002). The sandstones are believed to be braided river deposits (Catuneanu *et al*., 1998). There are also a few occurrences of siltstone, mudstone, and sporadic coal, but these are not abundant (Woodford and Chevallier, 2002).

Elliot Formation

This formation is early Jurassic in age and consists of predominantly reddish floodplain mudstones with minor crevasse splay and channel sandstones (Catuneanu *et al*., 1998). Aeolian influence increases upward in the formation, with the top of the Elliot being characterised by windblown fine-grained sandstones (Catuneanu *et al*., 1998). It is 500 m thick in the south, thinning to about 100 m in the north (Woodford and Chevallier, 2002).

Clarens Formation

The Clarens Formation formed between the early to the middle Jurassic period (Catuneanu *et al*., 1998) and is composed of cream or yellow fine-grained sandstones, sandy siltstones, and mudstones with subordinate coarse sandstones (Catuneanu *et al*., 1998). The depositional environment was aeolian-dominated (Catuneanu *et al*., 1998). The formation is 100 m thick in the north but up to 300 m thick in the south (Woodford and Chevallier, 2002)

3.4.1.5 The Drakensberg Group

The Drakensberg Group consists of flood basalts that erupted during the late Triassic until the early Cretaceous (Catuneanu *et al*., 2005). These tholeiitic basalts cover 80% of the land surface of Lesotho and are found in parts of the Free State, Eastern Cape, and the KwaZulu Natal provinces of South Africa (Woodford and Chevallier, 2002). The basalts in Lesotho have an average thickness of 1000 m with a maximum of 1400 m in the northwest (Woodford and Chevallier, 2002). It consists of individual lava flows with a thickness of 1-50 m (Woodford and Chevallier, 2002).

The group is separated informally into; the upper Lesotho Formation and the lower Barkley East Formation (Woodford and Chevallier, 2002). The lower Barkley East formation consists of thin flows, has a limited distribution and is 200 m thick. The upper Lesotho formation constitutes the majority of the Group (Woodford and Chevallier, 2002).

3.4.1.6 The Karoo Dolerite Suite

The Karoo Supergroup sediments were intruded into by sills and dykes in the course of extensive magmatic activity associated with one phase of the breakup of Gondwana (Chevallier *et al*., 2001). The Jurassic age (~180Ma) magmatism responsible for the suite occurred almost throughout the southern African continent (Chevallier *et al*., 2001). Figure 3.10 shows the sills emplaced in the main Karoo Basin.

The main Karoo Basin has been affected by a significant level of erosion, leaving the Karoo dolerites exposed. They show an uncommon level of tectonic complexity (Woodford and Chevallier, 2002). These dolerites are composed of an interconnected network of dykes and sills (Woodford and Chevallier, 2002). This dolerite suite is representative of the shallow feeder system of the Drakensberg flood basalts (Leyland, 2015). The sills are between a few metres to 200 m thick, while the dykes are 2 m to 10 m wide and 5 km to 30 km long (Leyland, 2015). Most dykes are homogenous in terms of their composition. However, some thick sills indicate a small internal differentiation (Leyland, 2015).

The emplacement of the dykes seems to have a lithological control. The density of intrusion is noted to decrease sharply on the divide between the lower and upper Ecca (Woodford and Chevallier, 2002). This is coincidental with the occurrence of the first sandstones in the Karoo Basin. The majority of the dykes are strata bound and are clustered between the upper Ecca and Beaufort Groups (Woodford and Chevallier, 2002).

Three major structural domains can be identified in the Karoo based on dyke distribution (Chevallier *et al*., 2001):

a) Western Karoo Domain: A zone of long and thick dykes trending east-west related to right-lateral shear deformation and north-northwest dykes characterise this domain, which stretches from Calvinia to Middleburg. The EW dykes can be followed for 500 km and are associated with NE p-type fractures and NW Riedel shears. The NNW dykes are regularly spaced, and their trend varies along their trajectory (Woodford and Chevallier, 2002)

b) Eastern Karoo Domain: It comprises two dyke swarms and extends from East London to Middleburg. One swarm has a curvilinear pattern trending EW along the coast and bending NNW to NS inland. The other has minor NNE trending dykes that likely represent extension (Woodford and Chevallier, 2002).

c) Transkei-Lesotho-Northern Karoo domain: It also has two major dyke swarms. Dykes with a NW trend in the Transkei (part of the Eastern Cape province) curving EW in the Free state and those trending NE that occur within and adjacent to the Lesotho basalts (Woodford and Chevallier, 2002).

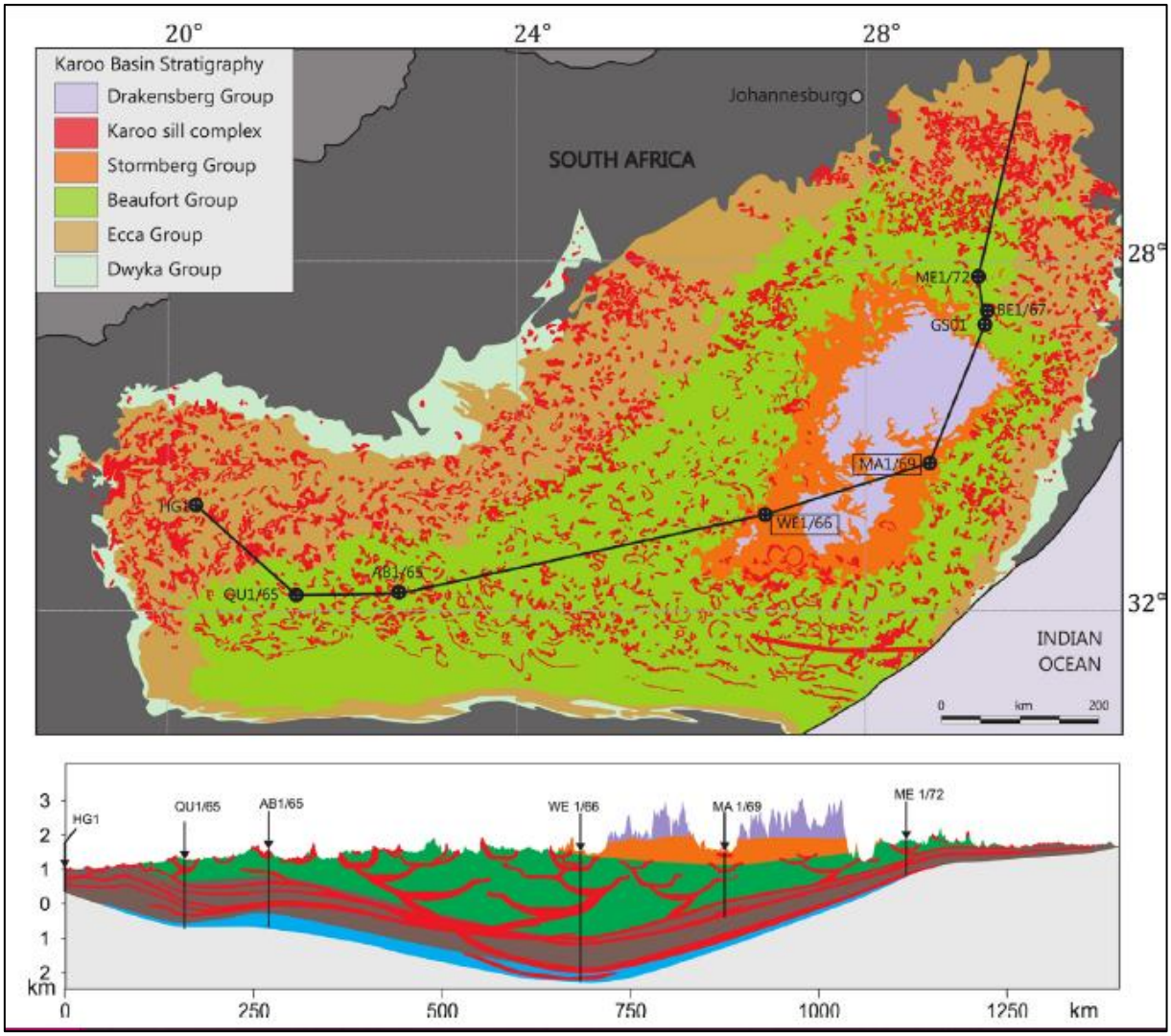

Figure 3.10: Sills emplaced in the Karoo Basin with the corresponding cross-section. (Modified from Svennson *et al.* (2012) in (Galland *et al.*, 2018)).

Figure 3.11 shows the structural domains identified. The Karoo dolerite dykes are sub-vertical and often have a dip above 70°. The dykes are commonly curved or dislocated at depth due to vertical offsetting resulting from vertical en-echelon segmentation or the interconnection of dykes between layers of sediment (Woodford and Chevallier, 2002). The dykes' attitude is illustrated in Figure 3.12, whose part a) shows the dislocated nature of the dykes. Fractures within the country rock are often associated with the emplacement of dykes.

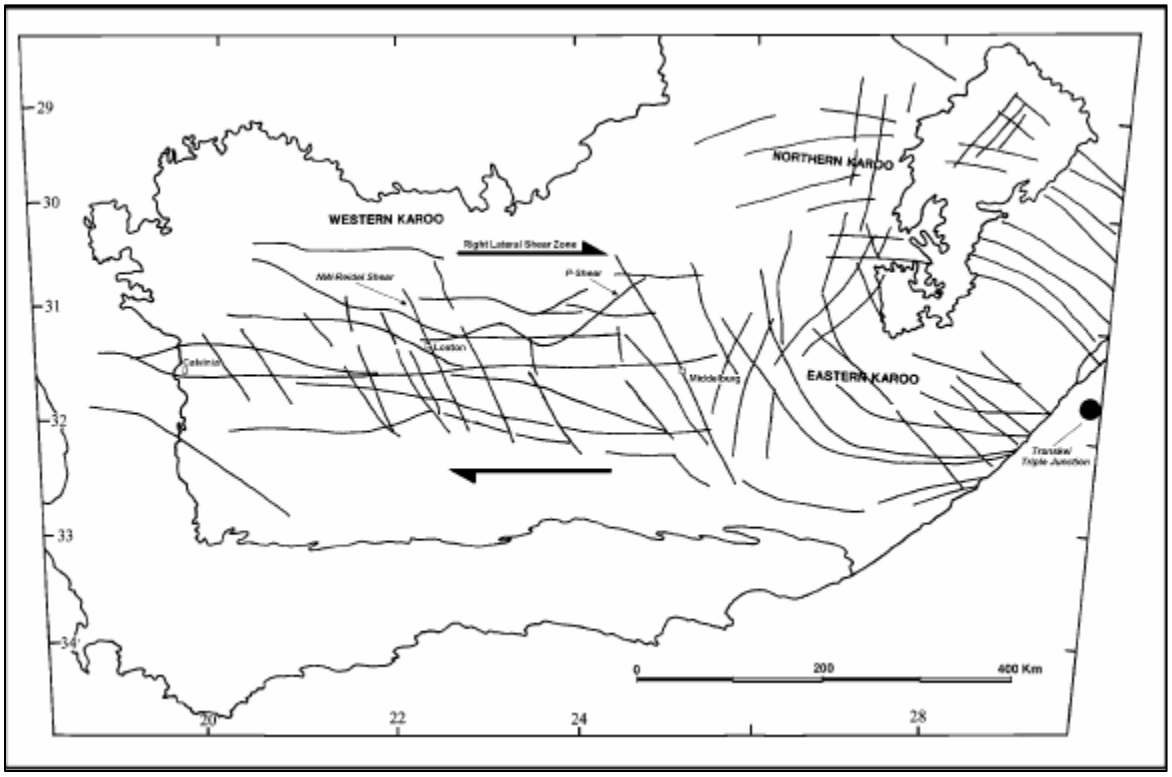

Figure 3.11: Structural domains of the Karoo Dolerites (Chevallier *et al*., 2001).

The emplacement-related fractures result in master joints parallel to the strike of the dyke that do not differ much from the thickness of the dyke itself (Woodford and Chevallier, 2002). Perpendicular to the edges of the dyke, thermal or columnar jointing occurs in the dyke, as shown in Figure 3.12 b). These perpendicular joints can extend up to 0.5 m within the country rock from the contact.

Near the dipping dyke, a localised up-warping of host rocks is often observed (Woodford and Chevallier, 2002), as illustrated in Figure 3.12 c). This upwarping is attributed to supergene formation of clays with a high expansion coefficient, which causes the apparent "swelling" of the host rock (Woodford and Chevallier, 2002). The way that the dykes cool is also apparent in the way they weather, with thick dykes (>8 m) having prominent chill margins and more prone to weathering. In contrast, thin dykes (<3 m) are more resistant to weathering and show a uniform pattern of shrinkage joints in outcrop (Woodford and Chevallier, 2002).

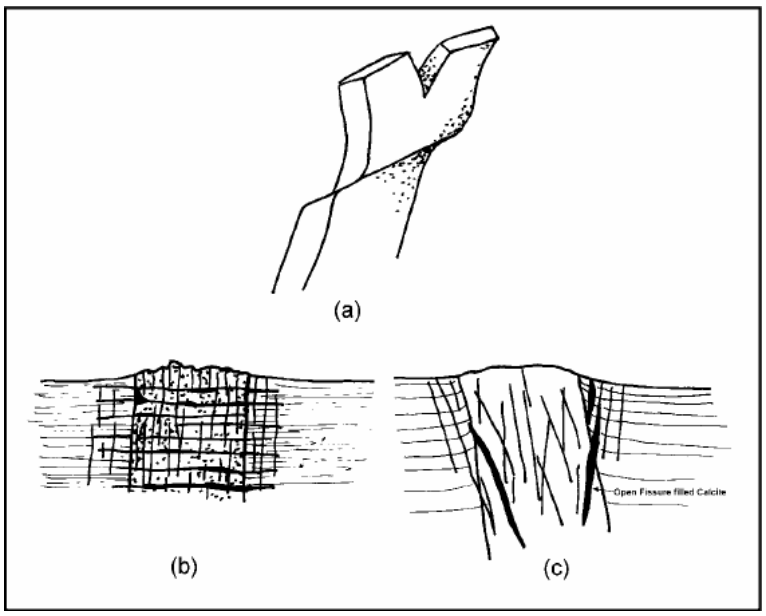

Figure 3.12: a) En-echelon dyke, b) Horizontal and vertical jointing within dyke, and c) Erosional unloading related jointing or fissures associated with tectonic reactivation and weathering (Woodford and Chevallier, 2002).

Dolerite sill and ring complexes are a major attribute of the present Karoo and share the same geographical distribution as the dolerite dykes (Chevallier *et al*., 2001). They are a very common form of intrusion within the basin and appear on satellite imagery as sub-circular saucer-like shapes whose rims are visible as topographical highs that outcrop in a ring-like manner (Chevallier *et al*., 2001). The dolerite sill to sediment ratio increases from the east of the basin, which shows that there was more intrusion in the elevated parts of the eastern basin (Woodford and Chevallier, 2002).

On a regional scale, the dolerite sills form a ring-within-ring structure. This typical structure can be seen in Queenstown, Eastern Cape, which is also regarded as a type area of these structures. It is also one of five major complex ring units in the basin. The dolerite ring structure of this town is shown in Figure 3.13. The sills show some stacking, and some inclined sills fed other similarly sized sills resulting in a box-like pattern (Woodford and Chevallier, 2002). The attitude and the stratigraphic level at which the sill intruded vary on the regional scale. More extensive sills occur towards the base of the Karoo, while the smaller ones are in the upper part of the Supergroup (Woodford and Chevallier, 2002).

At the bottom of the Karoo succession (at the contact between the Dwyka and Prince Albert Formations and between the Whitehill and Prince Albert Formations), long-wavelength undulating sills occur, structures similar to saucers are dominant in the middle (that is, within the Ecca and Beaufort) while at the top (below the Lesotho pile of basalt) flat-lying sills appear (Woodford and Chevallier, 2002).

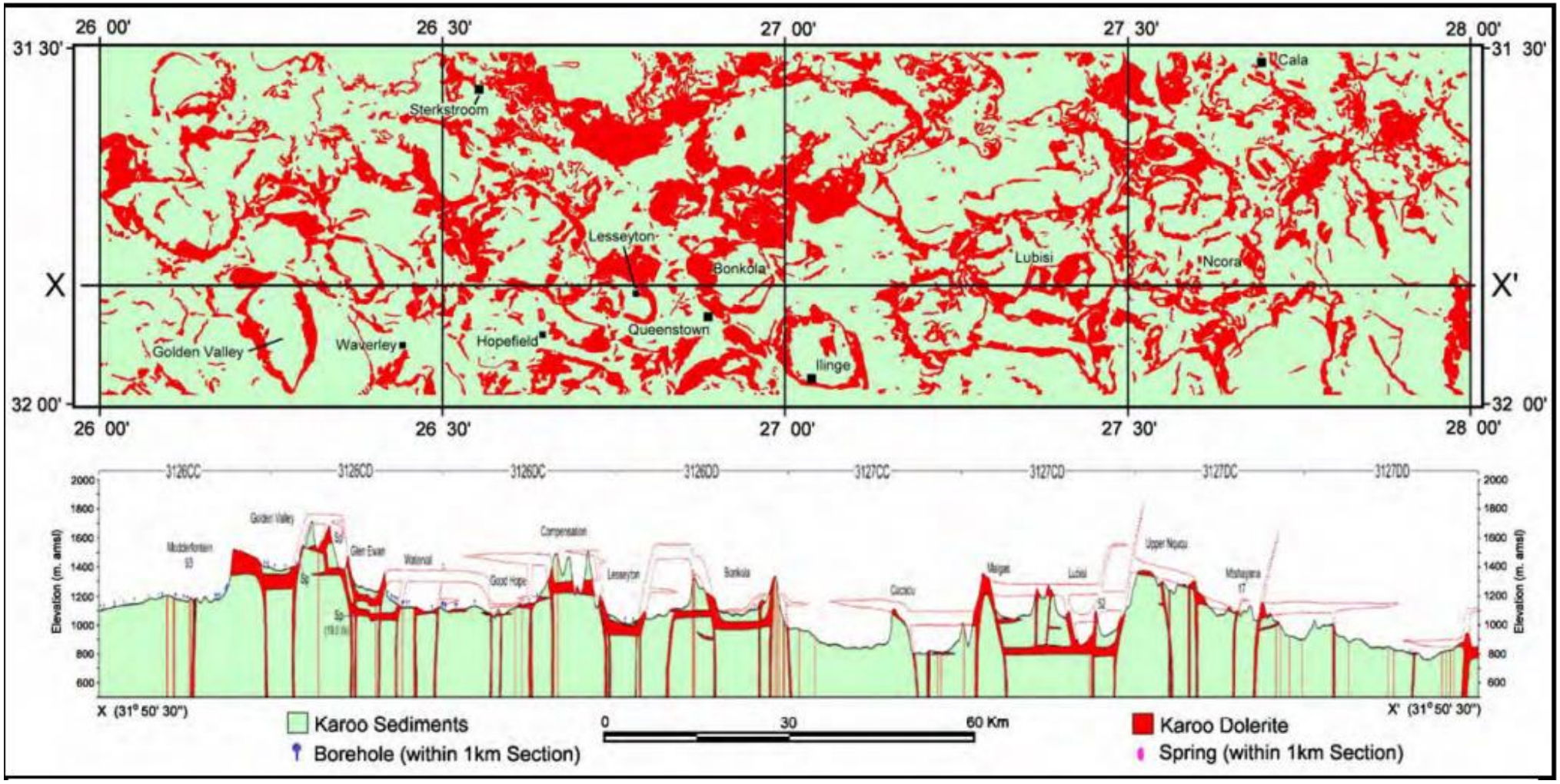

Figure 3.13: Queenstown ring and sill complexes with a corresponding cross-section (Woodford and Chevallier, 2002).

Chevallier *et al*. (2001) recognise three main types of fracturing within the dolerite sill and ring complex:

a) Well-developed vertical thermal columnar jointing in the flat-lying sill (Figure 3.14 f1)

b) Fractures parallel to the intrusion strike dominant in the inclined sheet (Figure 3.14 f2)

c) Open fractures that develop within the curved parts of the sill, which are often filled with secondary calcite and are well-developed, oblique or sub-horizontal (Figure 3.14 f3).

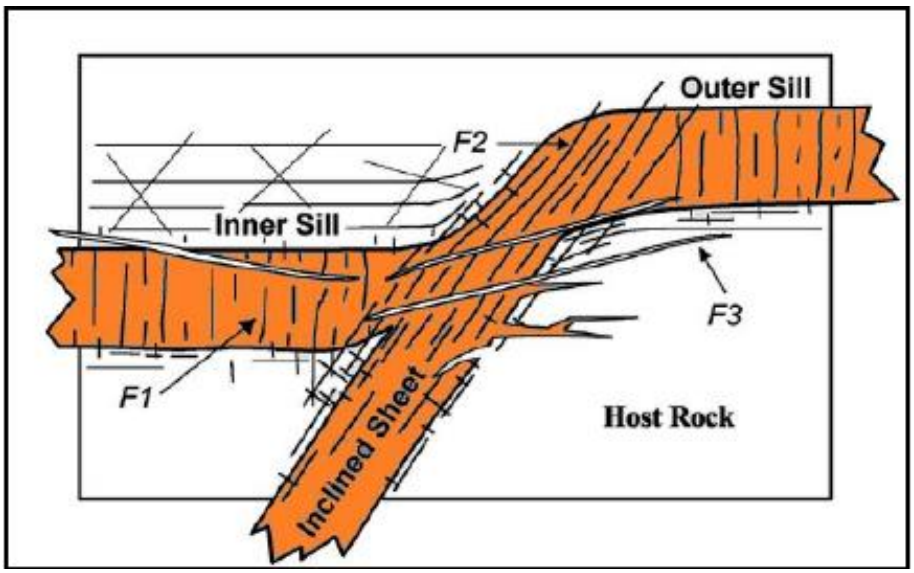

Figure 3.14: Fractures associated with sill and ring complexes (Chevallier *et al*., 2001)

The sill and ring complexes and dolerite dykes have an intricate relationship. The dykes are, in many instances, noted to feed the inclined sill sheets exerting some control on the ring complexes' shape, which can result in a jagged rim (Woodford and Chevallier, 2002). Some dykes branch out and merge with adjacent rings.

There are two models for the sill and ring complex emplacement. One envisages the sills as being laccolith shaped, thickening towards the centre, which is fed by dyke or plug, and the rings being the result of upwarping of overlying rock (Figure 3.15b). The other-the ring and dyke model describes a magma feeding system along the inclined sheet or the ring itself through a web of merged ring-dykes (Figure 3.15a). The 60° inward-dipping inclined sheet becomes an upper outer sill, which at the same time feeds a lower inner sill for this model.

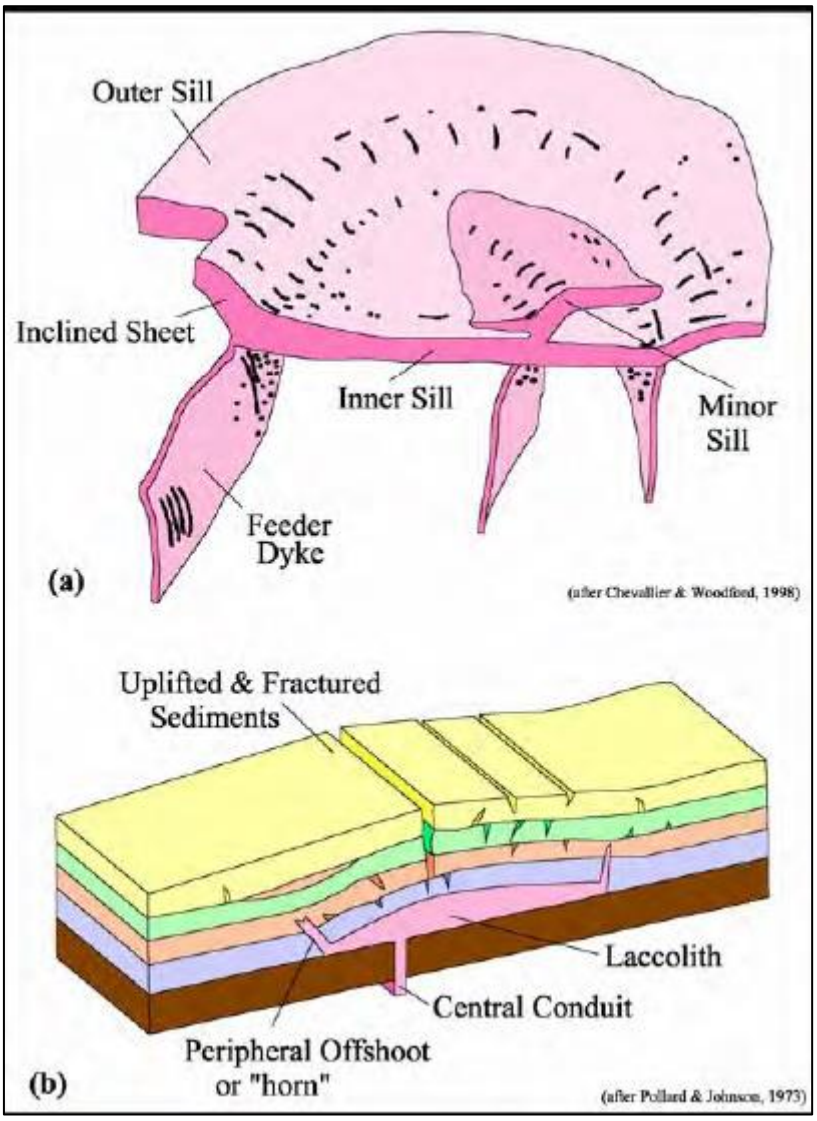

Figure 3.15: Dolerite sill and ring complexes models of emplacement a) ring/dyke model b) laccolith model (Woodford and Chevallier, 2002).

3.4.1.7 Dolerite breccia plugs and volcanic vents

These have a widespread geographic occurrence but are similar in texture, shape, size and hydrological properties (Woodford and Chevallier, 2002). Their occurrence is shown in Figure 3.16.

Dolerite Breccia Plugs

These are mainly confined to the Ecca and often occur in groups along the northern and western fringes of the Karoo Basin. Cluster diameter varies from a few hundred metres to fifty kilometres. These breccia plugs are normally found as small circular, low-relief hills with a diameter of 50-80 m (Woodford and Chevallier, 2002). Sometimes, they can be seen as negative relief features which are circular and have calcrete development. They may be identifiable by a white alteration halo around them in aerial photographs (Woodford and Chevallier, 2002).

Two facies can be identified (Woodford and Chevallier, 2002):

1. Molten Facies: The sediment is molten, baked, domed, re-crystallized, deformed, and contains xenolith from the underlying strata. Amygdales often occur, whose composition may be quartz and calcite, with grossular and vesuvianite to a lesser extent.
2. Breccia Facies: A true breccia with broken, crushed, and fractured rock fragments that have been re-cemented, often accompanied by mineralization of various minerals such as calcite, quartz, gypsum, or galena.

The molten facies is less resistant to erosion than the breccia facies and is the type most often encountered in the field (Woodford and Chevallier, 2002). It is proposed that when the early (lowermost dykes) intruded into the partially hardened "wet" sediments of the Karoo Supergroup, localised hydrothermal activity occurred. This caused the host sediments to become brecciated and also resulted in the mobilisation and upwards transportation of elements from the Prince Albert and Whitehill Formations (Woodford and Chevallier, 2002).

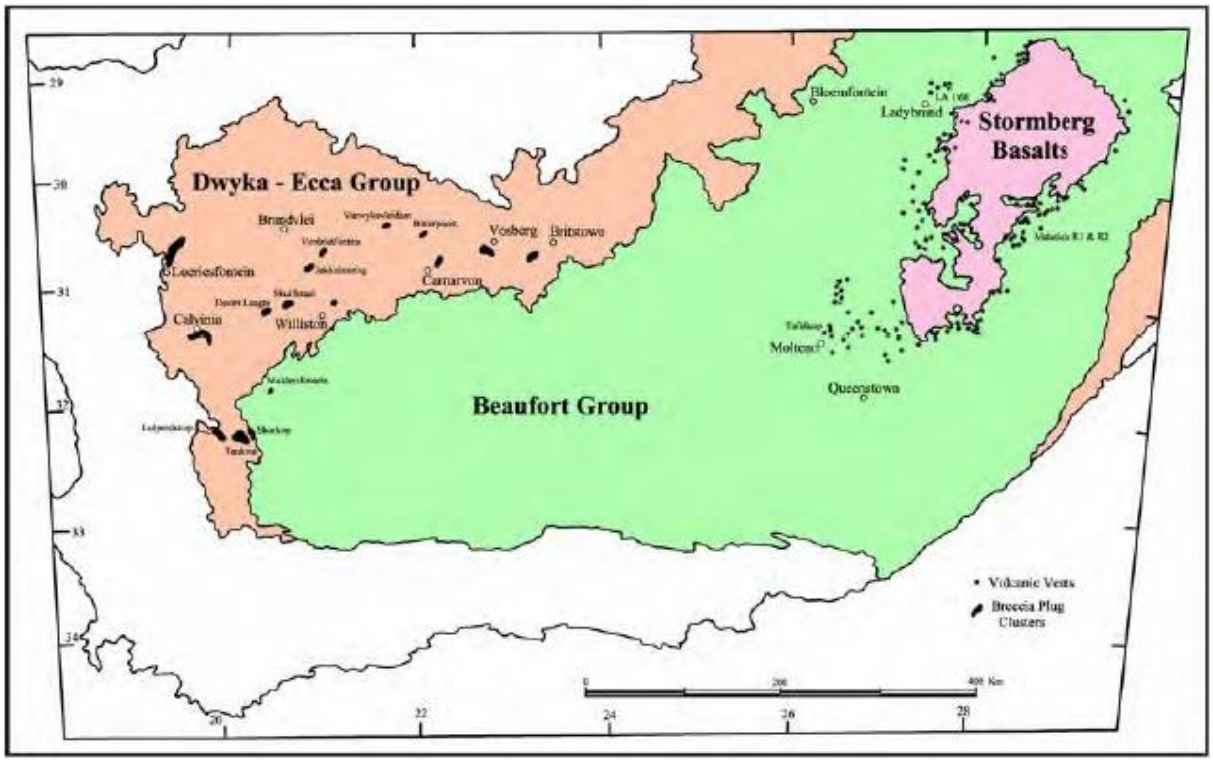

Figure 3.16: Geographic distribution of volcanic vents and breccia plugs in the main Karoo Basin (Woodford and Chevallier, 2002).

Volcanic Vents

Many occur at the foothills of the Drakensberg and are limited to the Clarens Formation. They are representative of the first volcanic eruptions that occurred before the lava flows. Their size varies from a few metres to some kilometres. They consist of yellowish tuff mixed with agglomerate, made of shattered and pulverised Clarens sandstone, and contain clasts of amygdaloidal basalt (Woodford and Chevallier, 2002).

Phreatic explosive activity is the likely cause of the formation of the volcanic vents. When magma encounters groundwater, phreatic explosions occur, leading to shattering, fluidisation and mobilisation of host sediments (Woodford and Chevallier, 2002).

3.4.1.8 Kimberlites and associated alkaline complexes

The kimberlites often exist as groups of linear or bow-shaped swarms or dykes and fissures related to some pipes, blows or enlargements (Woodford and Chevallier, 2002). The geographic extent of the kimberlites and linked fractures is shown in Figure 3.17. Several swarms can be distinguished in the area, but generally, a kimberlite swarm can be divided into smaller-sized sub-swarms (Woodford and Chevallier, 2002). Kimberlite fracture swarms are also made of parallel fissures and related joints or fractures. The space between each sub-swarm is close, some 10 m-50 m, with fissures 0.4 m-5 m wide (Woodford and Chevallier, 2002).

Kimberlite intrusions are often inconspicuous and are only encountered after drilling through 6 m-12 m of weathered material. On the surface, it can be visible as a sparse occurrence of weathered kimberlite called “green ground” or micaceous calcrete called “yellow ground” (Woodford and Chevallier, 2002). Kimberlite diatremes are not common in the western Karoo but are more common on the Kaapvaal craton. The manner in which kimberlites were formed has long been debated (Field *et al*., 2008).

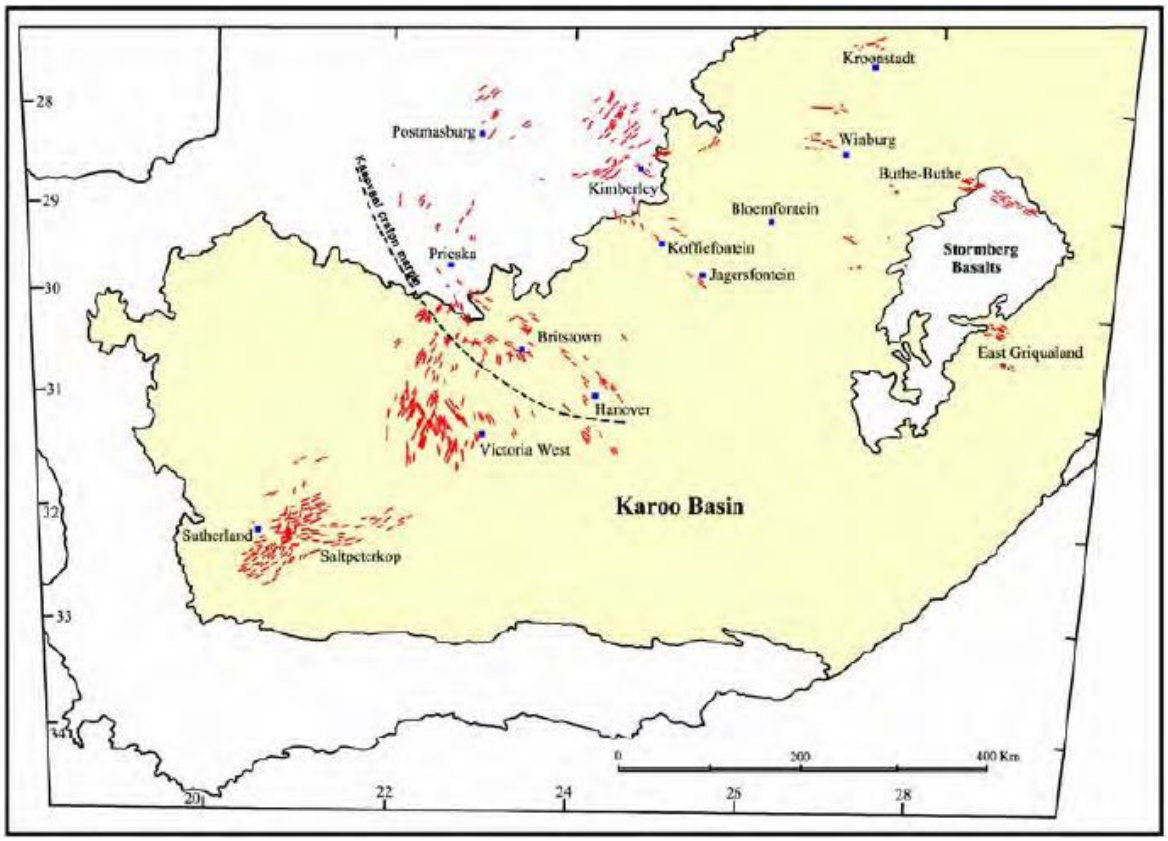

Figure 3.17: Geographic extent of Karoo Kimberlites and associated fractures (Woodford and Chevallier, 2002).

3.4.2 The Cape Supergroup

The Cape Supergroup is an assemblage of Early Palaeozoic aged rocks that outcrops along South Africa's southern and southwestern margins (Shone and Booth, 2005). Other similarly aged rocks, the Msikaba Formation and Natal Group, outcrop along the south-eastern margin of the country (Shone and Booth, 2005). These are correlated with the Cape Supergroup because of their lithological and age similarities. Figure 3.18 shows the location of these metasedimentary rocks.

The majority of the Cape Supergroup lies in a laterally continuous thrust and fold belt (Cape Fold Belt), which stretches for 1300 km along South Africa's southwestern coast (Hansma *et al*., 2016). The Msikaba Formation and Natal Group are relatively undeformed (Shone and Booth, 2005). According to Shone and Booth (2005), these sediments may have all been deposited in the Cape Basin. Only the rocks proper to the Cape Supergroup will be considered in this section.

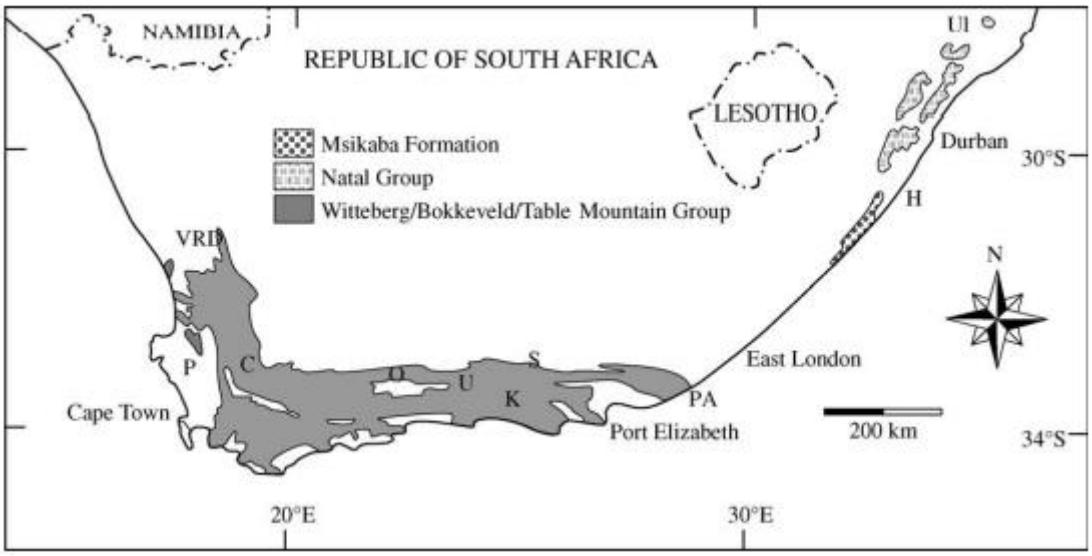

Figure 3.18: Location of the Cape Supergroup Outcrop. (C = Ceres, H = Hibberdene, K = Kareedouw, O = Oudtshoorn, P = Piketberg, PA = Port Alfred, S = Steytlerville, U = Uniondale, Ul = Ulundi, VRD = Vanrhynsdorp) (Shone and Booth, 2005).

The Cape Supergroup succession was deposited in a sea (the Agulhas) formed in an aborted rift on the ancient supercontinent Gondwana (Tankard *et al*., 1982; McCarthy and Rubigde, 2005). Pre-cape rocks consisting of quartzites, schists, gneisses and metamorphosed carbonates (Booth, 2011) and granites (Blake, Mlisa and Hartnady, 2010) form the basement of the Supergroup. The consensus is that the rocks were deposited between the early Ordovician and the Carboniferous before being subjected to deformation during the Permian to the Triassic (de Beer, 2002).

The Supergroup can be separated from youngest to oldest into three groups, namely (McCarthy and Rubigde, 2005):

- Witteberg Group

- Bokkeveld Group
- Table Mountain Group

The strata are generally composed of clastic metasedimentary rocks (mostly quartzites and phyllite), which have undergone nothing more than lower-grade greenschist metamorphism (Shone and Booth, 2005). Figure 3.19 shows the regional setting and lithological units of the Cape Fold Belt (CFB).

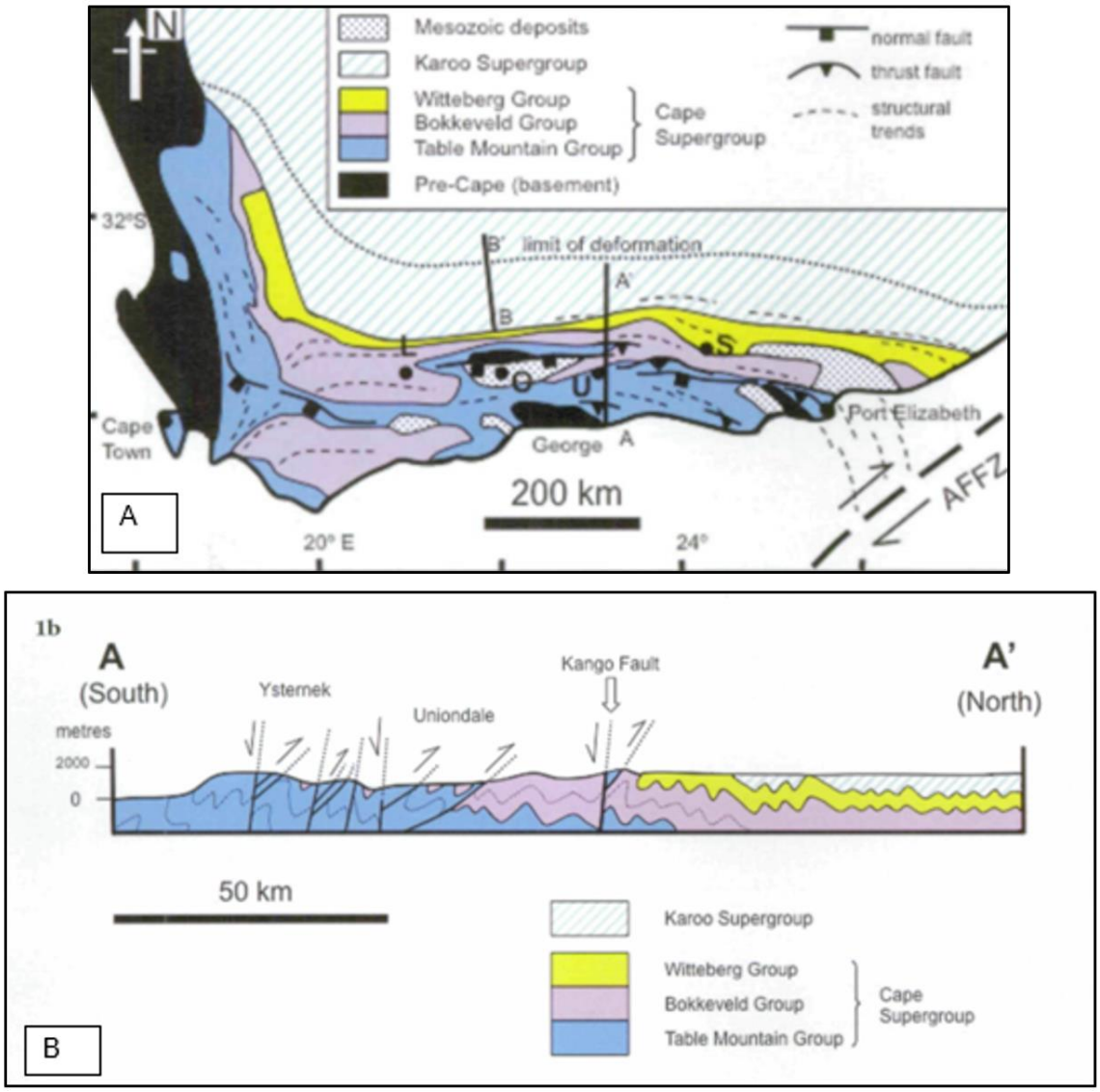

Figure 3.19: A. Map illustrating the regional setting of the Cape Fold Belt and its lithostratigraphic units. AFFZ - Agulhas Falklands Fracture Zone; S - Steytlerville; U = Uniondale; O = Oudtshoorn and L = Ladismith. B. is a cross-section from A-A' showing main structural characteristics (Booth, 2011).

3.4.2.1 The Table Mountain Group

This is the lowermost section of the Cape Supergroup. It was deposited between the early Ordovician and the Early Devonian time (Tankard *et al.*, 1982) in a shallow marine to terrestrial environment and

is composed of approximately 4000 m of quartz arenites, mudstones, and conglomerates (Mpofu *et al.*, 2020). It is underlain by the shales and mudstones of Malmesbury Group which have been intruded into by the Cape Granite Suite granites (Miller *et al.*, 2017).

The lithostratigraphic units vary in thickness in the western and eastern parts of the basin (Tankard *et al.*, 1982; Mpofu *et al.*, 2020). It can be divided into six units, which are given in Table 3.1. The Piekenierskloof Formation is the bottom unit of the TMG, whose lower contact with pre-cape rocks is an angular unconformity (Shone and Booth, 2005).

Table 3.1: The Table Mountain Group stratigraphy. Modified from (Tankard *et al.*, 1982; Mpofu *et al.*, 2020)).

Western Cape			Eastern Cape		
Formation	Thickness (m)	Lithology	Formation	Thickness (m)	Lithology
Nardouw Subgroup			Baviaanskloof	150	Shale, sandstone;marine invertebrates
			Skuwerberg	350	Sandstone, white weathering
	1100	Coarse grained quartz arenite; trace fossils	Goudini	250	Sandstone,brown weathering
Cedarberg	140	Fine grained sandstone, siltstone, and mudstone; marine invertebrates	Cedarberg	50	Shale, mudstone, fine grained sandstone
Parkhuis	120	Sandstone, conglomerate, diamictite	Peninsula	2150	Medium to coarse grained quartz arenite with quartz pebbles; trace fossils
Peninsula	1800	Medium to coarse grained quartz arenite with quartz pebbles; trace fossils	Sardinia Bay	950	Sandstone, conglomerate, phyllitic shale
Graafwater	400	Interbedded quartz arenite, siltstone, and mudstone; trace fossils			
Piekenierskloof	800	Conglomerate and coarse grained sandstone			

The Graafwater and Sardinia Bay Formations are about 700 km apart and outcrop at the western and eastern ends of the CFB, respectively (Shone and Booth, 2005). The former has an outcrop thickness of 424 m in its type area (de Beer, 2002), while the latter is 180 m thick in Sardinia Bay west of Gqeberha (Shone and Booth, 2005).

The Peninsula Formation outcrops in both the eastern and western parts of the CFB and is, in essence, a sequence of stacked thrust bounded quartzitic units (Shone and Booth, 2005). Large scale planar

and trough cross-bedding, low angle cross lamination, and horizontal cross lamination are observed in the Peninsula Formation (Shone and Booth, 2005).

Pakhuis Formation overlies the Peninsula Formation, and it comprises glacially derived sediment but is limited to the western section of the basin (de Beer, 2002). The Cedarberg Formation grades from the Pakhuis Formation. Its basal member is an important marker unit (de Beer, 2002; Shone and Booth, 2005). It outcrops continuously from the western to the eastern end of the CFB (de Beer, 2002).

The Nardouw Subgroup is separated into three formations; the lowermost Goudini Formation, the middle Skurweberg Formation, and the upper, laterally equivalent Rietvlei and Bavianskloof Formations in the west end of the belt (de Beer, 2002). It usually has an abrupt contact with the Bokkeveld Group dark shales, which it underlies (de Beer, 2002).

3.4.2.2 The Bokkeveld Group

This Group comprises a sequence of mudrocks with fresh black surfaces, dark grey to olive-coloured siltstones, and grey to olive-grey fine-grained sandstones (Shone and Booth, 2005). It was deposited in a deltaic environment, receiving large amounts of sediment, reaching a thickness of 1500 m in the Western Cape and 3200 m in the Eastern Cape (Tankard *et al*., 1982).

This assemblage of rocks is characterised by upwards coarsening sequences which imply it was deposited in a period of transgressions and regressions (Tankard *et al*., 1982). The stratigraphy of the Bokkeveld group is given in Table 3.2. In the sandstones of the Bokkeveld Group, wave ripple structures and hummocky stratification are common (Shone and Booth, 2005). A diverse range of fossils is found in the Bokkeveld Group (Tankard *et al*., 1982; Shone and Booth, 2005).

Table 3.2: The Bokkeveld Group stratigraphy. Modified from (Tankard *et al.*, 1982).

Western Cape				Eastern Cape			
Subgroup	Formation	Thickness (m)	Lithology	Subgroup	Formation	Thickness (m)	Lithology
Bidouw	Karoopoort	50	Siltstone and quartz arenite with shale interbeds	Traka	Sandpoort	400	Red shale, siltstone, quartz arenite
	Osberg	55	Feldspathic sandstone and quartz arentite				
	Klipbokopp	170	Mudstone, greywacke, and lithic arenite		Adolphspoort	620	Siltstone, quartz arenite
	Wuppertal	65	Quartz arenite, lithic arenite,siltstone				
	Waboomberg	200	Siltstone, quartz arenite, shale, black shale near top		Karies	1200	Shale, siltstone, quartz
Ceres	Boplaas	30	Quartz arenite and lithic arenite	Ceres	Boplaas	100	Feldspathic sandstone, quartz arenite, mudstone
	Tra-Tra	85	Mudstone, siltstone, subordinate sandstone		Tra-Tra	350	Mudstone, siltsone, sandstone
	Hex River	100	Arkose, lithic arenite, and quartz		Hex River	70	Lithic arenite, quartz arenite, siltstone, and sandstone
	Voorstehoek	115	Siltstone, shale, fine-grained sandstone		Voorstehoek	300	Siltstone, shale, fine-grained sandstone
	Gamka	135	Feldspathic sandstone, quartz arenite, mudstone		Gamka	200	Feldspathic sandstone, quartz arenite, mudstone
	Gydo	160	Black shale and siltstone		Gydo	600	Shale, siltstone, fine-grained sandstone

3.4.2.3 The Witteberg Group

It is a continuation of the Bokkeveld sedimentary patterns (Tankard *et al.*, 1982) and is the Cape Supergroup's northernmost outcrop (Mpofu *et al.*, 2020). The Witteberg primarily consists of thinly interbedded sandstones and shales with a horizon of diamictite at the top of the sequence (Shone and Booth, 2005; Mpofu *et al.*, 2020). Near-horizontal lamination, wave ripple structures, planar and trough crossbedding, and hummocky stratification are some sedimentary structures occurring in the Witteberg Group (Shone and Booth, 2005).

According to Tankard *et al*. (1982), the boundaries of the Witteberg are unclear due to its affinity with the Bokkeveld and the overlying Karoo. The stratigraphy of the Witteberg is given in Table 3.3. The Group is divided into three subgroups: Kommadagga, Lake Mentz, and the Weltevrede Subgroups (Mpofu *et al.*, 2020). Like the underlying Bokkeveld and TMG, the Witteberg has been subjected to thrusting and folding.

Table 3.3: The Witteberg Group lithostratigraphy. Modified from (Tankard *et al*., 1982; Mpofu *et al.*, 2020).

Western Cape				Eastern Cape				Interpretation
Subgroup	Formation	Thickness (m)	Lithology	Subgroup	Formation	Thickness (m)	Lithology	
				Kommadaga	Dirkskraal	175	Feldspathic sandstone, lithic arenite	Fluvial
					Soutkloof	170	Mudstone, shale, vervite	Proglacial lacustrine
					Swaartwaterspoort / Millers	100	Intertonguing sandstone, diamictite	Glaciofluvial, glaciogenic
Lake Mentz	Waaipoort	70	Mudstone, rhythmite, greywacke, thin conglomerate; fish and plant fossils	Lake Mentz	Waaipoort	340	Gray shale, mudstone, feldspathic sandstone; plant and fish fossils	Glaciofluvial and lacustrine
	Floriskal	60	Feldspathic sandstone; plant fossils		Floriskal	80	Shale, mudstone, quartz arenite; plant fossils	Fluvia and shore zones
	Kweekvlei	130	Black fossil shale		Kweekvlei	225	Shale, siltstone	Lacustrine shelft (?)
	Witpoort	310	Orthoquartzite, rare shale lenses		Witpoort	850	Orthoquartzite with rare shale lenses	Barrier sands, tidal flats
Weltervrede	Swartruggen	450	Siltstone, shale		Weltevrede	850	Shale, siltstone, thick orthoquartzite	Tidal flats, barrier sands of reworked delta, subaqueous delta
	Blinkberg	135	Interbedded sandstone					
	Wagendrift	185	Orthoquartzite, shale, siltstone, interbedded sandstone					

3.4.3 The Namaqua-Natal Metamorphic Province

The Kaapvaal Craton and its cover sequences are bound by the Namaqua-Natal Province. It was created during a specific, geochronologically defined tectonomorphic event and is a sizable area of uninterrupted structural fabric with definite borders (Cornell *et al*., 2006). This province occurs along the southern and western edges of the craton (Cornell *et al*., 2006). It comprises igneous and metamorphic rocks metamorphosed or formed from 1200 Ma to 1000 Ma during the Namaqua Orogeny (Cornell *et al*., 2006).

In the Northern Cape province, the rocks outcrop for 100 000 km^2 (Namaqua sector) while they outcrop for 20 000 km^2 in KwaZulu Natal (Natal sector) (Cornell *et al*., 2006). The Namaqua-Natal province geological extent is shown in Figure 3.20.

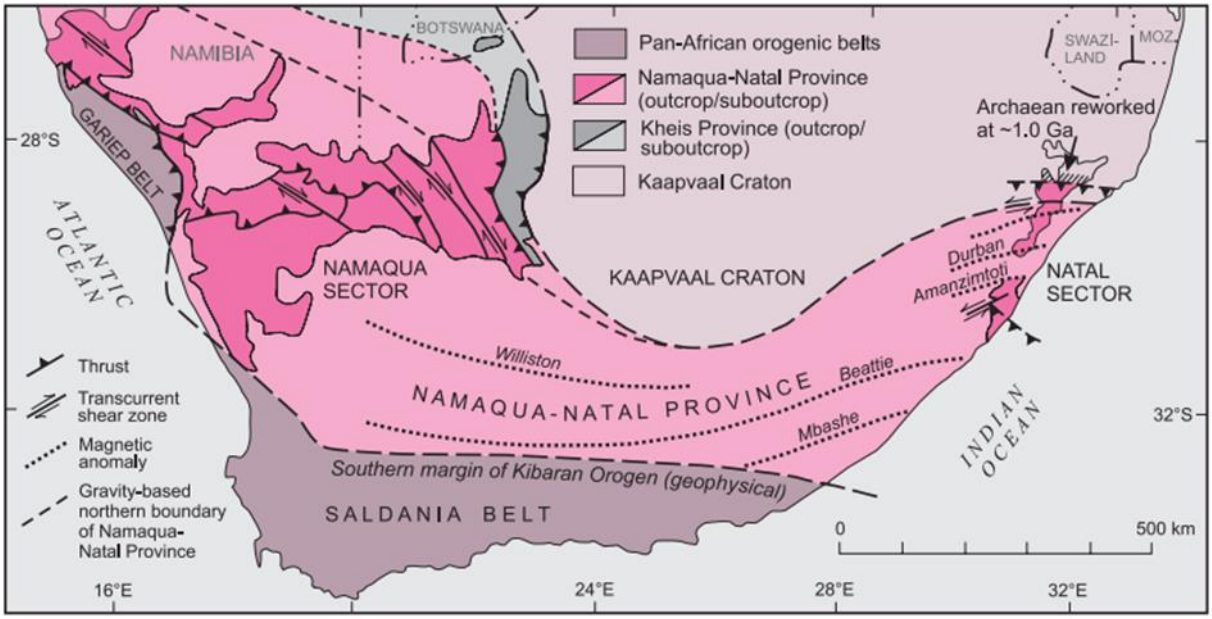

Figure 3.20: The Namaqua-Natal Province geological setting (Cornell *et al*., 2006).

The two sectors are segments of a continuous arcuate 400 km wide and 1400 km long orogenic belt beneath the Karoo Supergroup (Cornell *et al*., 2006). The Namaqua-Natal Province can be separated into several tectonostratigraphic terranes constructed during the Namaqua orogeny (Cornell *et al*., 2006). Three main components are (Cornell *et al*., 2006):

a) Reworked ~200 Ma Kheisian (late Palaeoproterozoic) rocks

b) Juvenile supracrustal and plutonic rocks ~1600 Ma-1200 Ma

c) Voluminous syn- and post-tectonic granitoids formed ~1200 Ma-1000 Ma

3.4.3.1 The Namaqua Sector of the Namaqua-Natal Province

The divisions of Thomas, Agenbacht, Cornell, *et al*. (1994) will be referred to here. The sector is flanked by the Kheis Province along its eastern margin (Figure 3.21), which has ~3000 Ma, ~2000 Ma, and ~1300 Ma low-grade supracrustal rocks (Cornell *et al*., 2006).

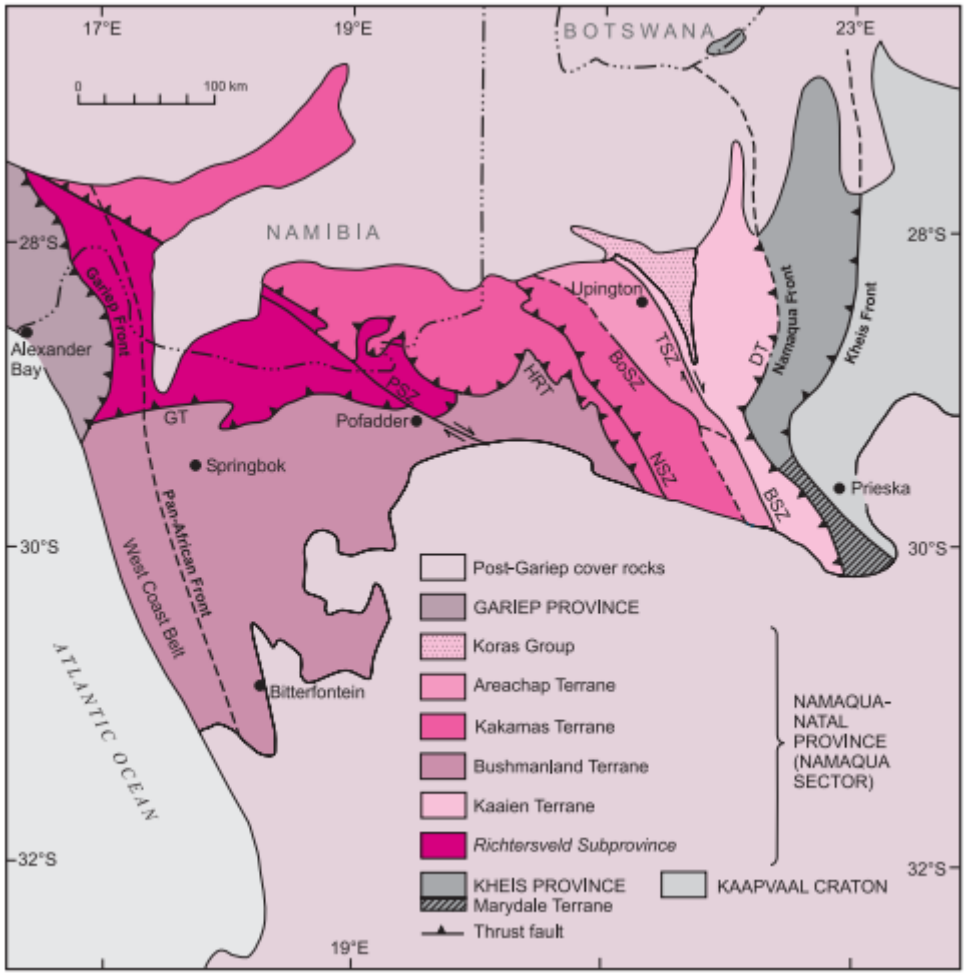

Figure 3.21: The Namaqua sector tectonic subdivision. PSZ: Pofadder Shear Zone, GT: Groothoek Thrust, NSZ: Neusberg Shear Zone, BoSZ: Boven Rugzeer Shear Zone, BSZ: Brakbosch Shear Zone, DT: Dabep Thrust, HRT: Hartbees River Thrust. (Cornell *et al*., 2006).

The Namaqua sector can be separated into five domains, as shown in Figure 3.21:

a. Richtersveld Subprovince: ~2000 Ma low to medium-grained supracrustal rocks and intrusions in the northwestern section (Cornell *et al*., 2006). It covers about 29000 km^2 and is bounded by thrusts. Its components are the Orange River Group, which comprises reworked volcaniclastic sediments and subaerial volcanic rocks, and the Vioolsdrif Suite, which is an extensive granitoid batholith (Cornell *et al*., 2006)

b. Bushmanland Terrane: ~2000 Ma granitic gneisses, 1600-1200 Ma amphibolite to granulite grade supracrustal rocks, and 1200-1000 Ma granitoids occur here. It is the sector's largest crustal block and covers an area of 60000 km^2 (Cornell *et al*., 2006). The terrane consists of three groups: a basement complex of granitic rocks, a mixed variety of supracrustal sequences rocks of sedimentary/volcanic origin, and suites of syn- and late-tectonic Namaquan intrusive rocks of granitic to charnockitic composition (Cornell *et al*., 2006).

c. Kakamas Terrane: It is on the east of the Bushmanland Terrane and is in contact with the Areachap terrane in the east. It consists of about 2000 Ma supracrustal metapelite, Namaquan granitoids and Namaquan fabric (Cornell *et al*., 2006). East of the Neusberg Shear Zone, calc-arenite and arenite dominate, whereas, in the west, slivers of high-grade metapelite and biotite-garnet paragneisses are predominant (Cornell *et al*., 2006).

d. Areachap Terrane: Juvenile ~1300 Ma arc-related supracrustal rocks and ~1000 Ma granitoids with a pervasive Namaquan fabric (Cornell *et al*., 2006). It consists of amphibolite-grade metabasic and intermediate granitoid gneisses of the Areachap Group intruded by Keimoes Suite granitoids (Cornell *et al*., 2006).

e. Kaaien Terrane: Bound by the Dabep Thrust in the east and the Brakbosch-Trooilapspan Shear Zone system in the west. It comprises deformed early Namaquan volcano-sedimentary rocks, Kheisian metaquartzites and undeformed but thermally metamorphosed bimodal metamorphic rocks. The thick sequences of deformed quartzites forming this terrane represent a shift from the Kheis Province and Kaapvaal Craton rocks to the Areachap Formation high-grade rocks (Cornell *et al*., 2006).

3.4.3.2 The Natal Sector of the Namaqua-Natal Province

This sector can be divided into three tectonostratigraphic terranes flanked by discontinuities and consists of very different rock types and metamorphic grades (Cornell *et al*., 2006). The rocks accumulated in a northeastern direction onto the Kaapvaal Craton's southern edge. The tectonic setting of the Natal sector is shown in Figure 3.22.

The northern margin of the sector is modelled as an imbricate thrust zone in which ophiolite rocks were obducted northwards onto the craton during the Namaqua Orogeny, while the boundary to the south is buried under a Phanerozoic cover (Cornell *et al*., 2006). Its contact with the Saldania belt was geophysically modelled. It is worth noting that WSW trending aeromagnetic anomalies several kilometres wide that form a striped pattern are typical of the Natal sector (Cornell *et al*., 2006). Tectonostratigraphic terranes of the Natal Sector are (A cross-section throughout the sector is shown in Figure 3.23):

i. Tugela Terrane: This is interpreted as an allochthonous ophiolite complex consisting of rocks of oceanic composition (Cornell *et al*., 2006). This complex was obducted onto the craton's southern margin (Cornell *et al*., 2006). It can be divided into a greenschist facies known as the Natal thrust belt in the north and the Natal thrust nappe in the south. The former is a 2-5 km wide, imbricate zone dipping south and is subdivided into the Ntingwe and Mfongozi Groups (McCourt *et al*., 2006). The Ntingwe Group comprises non-schistose dolomite,

limestone, shale, mudstone and conglomerate, while the Mfongozi Group is a bimodal succession of schistose metatholeiites alternating with quartz-muscovite schist (McCourt *et al*., 2006).

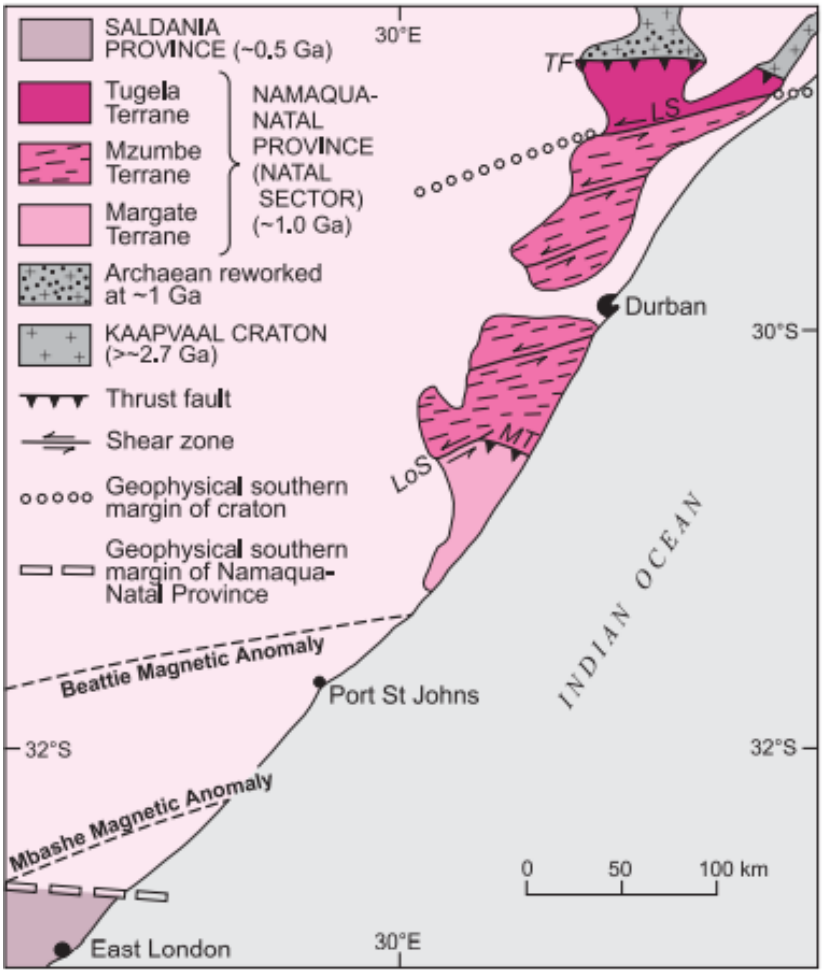

Figure 3.22: Namaqua-Natal province tectonic subdivisions of the Natal Sector. TF=Tugela Front, LS=Lilani-Matigulu Shear, LoS=Lovat Shear, MT=Melville Thrust (Cornell *et al*., 2006).

The Natal Nappe complex comprises a west plunging thrust stack, the nappes in the stack (top-down); Nkomo, Madidima, Mandleni, and Tugela thrust sheets (Cornell *et al*., 2006; McCourt *et al*., 2006). The nappes are composed of layered, locally garnetiferous, amphibolite, and migmatite, along with subordinate quartzo-feldspathic gneisses, rare metapelite (quartz + biotite + sillimanite + garnet), and magnetite quartzite (McCourt *et al*., 2006).

ii. Mzumbe Terrane: It comprises an older succession of amphibolite-grade supracrustal gneisses, which cover about 25% of the visible surface area, intruded by voluminous pre-, syn- and late-tectonic granitoid suites (Cornell *et al*., 2006). Its oldest rocks are part of the Mapumulo Group, which comprises amphibolite grade supracrustal gneisses. The group is further separated into the Quha Formation – a sequence of grey, biotite–hornblende–quartz–

plagioclase±garnet gneiss and migmatite of mostly intermediate composition, with interbanded amphibolite (plagioclase, hornblende ± quartz, and clinopyroxene) (McCourt *et al*., 2006). The other division is the Ndonyane Formation, characterised by strongly foliated felsic gneisses and migmatite. They consist of albite, quartz, biotite and microcline (McCourt *et al*., 2006).

iii. Margate Terrane: It is the southernmost element of the Natal Sector and extends south from the Melville Thrust to the phanerozoic cover rocks (Cornell *et al*., 2006; McCourt *et al*., 2006). Granitoid gneisses dominate this terrane. The oldest rocks belong to the Mzimkulu Group, which is in turn divided into the Leisure Bay, Marble Delta, and Mucklebraes Formations (McCourt *et al*., 2006). Meta pelitic rocks with subordinate calc-silicate gneisses are common in the Leisure Bay Formation. Carbonate rocks dominate the Marble Delta Formation, while mafic granulite and calc-silicate rocks characterise the Mucklebraes Formation (McCourt *et al*., 2006).

The Mzumbe and Margate Terranes were intruded by plutons and batholiths of voluminous rapaviki textured granitoid and charnorckite called the Origibi suite (Cornell *et al*., 2006). This intrusion followed the arc-continent collision that juxtaposed the two terranes (Cornell *et al*., 2006).

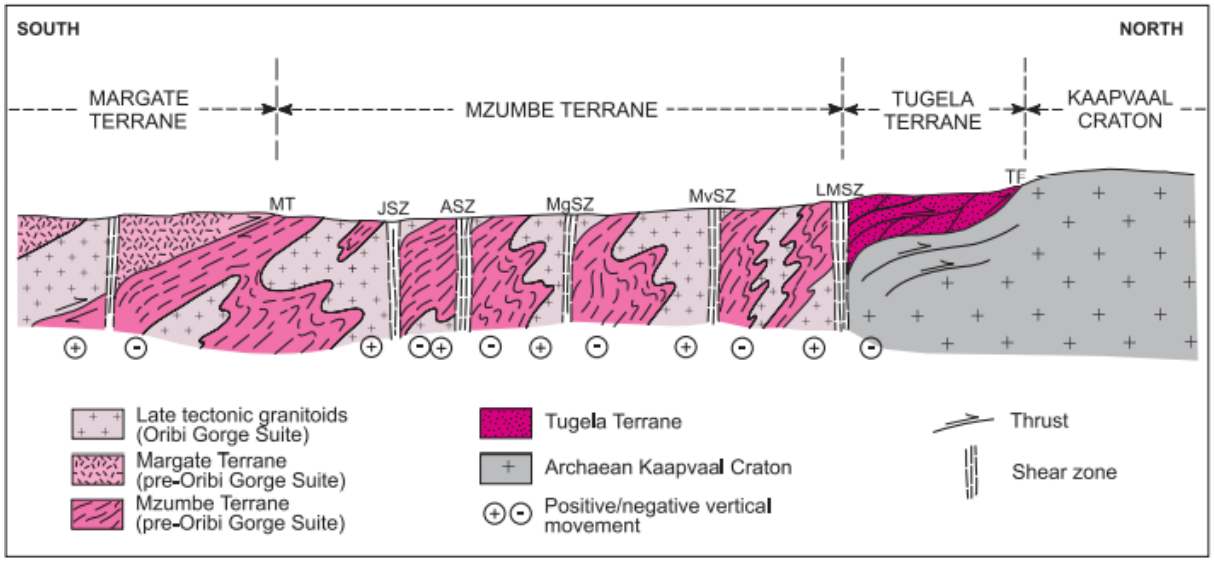

Figure 3.23: Schematic N-S cross-section through the Natal Sector. MvSZ = Mvoti Shear Zone, MT = Melville Thrust, MgSZ = Mgeni Shear Zone, LMSZ = Lilani-Matigulu Shear Zone, JSZ = Jolivet Shear Zone, ASZ = Amanzimtoti Shear Zone. (Cornell *et al*., 2006).

3.4.4 The Bushveld Igneous Complex

The Bushveld Igneous Complex (BIC) formed approximately 2060 Ma ago, covers an area of 65000 km^2 and is the largest known mafic intrusion on Earth (Eales and Cawthorn, 1996; Scoon and Viljoen, 2019). It consists of the Rustenburg Layered Suite, Lebowa Granite Suite, Rashoop

Granophyre Suite, and the Rooiberg Group (Mukherjee, Latypov and Balakrishna, 2017; Skursch *et al*., 2020). Figure 3.24 shows a simplified map of the Bushveld Igneous Complex. The Rashoop Granophyre Suite is omitted from the illustration.

The complex outcrops in four discontinuous lobes (western, far western, northern, and eastern) (Mukherjee, Latypov and Balakrishna, 2017). Bushveld Complex rocks have intruded into the Palaeoproterozoic age Transvaal Supergroup sedimentary rocks, which also form its basement (Mukherjee, Latypov and Balakrishna, 2017). The western and eastern lobes of the BIC are shown to be connected at depth; however, their connection with the northern and southern lobes remains ambiguous (Webb, Ashwal and Cawthorn, 2011).

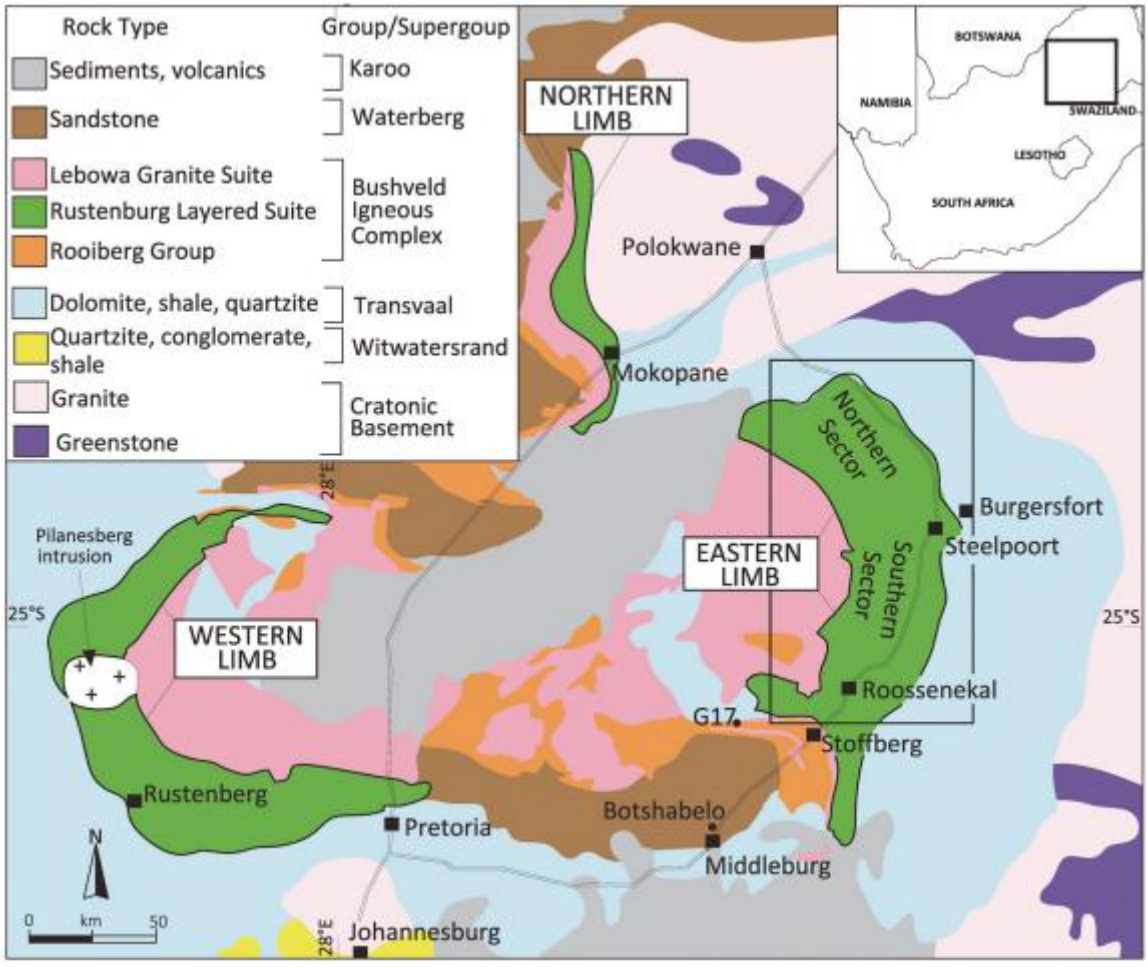

Figure 3.24 Regional geological map of the Bushveld Complex. The three main limbs of the Rustenburg Layered Suite are shown (Scoon and Viljoen, 2019).

3.4.4.1 The Rustenburg Layered Suite

The Rustenburg Layered Suite is the world's largest layered mafic intrusion (Scoon and Viljoen, 2019). It occurs in four limbs which surround the Lebowa Granite Suite, as shown in Figure 3.24 (Skursch *et al*., 2020), and a fifth limb (the southeastern limb inferred at depth). The cumulates of the

RLS are 7-9 km thick and are divided into five zones based on the appearance of different cumulus minerals (Eales and Cawthorn, 1996; Mukherjee, Latypov and Balakrishna, 2017):

i. Marginal Zone: Noritic to gabbro-noritic composition. It is hundreds of metres thick. The unlayered medium-grained rocks underlie most of the Complex (Eales and Cawthorn, 1996)

ii. Lower Zone (LZ): 2 km thick zone that is ultramafic in composition. Consists of harzburgite and orthopyroxenite (Mukherjee, Latypov and Balakrishna, 2017)

iii. Critical Zone (CZ): this zone has the highest concentration of chromitites. The zone is split into the Lower Critical Zone and the Upper Critical Zone (Mukherjee, Latypov and Balakrishna, 2017). The former is predominantly composed of orthopyroxenite, with harzburgite appearing in two intervals (Mukherjee, Latypov and Balakrishna, 2017). The upper critical zone is based on the appearance of the first cumulus plagioclase. This zone comprises norite, anorthosites, and pyroxenites (Mukherjee, Latypov and Balakrishna, 2017). The upper critical zone (Upper Group 2 and Merensky reef) contains large concentrations of platinum group elements (PGE) (Eales and Cawthorn, 1996).

iv. Main Zone (MZ): 2-3 km thick and has a composition of norites and gabbronorites. According to Eales and Cawthorn (1996), the boundary between the CZ and MZ is difficult to locate. The MZ cumulates lack olivine, chromian spinel, and the impressive layering of the CZ (Eales and Cawthorn, 1996)

v. Upper Zone (UZ): 1-2 km thick and consists of magnetite, gabbronorite, and anorthosite. The first occurrence of magnetite characterises this zone (Eales and Cawthorn, 1996)

3.4.4.2 The Lebowa Granite Suite

The Lebowa granite suite is a differentiated layered intrusion with an area of 30000 km^2 and is 1.5-3.5 km thick (Kinnaird, Kruger and Cawthorn, 2003). It is found beneath the felsic Rooiberg Group volcanics and the Rashoop Granophyre Suite sills (Kinnaird, Kruger and Cawthorn, 2003). These granites are younger than the RLS because feeder dykes of the granite cut through the RLS eastern limb (Kinnaird, Kruger and Cawthorn, 2003; Scoon and Viljoen, 2019). The LGS granites are generally alkali feldspar granites with iron-rich ferromagnesian minerals, silica content between 71% and 77%, low calcium oxide content, and a potassium oxide/sodium oxide >1 (Kinnaird, Kruger and Cawthorn, 2003).

LGS is divided into seven facies (SACS, 1980):

i. Nebo Granite: The most dominant member. Perthitic alkali feldspar, plagioclase, quartz, hornblende, and biotite are typical (Kinnaird, Kruger and Cawthorn, 2003). It contains fluoride

ii. Lease Granite: Aplitic facies.

iii. Bobbejaankop Granite: Red and coarse-grained granite which contains fluorite.

iv. Verena Granite: Coarse-grained porphyritic granite.

v. Balmoral Leucogranite: porphyritic texture.

vi. Makutso Granite: Locally porphyritic and biotite rich.

vii. Klipkoof Granite: medium to fine-grained.

The Lease and Bobbejaankop Granites are important textural variants of the Nebo granite (Hill *et al*., 1996). The Verena, Balmoral, Makutso, and Klipkoof Granites are geographically limited facies (Kinnaird, Kruger and Cawthorn, 2003).

3.4.4.3 The Rashoop Granophyre Suite

The Rashoop granophyre suite is confined to occurrences within granite or along the contact of the LGS with the RLS (Skursch *et al*., 2020). The suite is separated into three units based on variations in texture (Skursch *et al*., 2020). The units are (SACS, 1980):

i. Stavoren Granophyre: It has the largest volume and a ferroan composition. It consists of quartz, feldspar, hornblende, biotite and minor phases (Skursch *et al*., 2020). It consists predominately of coarse-grained intergrown quartz and alkali feldspar (Skursch *et al*., 2020). The other subdivisions are of similar composition to the Stavoren Granophyre.

ii. Zwartbank Pseudogranophyre: Composed of irregular quartz feldspar intergrowth

iii. Rooikop Granophyre Porphyry: Possesses a porphyritic texture.

A fourth unit called the Diepkloof Granophyre is defined. Its texture is similar to that of the Stavoren Granophyre but is of a different composition (Cawthorn *et al*., 2006)

3.4.4.4 The Rooiberg Group

The Rooiberg Group volcanics overlie unconformably the Pretoria Group volcano-sedimentary sequence of the Transvaal Supergroup (Jolayemi *et al*., 2020). The volume of the Group lies between 200000-300000 km^3, earning it a place among the world's largest silicic volcanic rock accumulations (Jolayemi *et al*., 2020). Age relations suggest that the Rooiberg is the oldest unit of the BIC. However, the overlap in the ages of the Rooiberg and the mafic components can not be overruled as the dating of the Group is incomplete (Jolayemi *et al*., 2020). The roof of the intrusive RLS is formed by the Rooiberg Group rhyolites (Jolayemi *et al*., 2020).

From the base to the top, the Rooiberg Group can be split into four formations:

i. Dullstroom Formation: The rhyolites of this basal formation are reddish-brown to grey, are massive or have localised flow banding. It has a microcrystalline groundmass and is devoid of phenocrysts (Jolayemi *et al*., 2020).

ii. Damwal Formation: It is reddish-brown, aphanitic, and has phenocrysts. Its microcrystalline groundmass comprises quartz, plagioclase, and subordinate k-feldspar, while the phenocrysts are of plagioclase, k-feldspar, and quartz (Jolayemi *et al*., 2020)

iii. Kwaggasnek Formation: The microcrystalline groundmass of these rhyolites is dominated by quartz and plagioclase. Flow banding is more pronounced, and phenocrysts of quartz and plagioclase are present in minor amounts, with chlorite and hornblende as accessory phases. Some vesicles occur, with some being amygdales of quartz or chlorite (Jolayemi *et al*., 2020). Spherulites can be up to 3 m in diameter (Jolayemi *et al*., 2020)

iv. Schrikkloof Formation: Displays a microcrystalline to cryptocrystalline groundmass of feldspars and quartz. Phenocrysts include feldspar, plagioclase, and quartz (Jolayemi *et al*., 2020). The presence of clay minerals such as illite shows that these rocks have undergone alteration.

The position of the felsic Rooiberg Group in relation to other Bushveld Complex members is shown in Figure 3.25. Thicknesses of Rooiberg formations, magma types, and main lithologies are also summarised.

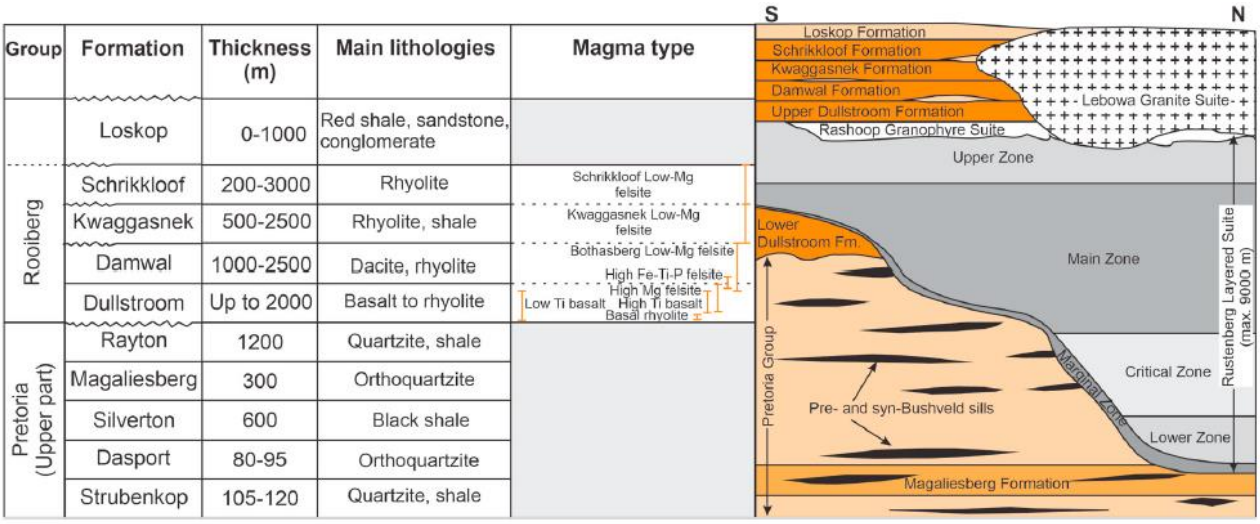

Figure 3.25: Schematic of Rooiberg Group lithologies and their relation with the other units of the BIC (Jolayemi *et al*., 2020).

3.4.5 The Transvaal Supergroup

The Transvaal Supergroup assemblage is conserved in three basins, the main Transvaal Basin, the Griqualand West Basin and the minor Kanye Basin in Botswana towards the west of the main

Transvaal Basin (Bumby *et al*., 2012). This Supergroup unconformably overlies the Ventersdorp Supergroup and was subjected to the Bushveld Igneous Complex intrusion in the main basin (Bumby *et al*., 2012). The succession was deposited between 2650 Ma and 2050 Ma (Moore, Tsikos and Polteau, 2001). The Transvaal Supergroup distribution is shown in Figure 3.26. Only the main Transvaal Basin and the Griqualand West Basin will be considered here.

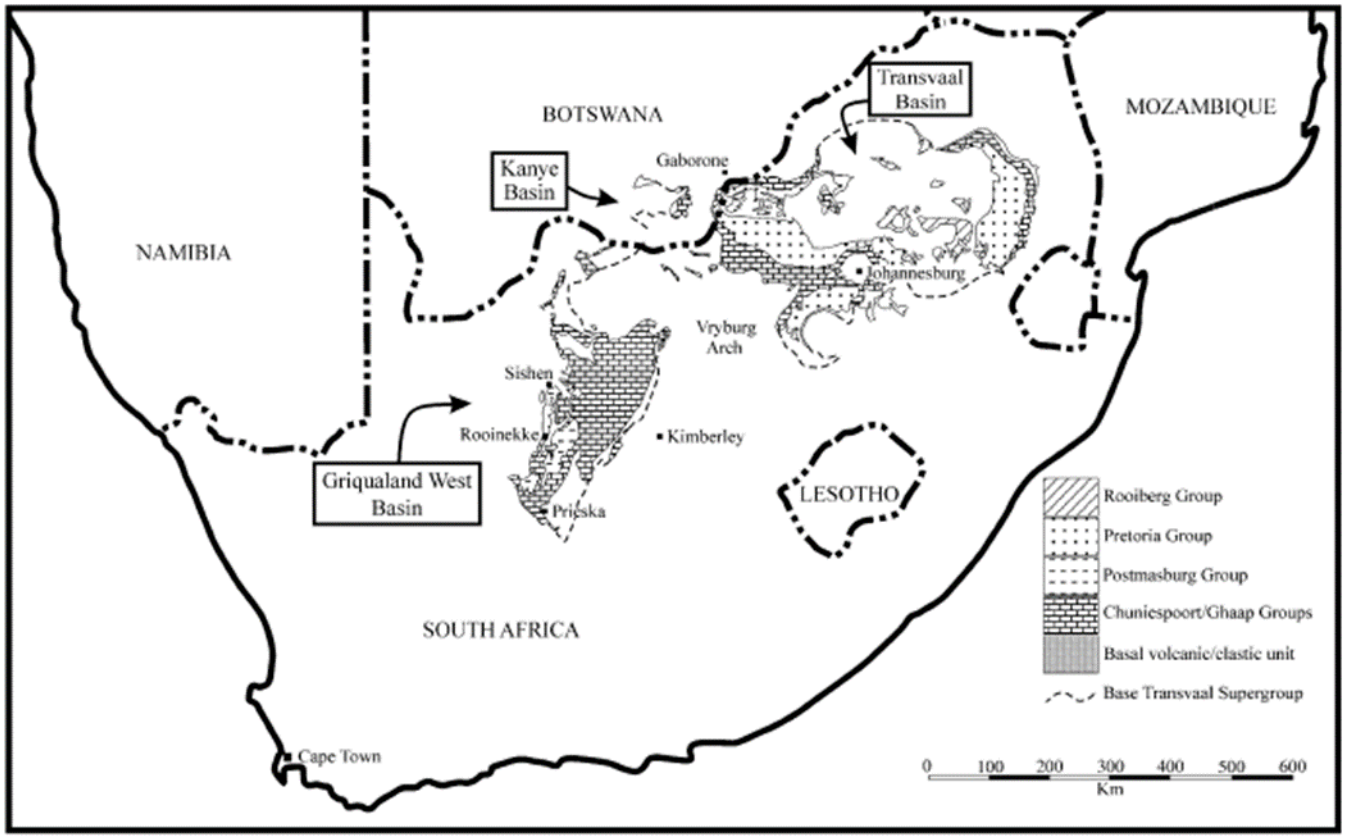

Figure 3.26: The Transvaal Supergroup distribution within its basins. The Rooiberg Group of volcanics of the Bushveld Complex are shown for reference (Moore, Tsikos and Polteau, 2001).

The Transvaal Supergroup (in the main basin) is divided into; basal protobasinal rocks, the Black Reef Formation, Chunniespoort Group and the Pretoria Group (Bumby *et al*., 2012). The protobasinal rocks are found only in the Transvaal Basin. The Griqualand West equivalents of the other rocks are the Vryburg Formation, Ghaap Group and the Postmasburg Group, respectively (Moore, Tsikos and Polteau, 2001; Bumby *et al*., 2012; Franchi and Mapeo, 2019).

3.4.5.1 Protobasinal rocks

These rocks were deposited in separate, fault-associated basins recognized as small-deep pull-apart basins related to strike-slip faults or larger rift basins related to extensional tectonism (Catuneanu and Eriksson, 1999). The Protobasinal rocks' basin-fill successions are preserved in isolated areas (Catuneanu and Eriksson, 1999). Figure 3.27 summarises the large-scale geometry of the basins, facies association and their inferred conditions of deposition (Bumby *et al*., 2012).

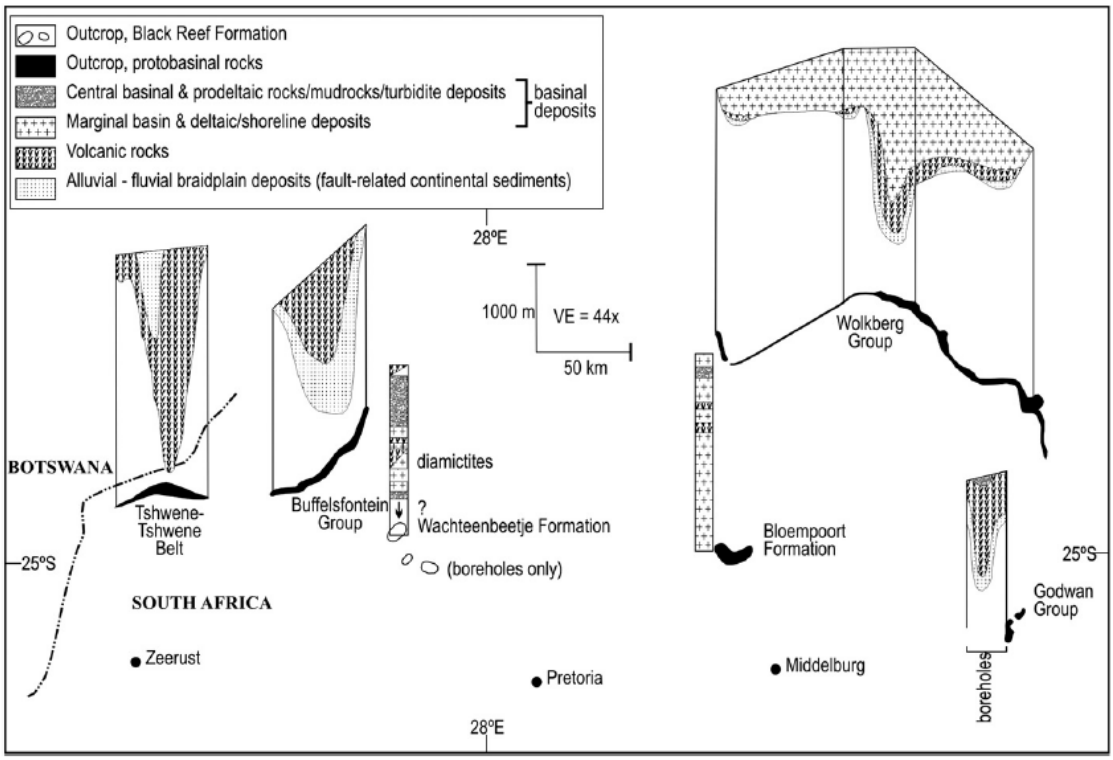

Figure 3.27: Fence diagram showing the Transvaal protobasinal rocks geometry and inferred depositional facies (Bumby *et al*., 2012).

3.4.5.2 The Black Reef and Vryburg Formations

The Black Reef Formation is made of about 30-60 m thick sandstones and overlies the protobasinal rocks (Bumby *et al*., 2012) unconformably. It may be divided into a lower upwards-fining sequence, consisting of basal conglomerates that grade into mature quartz arenites and mudstones, succeeded by an upper upwards-coarsening sequence of sandy rocks (Catuneanu and Eriksson, 1999). Figure 3.28 shows a generalised section through the Black Reef Formation.

In the Griqualand West basin, the Vryburg Formation is often correlated with the Black Reef Formation (Franchi and Mapeo, 2019). It overlies the Ventersdorp Supergroup unconformably and consists of about 30-100 m thick shales, siltstones, quartzites, and volcanic rocks (Bumby *et al*., 2012; Franchi and Mapeo, 2019).

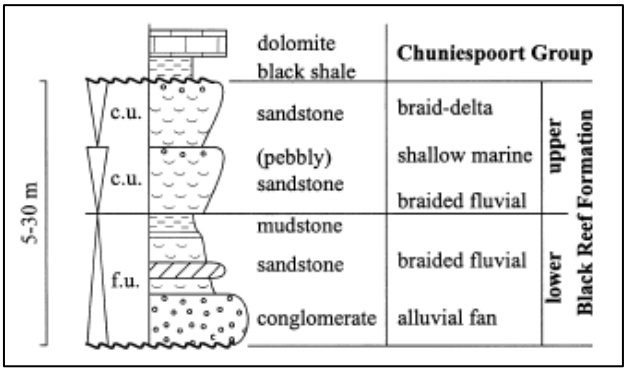

Figure 3.28: The Black Reef Formation generalised vertical profiles and environments. c.u. = coarsening upwards, f.u.= fining upwards (Catuneanu and Eriksson, 1999).

3.4.5.3 The Chunniespoort and Ghaap Groups

The Chunniespoort Group overlies the Black Reef Formation in the Transvaal Basin unconformably (Catuneanu and Eriksson, 1999). The group consists of seven formations with a sheet-like geometry (Catuneanu and Eriksson, 1999). The five formations of the Malmani Subgroup (Oaktree, Monte Cristo, Lyttelton, Eccles, and Frisco Formations) consist primarily of dolomites. They are differentiated on the basis of the type of stromatolite they have, their chert content, rare quartzites and interbedded subordinate carbonaceous mudstones (Catuneanu and Eriksson, 1999). This ~1200 m thick stromatolitic package grades into the Penge Formation, which is about 640 m thick (Catuneanu and Eriksson, 1999; Bumby *et al*., 2012).

The Penge Formation is comprised of macro- to micro-banded iron formation (BIF) with shard structures, minor interbedded carbonaceous mudstones and interclastic iron formation breccias (Catuneanu and Eriksson, 1999). A ~1100 m thick, mixed assemblage of chemical and clastic sedimentary rocks called the Duitchsland Formation overlies the Penge Formation (Bumby *et al*., 2012). It is the Chunniespoort Group's topmost formation and comprises dolomitic mudstones with interbedded dolomites and quartzites, a thick body of chert breccia, paleosols and two thin lava beds (Catuneanu and Eriksson, 1999).

The Ghaap Group, which is the equivalent of the Chunniespoort Group in the Griqualand West Basin, is more than 2500 m thick (Bumby *et al*., 2012). It is divided into the Schmidtsdrif, Campbellrand, Asbestos Hills, and Koegas Subgroups (Moore, Tsikos and Polteau, 2001). The basal Schmidtsdrift Subgroup lies unconformably on either the Ventersdorp Supergroup lava or upon crystalline Archaen Basement (Polteau, Moore and Tsikos, 2006). It comprises shales, quartzites, siltstones and lava (Polteau, Moore and Tsikos, 2006). The overlying Campbellrand Subgroup consists of a thick succession of stromatolitic limestones and dolomites, as well as some shale and chert (Polteau, Moore and Tsikos, 2006).

The Asbestos Hills Subgroup overlies the Campbellrand Subgroup conformably and consists predominantly of BIFs (Polteau, Moore and Tsikos, 2006). It is divided into the lower Kuruman Formation with microbanded BIFs and the upper Griquatown Formation with clastic-textured BIFs (Polteau, Moore and Tsikos, 2006). The Koegas Subgroup is the topmost unit of the Ghaap formation and is only preserved in the southwestern part of the basin (Prieska sub-basin) (Polteau, Moore and Tsikos, 2006). This subgroup consists of five formations (Pannatjie, Doradale, Kwakwas, Naragas, and Rooinekke Formations) comprising quartz wacke, shales, BIF, slate, and dolomites (Polteau, Moore and Tsikos, 2006).

3.4.5.4 The Pretoria and Postmasburg Groups

The Pretoria Group (Transvaal Basin) consists of 14 formations (Catuneanu and Eriksson, 1999), as shown in Figure 3.29. In general, the group encompasses about 6-7 km of argillaceous sedimentary rocks, subordinate interbedded sandstones, and two volcanic intervals (Bumby *et al*., 2012).

The lowermost formation of the Postmasburg Group, the Makganyane Formation, is developed all through the Griqualand West Basin (Polteau, Moore and Tsikos, 2006). The Makganyane Formation is separated from the Ghaap Group by an unconformity (Polteau, Moore and Tsikos, 2006). It ranges from 3 m to 500 m thick (Polteau, Moore and Tsikos, 2006). The formation consists of various rock types, such as massive to coarsely bedded diamictites, BIFs, shales, sandstones and stromatolite bioherms, with occurrences of carbonates set in a ferruginous matrix (Polteau, Moore and Tsikos, 2006).

The Ongeluk Formation is separated from the diamictites of the Makganyane Formation by a 1-3 m thick tuffaceous turbidite unit (Polteau, Moore and Tsikos, 2006). The Ongeluk Formation consists of continental flood-type basaltic andesites in which pillow lavas are common (Polteau, Moore and Tsikos, 2006). The overlying Voelwater Subgroup has a transitional contact with the Ongeluk Formation, the two being separated by black volcanic tuffs, hyaloclastites, and red haematitic jaspilites interbedded with BIF and diamictite (Polteau, Moore and Tsikos, 2006).

The Voelwater Subgroup is separated into two formations. The basal Hotazel Formation comprises BIF and diamictite lenses. Alternating chert-rich and magnetite-rich bands are typical of the Hotazel Formation (Polteau, Moore and Tsikos, 2006). It can be split into a lower, carbonate-poor member and an upper carbonate-rich one (Polteau, Moore and Tsikos, 2006). The overlying Mooidrai Formation is characterised by iron-bearing limestone, dolomite and minor chert (Polteau, Moore and Tsikos, 2006). The Mooidraai Formation has a conformable contact with the underlying Hotazel Formation and is the uppermost unit of the Transvaal Supergroup in the Northern Cape (Polteau, Moore and Tsikos, 2006).

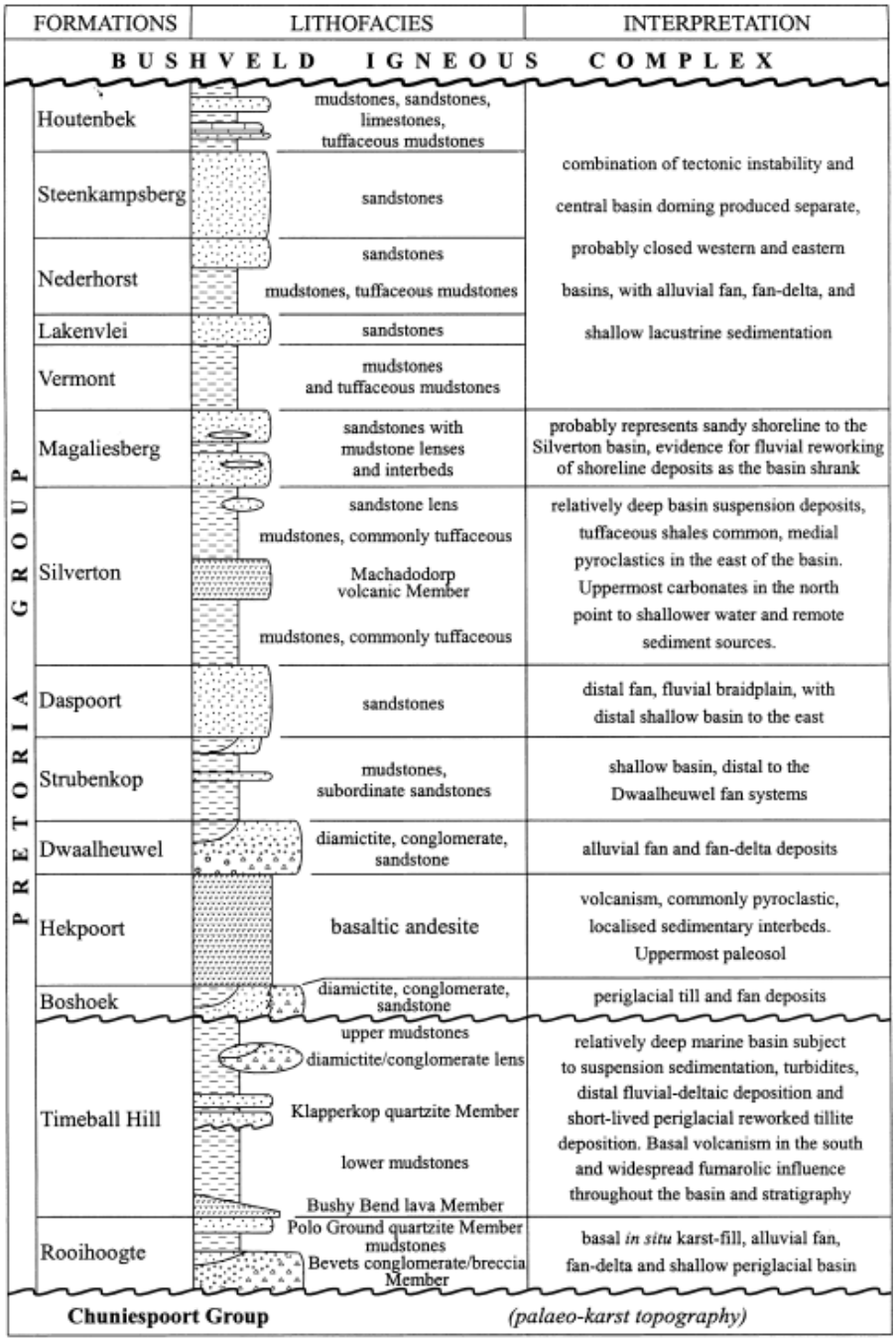

Figure 3.29: Lithostratigraphy of the Pretoria Group (Catuneanu and Eriksson, 1999).

3.4.6 The Ventersdorp Supergroup

The Neoarchaean (2714-2709 Ma) Ventersdorp Supergroup is a predominantly volcanic succession of rocks with a preserved thickness of approximately 5100 m and covers an area of 300000 km^2 (Eriksson *et al*., 2002; Humbert *et al*., 2019). It overlies the Witwatersrand Basin and other cratonic rocks unconformably (Bumby *et al*., 2012). The supergroup is separated into three units; the basal Klipriviersberg Group overlain by the Platberg Group, and the Bothaville and Allanridge Formations (Pniel Group) (Humbert *et al*., 2019). The Ventersdorp Supergroup and similar-aged dyke swarms distribution is shown in Figure 3.30.

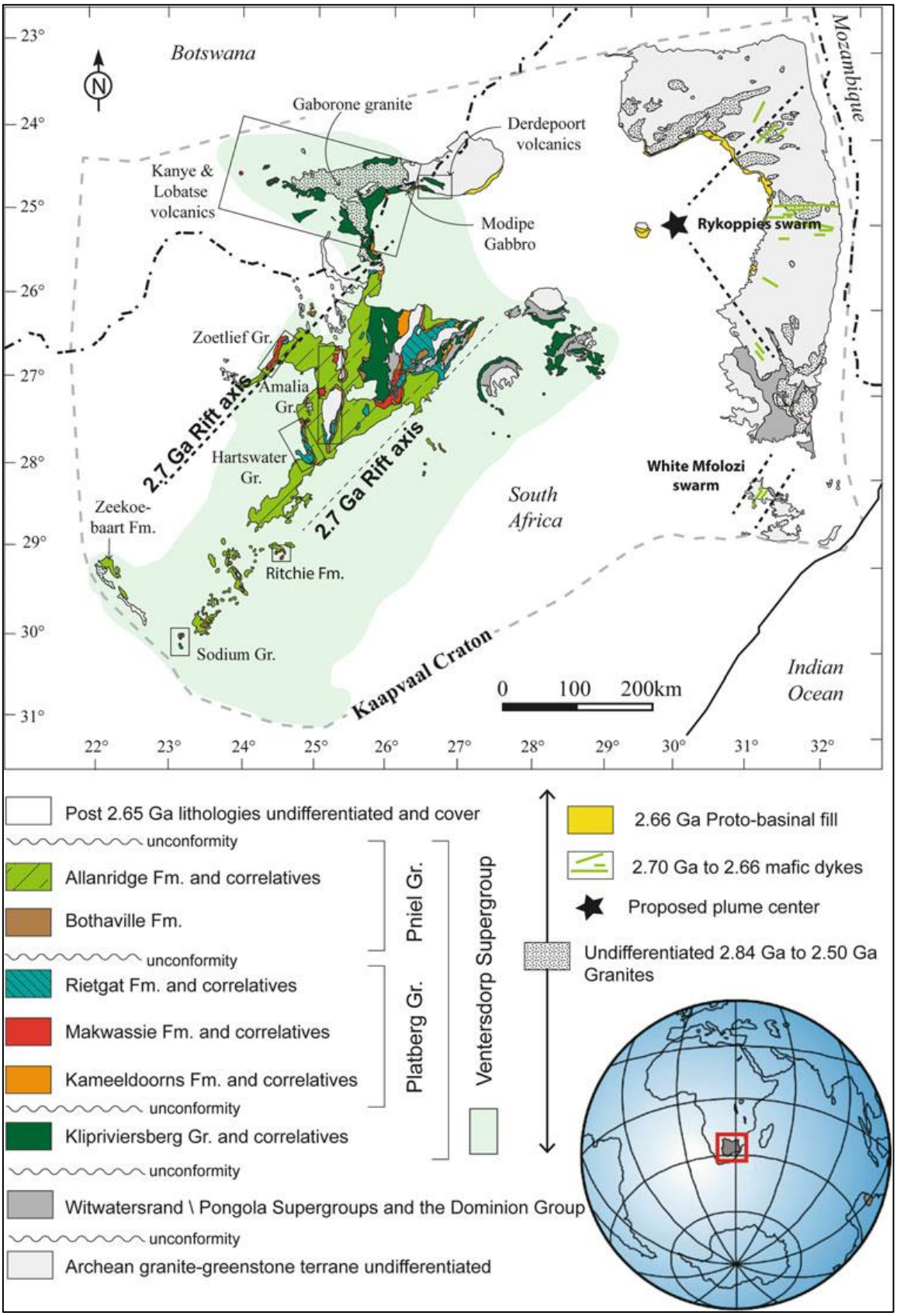

Figure 3.30: The Ventersdorp Supergroup's distribution on the Kaapvaal Craton (Humbert *et al.*, 2019).

3.4.6.1 The Klipriviersberg Group

The Klipriviersberg Group is the basal unit of the Ventersdorp Supergroup and is an approximately 1.5 km-2 km thick, locally komatiitic flood basalt (Bumby *et al*., 2012). It is split into the basal Venterspost Formation (~44 m thick), which is comprised of a conglomerate-(lava)-quartzite-shale succession with upper and lower units with komatiitic-basaltic lava between them (Eriksson *et al*., 2002).

The remainder of the Klipriviersberg Group consists of lavas with high magnesium and komatiite at the base and transition into tholeiitic basalts (Eriksson *et al*., 2002). This section can be divided into six formations based on features such as colour or the presence of amygdales (Humbert *et al*., 2019). These are the Westonaria, Alberton, Orkney, Jeanette, Loraine and Edenville Formations (Humbert *et al*., 2019). These formations constitute the bulk of the group.

3.4.6.2 The Platberg Group

An angular unconformity divides the graben fills of the Platberg Group from the underlying Klipriviersberg Group (Humbert *et al*., 2019). It is divided into four formations (Eriksson *et al*., 2002):

- Kameldoorns Formation: A clastic wedge deposit with immature sedimentary rocks interbedded with volcanic rocks
- Geodgenoeg Formation: Consists of intermediate feldspar porphyries with minor non-porphyritic mafic lavas. Rarely, minor tuffaceous rocks are interbedded with the mafic lavas and porphyries.
- Makwassie Formation: It consists of quartz-feldspar porphyries. The lava compositions are rhyolitic to dacitic and are interbedded with andesitic lava flows and thin sedimentary beds.
- Reitgat Formation: This uppermost part of the Platberg Group is composed of mafic lavas (often porphyritic and amygdaloidal), lesser intermediate volcanic rocks, tuffs and interbedded sedimentary rocks (such as gritstones, arkosic sandstones, tuffaceous siltstones, and stromatolitic cherty limestones).

3.4.6.3 The Pniel Group

The Bothaville and Allanrigde Formations that comprise this group have a blanket-like geometry and overlie the Platberg Group unconformably (Humbert *et al*., 2019).

a. Bothaville Formation: It is a predominantly arenaceous formation about 400 m thick (Eriksson *et al*., 2002). The formation is characterised by tuffaceous argillites found locally

and greywacke sandstones with mature quartzose sandstones (now quartzites) (Eriksson *et al*., 2002).

b. Allanridge Formation: It is about 750 m thick and consists of predominantly fine amygdaloidal and porphyritic andesites (Humbert *et al*., 2019). Basaltic komatiites are found at the bottom of the formation (Humbert *et al*., 2019).

3.4.7 The Witwatersrand Supergroup

The Witwatersrand Basin hosts the largest known gold anomaly on Earth, with approximately a third of all gold historically mined originating from the Witwatersrand. The Witwatersrand Basin overlies middle Archaean granitoids and greenstones of the Kaapvaal Craton and is found in the middle of the Kaapvaal craton (Bumby *et al*., 2012; Humbert *et al*., 2019). The Witwatersrand Supergroup rocks overlie the tholeiitic basalt lavas and quartzites of the 3.07 Ga Dominion group (Dankert and Hein, 2010). The Witwatersrand Basin also hosts the approximately 2023 Ma Vredefort Structure, which is the oldest and largest known impact structure on the planet (Frimmel, 2019).

The Witwatersrand Supergroup is composed of 8 km of mostly siliciclastic metamorphosed sedimentary rock (Dankert and Hein, 2010). It is split into the Central Rand and West Rand Groups (Frimmel, 2019). The Witwatersrand Supergroup's known distribution on the surface and in the subsurface is shown in Figure 3.31, while its stratigraphy is shown in Figure 3.32.

3.4.7.1 The West Rand Group

The West Rand Group is characterised predominantly by shale and quartzites in equal proportions, with subordinate conglomerate beds (Frimmel, 2019). The group is divided into three subgroups, as shown in Figure 3.32 (Frimmel, 2019):

- Hospital Hill Subgroup: At the base of this subgroup is the Orange Grove Formation which consists of conglomerate and fluvial sandstone (Frimmel, 2019). It is overlain by the marine shale with iron intercalations of the Parktown Formation. The Brixton Formation, which follows, consists of tidal sandstone and lesser mudrock. Finally, the topmost unit of this Subgroup, the Bonanza Formation, consists of fluvial sandstone with intercalations of polymictic pyritic conglomerates in the west of the basin (Frimmel, 2019).
- Government Subgroup: This Subgroup was deposited during a period of fluctuating sea level, which led to great variability in lithology (McCarthy and Rubigde, 2005). The Promise Formation at the base of this subgroup consists of a laterally extensive diamictite overlain by shallow marine ferruginous shale and littoral sandstone. An upwards-coarsening sequence of sandstone follows (Frimmel, 2019). Shale, intercalated glaciogenic diamictite and iron

formation form the Coronation Formation. It underlies the quartz wacke of the Tusschenin Formation. The Palmietfintein Formation is dominated by magnetic marine shale, while the overlying Elandslaagte Formation consists of conglomerate and sandstone (Frimmel, 2019). Marine mudstone and sandstones form the Afrikander Formation, the topmost unit of the government subgroup.

- Jeppestown Subgroup: A major hiatus exists between the Jeppestown Subgroup and the underlying Government Subgroup (Frimmel, 2019). At the base of this subgroup lie the fluvial conglomerates and an upwards-fining sequence of sandstone that constitute the Koedoeslaagte Formation. The Reitkuil Formation, which overlies it, consists of magnetite mudstone followed by the conglomerates and feldspathic sandstones of the Babrosco Formation. 250 m thick basaltic andesite lava flows characterise the Crown Formation, which is succeeded by the Roodepoort Formation sandstone and ferruginous, partially magnetic mudstone (Frimmel, 2019). The Maraisburg Formation, which consists of sandstone and subordinate conglomerates, marks the top of the West Rand Group (Frimmel, 2019).

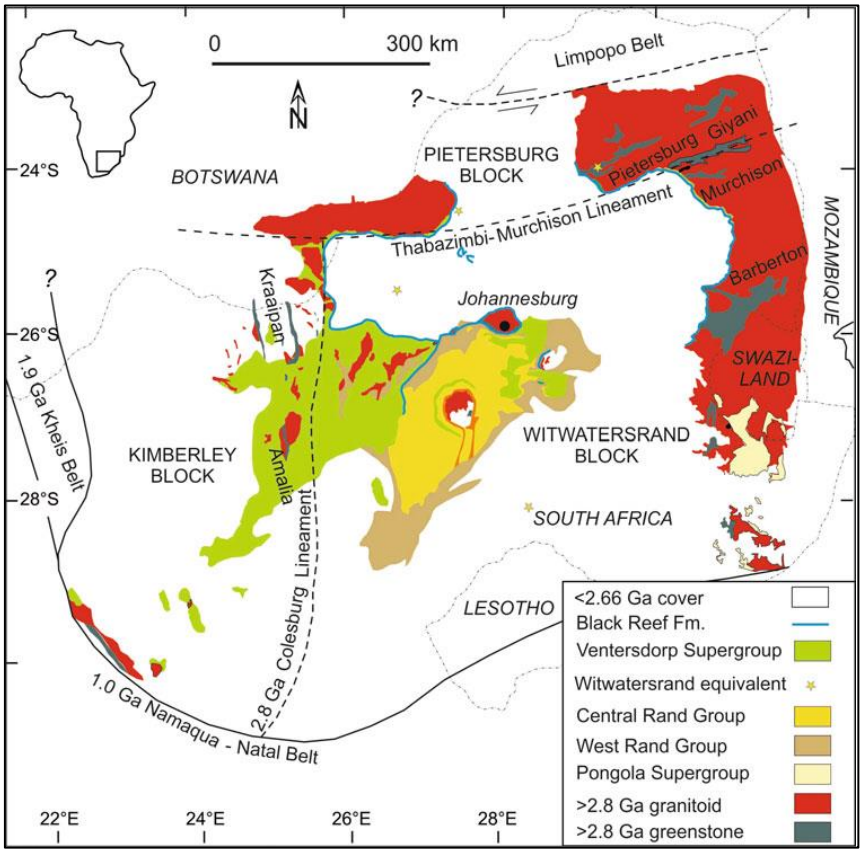

Figure 3.31: The known extent of the Witwatersrand Supergroup. Stars indicate locations of Witwatersrand age rocks encountered during drilling (Frimmel, 2019).

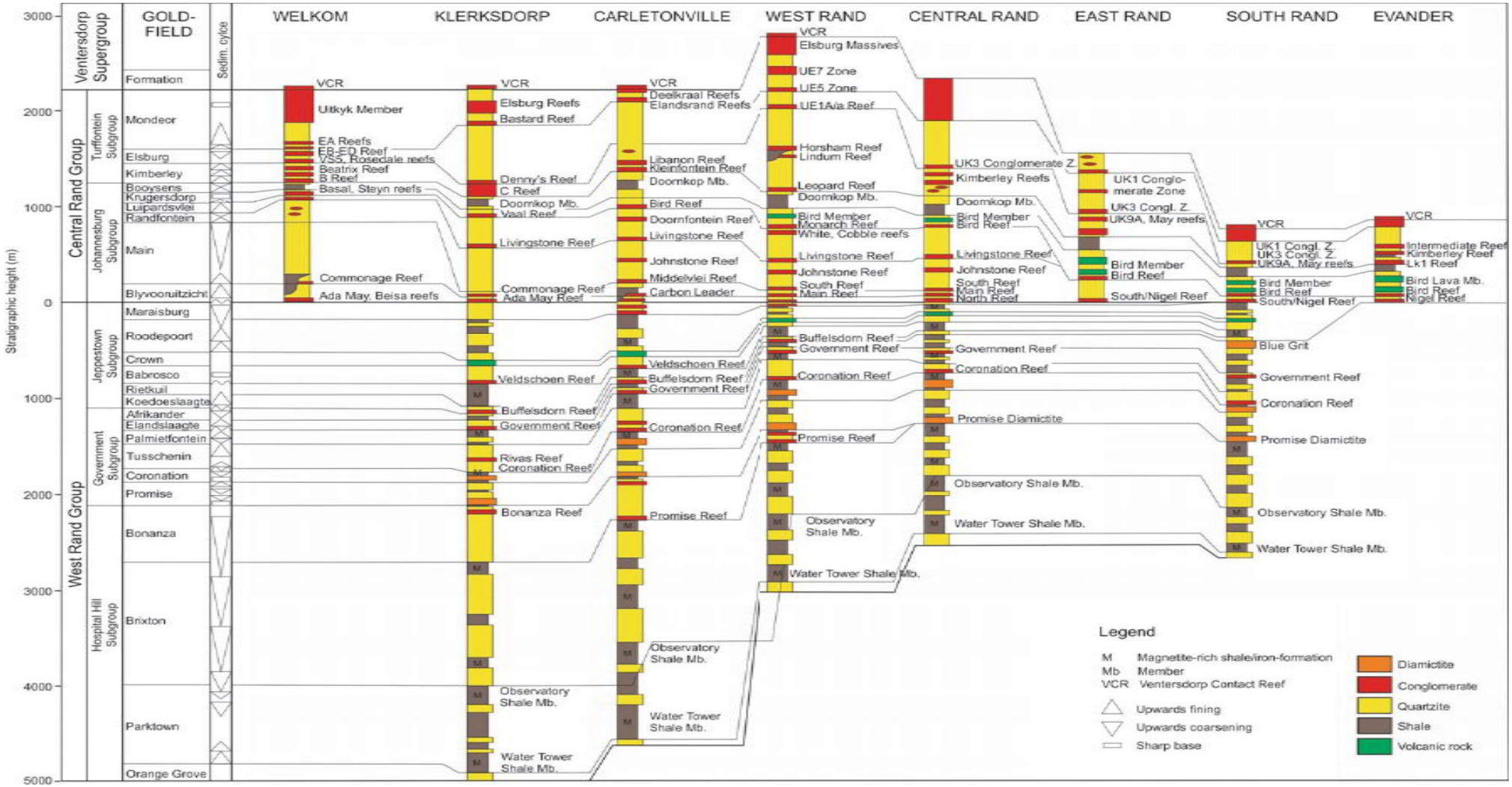

Figure 3.32: The Witwatersrand Supergroup stratigraphy and correlation between the different goldfields. Modified from McCarthy, (2006) in (Frimmel, 2019).

3.4.7.2 The Central Rand Group

The Central Rand Group generally comprises sandstone, auriferous conglomerate and intercalated shales and is approximately 2800 m thick (Dankert and Hein, 2010). It overlies the West Rand Group conformably and unconformably (Dankert and Hein, 2010). It is separated into the Johannesburg and the Turffontein Subgroups (Frimmel, 2019).

- Johannesburg Subgroup: This subgroup is mostly an accumulation of fluvial braid-plain deposits that are arenitic in nature. Most of the subgroup formations consist of conglomerate at the base, followed by quartzite, as shown in Figure 3.32 (Frimmel, 2019). Krugersdorp Formation basaltic lava is the only magmatic activity recorded in the Central Rand Group. The topmost Booysens Formation is anomalous because it consists of marine shale, even though fluvial deposits dominate the Central Rand Group (Frimmel, 2019).
- Turffontein Subgroup: There is a major hiatus between the Booysens Formation and this subgroup of the Central Rand (Frimmel, 2019). It is divided into the conglomerate beds and quartzites of the Kimberly, Elsburg and Mondeor Formations, with increased occurrence of conglomerate upwards in the sequence (Frimmel, 2019).

3.4.8 The Barberton Sequence

The term “greenstone”, according to Anhaeusser (2014), describes Archaean age deformed and metamorphosed volcano-sedimentary rocks usually surrounded by gneissic and granitic rocks. Several of these belts occur on the Kaapvaal craton as belts, remnants or fragments of greenstones (Brandl *et al*., 2006). Some greenstone belts on the Kaapvaal are shown in Figure 3.33. The Barberton Greenstone Belt is of particular interest.

The Barberton Greenstone Belt is a mid-Archaean (3600-3100 Ma) volcano-sedimentary remnant that is completely surrounded by granitoids of the Kaapvaal craton (Brandl *et al*., 2006). It covers a 120 km × 50 km area, is strongly folded and is trending ENE (Brandl *et al*., 2006). The combined thickness of the Barberton Greenstone Belt lies between 15 km-21 km (Anhaeusser, 2014). The Barberton Greenstone Belt is known for some of the earliest mineralisation of gold and has been used as a type locale for studying Archaean rocks (Agangi *et al*., 2019). Its rocks are situated south and south-east of Nelspruit but also occur in northwestern eSwatini (Kröner *et al*., 2019).

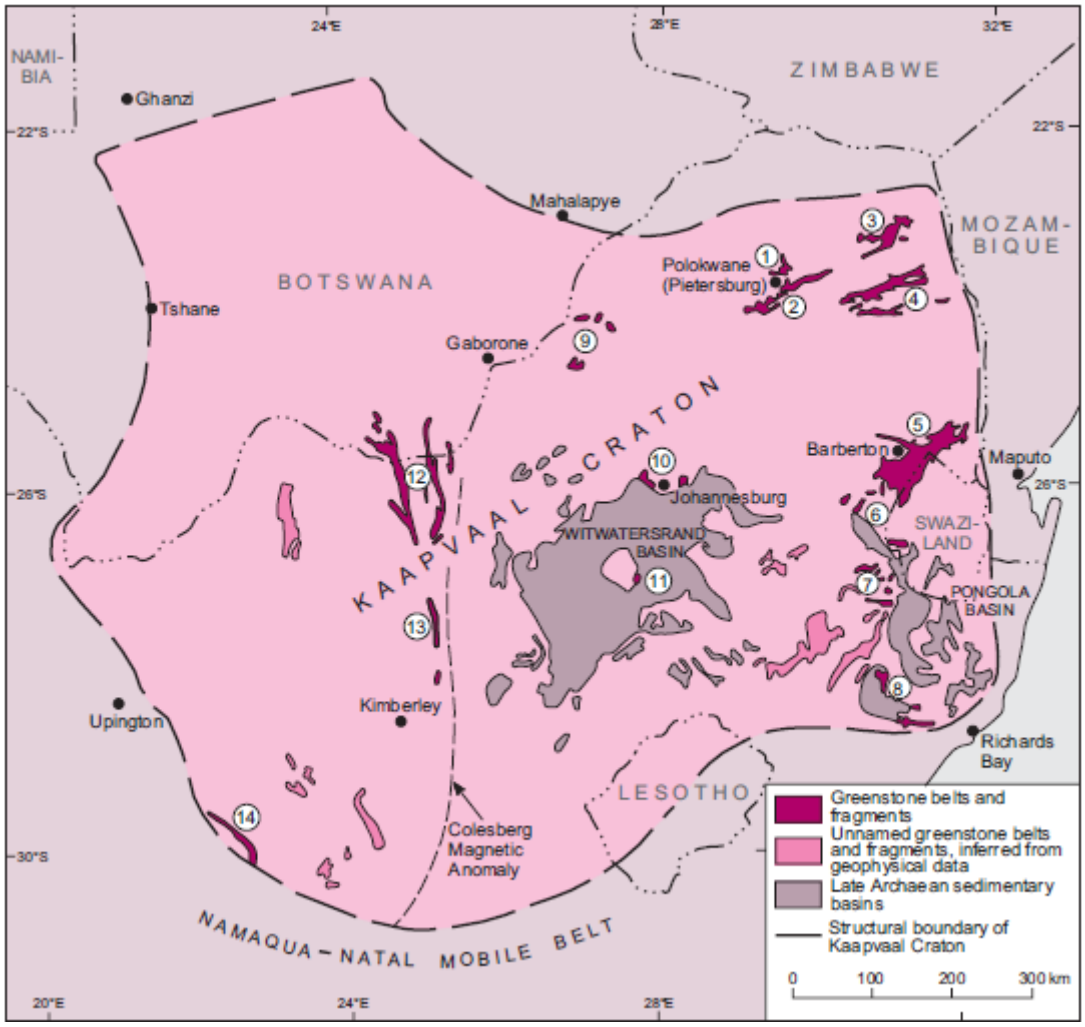

Figure 3.33: Various greenstone belts and fragments' distribution on the Kaapvaal Craton. 1. Rhenosterkoppies; 2. Pietersburg; 3. Giyani (Sutherland); 4. Murchison; 5. Barberton; 6. Weergevonden, Schapenburg; 7. Assegaai, DeKraalen, Commondale; 8. Nondweni-Ilangwe; 9. Makoppa Dome; 10. Johannesburg Dome; 11. Vredefort Dome; 12. Kraaipan; 13. Amalia and 14. Marydale (Brandl *et al.*, 2006).

The Barberton Greenstone Belt rocks are stratigraphically grouped into the Barberton Supergroup, divided into the Onverwacht, Fig Tree and Moodies Groups (Brandl *et al*., 2006). The geological map of the Barberton Supergroup is shown in Figure 3.34.

3.4.8.1 The Onverwacht Group

The largely ultramafic to mafic Onverwacht Group is separated into six formations (Brandl *et al*., 2006), as illustrated in Figure 3.35. The lowermost Sandspruit Formation, with a thickness of 2135 m, is developed as isolated remnants of the ultramafic to mafic amphibolite surrounded by plutons trondhjemitic gneisses (Brandl *et al*., 2006). Minor metasedimentary units consisting of chert, BIF, calc-silicate rocks, and arkoses occur. The overlying Theespruit Formation is about 1890 m thick and is composed of a variation of metamorphosed lavas, tuff and basalts (Brandl *et al*., 2006). Autoclastic

units forming distinct sericitic aluminous and siliceous schistose beds with subordinate chert and felsic pyroclastic, volcaniclastic units are diagnostic features of the formation.

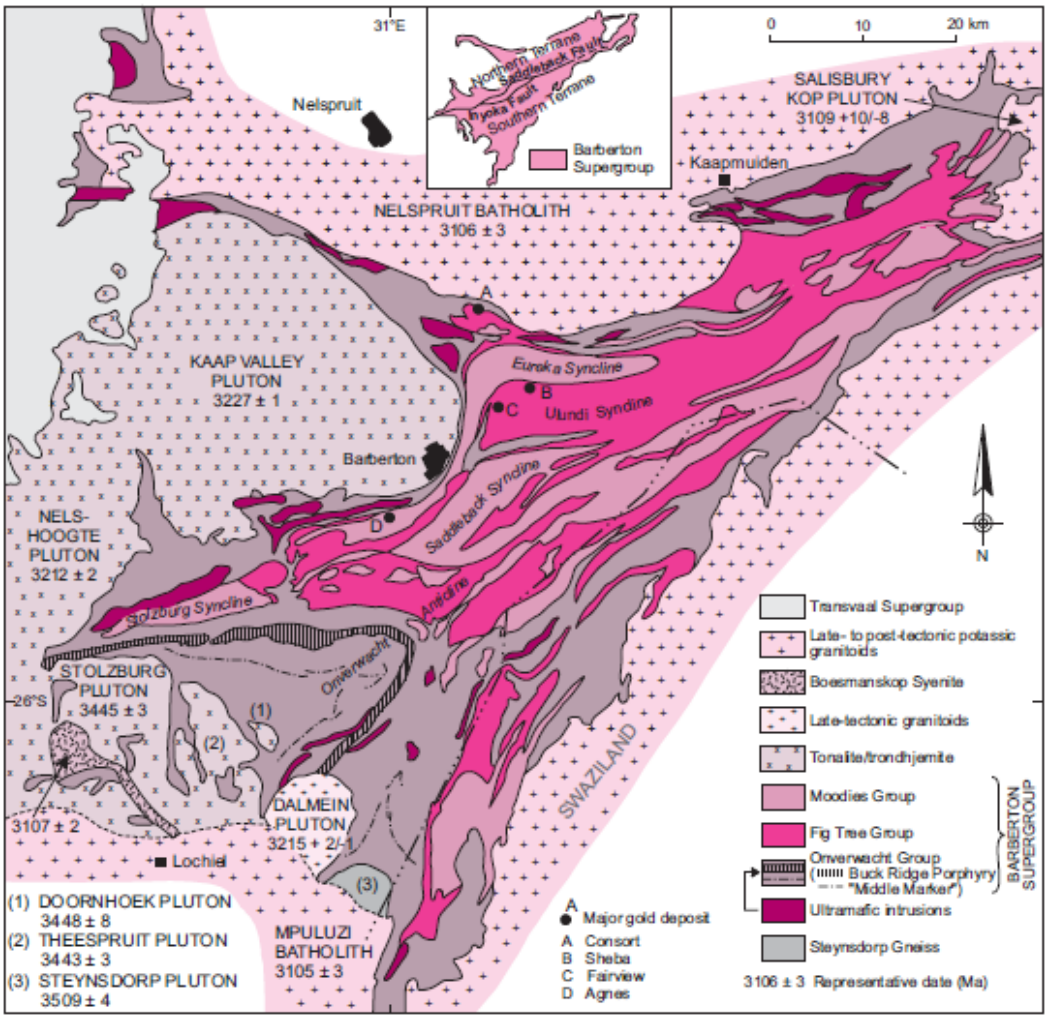

Figure 3.34: A geological map of the Barberton Greenstone Belt (Brandl *et al*., 2006).

The Komati Formation is up to 3500 m thick and comprises minor metatholeiite, komatiitic basalt, metamorphosed komatiite, and small intrusive bodies of soda-rich porphyry (Brandl *et al*., 2006). It is overlain by the Hooggenoeg Formation, which is about 4850 m thick and comprises thick cycles of pillowed tholeiitic basalts that progress upwards into thinner cycles of dacitic to ryhodacitic lavas capped by chert (Brandl *et al*., 2006).

The Middle Marker, which consists of iron oxide, carbon- and silica-rich chert layers, lies in this formation (McCarthy and Rubigde, 2005). The Kromberg Formation consists of 1700 m of pillowed and massive basalt and komatiite, black and banded chert and mafic lapilli tuff. Komatiitic lavas and massive komatiite comprise the topmost Mendon Formation (Brandl *et al*., 2006).

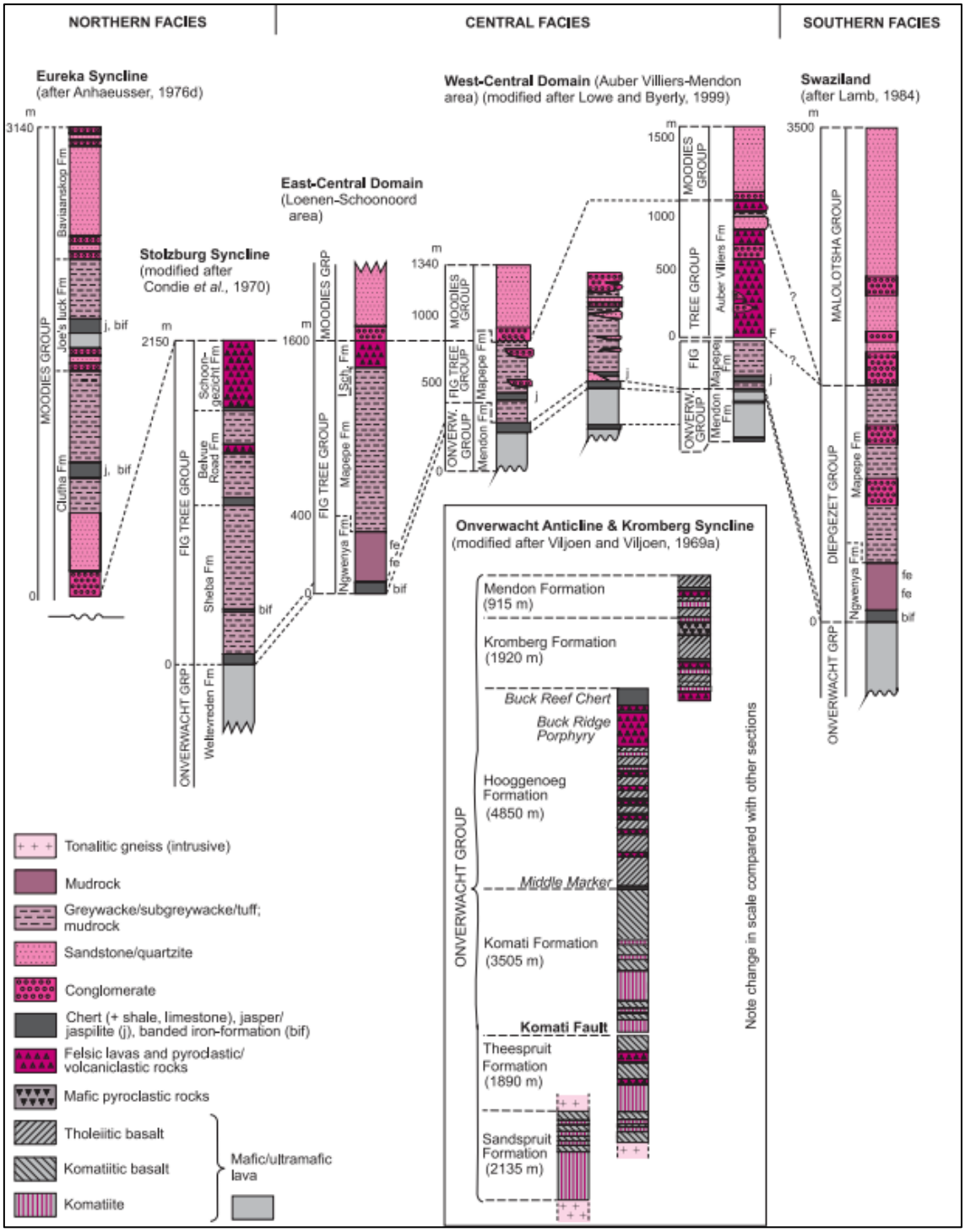

Figure 3.35: Simplified Stratigraphic sections through the Barberton Greenstone Belt and main structural domains (Brandl *et al.*, 2006).

3.4.8.2 The Fig Tree Group

The Fig Tree Group conformably lies atop the Onverwacht Group and is composed in general of sandstones, siltstones and carbonaceous mudstones (McCarthy and Rubigde, 2005). In the northern region, the Fig Tree Group is divided into the Sheba Formation with turbiditic lithic greywacke and shale; the Belvue Road Formation, consisting of turbiditic siltstone, shale and chert, greywacke and coarse volcaniclastic rocks and altered komatiitic lava with a black chert near the top; and the

Schoongezicht Formation, composed of approximately 550 m of coarse, felsic, volcaniclastic sandstone, breccia, conglomerate, mudstone and shale (Brandl *et al*., 2006).

South of the Inyoka fault (southern region), the Fig tree is divided into the Loenen, Ngwenya, Mapepe and the Auber Villiers Formations (Brandl *et al*., 2006). Figure 3.35 shows the Fig Tree Group formations in different domains (Brandl *et al*., 2006).

3.4.8.3 The Moodies Group

The Moodies Group is at the top of the Barberton Supergroup (McCarthy and Rubigde, 2005). It is developed as structurally isolated blocks and remnants and is split into three formations (Figure 3.35). These are the Clutha, Joe's Luck and Baviaanskop Formations (Brandl *et al*., 2006). Each of the formations is representative of an upwards fining sequence composed of a unit of conglomeratic quartzose sandstone at the base, succeeded by a thick unit of finer-grained quartzose sandstone, siltstone and shale (Brandl *et al*., 2006). The total thickness of this Group is about 3140 m (Brandl *et al*., 2006). The bottom of the Moodies is distinguished by well-defined cobble and pebble conglomerates or conglomeritic sandstones found below the first appearances of quartz-rich sandstone (Johnson *et al*., 2006).

3.4.9 The Kalahari Group

Up to this point, the deposits discussed were consolidated. The late Cretaceous to Cenozoic sediments of the Kalahari group cover rocks that are 3600 Ma old (Jonker and Abiye, 2017). The Kalahari Group largely consists of unconsolidated materials. The topmost aeolian unit of the Group can be traced from the Northern Cape Province to 2° north of the equator (Partridge *et al*., 2006). The Kalahari Group's extent in southern Africa is shown in Figure 3.36.

The Kalahari Group is divided into the following formations, as illustrated in Figure 3.37 (Partridge *et al*., 2006):

- Wessels Formation: It is the basal unit and consists of clayey gravel.
- Budin Formation: This formation comprises mostly brown and red clays and may consist of calcified root casts and thin pebble layers near its base.
- Eden Formation: Red, brown or yellow poorly consolidated sandstones characterise this formation. It becomes disaggregated towards the top and shows a gradational contact with the underlying Budin Formation.

- Mokalanen Formation: It is composed of calcretes and can be split into a sandy limestone overlain by a conglomerate with a calcareous matrix.
- Obobogorop Formation: It comprises pebble and boulder clasts derived from erosion of the Dwyka tillite.
- Gordonia Formation: The red aeolian sands of this formation hide the majority of the underlying Kalahari Group sediments. The sand has a thickness of 30 m and is comprised of rounded quartz clasts with a haematite coating (Partridge *et al*., 2006).

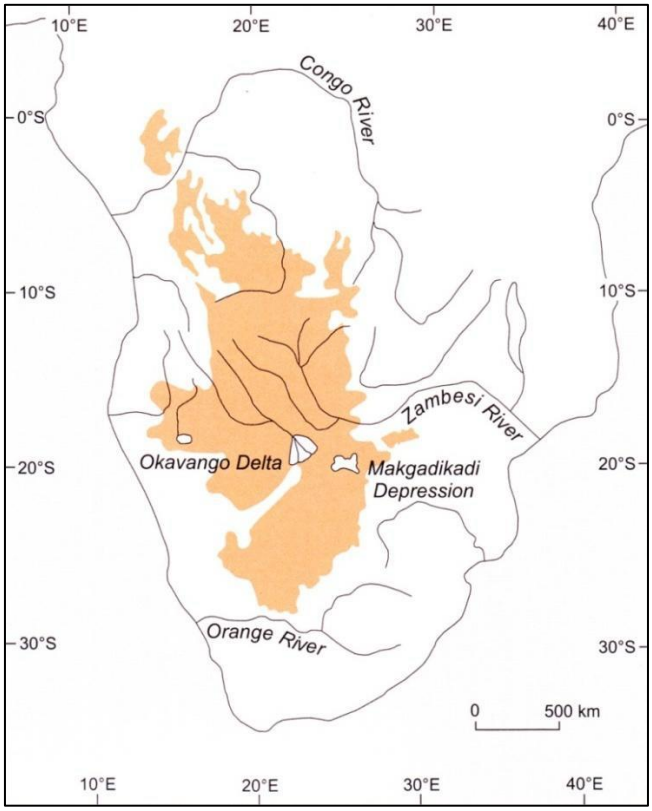

Figure 3.36: Kalahari Group sediments distribution (Partridge *et al*., 2006).

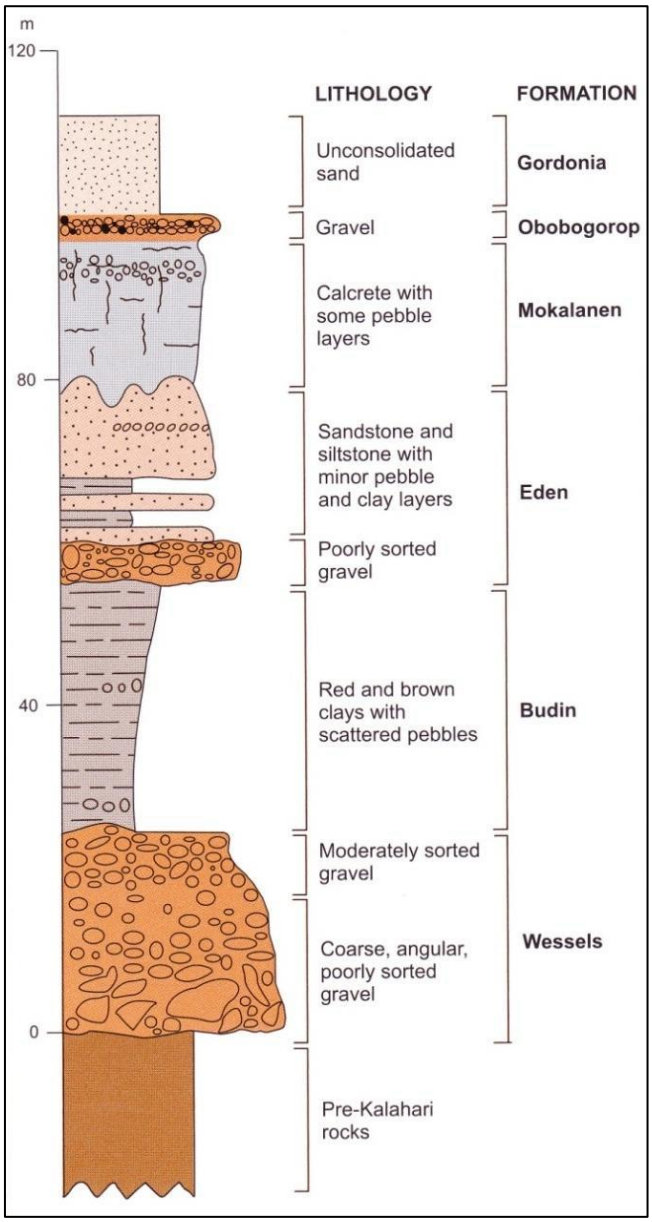

Figure 3.37: A generalised section through the Kalahari Group (Partridge *et al*., 2006).

3.5 GENERAL GEOHYDROLOGY OF SOUTH AFRICA

It has been shown that South Africa extends across different climatic and geological areas, which results in a wide range of hydrogeological characteristics that determine the nature of the aquifers in the country. The diversity seen in these characteristics is reflected in the occurrence, quality and movement of groundwater. South African aquifers can be divided into (Nel, 2017; Mvandaba *et al*., 2019):

a. Aquifers in the Karoo

b. Dolomitic aquifers

c. Basement granites

d. Table Mountain Group deposits

e. Aquifers in unconsolidated sands

f. Aquifers in hard rock formations

At a broader scale, aquifers in South Africa can be divided into four classes (Du Toit and van Lelyveld, 2014):

- Intergranular (Class A): It describes a water-saturated zone that is often unconsolidated but may occasionally be partially consolidated. Water moves through and is stored in intergranular interstices. Alluvial deposits or weathered crystalline rock are some materials that fall under this aquifer class (Du Toit and van Lelyveld, 2014).
- Fractured (Class B): This type occurs in fissured and fractured bedrock. The principal water strike may be along the contact between two rock formations or within fractures in the rock. The groundwater is transmitted and stored in fractures, joints or fissures. Groundwater may flow between the fractures and the matrix called bilinear flow. In the case of a connected fracture network, the aquifer is a double porosity reservoir (van Tonder *et al*., 2001). The fractured aquifer can be formed by arenaceous sedimentary rocks or igneous rocks (Du Toit and van Lelyveld, 2014)
- Karst (Class C): This class refers to carbonate rocks where groundwater is transferred and stored in fractures that are enlarged by chemical dissolution. Such can occur in dolomites or limestones.
- Intergranular and Fractured (Class D): This class comprises a fractured area overlain by a saturated weathered zone. Water moves between the two zones with fractures creating preferred flow paths and weathered material providing storage. This form of aquifer is common in South Africa.

The distribution of the broad classes of aquifers is illustrated in Figure 3.38. Each aquifer class is then subdivided based on yield (Du Toit and van Lelyveld, 2014):

- Aquifers of yields >5 L/s are classified as high-yielding and are suitable to supply urban areas or large-scale irrigation.
- 2.0 L/s – 5.0 L/s are moderately yielding, appropriate for domestic supply to small towns or small-scale irrigation.
- 0.5 L/s- 2.0 L/s have a moderately low yield. These can irrigate community plots or be used as the rural domestic supply.

- 0.1 L/s- 0.5 L/s are low-yielding and can supply single homesteads, stock watering or small rural villages. These are typically equipped with hand pumps or windblown pumps.
- Aquifers with yields of 0-0.1 L/s are classified as very low yield (Du Toit and van Lelyveld, 2014).

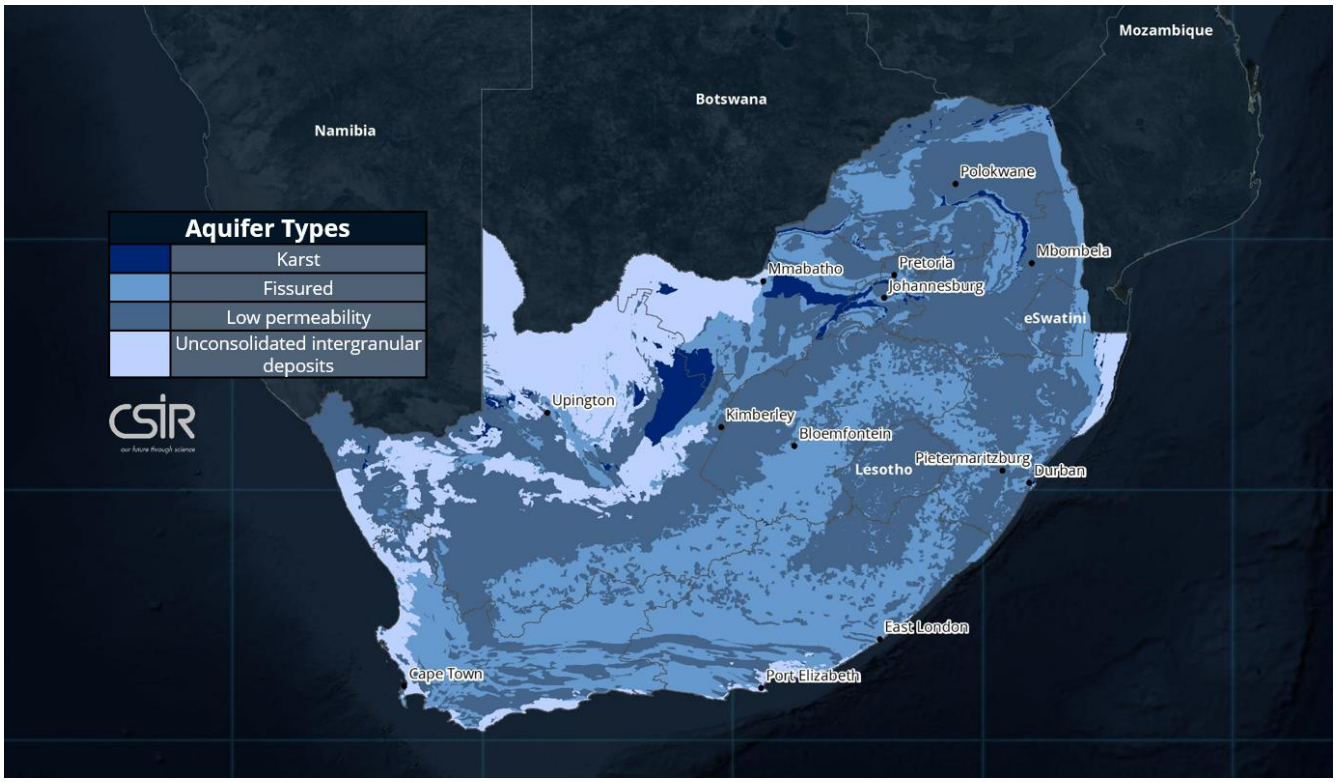

Figure 3.38: Types of aquifers in South Africa. Modified from (Mvandaba *et al*., 2019).

These classes of aquifers are illustrated in the 1:500 000 General Hydrogeological map series developed by the Department of Water and Sanitation (DWS), then known as the Department of Water Affairs and Forestry), which consists of 23 map sheets (Du Toit and van Lelyveld, 2014). Information on the groundwater quality observed from known boreholes is maintained in the National Groundwater Archive.

The different aquifer types and yields translate into different groundwater potentials throughout the country as shown in Figure 3.39.

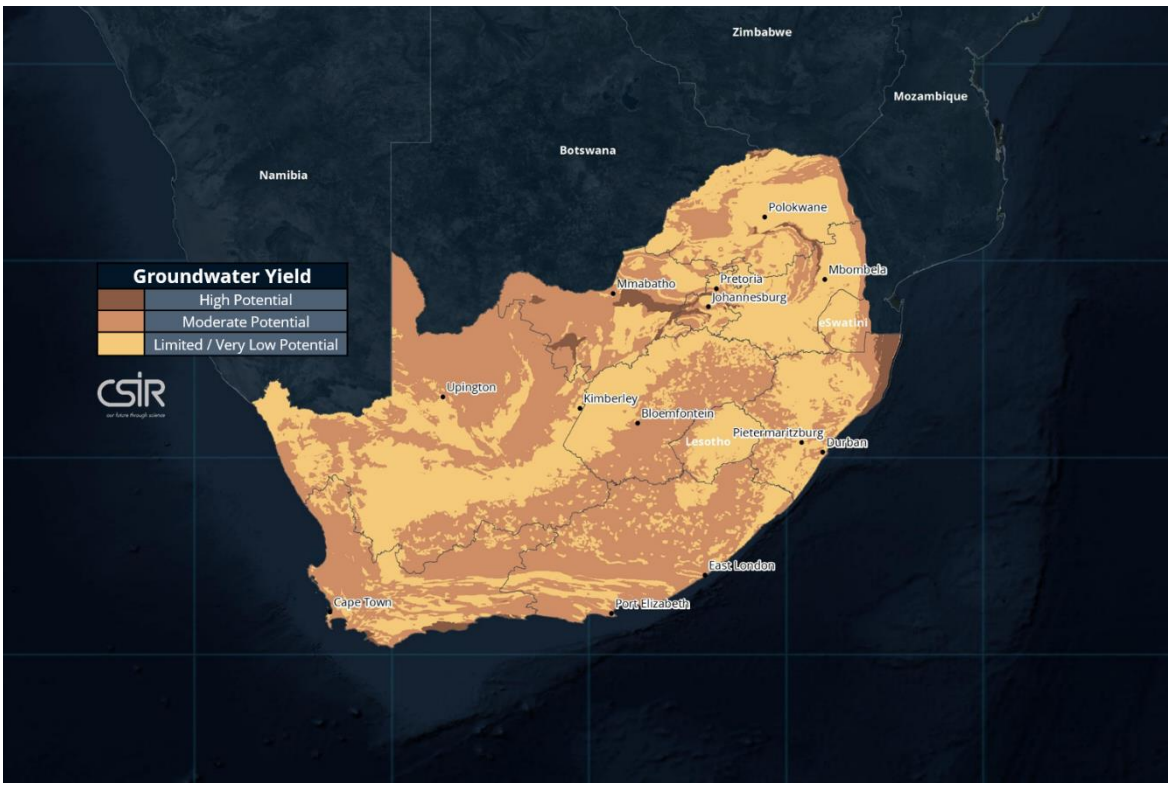

Figure 3.39: Potential Groundwater Yields in South Africa (Mvandaba *et al*., 2019).

In a given environment, there are different features that can be typically targeted during exploration that produce geophysical anomalies. How well a geophysical method can resolve such anomalies is related to its efficacy in the particular environment (Chandra, 2015). The subsequent sections in this chapter will describe the potential targets for geophysical groundwater exploration and the general geohydrology in the geological environments of interest.

3.5.1 General geohydrology of the Karoo Supergroup

The Karoo covers a sizeable proportion of the country; because of its large extent, its hydrogeology is quite variable, with different yields depending on the local characteristics. Typical Karoo aquifers are mudstones, siltstones, sandstones and shale (Gomo and Ligavha-Mbelengwa, 2020).

3.5.1.1 Dwyka Group

The group is characterised by low hydraulic conductivities and generally has very low yields of 0.1 L/s to 0.5 L/s. The Dwyka diamictites have virtually no primary porosity, so groundwater is confined to fractures or jointing (Meyer, 2003; Ndlovu, Demlie and Butler, 2019). However, it is often considered an aquitard due to its low yields (Woodford and Chevallier, 2002). Some exploitable targets exist where there are sand gravel deposits, but water from the Dwyka is usually saline (Woodford and Chevallier, 2002). Average EC values in the Dwyka Group rocks are about 200 mS/m (Meyer, 2003). The Dwyka diamictite has low resistance to weathering, and the weathered zone can also be a potential aquifer (GHT Consulting, 2013).

3.5.1.2 Ecca Group

The dense shales of the Ecca have led to it being disregarded as a groundwater source (Woodford and Chevallier, 2002; Lourens, 2013). The bulk densities and porosities of the Ecca rocks increase from the northern to the southern and southeastern reaches of the basin (Woodford and Chevallier, 2002). It is worth noting that the shales of the Ecca behave as aquitards in the vertical direction and aquifers in the horizontal (Lourens, 2013). Groundwater in the Ecca is normally associated with dolerite contact zones, bedding planes and joints (Meyer, 2003). Although the Ecca is often overlooked, high-yielding boreholes occur in the Petrusburg area in the central Free State, likely due to the presence of high porosity calcretes (Meyer, 2003). The deltaic sandstone facies has low permeability due to poor sorting and diagenesis, which have lowered the primary porosity of the rocks (Woodford and Chevallier, 2002).

3.5.1.3 Beaufort Group

The intergranular and intergranular and fractured classes of aquifers occur in the Beaufort Group (Meyer, 2003). Median yields of 0.1 L/s-0.5 L/s and 0.5 L/s-2 L/s are reported for the group (Baran, 2003; Meyer, 2003). Primary permeabilities in the Beaufort are often low, with the aquifer behaviour further complicated by the migration of the meandering rivers which formed them. This causes the Beaufort aquifers to have multiple layers and varying thicknesses (GHT Consulting, 2013). Coarser, more permeable rocks in the group are lens-shaped, which gives high-yielding boreholes in the Beaufort limited productivity without recharge (GHT Consulting, 2013). Groundwater in the Beaufort usually has an alkaline nature (Baran, 2003).

3.5.1.4 Stormberg Group

The arenaceous Molteno Formation has persistent sedimentary bodies and a sheet-like geometry, all favourable conditions for groundwater storativity (Woodford and Chevallier, 2002). According to Baran (2003), boreholes drilled in the Molteno had yields of 0.1 L/s-2 L/s. The argillaceous Elliot Formation has low permeability, although its mudstones are very porous and can store large volumes of water (Woodford and Chevallier, 2002). The Clarens Formation's well-sorted, fine-grained sandstones have high and uniform porosity and are expected to be an ideal aquifer. However, due to low permeability and poor fracturing, the formation has low hydraulic conductivity. Median yields within the Clarens are reported between 0.5 L/s-5 L/s (Meyer, 2003).

3.5.1.5 Drakensberg Group

The high elevation of the areas underlain by the Drakensberg extrusives has led to little or no development of boreholes. The Drakensberg falls into the intergranular and fractured aquifer class. Groundwater can be found within weathered zones in the lava and the jointed transitional zone

between weathered and fresh lava (Meyer, 2003). The contact between the Drakensberg and Clarens below is significant to groundwater storage and movement, as shown by the numerous springs at the contact (Woodford and Chevallier, 2002).

3.5.1.6 Karoo Dolerite Suite

Dolerite sills and dykes that have intruded into the Karoo represent significant features for groundwater potential. Dykes and sills may create preferential flow paths for groundwater along their contacts and associated fractures and jointing. Sills and dykes often cut across multiple sedimentary bodies and have different dips, complicating groundwater interception depth (Meyer, 2003). Groundwater in the dolerite intrusion occurs in interstices in weathered dolerite and the transitional zone between the weathered and solid dolerite body (Ndlovu, Demlie and Butler, 2019). The yield for boreholes drilled into or along dolerite bodies is highly variable (Chevallier, Goedhart and Woodford, 2001).

3.5.1.7 Dolerite breccia plugs and Volcanic vents

Breccia plugs and volcanic vents are highly permeable features that are targets of interest for extracting groundwater. However, sustainable yield is determined by the properties of the host rock in which they are found. Yields exceeding 8 L/s can be encountered in intensely brecciated parts of plugs, but the plug itself is but a conduit for groundwater flow (Woodford and Chevallier, 2002).

3.5.1.8 Kimberlites and associated alkaline complexes

Clusters of kimberlites represent significant fractured domains on the regional scale. On a local scale, kimberlite dykes are only weakly jointed and only have low permeability. Kimberlite fissures are normally clogged by clays produced during the decomposition of the kimberlites, so boreholes drilled into them commonly have low yields. Local and regional faults associated with kimberlite emplacement can give appreciable amounts of groundwater (Woodford and Chevallier, 2002).

3.5.2 General geohydrology of the Cape Supergroup

The Cape Supergroup is found along the southern and southwestern margins of the country; as such, it constitutes a significant feature for potential groundwater occurrence. It is important to note that the coastal Cenozoic deposits, which in some areas overlie the Cape Supergroup unconformably, are also important primary aquifers that can be encountered. The Cape Supergroup aquifers are generally secondary aquifers.

3.5.2.1 Table Mountain Group

Groundwater development in the Cape Supergroup is often targeted at Table Mountain Group. The TMG is a fractured rock aquifer that extends 248000 km^2 with 37000 km^2 exposed at the surface, which makes it one of the most important aquifers in South Africa (Xu *et al.,* 2009). The TMG is strongly compartmentalised by basement rocks and fault zones. The Kango-Baviaanskloof fault and the Worcester fault, which are regional faults, influence TMG distribution (Xu *et al.*, 2009).

The thickness of the aquifer is about 500 m to 4000 m (Miller *et al.*, 2017). This aquifer is conceptualised into three main aquifer units; the Peninsula Aquifer of the Peninsula Formation, the Nardouw Aquifer comprising the Nardouw Subgroup and the Cedarberg aquitard, which separates the two (Miller *et al*., 2017). The Piekernerskloof aquifer overlain by the Graafwater aquitard is limited to the western section of the Cape Fold Belt. The Peninsula and Nardouw aquifers have low primary porosity, and groundwater flow is mainly through the heterogeneous fracture networks controlled by folding and faulting of the TMG. Hydraulic conductivity, water table position and flow rates are highly variable in different parts of the aquifer (Miller *et al*., 2017). Water quality in the Peninsula Formation has TDS <100 mg/l with TDS <50 mg/l often encountered. Abstraction occurs at various locations with the TMG at rates of ~30 L/s (Miller *et al*., 2017).

Xu *et al.* (2009) proposed a sustainable yield of $<1x10^9$ m^3/year for the TMG. The hydrogeological boundary of hydrogeological units in the TMG is controlled by lithology, geomorphology, recharge/discharge boundaries, and faulting. According to (Xu *et al.*, 2009), the TMG can be divided into 15 hydrogeological units based on these different factors influencing the hydrogeological boundary. The units are illustrated in Figure 3.40.

In a more general sense, in terms of the strata, the TMG has four categories being:

a) horizontal strata aquifer such as the Cape Peninsula

b) fold strata such as synclines, anticlines and monoclines

c) fracture zone aquifers

d) composite aquifers

These categories are illustrated in the model in Figure 3.41.

Faults play a major role in groundwater occurrence in the TMG. However, the majority of faults are often recemented through and can serve as barriers to groundwater flow with fracture zones as conduits. Transmissivity estimates in the TMG are highly variable due to the complexity and anisotropic nature of hydraulic properties at different sites (Xu *et al.*, 2009). Springs with an array of discharge rates also occur within the TMG.

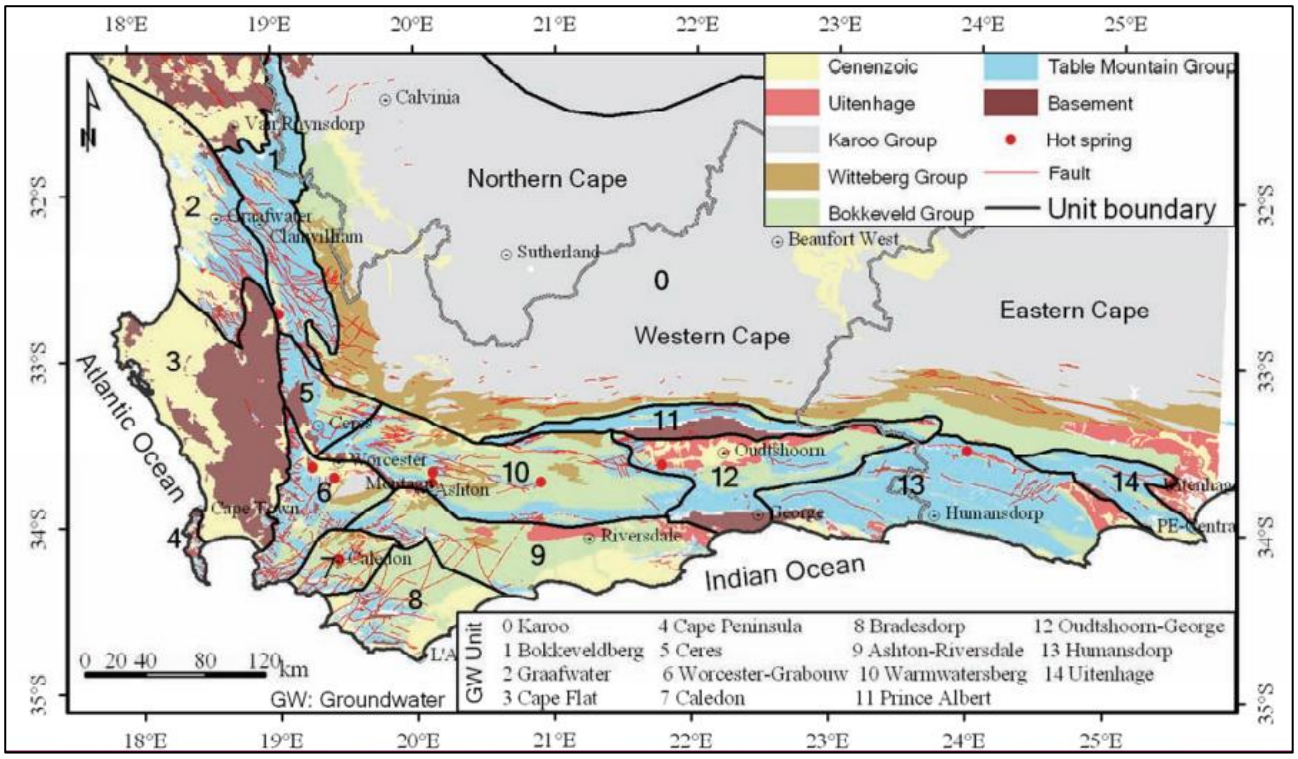

Figure 3.40: The 15 hydrogeological units of the TMG (Xu, Lin and Jia, 2009).

3.5.2.2 Bokkeveld Group

The primarily argillaceous Bokkeveld can be considered as a secondary aquifer, that is, a fractured aquifer. However, this argillaceous nature makes it behave more like an aquitard (Miller *et al.*, 2017). The Bokkeveld is part of an aquitard known as the Gydo mega-aquitard (Blake *et al.*, 2010). In this group, the ratio of arenaceous to argillaceous materials has a bearing on groundwater occurrence. Formations with more arenaceous material tend to have higher yields. For example, the sandstone layers within the Ceres Subgroup have higher yields of up to 5 L/s, although the volumes cannot be sustained over the long term (Lourens, 2013). In the sandstone poor Bidouw Subgroup yields below 1 L/s can be expected (Meyer, 2001).

The aquifers of the Bokkeveld generally have less faulting and low yields and are characterised by high TDS. Groundwater from the shales and limestones of this group is mostly alkaline and can be brackish in some cases (Mokoena *et al.*, 2020; Mokoena *et al.*, 2021). The EC values in the Ceres Subgroup are 30 mS/m-400 mS/m, while those of the Bidouw/Traka Subgroup can be well above 400 mS/m (Meyer, 2001).

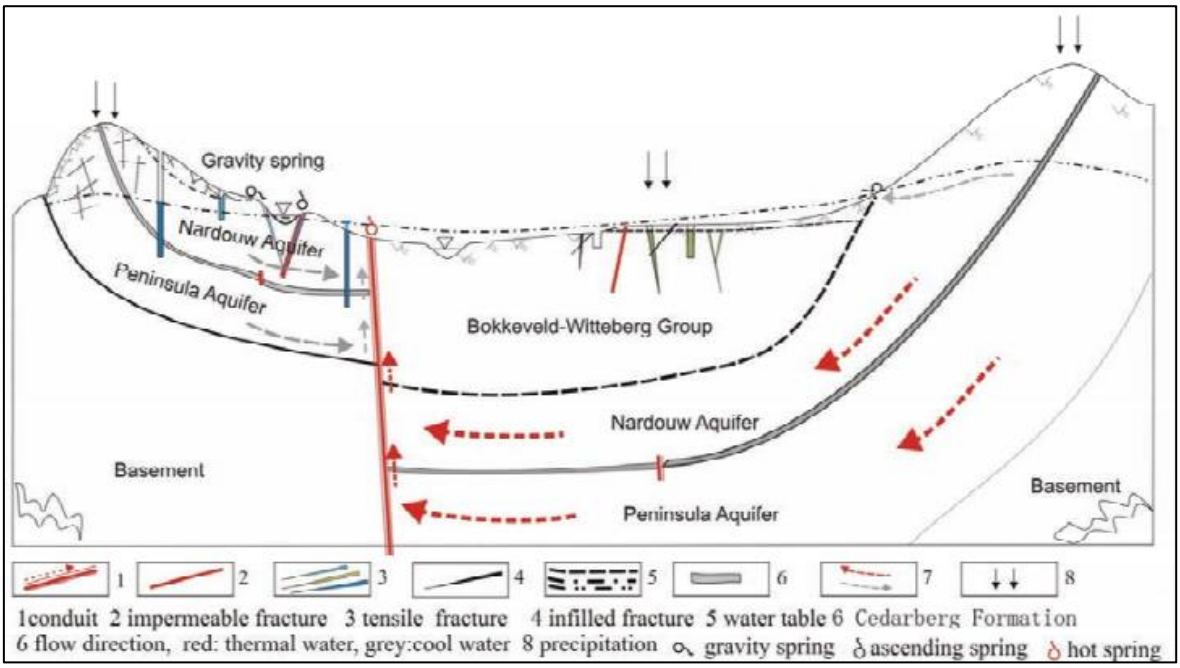

Figure 3.41: The TMG composite aquifer model (Xu, Lin and Jia, 2009).

3.5.2.3 Witteberg Group

This group can also be considered a secondary aquifer. EC values within the Witteberg shales are between 200 mS/m and 700 mS/m. The ratio of arenaceous to argillaceous materials also plays a role in the yields encountered within this group. In sandstone-rich formations, yields of 5 L/s are encountered, while yields above 2 L/s are rare in shaly formations (Meyer, 2001). Water from the shale units is usually saline. The groundwater, which mostly occurs in fractures in the shales and quartzites, is generally of bad quality (DWS, 2011a). The poor yields and water quality make the Witteberg unsuitable for use, hence not much study is done on groundwater in this group.

3.5.3 General geohydrology of the Namaqua-Natal Metamorphic Province

The geological character of the Natal and the Namaqua Sectors of the Natal metamorphic complex may be similar. However, the two sectors are located in different climatic regions of the country, which means that the groundwater quality and degree of exploitation are not the same for the two. The Natal sector, located in a wetter region is not often exploited, whereas in the dry Namaqua region, groundwater is the most important water source. Generally, water is found in schists and in fractures in granites. Older granites in the provinces have more water potential due to erosion they have incurred. Water is also common on fault zones with the dip of fault zones also being important to groundwater potential in the Namaqua-Natal Metamorphic provinces (DWS, 2011b).

3.5.3.1 Natal Sector

The rocks of the Natal sector are classified as intergranular and fractured aquifers. The weathered intergranular zone overlies a fractured zone. This intergranular system has a high porosity but, due to

its high clay content, has low hydraulic conductivity. Water in the natal sector is associated with near-surface weathering, fracturing and dolerite intrusions (King, 2002). The weathered zone is no more than 25m thick and is in hydraulic connectivity with the fractured bedrock (King, 2002). Yields in the Natal sector rocks range around 0.1 L/s-0.5 L/s and 0.5 L/s-2.0 L/s (Lin and Lin, 2019). Water quality in the rocks is generally good; however, fluoride values of 2 mg/l are sometimes reported in argillaceous metamorphic rock aquifers.

3.5.3.2 Namaqua Sector

Although there is a variety of different rock types in the sector, the rocks are similar in that they virtually have no primary porosity but have secondary porosity due to weathering and fracturing (Vegter, 2006). In the Namaqua sector, groundwater occurrence is thus more dependent on the degree of weathering and fracturing than on the rock type or lithostratigraphic unit (Vegter, 2006). The aquifers generally have low storativity, but there is higher transmissivity where fractures occur. Groundwater flow is complex because of heterogeneity associated with mechanical discontinuity as a result of fractures (Friese *et al*., 2006). In Namaqualand, aquifer systems are confined to narrow and open valleys related to fault zones. The groundwater possesses a strong NaCl character and is generally saline. Average yields in the Namaqualand basement rocks are 0.2 L/s-2 L/s (Friese *et al*., 2006).

3.5.4 General geohydrology of the Bushveld Igneous Complex

At a regional scale, the Bushveld Complex can be classified as an intergranular and fractured aquifer. It can be conceptualised into a two-layer aquifer model; a shallow weathered system which may be connected to alluvial aquifers associated with river systems and a deeper fractured bedrock system (Titus *et al*., 2009). The weathered zone varies in thickness between 12 m and 50 m. Where the weathered zone is close to river courses it is overlain by alluvial aquifers.

The deeper fractured bedrock comprising anorthosites norites and pyroxenites of the BIC has a low matrix hydraulic conductivity. Groundwater flow is through interconnected fracture systems that have the potential for rapid flow from the overlying weathered system to greater depths along the interconnected conductive zones. The shallow weathered zone shows a Mg-Ca-HCO3 water type while the deeper one shows a Na-Cl facie (Titus *et al*., 2009). The weathered overburden has a low transmissivity but high storativity with pumping tests in the region yielding transmissivities of 3-8 m^2/d. Storativity values are variable. Transmissivities of up to 500 m^2/d and storativities of 0.15 have been determined for highly transmissive zones (Titus *et al*., 2009).

78% of some 300 boreholes drilled into the Rooiberg Group had yields less than 2 L/s, while 55 had yields in excess of 5 L/s (Du Toit and Sonnekus, 2014a). Water quality is good to moderate, with EC

a harmonic mean of 26.15 mS/m. The Rashoop granophyre is generally of low groundwater potential with low storage capacity, although some yields between 0.5 and 2 L/s do occur (Du Toit and Sonnekus, 2014a). In the Rustenburg layered suite, median yields are about 1 L/s, with some boreholes with yields as high as 25 L/s being encountered (Du Toit and van Lelyveld, 2014). In some mines located within the RLS, large volumes of water are intercepted at depths of 300 m where there is fractured anorthosite (Du Toit and van Lelyveld, 2014)..

The Lebowa Suite granites seem to have low groundwater potential, although good yields in excess of 5 L/s can occur occasionally (Du Toit and van Lelyveld, 2014). Water in the Lebowa suite has a high fluoride content, with 52% of 638 boreholes analysed having a fluoride content greater than 1.5 mg/L (Du Toit and Sonnekus, 2014a).

3.5.5 General geohydrology of the Transvaal Supergroup

3.5.5.1 Black Reef and Vryburg Formations

The quartzites of these formations are classified as fractured rock aquifers, and they possess low permeability (Mndaweni, Naicker and Blake, 2019). The Black reef is located in mountainous areas and is not easily accessible. Thus, its hydrogeological character is not well studied (Du Toit and Sonnekus, 2014a). Most yields in the formations are less than 2 L/s, while EC values in some are about 34 mS/m (Barnard, 2000). The water level depth in the formation is determined by the groundwater movement direction between the formation and adjoining dolomites of the Chunniespoort and Ghaap Groups (Barnard, 2000).

3.5.5.2 Chunniespoort and Ghaap Groups

The carbonates of these groups are some of the most important aquifers in the country. The carbonate rocks do not have primary porosity, but due to karstification, they have developed a very high storage capacity (DWS, 2011c). In this process, rainwater takes up carbon dioxide in the air and soil, forming a weak carbonic acid. The weakly acidic groundwater circulating along fractures, faults and joints in the dolomites causes leaching of the carbonate, leaving insoluble residual materials and eventually creating cavities in the subsurface filled with groundwater (Oosthuizen and Richardson, 2011). Figure 3.42 shows a conceptual model of a typical karst landscape in South Africa.

The Malmani and Campbellrand Subgroup cover the largest karst area in Southern Africa, about 63% of total karst or 31000 km^2 in the region (Masilela and Beckedahl, 2022). The Malmani Subgroup dolomites and limestones form a fractured karst aquifer with sustainable yields of 2 L/s to 5 L/s, although high yields above 10 L/s are possible (Mndaweni, Naicker and Blake, 2019). The karstic aquifers are compartmentalised by dolerite dykes which act as barriers to flow. The banded iron

formations that overlie the carbonates have moderate to good potential as they are located in a high rainfall region. Yields in the BIFs are 0.5 L/s-2 L/s (Du Toit and Sonnekus, 2014a).

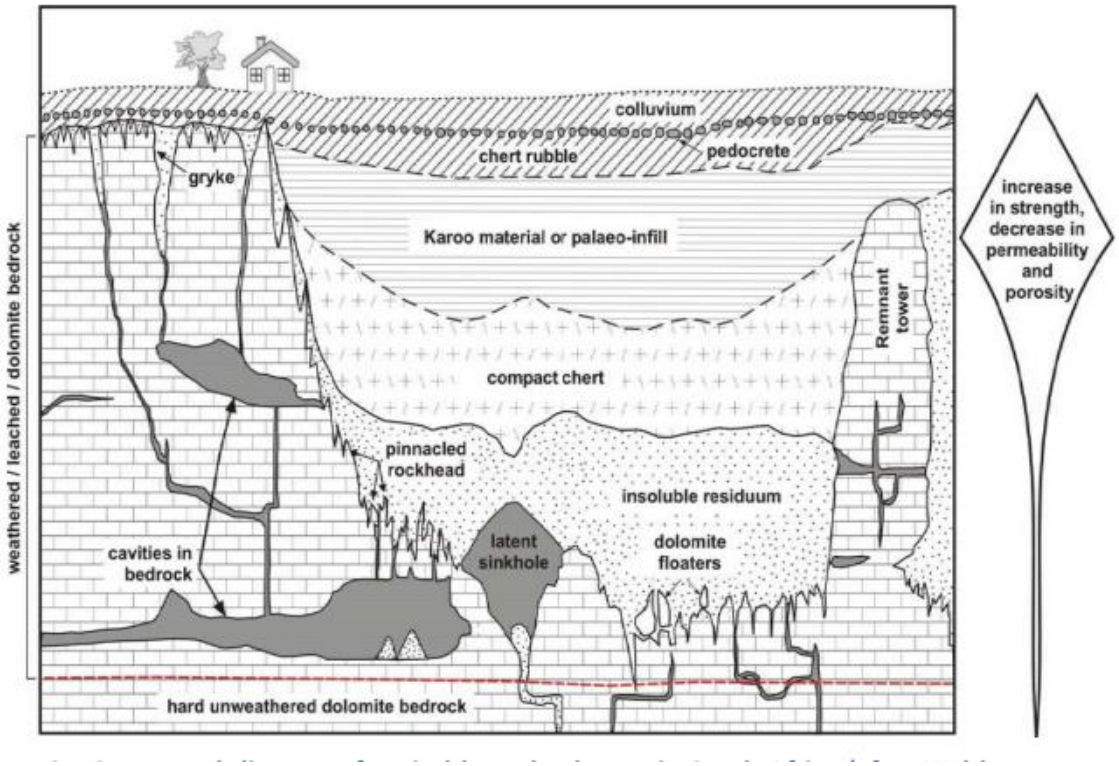

Figure 3.42: Typical Karst landscape in South Africa (Waltham and Fooks (2003) in (Oosthuizen and Richardson, 2011)).

3.5.5.3 Pretoria and Postmasburg Groups

The arenaceous lithologies of the Pretoria Group and the Postmasburg Group are classified as fractured aquifers (Du Toit and Sonnekus, 2014b). The argillaceous formations, which constitute the majority of the Pretoria Group are classified as intergranular and fractured. The shales which have been metamorphosed to hornfels have diminished water-bearing properties, and the group is often considered an aquitard (Du Toit and van Lelyveld, 2014; Mndaweni, Naicker and Blake, 2019). Median borehole yields in these intergranular and fractured facies are 0.8 L/s.

3.5.6 General geohydrology of the Ventersdorp Supergroup

The volcanic and sedimentary rocks of the Ventersdorp have low porosity and hydraulic conductivities. The groundwater in the Klipriviersberg is associated with weathering basins and the transitional zone between weathered and fresh lava (Barnard, 2000). Yields less than 2 L/s are common, groundwater generally occurs at 10-25 mbgl, and EC is about 60 mS/m (Barnard, 2000).

The Platberg Group has moderate groundwater potential with yields greater than 2 L/s often encountered (Barnard, 2000). Water is often associated with the transitional zone between the weathered and fresh rock. Andesitic lavas have similar hydrogeological characteristics to the other

formations, although average EC is 57 mS/m, and the groundwater from those areas is slightly alkaline (Barnard, 2000).

3.5.7 General geohydrology of the Witwatersrand Supergroup

This rock assemblage constitutes a fractured aquifer type. Dykes act as important conduits for groundwater flow and compartmentalize the water. Main water-bearing structures are fractured and weathered zones. The Black Reef quartzites are intensively fractured and provide a medium for vertical recharge of the Witwatersrand aquifer (Abiye *et al*., 2011).

The Central Rand Group weathers to sandy soil that may locally promote recharge. Groundwater generally discharges out through seeps or springs along the floor and slopes of principal valleys in the West Rand Group, although there are no known springs in the Central Rand Group (Barnard, 2000). According to Barnard (2000), groundwater quality can be considered good, with average EC of 37 mS/m and 29 mS/m for the West Rand and Central Rand Groups, respectively. The aquifer is considered a low to moderate yielding system, with the majority of boreholes having yields less than 2 L/s, although yields >5 L/s are sometimes reported with a maximum of 30 L/s encountered (Barnard, 2000).

The water level is generally between 10 mbgl and 25 mbgl. Although the Witwatersrand is low yielding, it lies adjacent to the karst Malmani Subgroup aquifers and water ingresses into the Witwatersrand mines (Durand, 2012). As mines were closed and abandoned, mine voids were filled and decantation occurred. However, the pyrite and other sulphates in the gold fields were dissolved by the water and discharged into the surrounding surface waters and groundwater bodies as Acid Mine Drainage, with rendered the water in some parts of the supergroup unusable (Durand, 2012).

3.5.8 General geohydrology of the Barberton Sequence

Similar to other greenstone belts, the rocks of the Barberton are classified as fractured rock aquifers. The metabasalts and granites that comprise this Supergroup are impermeable. Fractures in the granites are often filled with quartz veins which lower the groundwater potential in the granites significantly (Sami *et al*., 2002a). The metabasalts are not often subject to those quartz-filled fractures.

In general, groundwater strike, according to Du Toit and Sonnekus (2014b), in the Barberton is less than 70 mbgl. The water samples taken from this area have elevated sodium levels with a dominant bicarbonate character. Static water levels are also shallow, which suggests that groundwater likely occurs in the weathered zone (Du Toit and Sonnekus, 2014b).

3.5.9 General geohydrology of the Kalahari Group

The Kalahari is considered an intergranular aquifer system due to its primarily unconsolidated nature. The Karoo rocks which underlie the Kalahari are important for locating groundwater. The lime-rich clay layers of the Kalahari have a higher storage capacity than the underlying Karoo but a lower permeability. Groundwater is intercepted in the lower formations, that is, the Wessels, Budin, and Eden Formations (Lourens, 2013). The Kalahari is located in an arid part of the country with very low rainfall, and there is limited recharge. Groundwater quality in the region is complex. According to Martinelli (1975), the water quality depends on the degree of natural recharge in areas of concentrated run-off and the development of appropriate sandy layers. Where there are favourable recharge conditions, lenses of fresh water are expected to be overlying brackish water.

Generally, water levels vary between 40 mbgl and 50 mbgl, but the water level can be up to 150 m deep (DWS, 2011d). Yields are quite low, between 0.2-1 L/s. The Kalahari is not an ideal aquifer; other primary aquifers in the country, such as the Cenozoic Sandveld Aquifer that overlies the Cape Supergroup, and older rocks have better potential. The Sandveld, for example, generally has shallow water levels and can be considered high yielding (Conrad, Nel and Wentzel, 2004).

3.6 POTENTIAL GEOLOGICAL TARGETS FOR GEOPHYSICAL GROUNDWATER EXPLORATION

3.6.1 Introduction

Targets of exploration vary according to the specific environment. Different geological formations have unique characteristics that translate into different targets. Typical features that increase groundwater potential in the selected environments are summarised in this section.

3.6.2 Targets in the Karoo Supergroup

Groundwater flow in Karoo aquifers is fracture-dominated. Several areas and features of the Karoo make for favourable targets due to their higher permeability. These are often associated with dolerite dykes and ring structures, dolerite sill margins, thick alluvial deposits, and folded and faulted formations (Murray *et al.*, 2012).

a. Dolerite Intrusions: These bake, deform and fracture sedimentary rocks, creating zones of higher transmissivity along their contacts. They may also bar groundwater flow. According to Woodford and Chevallier (2002), there is a higher probability of intersecting groundwater in boreholes drilled into or next to dolerite dykes. Dolerite is strongly magnetic, which makes it particularly easy to detect using the magnetic method.

b. Thick Alluvial Deposits: Some thick occurrences of alluvium are found in various areas across the main Karoo Basin. If they are coarse-grained and thick with high permeability, they form very productive aquifers (Murray *et al.*, 2012). Groundwater potential is also significant where such alluvial deposits overlie fractured aquifers. For example, the Quaternary coastal deposits of the Maputaland Group (which overlie the Karoo Supergroup in Natal) comprise alluvium, aeolinites and estuarine deposits, among others, constitute intergranular aquifers with yields between 0.5 L/s and 2 L/s (Ndlovu, Demlie and Butler, 2019).

c. Folded and faulted formations: Deformation and faulting that have affected such formations have led to their increased permeability. According to Murray *et al.* (2012), faulting within the main Karoo basin has a limited extent, but the folding at the southern margin is significant.

d. Type of host rock: Fractured sandstones are more permeable than fractured mudstones. Therefore, groundwater potential is typically higher in more arenaceous than argillaceous formations.

3.6.3 Targets in the Cape Supergroup

The preferred targets of exploration in the Cape Supergroup lie mostly within the TMG. The Bokkeveld and Witteberg Group Formations are generally avoided. The mountainous terrain makes it so that drilling is normally confined to foothills. The topography is also taken into consideration when choosing the geophysical methods used in exploration.

Formations often targeted are the Piekenierskloof Formation, Peninsula Formation and the Nardouw Subgroup (Rosewarne and Weaver, 2002). The bottom of the Bokkeveld is also sometimes targeted where the prime formations are not accessible. The contact between the Nardouw Subgroup quartzites and the Gydo Formation shales due to fracturing that occurred there makes the contact another ideal target (Rosewarne and Weaver, 2002).

Specific target features are:

- Major regional fault systems which extend over hundreds of kilometres. However, they require drilling to depths over 250 m for optimal results
- Local faults and fractures associated with folding and local stress fields
- Bedding planes, especially in the thinly Bedded Nardouw aquifers

Locating a favourable fracture system in the TMG is quite important for the siting of successful boreholes. However, the TMG also has some adverse features, such as breccia or mylonite, that can lower hydraulic conductivity (Rosewarne and Weaver, 2002).

3.6.4 Targets in the Namaqua-Natal Metamorphic Province

In the Natal sector, groundwater occurrence is associated with the fracturing and weathering of the metamorphic and igneous rocks. Therefore, preferred target features are the major fault systems, intrusions of dolerite and the weathered zone (Lourens, 2013). According to Vegter (2006), water in the Namaqua hard rock aquifers is generally struck in the fractured rock beneath the weathered zone and not in the transition zone between the weathered and fresh bedrock as is typically seen in wetter regions.

Zones of intense fracturing, shearing, jointing and brecciation are the preferred targets in the Namaqua sector. However, it must be noted that loss or decrease of fracture permeability may occur due to weathering of fracture surfaces and the formation and deposition of clays. Secondary openings may also be reduced or destroyed by epidotisation, silicification, and chertification of mylonite (Vegter, 2006). A large portion of the area underlain by the Namaqua sector strata is blanketed by a low resistivity layer, which makes it difficult to distinguish unweathered but fractured rock and solid rock (Vegter, 2006).

3.6.5 Targets in the Bushveld Igneous Complex

Groundwater targets in the Rooiberg Group include faults and their associated shear zones, fracture zones, dyke contacts, the contact with overlying sandstones (Waterberg Group) and lava flow contacts. The depth to groundwater level is in general less than 30 m (Du Toit and Sonnekus, 2014a). In the Rashoop granophyre, water occurs in fracture zones, dyke contacts and faults.

Water occurs in weathered and fractured rock as well (Du Toit and van Lelyveld, 2014). Botha and Van Rooy (2001) showed that the intrusive carbonate complexes within the BIC may also be targeted, such as the Spitskop Complex within the Nebo granite of the Lebowa Suite. The carbonatite complex, due to its low silica content, tends to weather more easily than the surrounding granites, forming a regional topographical low. These lows tend to form recharge zones, and many successful boreholes are located within these features (Botha and Van Rooy, 2001)

3.6.6 Targets in the Transvaal Supergroup

The dolomitic rocks are the main targets due to their high yield capability. Therefore, the Malmani, Campbellrand and Schmidtsdrift Subgroups are important targets. Contacts between the dolomite and dolerites are often fractured and subject to preferential dissolution and form groundwater flow paths (Mndaweni, Naicker and Blake, 2019). Higher yields are also experienced in areas overlain by thick, saturated sandy to gravelly alluvium. Large regional fractures, shear zones and fractures resulting from offloading are also associated with higher yields (Mndaweni, Naicker and Blake, 2019).

Karstification zones are however sometimes filled with rubble making drilling in these areas difficult. Deformation, metamorphism and fluid movement have resulted in a range of mineralisation in the Transvaal, leaving its aquifers vulnerable to pollution from mining activities. Groundwater level drawdown can also lead to subsidence and sinkhole formation in these dolomite underlain areas (Oosthuizen and Richardson, 2011).

3.6.7 Targets in the Ventersdorp Supergroup

There is no specific formation to target in this assemblage. However, the deepest part of a weathered basin is the best target for groundwater resources in the Ventersdorp. Fractures or fault planes associated with regional fault systems are associated with good-yielding boreholes. The transition zone between weathered and fresh rock and dolerite dykes are also good targets for groundwater (Lourens, 2013).

3.6.8 Targets in the Witwatersrand Supergroup

The following features are favourable targets in the Witwatersrand Supergroup:

- The contact zone between sediments and intrusive sills
- Deeply weathered shale formations
- Weathered lithological contacts
- Regional faults and associated fractures

The shales weather more intensely, forming better aquifers. Low-lying areas are also more favourable as contacts and bedding planes there are more weathered (Barnard, 2000).

3.6.9 Targets in the Barberton Sequence

The preferred targets are the metabasalts, especially when they are fractured by dykes and faults. Fractures in this region have three strike directions, NW-SE, N-S and NE-SW, which are expressed in morphological features such as valleys, gorges, or other depressions visible in aerial photographs. Some important points to note during exploration (Sami *et al*., 2002a):

- Dykes and sills have had low-yielding boreholes and seem to not be of importance.
- Shear zones are often filled with clay gouge reducing their permeability.
- Major faults and thin dykes close to fault zones are the best targets for exploration. Dip-slip and strike-slip faults are water-bearing and associated with cavities that enhance the permeability of the rocks.

- The EM and DC resistivity are good tools for exploration in this environment. DC resistivity is able to resolve deep fractures, faults, and weathered zones.

3.6.10 Targets in the Kalahari Group

According to Van Wyk (2011), locating and mapping paleochannels or valleys is the best approach to finding groundwater in the Kalahari Group. Targeting current river systems where the group's thickness is less than 180m so that areas with significant leaching at the edge of the basin can be penetrated is also ideal (Lourens, 2013). Martinelli (1975) also emphasised the need to target surface drainage lines in this region. Regional fault systems are other important targets. As previously mentioned, the Wessels, Budin, and Eden Formations are the formations in which groundwater is intercepted.

CHAPTER 4:
GEOPHYSICAL GROUNDWATER EXPLORATION IN SOUTH AFRICA

4.1 INTRODUCTION

In this chapter, various case studies where geophysics was used in groundwater prospecting are summarised. The case studies have variable extent, some being small studies for local water supply and others being regional studies. Most studies used a combination of tools to aid groundwater exploration. For the sake of efficiency, emphasis is placed only on sections of the studies relating to geophysics.

4.2 PUBLICATIONS ON GEOPHYSICAL GROUNDWATER EXPLORATION

Geophysical groundwater exploration in South Africa is not well documented, and there is a general lack of publications relating to the subject in the public domain. In this section, various published papers relating to geophysical groundwater are summarised. The majority are journal articles, and others are published thesis or conference papers.

4.2.1 Applications of geophysical prospecting in the Union of South Africa

Enslin (1955) wrote a paper on the applications of geophysical prospecting in the Union of South (later the Republic of South Africa). One of the applications for which it was used was in groundwater exploration to choose drilling targets. In 1950, 95% of 300000 known boreholes were sited without geophysics. However, Enslin (1955) predicted a rise in the use of geophysics in groundwater exploration as technology advances, as geological observation alone is insufficient in groundwater exploration. Geophysical techniques were chosen so that interpretation could be conducted in the field to minimise costs and allow the operation to be flexible.

Magnetic methods were used to identify contacts between sedimentary and igneous rocks. The contacts could be identified by taking traverses across the vertical magnetic field of the dyke as the majority of dykes are strongly magnetic. Enslin (1955) also describes an anomaly interpretation method that could determine the contact of the dyke with the host rock with an accuracy of 30-60 cm.

50% of boreholes were drilled into igneous rocks, marking the importance of weathering basins. These are detected through resistivity methods where routine surveys used the Wenner configuration. Enslin (1955) divided these basins into those where free water conditions exist and form cones of depression and those in which confined water is pumped, and cones of pressure relief are formed.

Narrow water-bearing structures such as fault planes could be detected by electromagnetic methods. These methods were used as supplementary surveys to the resistivity method in areas where there was rapid resistivity variation in the lateral and vertical. Geophysics in the union was also used in gold (gravity and magnetics) and other mineral (SP or radioactivity logging) prospecting as well as for engineering studies.

4.2.2 Kalahari Gemsbok National Park

Vertical Electrical Sounding was carried out to delineate the interface between fresh and saltwater in the Kalahari, as it was observed that freshwater lenses overlay saltwater in the region (Martinelli, 1975). This was to prevent unnecessary drilling into the saline water and to avoid drilling boreholes in unsuitable areas.

For a formation of uniform porosity, a change in resistivity is indicative of changes in the conductivity of the saturating liquid; therefore, the saline/fresh interface can be detected. Figure 4.1 shows the result of the calibration soundings to establish hydrogeophysical parameters in the area. An increase in salinity is indicated by decreased resistivity in the field curve. Seventy-five electrical soundings were conducted in the area. Four boreholes were eventually drilled, with three/four having a resistivity of 4-7 ohm.m (Martinelli, 1975).

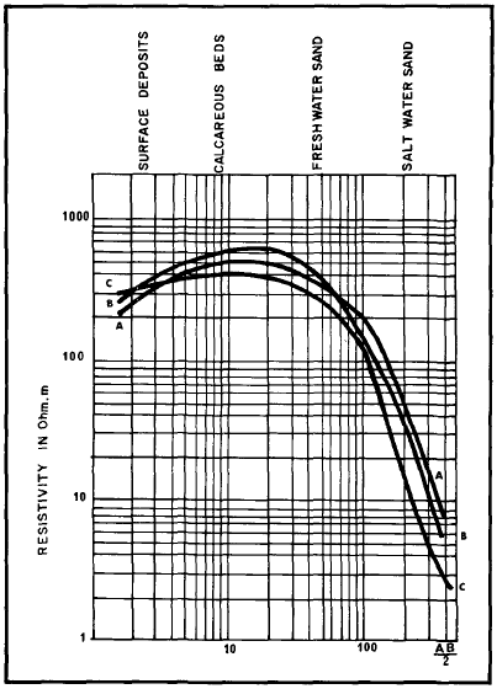

Figure 4.1: Electrical soundings from Kalahari Gemsbok National Park (Martinelli, 1975).

4.2.3 Applicability of geophysical methods for groundwater exploration in the central Limpopo Mobile Belt

Du Toit (1989) wrote a report for the then Department of Water and Sanitation (DWS) to establish the most suitable geophysical methods for siting boreholes in the Swartwater and Beauty border areas in Limpopo. The magnetics, resistivity, and electromagnetic methods were used in the study. The area in question is part of the central zone of the Limpopo Mobile Belt where there is granulite grade metamorphism and primary structures cannot be identified due to the intense folding and faulting that has affected the area. Lithologies in the region include metaquartzite, amphibolite, marble, metapelites, and calc-silicates.

Targets were identified from aerial photographs and topo-cadastral maps. Traverses were then conducted perpendicular to the chosen target feature for each method under investigation with 300 m long lines (Du Toit, 1989). Finally, the geophysical data were interpreted, and boreholes drilled at identified sites (Du Toit, 1989). The study found that the use of a single method is inadequate for siting boreholes in the LMB. It was recommended that magnetics, resistivity and at least two profiling techniques, such as two different EM profiling techniques or EM profiling with resistivity profiling, be used. The profiling combination was chosen based on conductivity, depth to the water table, and thickness of overburden. If minimum equipment is available, Du Toit (1989) recommended the use of the Geonics EM34.

4.2.4 Groundwater exploration in the Kalahari Basin

According to Botha and Vorster (1993), the DC resistivity and gravity methods had been the preferred methods of groundwater exploration in the Kalahari Basin. However, unpredictable variations in rock density and resistivity, as well as high contact resistance, limit the applicability of these techniques in the region. The time-domain electromagnetic method (TDEM) was applied successfully to map the Kalahari total thickness, although individual layers could not be resolved. Possible fault zones were also detected by the TDEM. High-resolution seismic surveys were also conducted which were able to discern the different layers of the subsurface. The Kalahari sand cover in one site was 200 m thick, overlying a 40 m thick clay layer and a freshwater gravel and clay aquifer beneath (Botha and Vorster, 1993). The results of the surveys were not provided.

4.2.5 Groundwater exploration in the Nebo granite

In the 1990s, many boreholes were drilled into the Nebo granite of the Lebowa Granite Suite as part of a drought relief program (Botha *et al.*, 2001). Out of 100 boreholes, 51 were dry, 42 had yields of 0.1-1 L/s, while 7 had yields of 1.0-3.0 L/s (Botha *et al.*, 2001). Results such as these caused the area to be declared unsuitable for drilling. However, this result was likely due to poor interpretation of

geophysical data; hence, an integrated multidisciplinary approach using airborne and ground geophysics, geology, structural mapping, orthophotos and topo cadastral maps was developed to site boreholes (Botha *et al.,* 2001).

Two sites of 100 km^2 and 10 km apart were chosen for the study (Botha *et al.,* 2001). Site 1 had a large number of outcrops, while site 2 had a significant cover of overburden. Once optimum survey parameters were determined from site 1, they were applied to site 2. Pre-existing multidisciplinary data were entered into a GIS database and evaluated to check its applicability.

Three airborne geophysical techniques were flown over site 1 to plan the optimum exploration program. These were frequency domain electromagnetic (DIGHEM^{v}), total field magnetics (Scintrex H8 vapour type), and radiometric (consisting of Th, U, K, and total count measurements). EM focus was to identify regional structures, such as faults, while the airborne magnetics were to identify and map different lithological units and structures. Radiometric data can delineate faults and different lithological units (Botha *et al.,* 2001).

Targets of exploration were identified from the airborne data interpretation, and a ground geophysical survey was conducted as a follow-up. This groundwork consisted of an electromagnetic survey using the Geonics EM34 and a magnetic survey using the Geometrics G856-X proton precession instrument. Ground survey lines were about 400 m long (Botha *et al.,* 2001). Similarly, an airborne geophysical survey was flown over site 2, and a ground geophysical survey was done after targets were identified. A max-min horizontal loop electromagnetic and a magnetic survey were also conducted at site 2.

Drilling positions were identified, and boreholes were drilled. At site 1, 92.3% of sites were successful, with 46% of sites yielding >2.0 L/s. The project was able to demonstrate that a regional approach to exploration is necessary before an area can be declared unsuitable for groundwater exploration.

4.2.6 Groundwater exploration in Mamre

Fraser (2001) conducted an integrated geophysical groundwater exploration survey in Mamre, 50 km north of Cape Town. The town is underlain by the shales and phyllites of the Tygerberg Group of the Malmesbury Formation. Yields in these metasediments are low. Granites of the Darling Pluton, Cape Granite Suite have intruded into the shales and phyllites. The package is overlain in some places by the unconsolidated Bredasdorp Formation sands that also possess low yields. Three geophysical methods, the electromagnetic, seismic and magnetic methods, were applied during the survey. Data was acquired along a 1100 m section of road to Mamre (Fraser, 2001).

To collect seismic data, a Bison 24-channel seismograph with a sledgehammer striking a wooden block was the source, and uni-axial geophone receivers were employed. Data were processed in the Winseis software. The stacked seismic data that resulted is shown in Figure 4.2 a). It is shown as a time section because the weathered layer had a complex velocity that did not allow for it to be converted to a depth section (Fraser, 2001). The velocity was 2000 m/s in the north and 4000 m/s in the middle and south, which correlates with the expected response for the geology (Fraser, 2001). At 30 ms, there is a prominent reflection that shows the base of the weathered zone. Depth to layers was calculated from the velocity data.

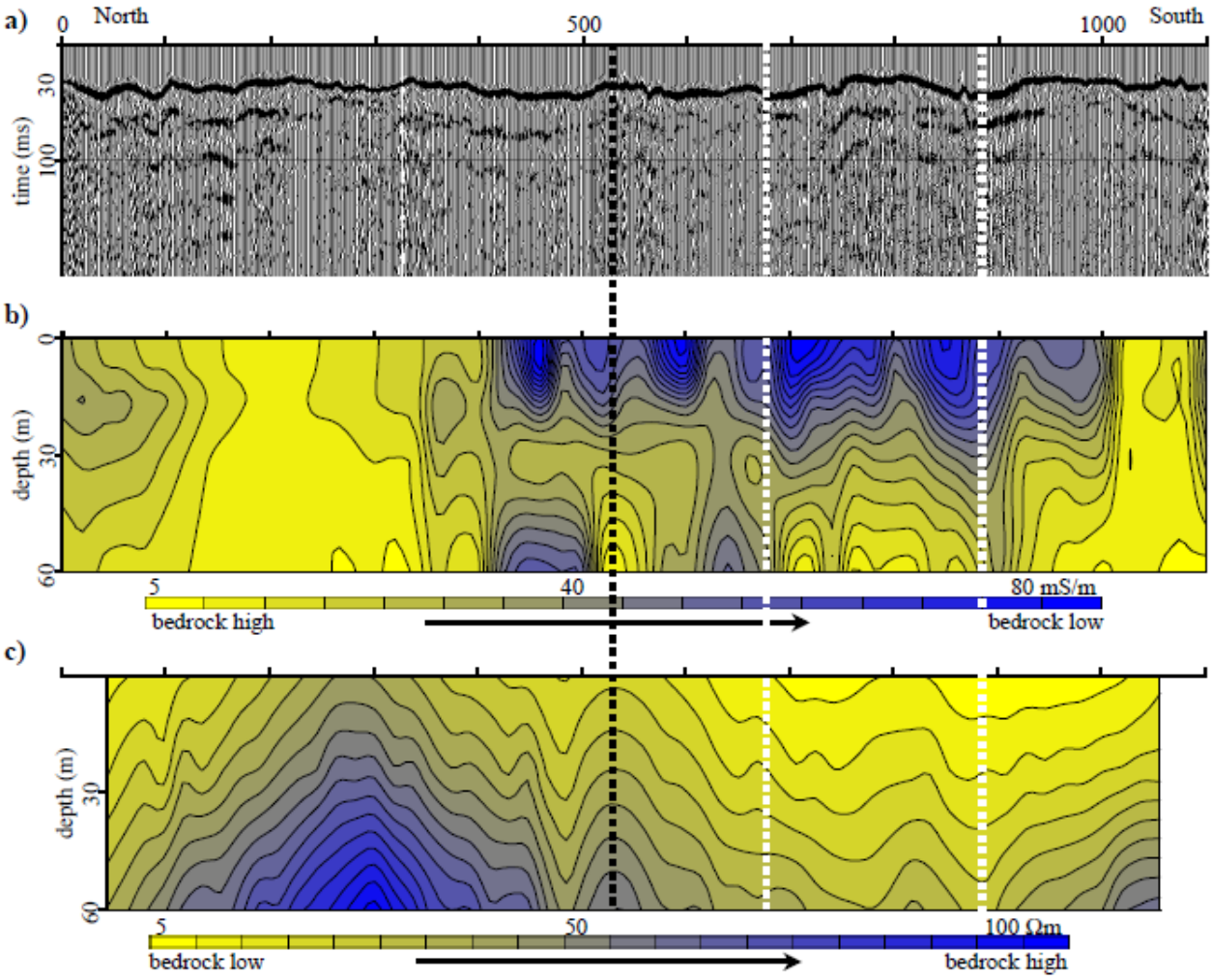

Figure 4.2: Modelled geophysical data a) seismic (stacked) b) EM c) resistivity (Fraser, 2001).

The electromagnetic survey was conducted with the Geonics EM34 through four traverses. Interstation spacing was 10 m, the horizontal dipole orientation was used at intercoil spacings of 10 m, 20 m, and 40 m, while the vertical dipole was used with intercoil spacing of 60 m. The data was contoured in Surfer software and is displayed in Figure 4.2 b). The data was then interpreted using the borehole log (borehole indicated by the black stippled line) for comparison (Fraser, 2001). Conductivity at the borehole decreases from 58.3 mS/m at 7.5m to 12.2 mS/m at 60 m, which is consistent with the bedrock observed at depth from the borehole log (Fraser, 2001).

The Barlow Res unit was used to collect resistivity data in the Wenner array. Electrode spacings of 20 and 50 m were used with a maximum spread of 150 m (Fraser, 2001). Resistivity data, as shown in Figure 4.2 c), correlated well with conductivity data increasing from surface to greater depth. Higher resistivity in the north is attributable to sandy cover in the area. The three data sets were all in agreement with each other and the available borehole log. Proposed borehole locations are shown by the white stippled lines in Figure 4.2.

4.2.7 Groundwater exploration in geologically complex terrain

To secure sustainable water supply in rural areas, the Department of Water Affairs and Forestry identified the need to develop a comprehensive approach for groundwater exploration in complex terrain (where water demand was expected to grow). The multidisciplinary approach adopted included structural geological mapping, tectonics, strain analysis, LANDSAT image interpretation and geophysical methods combined to determine the geodynamics of a region and identify geological structures where groundwater could be located. The primary objective of the project was to investigate the groundwater potential of the geologically complex terrain. Four research areas were chosen which were underlain by the Dywka Group, Limpopo Mobile Belt (LMB), Natal Metamorphic Provinces, and the Barberton Supergroup (Sami *et al.* 2002a).

The geophysical methods recommended were the magnetic and electromagnetic methods. For the Dwyka Group portion of the project, a research area of about 600 km^2, 12 km SE of Harding in KwaZulu Natal was explored (Sami *et al*., 2002b). Regional scale faulting occurs throughout the study area, trending NNW to NNE. These north-trending faults produced prominent graben structures to the East of the study area. Lineaments were examined based on their length, width, orientation, and frequency from LANDSAT data. The geophysical surveys for the area were then conducted over the identified lineaments (Sami *et al*., 2002b).

According to Sami *et al.* (2002a), 75% of water strikes occur at depths greater than 60 m, so methods were selected to be able to investigate to those depths. The methods chosen were the Max-Min Horizontal Loop Electromagnetic Method (HLEM) and ground magnetics. The HLEM is a frequency domain EM method with a moving source moving receiver system (Sami *et al*., 2002a). A total of 23 profiles were completed in various parts of the study area (Sami *et al*., 2002a). The geology of the site is unfavourable to groundwater occurrence; therefore, groundwater abstraction should be limited to hand pump schemes. Sami *et al.* (2002a) report that the exploration method employed was able to increase the drilling success rate in this region from a historical 12% to 50% in the study.

Another area- part of the Natal Metamorphic Province- of 1300 km^2, 30 km NW of Stanger and 75 km north of Durban in KwaZulu Natal was explored (Sami *et al*., 2002a). The metamorphic complex underlies 15% of rural KZN, and although water needs were met primarily through surface water

resources, groundwater could become increasingly important during drought (Sami *et al.,* 2002a). The region was included in the study for that reason. This area forms an elongated belt from the Valley of a Thousand Hills to the Tugela River and falls in the Mzumbe Terrane (Sami *et al.,* 2002b, a).

Geophysical investigations were completed at structural features believed to be under conditions of tensional or compressional strain determined from tectonic interpretation and strain analysis of field outcrop mapping. Specifically, targets were identified from aerial photographs and LANDSAT imagery interpretation. Target features included lineaments in all four major stress directions at geological structures such as fault lines, mylonite zones, dykes, lithological contacts of dipping strata and undifferentiated lineaments.

In addition to the Max-Min HLEM at various frequencies and ground magnetics, electrical resistivity sounding in the Schlumberger array (to determine weathering depth and bedrock fracturing) were used to conduct the survey. 13 electrical resistivity soundings, 29 magnetic profiles, and 26 electromagnetic traverses were conducted throughout the study area (Sami *et al*., 2002b). The multifaceted approach raised the drilling success rate from 54% (National Groundwater Database) to 89% in this part of the study (Sami *et al*., 2002a). The median yield was also increased from 0.1 L/s to 1.8 L/s (Sami *et al.,* 2002a).

The third case study region was underlain by Sandspruit, Theespruit and Komati Formations of the Onverwatch Group. The study area is southeast of Barberton, ~15 km from the eSwatini border in the districts of Tjakastad and Steynsdorp. As with the others, structural analysis, aerial photography, and LANDSAT lineaments were used to select target locations for geophysical exploration (Sami *et al*., 2002b). Dip-slip and strike-slip faults were water-bearing and associated with cavities that enhanced the greenstones' permeability. Geodynamic and stress analyses also suggest that structures with a NNE-SSW direction are likely to be under extension and open and are thus primary targets. Generally, the metabasalts are the best targets (Sami *et al.,* 2002a). The electromagnetic (Max-Min HLEM), magnetic and resistivity (electrical sounding) methods were also employed. There were 27 traverses that were conducted perpendicular to the lineament directions. In this region, the drilling success rate rose from a historic 50% to 89% (Sami *et al*., 2002a). The median yield was also increased from 0.4 L/s to 1 L/s (Sami *et al*., 2002a).

The Limpopo Mobile Belt region was split into two study areas i) and ii). Study area (i) was in the west of the LMB where a quaternary sand cover overlies metamorphic rocks and is 1200 km^2 (Sami *et al*., 2002b). Its southern boundary is formed by several ENE-WSW running faults and bound by the Limpopo River in the north. Study area (ii) was 1000 km^2 and is also bound in the north by the Limpopo River and in the South by ENE-WSW faults that separate the LMB metamorphics from the

Karoo Clarens (Sami *et al.*, 2002b). The magnetic, Max-Min HLEM and resistivity surveys were also conducted in this area. For the LMB, borehole success was observed to increase from 44% to 66% and the median yield from 0.39 L/s to 3.9 L/s (Sami *et al.*, 2002a)

4.2.8 Dayspring children's village

The Dayspring Children's Village is a school located ~70 km NW of Johannesburg. The area in which the school is found was invaded by water-consuming eucalyptus trees. A continuous geophysical survey was conducted to quantify the effect of removing the trees on the groundwater and to better select a drilling site. Geophysical data consisting of gravity, aeromagnetic, airborne electromagnetic, electrical resistivity, and seismic data were collected onsite to determine the relationship between the groundwater and trees. (Webb *et al.*, 2011b). The school lies on EW striking Silverton Formation shales of the Pretoria Group, interlayered with diabase sills with cross-cutting NS syenite dykes. Magaliesberg quartzites are encountered to the north of the site.

Figure 4.3 shows the modelled resistivity data for profile 17, a) was collected at the end of the rainy season and b) at the end of the dry season, while c) shows the difference between the two. Line 17 was closest to the line of trees, and there was a noticeable increase in resistivity between the rainy and dry seasons, possibly due to the use of groundwater by the trees in the top 8-15 m. A break halfway along the line may be a possible fracture that the trees are using to access water. This fracture was mapped from the other resistivity surveys (Webb *et al.*, 2012).

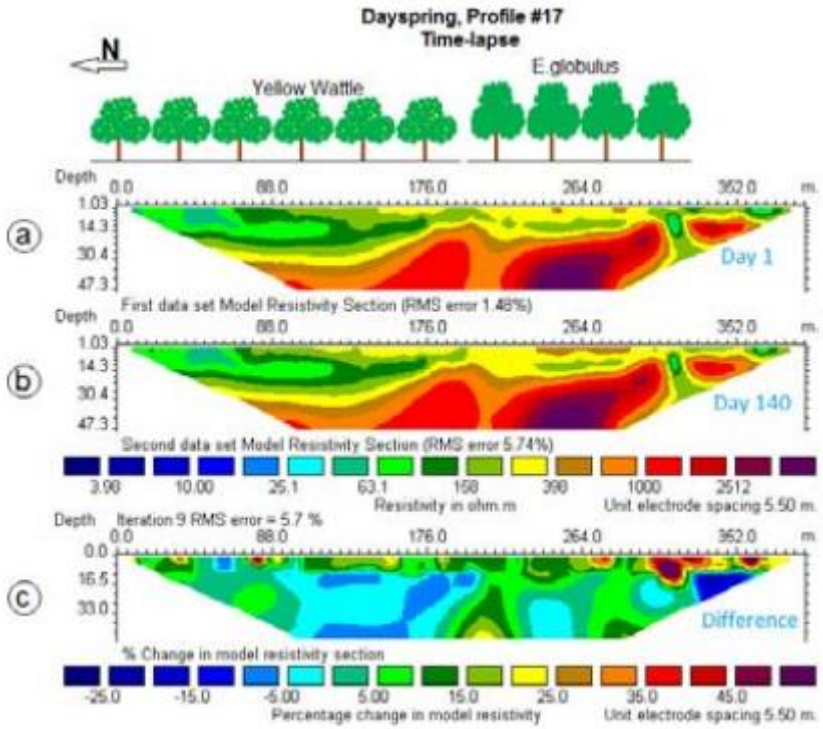

Figure 4.3: Line 17 a) April (end of rainy season), b) September (end of dry season), c) difference (Webb *et al.*, 2012).

4.2.9 Groundwater exploration in the Capricorn District in Limpopo

Regional potential targets of groundwater were identified for the Capricorn District Municipality in Limpopo (Sakala *et al.*, 2014). The area in question consists of high-grade in the north and low-grade archaean granitoid greenstone terrain of the Kaapvaal craton to the south. Goudplaats-Houtrivier Group tonalitic and trondhjemitic gneisses dominate most of the study area. The Sand River gneiss of the Limpopo Mobile Belt is dominant in the north. Complex folding and banding with extreme deformation can be observed in these rocks. EW and NS striking structures cross-cut various rock types in the north of the area.

Borehole yields in the crystalline aquifers of the region are <1 L/s but can be as high as 75 L/s in weathered and fractured regions. For the project, airborne magnetic data and satellite imagery were used to map lineaments and delineate fracture zones. The aeromagnetic data were collected from a survey flown in 2009 with a flight line separation of 200 m. The Cessna 210 was flown at 60 km/h at a clearance of 80 m. Magnetic data were recorded using the Geometrics G803 magnetometer with 1.0 nT accuracy. The total field magnetic data were recorded with the Geometrics G822A Caesium Vapour magnetometer with 0.01 nT resolution and a measuring frequency of 10 Hz. A Geometrics G856AG proton precession magnetometer was used as a ground base station to monitor diurnal variations (Sakala *et al.*, 2014)

The acquired data were interpreted to identify dykes, lineaments and magnetic source bodies that may have influence on groundwater occurrence. A digital elevation model was also used to supplement the study. An integration of lineaments from the aeromagnetic survey, Landsat imagery, and normalized difference vegetation index (NDVI) was able to determine that the north and central parts of the site were feasible for groundwater occurrence while the southern parts were dry with bare soil (Sakala *et al.*, 2014).

4.2.10 Groundwater exploration in Tsineng

Mokgatle (2016) conducted a study to assess groundwater in Tsineng, Northern Cape. The study area fell within the Ghaap Group in the Griqualand West Basin of the Transvaal Supergroup. Airborne geophysical investigations were conducted using the Skytem system, which is a helicopter-borne time-domain electromagnetic system. The TDEM results were used to identify subsurface resistivity contrasts and showed that some dykes in the area have detectable resistivity contrasts. The area is also underlain by the Kalahari sands, and the TDEM has the ability to determine soil conductivity at different depths. From the airborne survey results, ground geophysical targets were identified.

Gravity was used as decreases in gravitational acceleration can show the presence of cavities for karst aquifers. The EM was chosen because it is not made inefficient by a high resistivity cover and can

detect faults and conducive areas around dykes and weathered zones. Dykes are also often strongly magnetic, so the magnetic method was included in this extensive study. 2D ERT was also conducted where possible changes in lithology were detected by the other methods to obtain a model of the subsurface resistivity and verify other methods. Profile lines were perpendicular to identified targets. The ground geophysical survey confirmed the presence of structures identified from the airborne survey, such as faults and different lithologies. Drilling targets were then selected from the ground results, mostly along two major fault systems and dykes identified in the surveys. Sixty out of 78 drilled boreholes struck water and were declared successful. The highest-yielding boreholes were located along those major faults in the area. Hydraulic tests and chemical analyses were also conducted as part of the study (Mokgatle, 2016).

4.2.11 Polile Tshisa Hot Spring

Hot springs are indicators of groundwater circulation at great depth along fault zones and neotectonics. Their characterization can help infer the occurrence of structures favourable for groundwater potential. Therefore, Madi *et al.* (2016) conducted a study to characterise the Polile Tshisa hot spring in the Eastern Cape using magnetic and electromagnetic methods. The area is underlain by sandstones of the Molteno Formation, characterised by intense weathering and kaolinisation. The hot spring is possibly hosted within a regional fault that connects other hot springs along it. Figure 4.1 shows the geological map of the region and the hot springs.

Magnetic data were obtained using the Geometrics Proton Procession Magnetometer (G-859) with a cycle time of 1.5 s, 0.1 nT resolution, an accuracy of 0.5 nT, and a gradient tolerance of 1000 nT (Madi *et al*., 2016). Data were acquired around the hot spring along four lines (NW-SE. N-S, NE-SW) and the magnetic map produced at grid size 14m is shown in Figure 4.5. Three magnetic profiles were extracted from the magnetic map, one of which is shown in Figure 4.6. The two peaks may be due to the presence of dykes that can be targeted for groundwater.

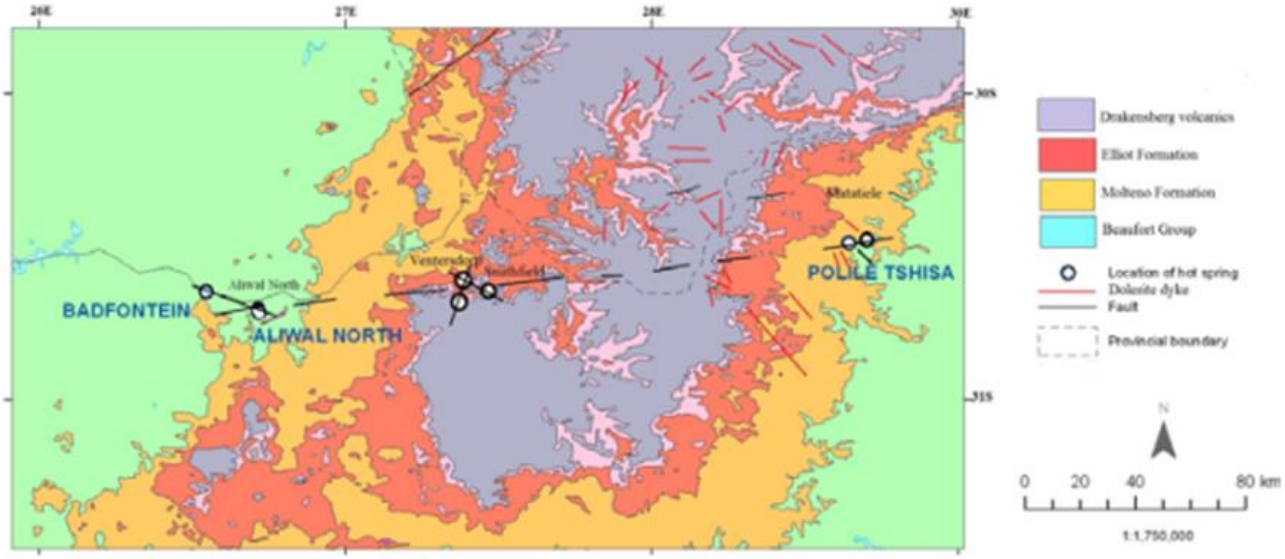

Figure 4.4: Geological map showing the hot springs and structures in the Eastern Cape neotectonic belt. (Madi *et al*., 2016).

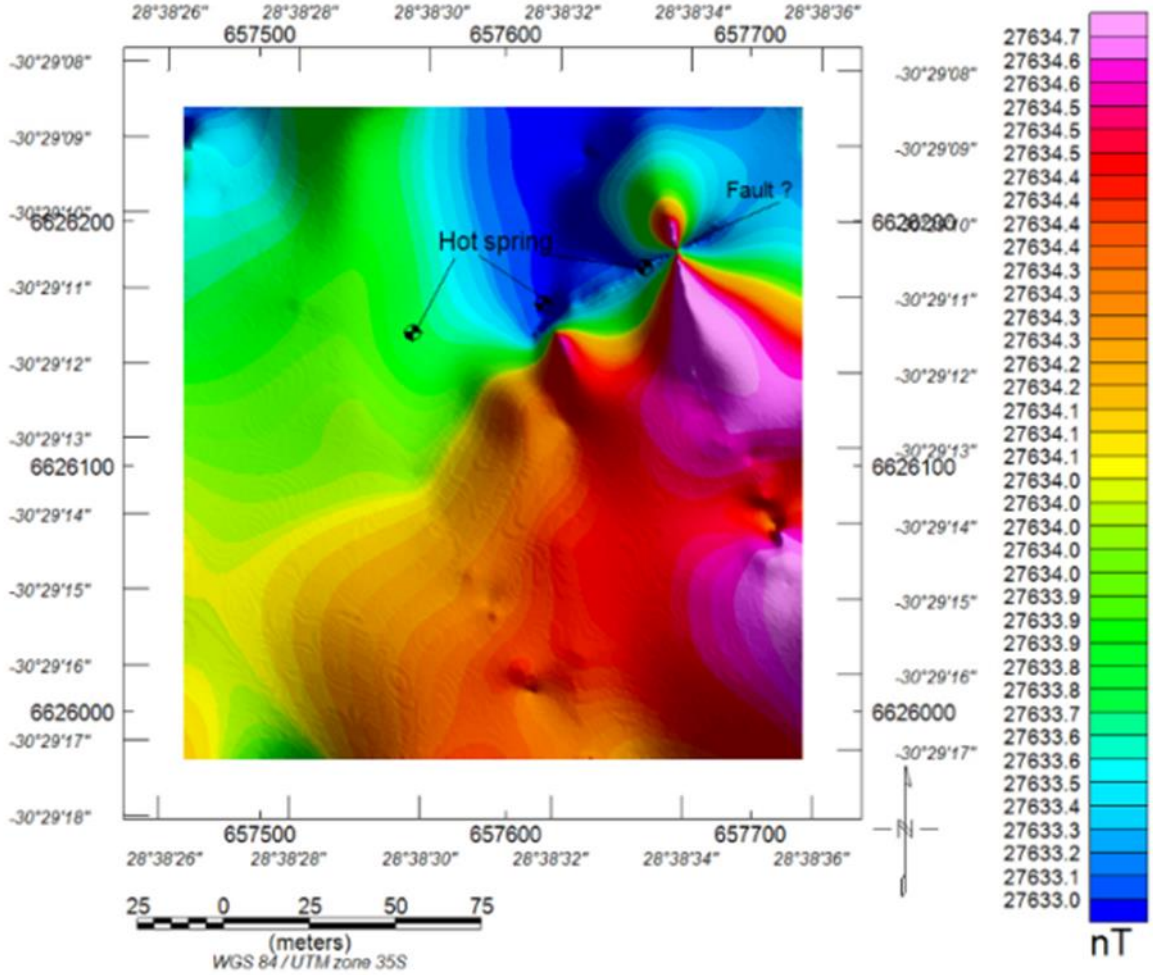

Figure 4.5: Magnetic Map at grid size 14m (Madi *et al*., 2016).

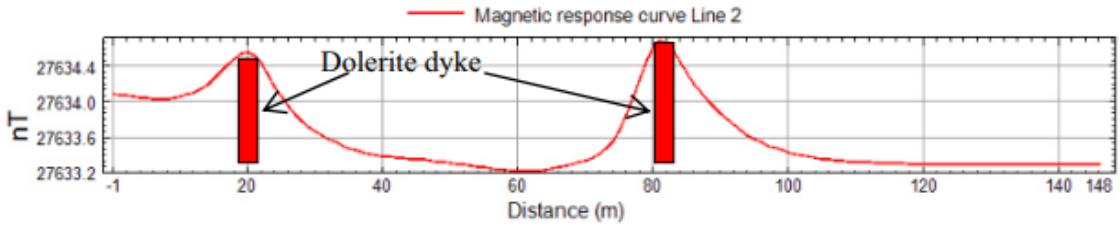

Figure 4.6: NW-SE Magnetic profile (Madi *et al.*, 2016).

The electromagnetic survey was conducted along three profiles. Lines 1 and 2 were SE-NW, and line 3 was NE-SW (Figure 4.7). The vertical (VD) and horizontal dipole (HD) modes were set with intercoil spacing of 20 m and 10 m station spacing (Madi *et al*., 2016). The line 1 profile is shown in Figure 4.8. HD is higher than VD, which indicates a decrease in conductivity at depth. A positive anomaly (VD) at 170 m shows a possible weathered and fractured zone, and a negative anomaly (HD) may be a vertical dyke (Madi *et al*., 2016).

The anomalies in the VD at 60 and 130 m are possible dykes separated by a fault (Madi *et al*., 2016). This indicates a good potential for a productive well in the area. A depth conductivity model from Line 1 data was constructed (Figure 4.9) and shows two high conductivity zones (≥ 30 mS/m) in the southeastern end and at 175 m and beyond. Both zones are ~8 m deep and are interpreted to be weathered sandstones. The broken black lines are interpreted faults (Madi *et al*., 2016).

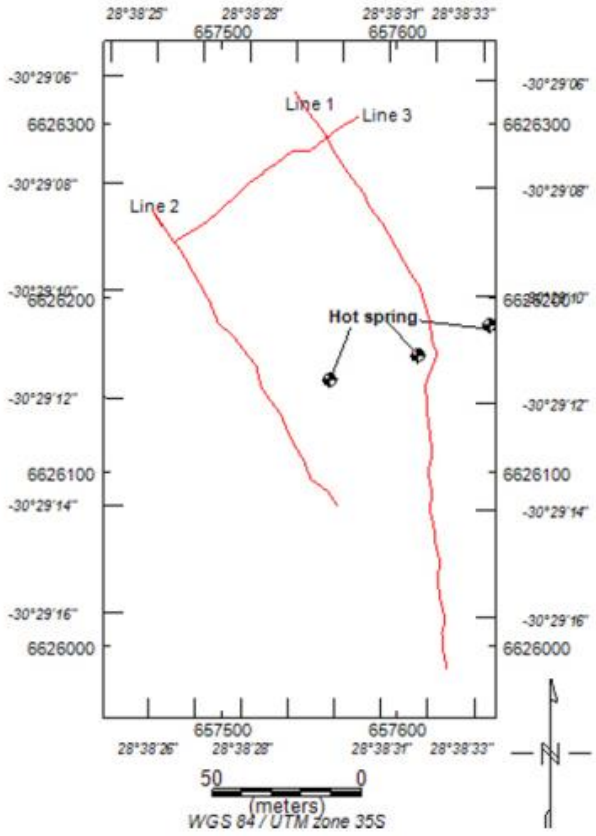

Figure 4.7: EM survey lines (Madi *et al*., 2016).

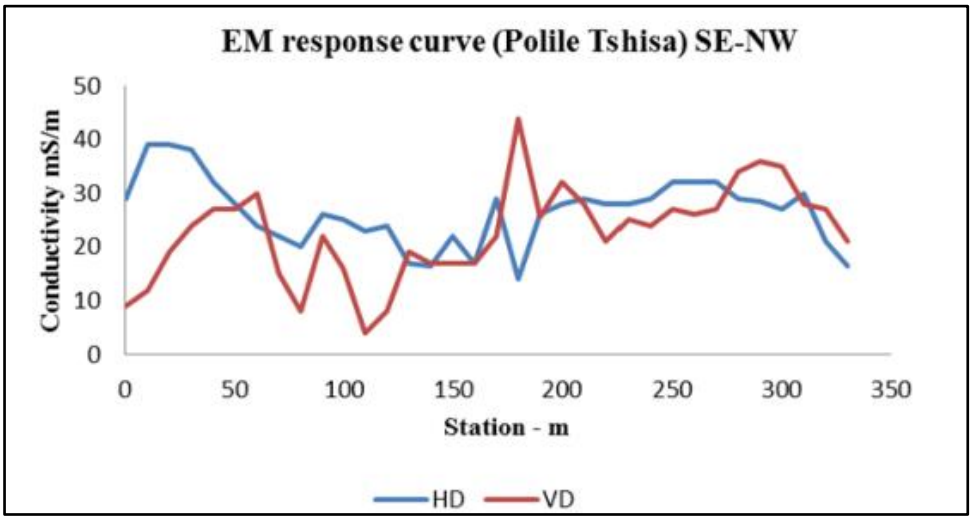

Figure 4.8: Line 1 EM curve (Madi *et al*., 2016).

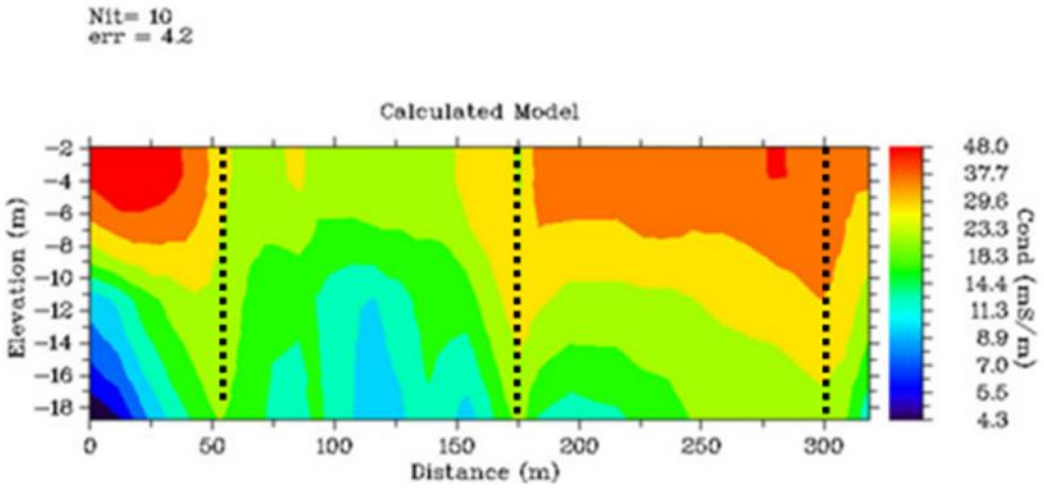

Figure 4.9: Polile Tshisa hot spring depth-conductivity model (Madi *et al*., 2016).

4.2.12 Feasibility plan for groundwater resource development of the Malmani Dolomites within the Olifants River Water Supply System

The consultant led a project to determine the Malmani Subgroup dolomites' potential along the Limpopo and Mpumalanga escarpment as a potential water source. The main aims of the study were to augment the water supply to the Olifants River Water Supply System (ORWSS) by securing groundwater use in the area and to find if artificial aquifer recharge is possible (DWS, 2017). The area of interest is 1600 km^2 and falls within several local municipalities (DWS, 2017). The dolomites form a karst aquifer.

Geophysical surveys of potential wellfield sites of the area were undertaken to site boreholes to be drilled. The primary methods used in this survey were electromagnetic and ground magnetics along the same traverse lines (DWS, 2017). These surveys were conducted in five priority potential wellfield target zones (WFTZ). Targets were:

- PR01 with four survey lines totalling 4.4 km.
- BR01 with three survey lines totalling 5.8 km.
- TR01/TR03 with three survey lines totalling 3.4 km
- OR01 with four survey lines and a total of 5.9 km
- PV01 with four traverse lines totalling 4.8 km

The ground conductivity survey was conducted using the Geonics EM-34 set up in the horizontal and vertical dipoles with an intercoil spacing of 20 and 40 m. The depth of investigation was approximately 60 m (DWS, 2017). Potential groundwater-bearing fractured dolomite can be identified by elevated apparent conductivities of 10 mS/m to 30 mS/m within fault systems or adjacent to dolerite dykes (DWS, 2017). A magnetometer was used to conduct a ground magnetic survey. This allowed the dolerite dykes and mineralised iron-rich zones in large fault systems to be identified. These appear as spikes within the magnetic data (DWS, 2017). Only a few results obtained for some of the survey lines are outlined here.

PR01- Pilgrims Rest-Blyde WFTZ geophysical survey

The survey was conducted on 3rd-7th April 2017. Preliminary lines were changed slightly due to access issues. Figure 4.10 shows the potential wellfield site (red polygon) geophysical lines in blue while the preliminary lines are green. Pink lines are adjacent WTZ, light blue are other potential wellfield sites which have not been investigated while white lines refer to geological features such as faults or dykes. The start and end markers of the survey are also shown (DWS, 2017).

Based on the features interpreted from the surveys, potential borehole sites were identified. Three priority potential borehole targets and two alternatives were identified for Line 1. These were along a fault/fracture zone and adjacent to an identified dolerite dyke (DWS, 2017).

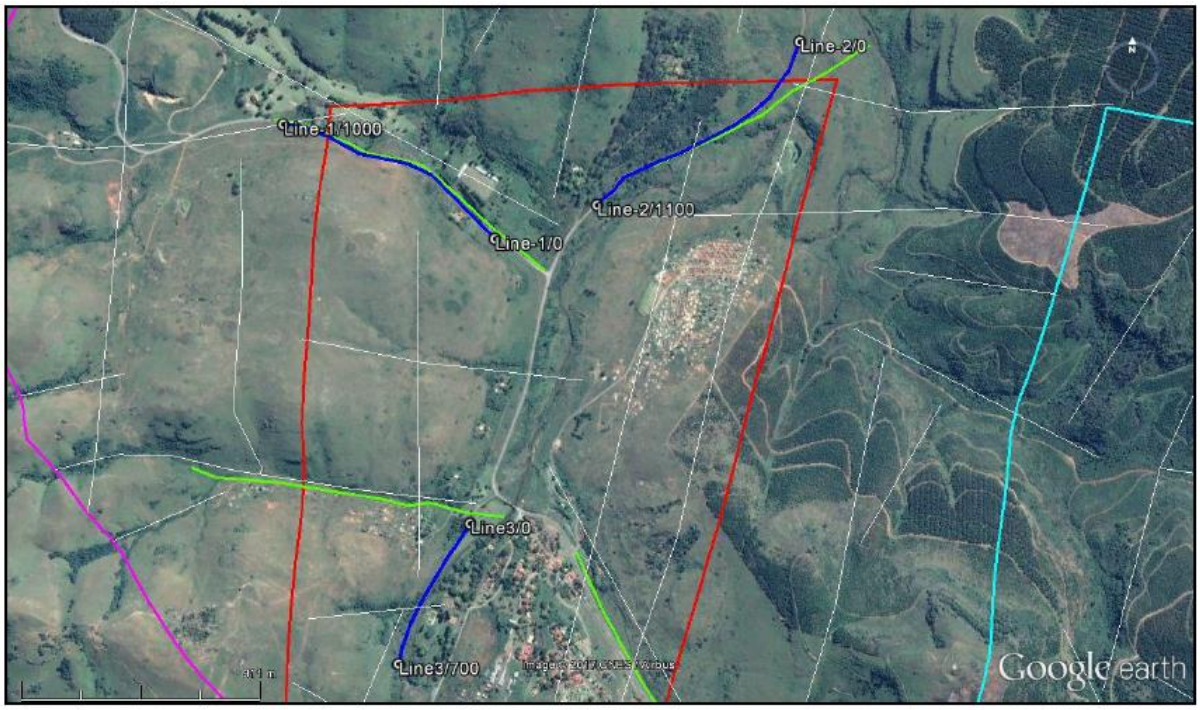

Figure 4.10: PR01 Geophysical traverses (DWS, 2017).

Figure 4.11 shows the modelled result of the electromagnetic and magnetic surveys conducted on line 1. The EM34 horizontal dipole with a 20 m intercoil spacing is light green, and the 40 m is black. While the vertical dipole of 20 m is pink and the 40 m is red lines. Navy blue lines show the magnetics.

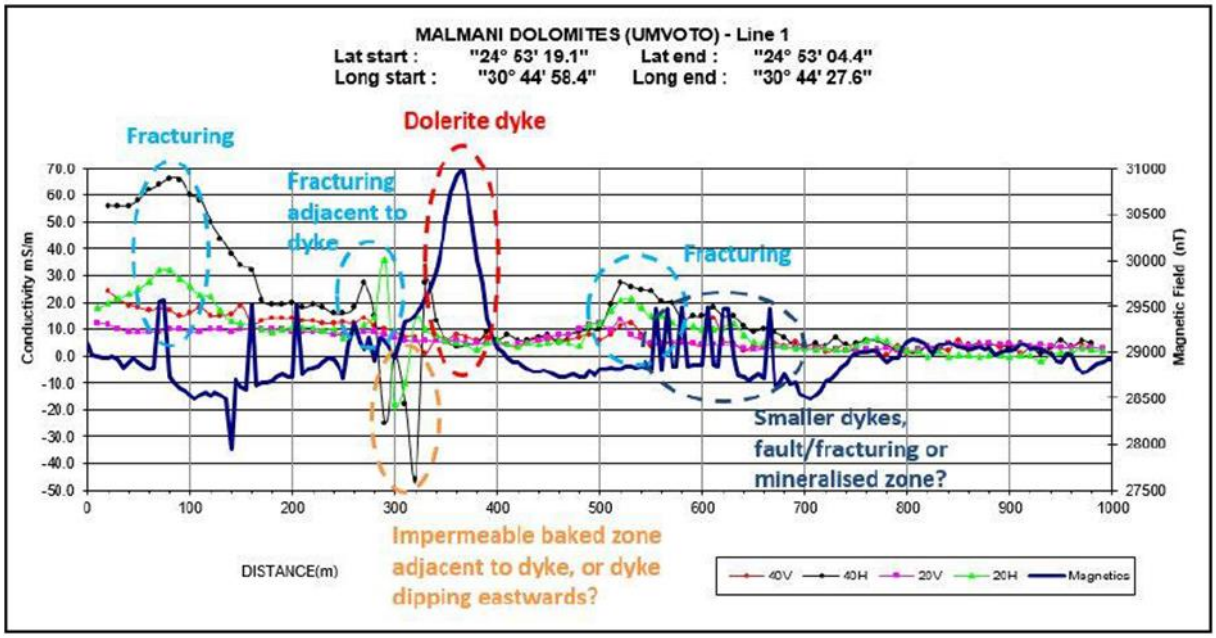

Figure 4.11: Line 1 conductivity and magnetic profile (DWS, 2017).

The fractured zones were identified as high conductivity zones of 10-30 mS/m or spikes in both the 20 m/40 m vertical and horizontal dipoles. In contrast, spikes in the magnetic data are attributed to

the presence of dolerite dykes (DWS, 2017). Figure 4.12 shows the modelled results overlain with the priority drilling sites (PR01) identified and the alternative drill sites (a1/a2 respectively).

The priority boreholes are shown in Figure 4.12 by dark blue circles, while the light blue circles are alternative sites. The priority drilling sites target a N-S-orientated fracture zone adjacent to and northwest of a dyke with a N-S striking and potentially eastward dipping dyke (DWS, 2017).

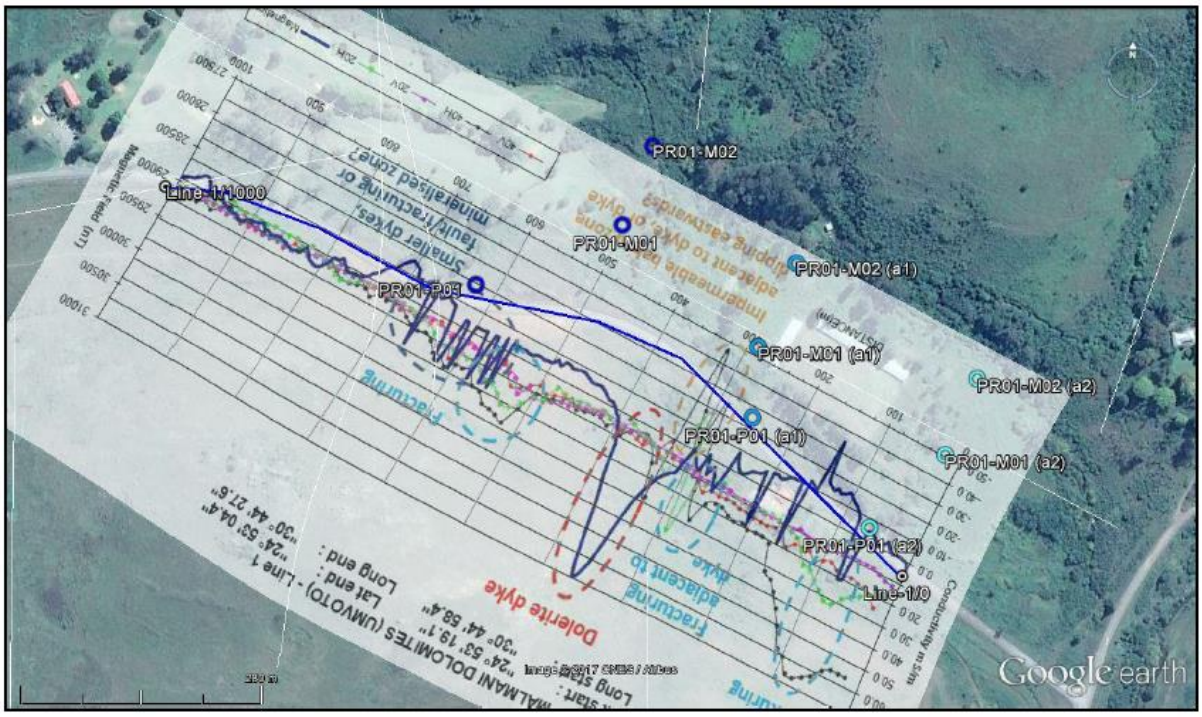

Figure 4.12: PR01 line 1 results overlain with borehole locations (DWS, 2017).

The fracture zone for the potential target is at about 500 m-600 m along the survey line, while the alternative sites target fracturing at around 260-280 m and 60-100 m adjacent and southeast to the main dyke along the traverse.

Blyde River Valley WFTZ- BR01 Geophysical survey

Four EM34 and magnetic lines were surveyed as part of the project between the 8th and 12th of May 2017 for this potential well field site. Figure 4.13 shows the traverse lines for the potential well field site. Preliminary lines are green, while actual traverses are blue and show start and end positions (DWS, 2017). Pink lines are adjacent WFTZ, light blue lines are potential WFTZ not included in this phase of investigation while white lines are geological features such as dyke or faults (DWS, 2017).

Line 1 in this survey was orientated NNW-SSE and was 1.1 km long. Along this traverse, alternative (BR01-a1) drilling sites were identified. They target fracturing adjacent to and between two main large NW-SE-orientated dolerite dykes at 560 m and 900-940 m along the traverse (DWS, 2017). Line 1 results are shown in Figure 4.14. Anomalous peaks identified as dolerite dykes are circled in red with fractures circled in blue.

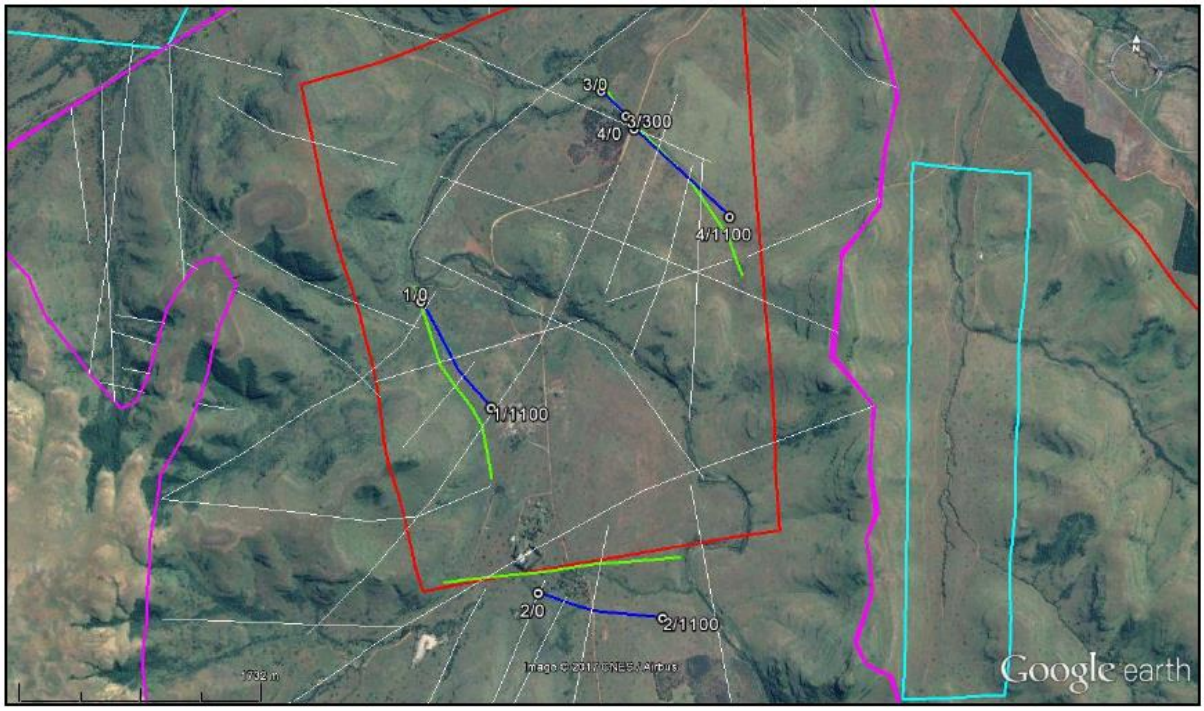

Figure 4.13: BR01 Geophysical traverses (DWS, 2017).

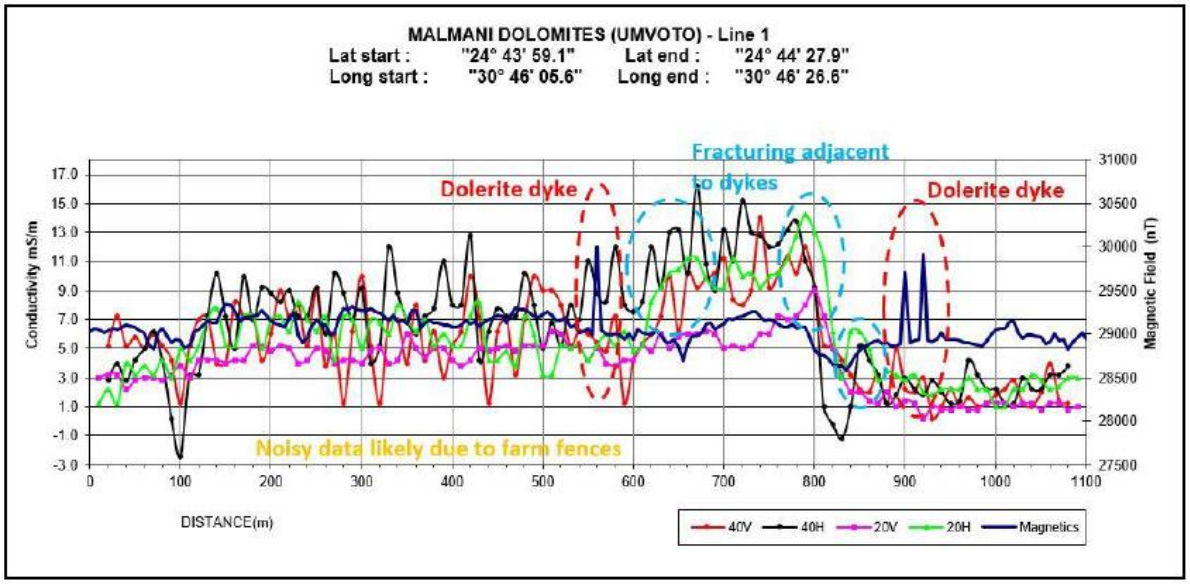

Figure 4.14: BR01 Line 1 conductivity and magnetic profile (DWS, 2017).

The noise in the obtained model is attributed to the presence of farm fences within the survey area. Figure 4.15 shows Line 1 survey modelled results overlain with alternative borehole sites shown with light blue circles (DWS, 2017). The influence of anthropogenic features is one issue to be taken into consideration when a geophysical method is chosen.

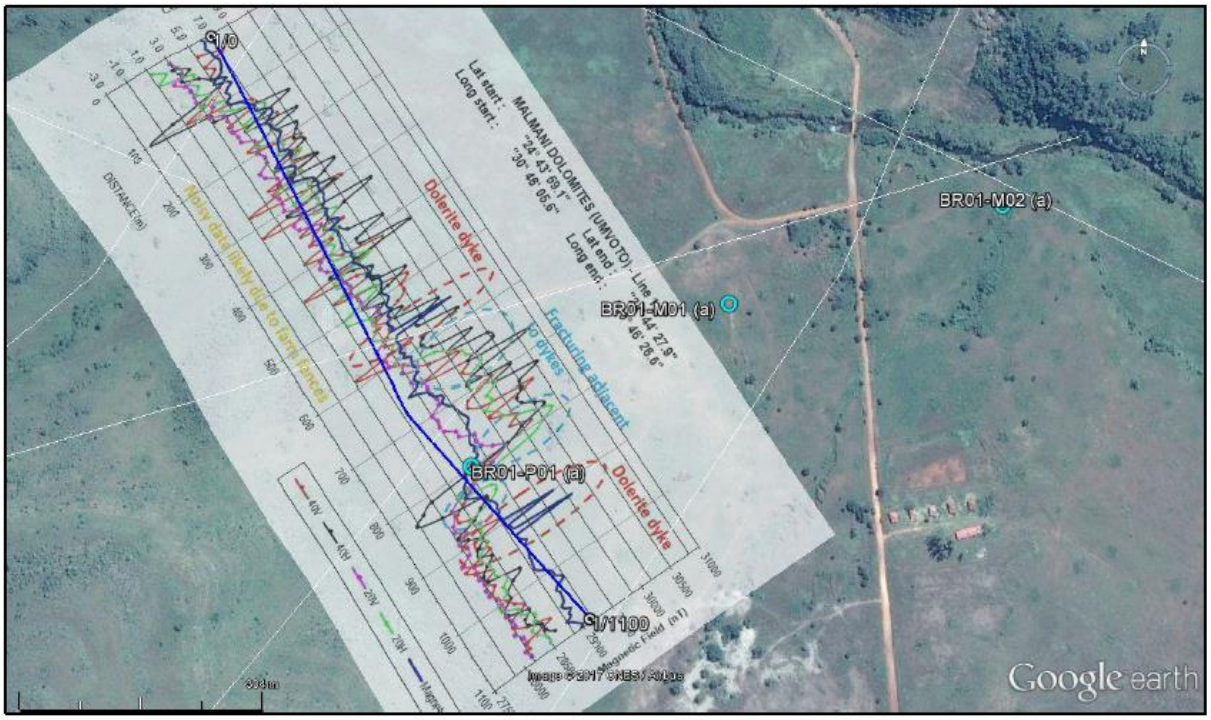

Figure 4.15: BR01 line 1 survey results overlain with borehole locations (DWS, 2017).

Line 2 was WNW-ESE orientated and about 1.1 km in length. Three priority boreholes on this line target a fault structure with a NNW-SSE orientation around 60-120 m along the survey line. The fault is adjacent to and west of a large NNW-SSE striking dolerite dyke (DWS, 2017). Figure 4.16 shows the results modelled for this line, and Figure 4.17 shows the results overlain with potential targets. The data for line 2 are also slightly noisy due to the fences in the area. However, the features in the subsurface can be discerned. Spikes in the EM34 data represent the fractures related to faulting and fracturing adjacent to the dolerite dyke.

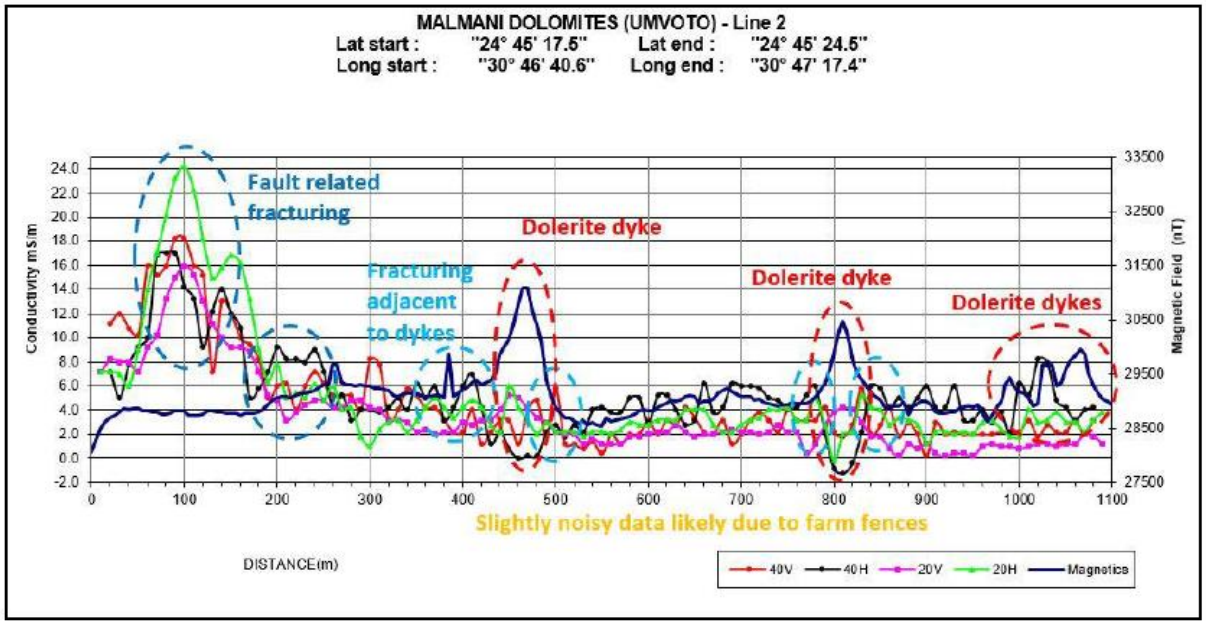

Figure 4.16: BR01 line 2 conductivity and magnetic profile (DWS, 2017).

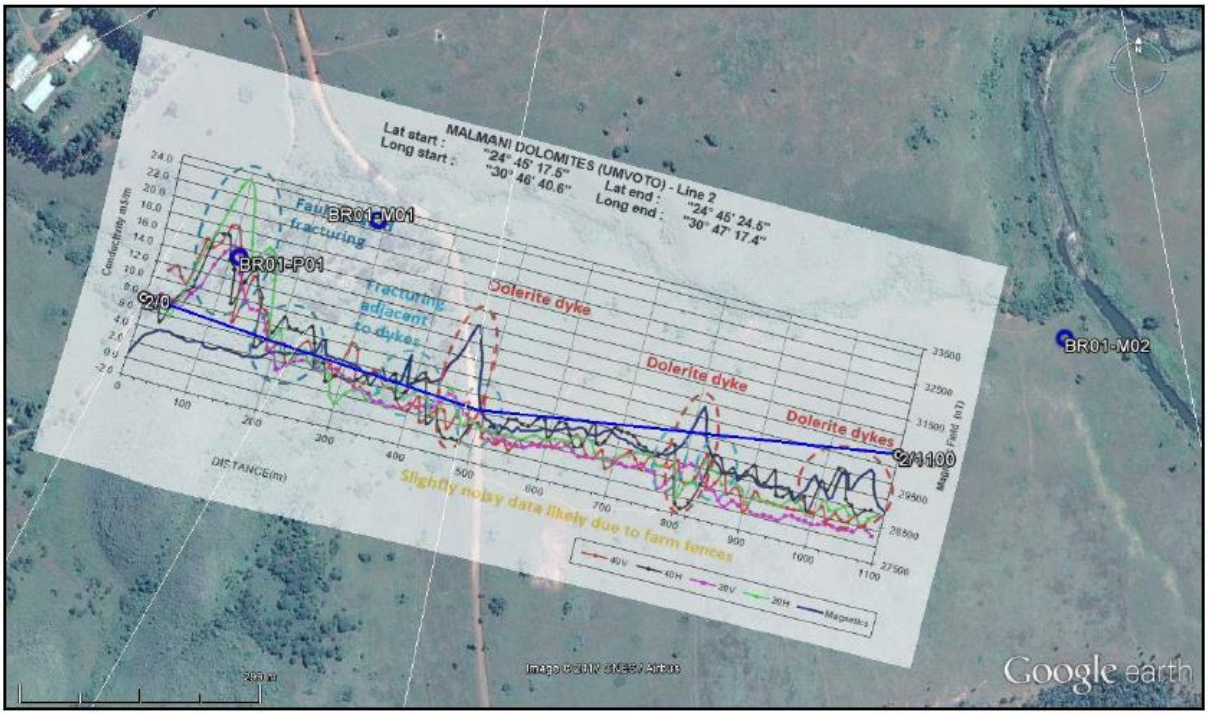

Figure 4.17: BR01 line 2 modelled results overlain with potential borehole targets (DWS, 2017).

Exploration drilling and pump testing ensued after the extensive geophysical surveys in the five potential wellfield target zones. Three boreholes were drilled for the Pilgrims Rest Blyde PR01 WFTZ, while four boreholes were drilled in the Blyde River Valley BR01 WFTZ. The BR01 yields were very low (<0.5 L/s or dry) and were made to be monitoring boreholes (DWS, 2017). Further EM, magnetic and airborne geophysical surveys were recommended for more precise siting of boreholes in the WFTZs with higher groundwater potential (DWS, 2017).

4.2.13 Makula Village groundwater potential

Ratshiedana *et al.* (2018) conducted a study in Makula Village, Limpopo, to investigate structures that possess groundwater potential. The village is underlain by the rocks of the Soutpansberg Group, which is a volcano-sedimentary succession. Clastic sediments such as shale, conglomerates and greywacke are found in the basal formations, while near the top of the succession, iron-rich basalts are intercalated with the sediments. The magnetic method was used due to the magnetic nature of the rocks in the area. A Proton Precession Magnetometer (G-856) was used to collect the data, with a Garmin GPS used to locate all sampling points. Six traverses, 1 km long and 500 m apart, were conducted with station spacings of 20 m (Ratshiedana *et al.*, 2018). The profiles were taken perpendicular to the strike.

The magnetic data was reduced and processed. One of the magnetic profiles generated after all the processing steps were conducted is shown in Figure 4.18. The vertical axis shows magnetic intensity in nT. The alternating magnetic highs and lows suggest contacts between different lithologies, the

water-bearing sediments and the magnetic basalts (positive anomalies) or the presence of faults (negative anomalies). The vertical derivative of the magnetic data was taken to sharpen and enhance anomalies, and a contour map was generated (Figure 4.19). SW-NE-orientated lineaments of low magnetic intensity can be observed, which are likely contacts or faults. The magnetic survey was thus able to successfully delineate structures that are potentially water-bearing in Makula (Ratshiedana *et al*., 2018).

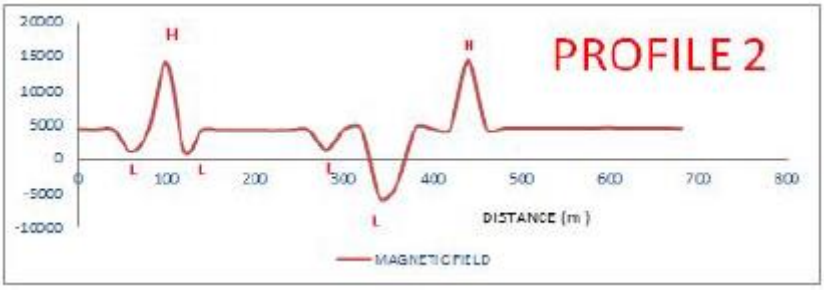

Figure 4.18: Makula magnetic profile 2. Modified from (Ratshiedana *et al.*, 2018).

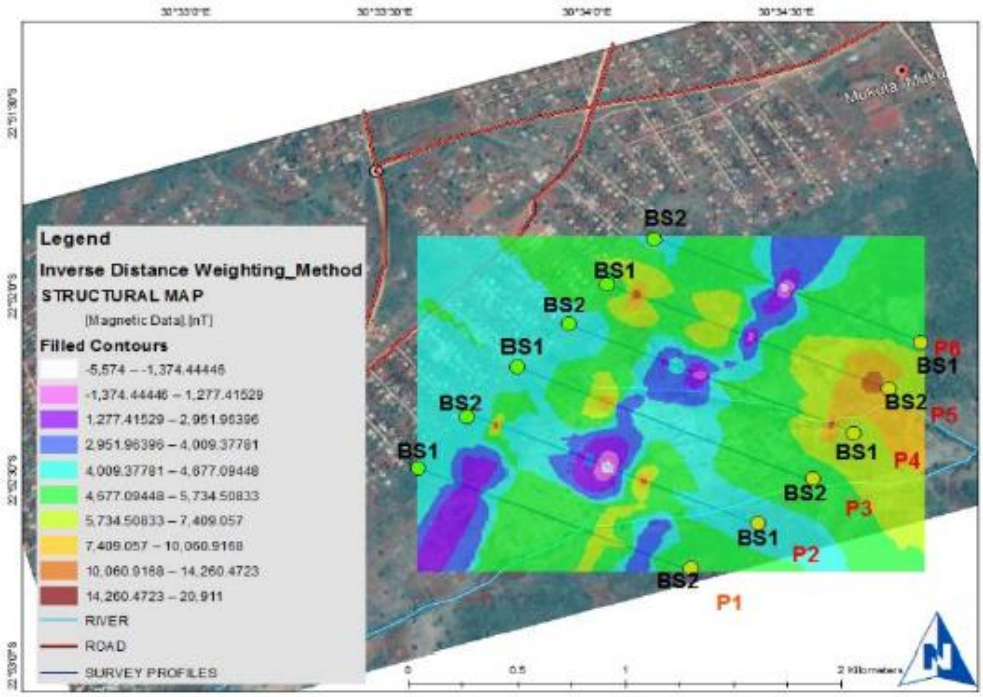

Figure 4.19: Vertical Derivative contour map (Ratshiedana *et al*., 2018).

4.2.14 Groundwater exploration in Limpopo using remote sensing and geophysics

Magakane (2019) conducted a study in an area in Limpopo Province underlain by the Archaen-age Limpopo Mobile Belt Rocks, the Soutpansberg volcano-sedimentary sequence and the Karoo sedimentary cover. Remotely sensed data, which contained lineaments, lithologies, land, slope, and land cover, were used to create groundwater potential maps. Several geophysical surveys were then conducted to validate the groundwater potential zones.

Regional aeromagnetic data was obtained for the area. The data was recorded using a proton precession magnetometer at an average height of 100-150 m above the ground with 1 km lines (Magakane, 2019). The data was reduced, and spurious noise was removed before interpretation. Reduction to the pole, high pass filters and manual digitizing of the data were conducted. Figure 4.20 shows the total magnetic field intensity for the study area, which is consistent with the complex geology in the region. Elongated bodies with high magnetic signatures are observed, which may be dolerite dykes while low magnetic signatures relate to metasediments in the area.

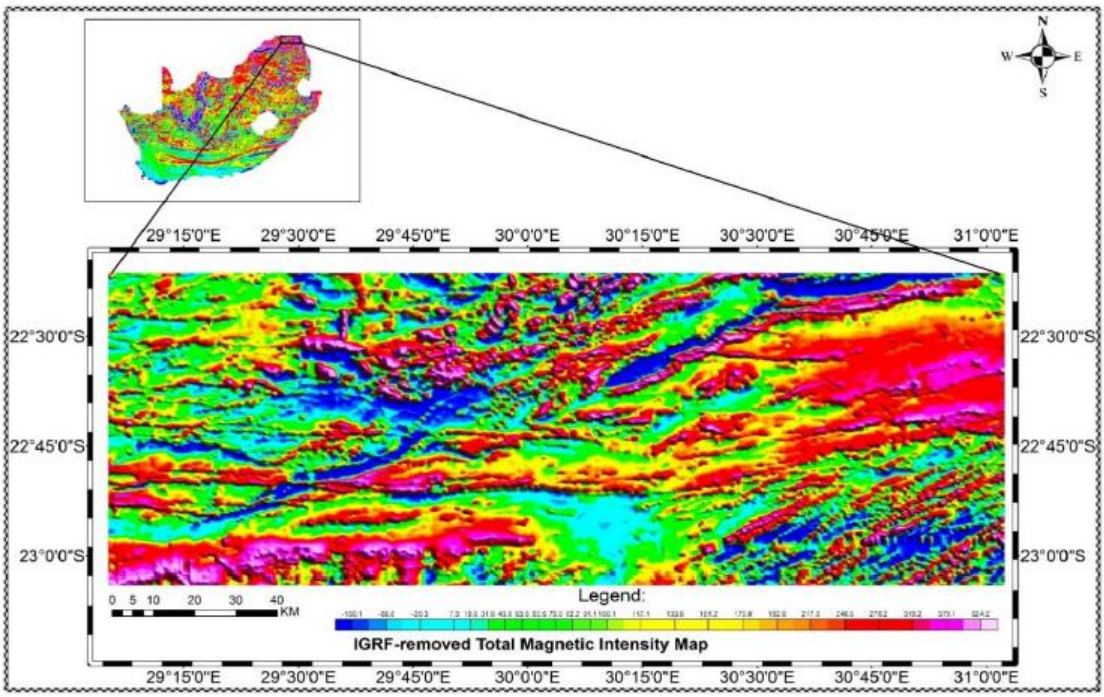

Figure 4.20: Total Magnetic Intensity for the study area (Magakane, 2019).

Target areas identified from the remote sensing and aeromagnetic data were further investigated by means of a ground resistivity survey. VES was conducted in the Schlumberger array using the Ares G v5.0 Resistivity and IP imaging equipment on two near parallel profiles. The VES data was input into IP2Win software to interpret the resistivity sounding curves by curve matching (Figure 4.21). Four layers were determined from the curve matching.

A resistivity cross-section (Figure 4.22) was then constructed from the data of the two profiles. The topmost layer with an apparent resistivity of 160-190 Ωm is consistent with unsaturated topsoil. The second layer has low apparent resistivities of 4-6 Ωm with a varying thickness of 3-9 m across the profiles. It was interpreted as a saturated, weathered layer, a potential groundwater target. The third geoelectric layer, with an apparent resistivity of 6-30 Ωm, is interpreted by fractured and saturated rock, while the fourth layer (14000 Ωm) is bedrock (Magakane, 2019). The integration of remote sensing and geophysical data was able to successfully determine groundwater potential zones, which were also compared to existing borehole yield data available in the region (Magakane, 2019).

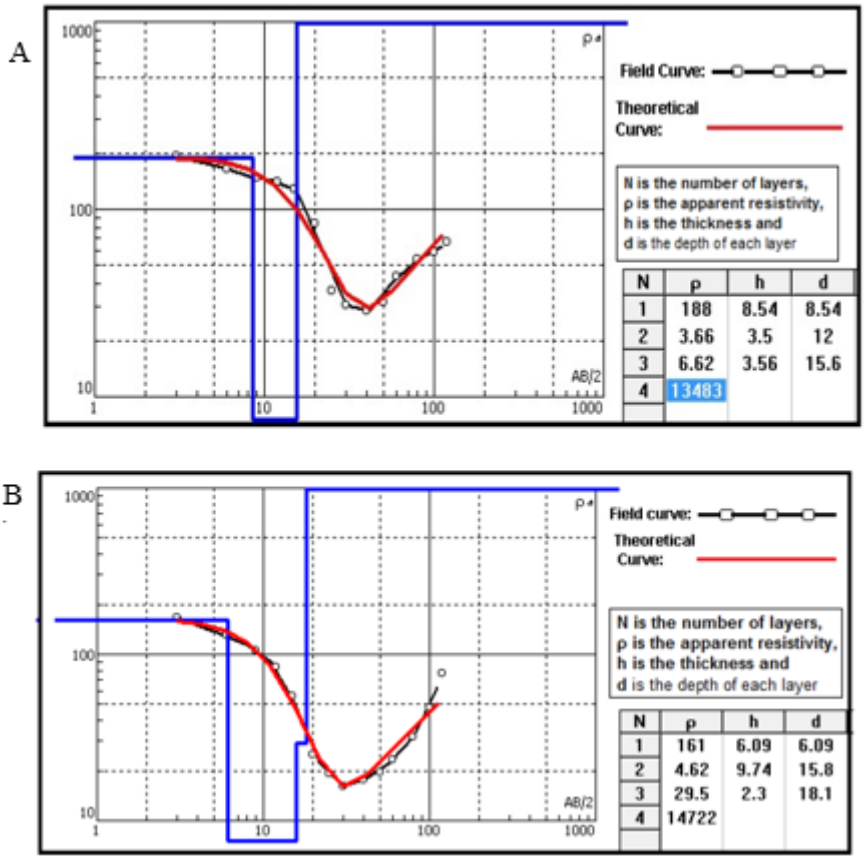

Figure 4.21: Resistivity curves for site A and site B at Masea in the study area (Magakane, 2019).

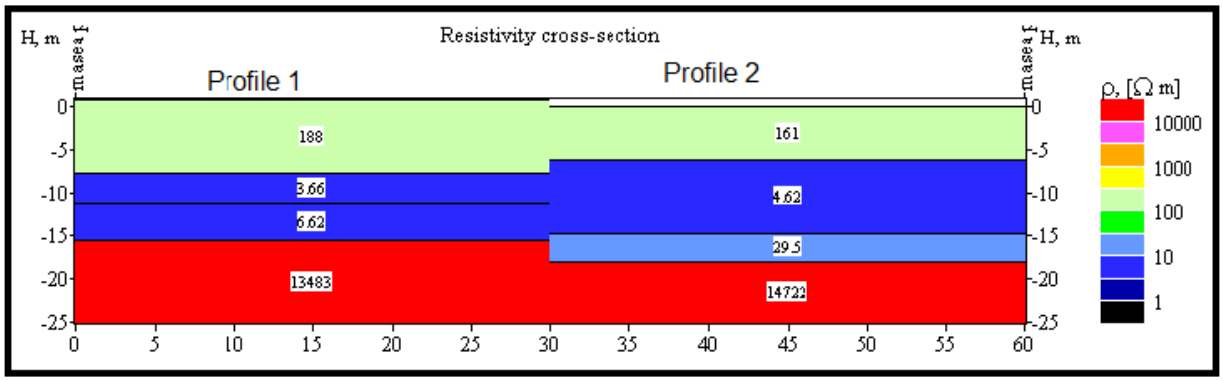

Figure 4.22: Resistivity section at Masea in the study area (Magakane, 2019).

4.2.15 Ndlambe Municipality

The study investigated the groundwater potential in the Ndlambe Municipality, Eastern Cape using various methods. Remote sensing was used to map lineaments in the region (from LANDSAT data), surface geology observation was done, and subsurface lithology was explored by means of four borehole logs (Mpofu *et al.*, 2020). The area in question is set in the Cape Fold Belt. Outcrops of the Dwyka Group occur nearby. The regional geology map of the municipality is shown in Figure 4.23.

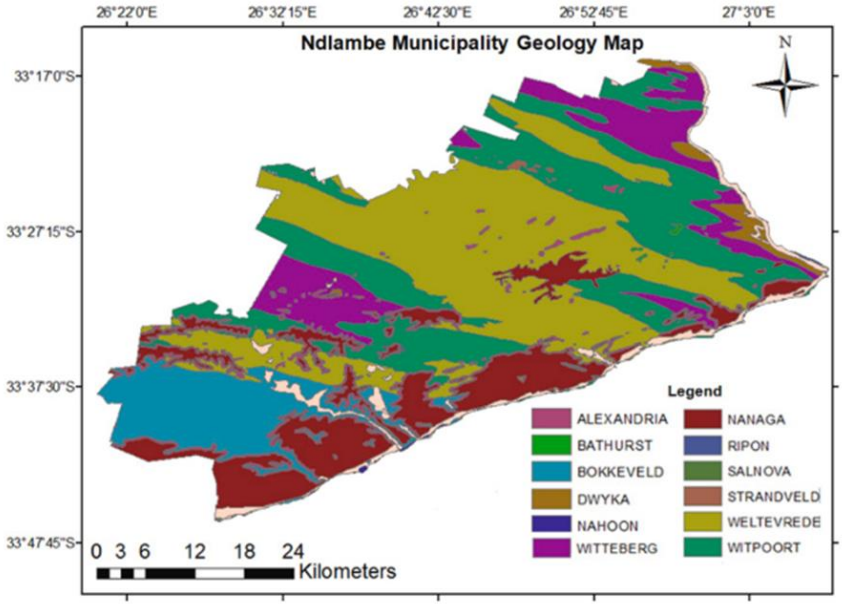

Figure 4.23: Ndlambe regional geology (Mpofu *et al.*, 2020).

As part of the study, vertical electrical sounding (VES) and electrical resistivity profiling (ERP) were undertaken. Two resistivity instruments were used, the Geotron resistivity meter (G41) and the Sycal Pro resistivity meter. The Geotron was used to produce apparent resistivity pseudosections and inverse model resistivity in the Schlumberger array. The distance between current electrodes AB/2 was increased from 1.5 m to a maximum of 100 m (Mpofu *et al.*, 2020). Four VES were conducted. Data were collected with the Sycal pro in the dipole-dipole array, with three lines of investigation (line 1=320 m, line 2=480 m, line 3=320 m). The calculated apparent resistivity from the Geotron data was then plotted against AB/2 on a log-log graph, and the acquired data were plotted on sounding curves. The theoretical VES curves were generated using the Win Resist program. Data collected from both instruments were processed in the RES2DInv to produce 2D electrical resistivity models from apparent resistivity pseudo-sections (Mpofu *et al.*, 2020).

At site 1, electrical resistivity imaging was conducted in the Schlumberger and dipole-dipole array with a spread of 350 m and electrode spacing of 10 m. The dipole resistivity depth model is shown in Figure 4.24, while Figure 4.25 shows the inverse resistivity model. Resistivity values range from 6.63-5755 Ωm (Mpofu *et al.*, 2020). The low resistivities on the surface could be attributed to weathered moist sandstone with clay, high resistivity zones are indicative of fresh bedrock. Intermediate resistivity layers (120 Ωm and 317 Ωm) may characterise weathered sandstone and quartzite. Based on the profile, regions associated with fractures (110 and 120 m; 200 and 230 m) could be potential sites for borehole drilling (Mpofu *et al.*, 2020). Figure 4.26 shows the resistivity curves generated for site 1. There are three layers; the second layer consists of fractured and weathered sandstone, while the third is a high resistivity layer (970 Ωm).

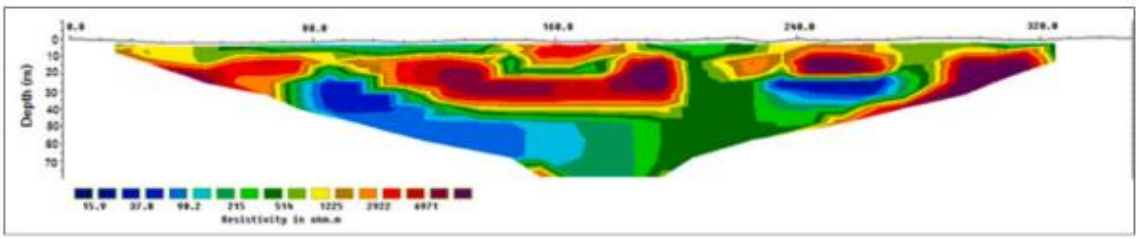

Figure 4.24: Site 1: Dipole-dipole resistivity model (Mpofu *et al.*, 2020).

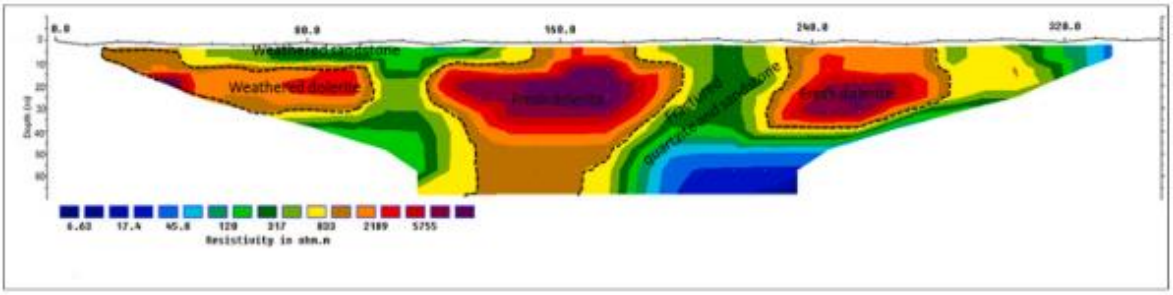

Figure 4.25: Site 1: Schlumberger array depth model (Mpofu *et al.*, 2020).

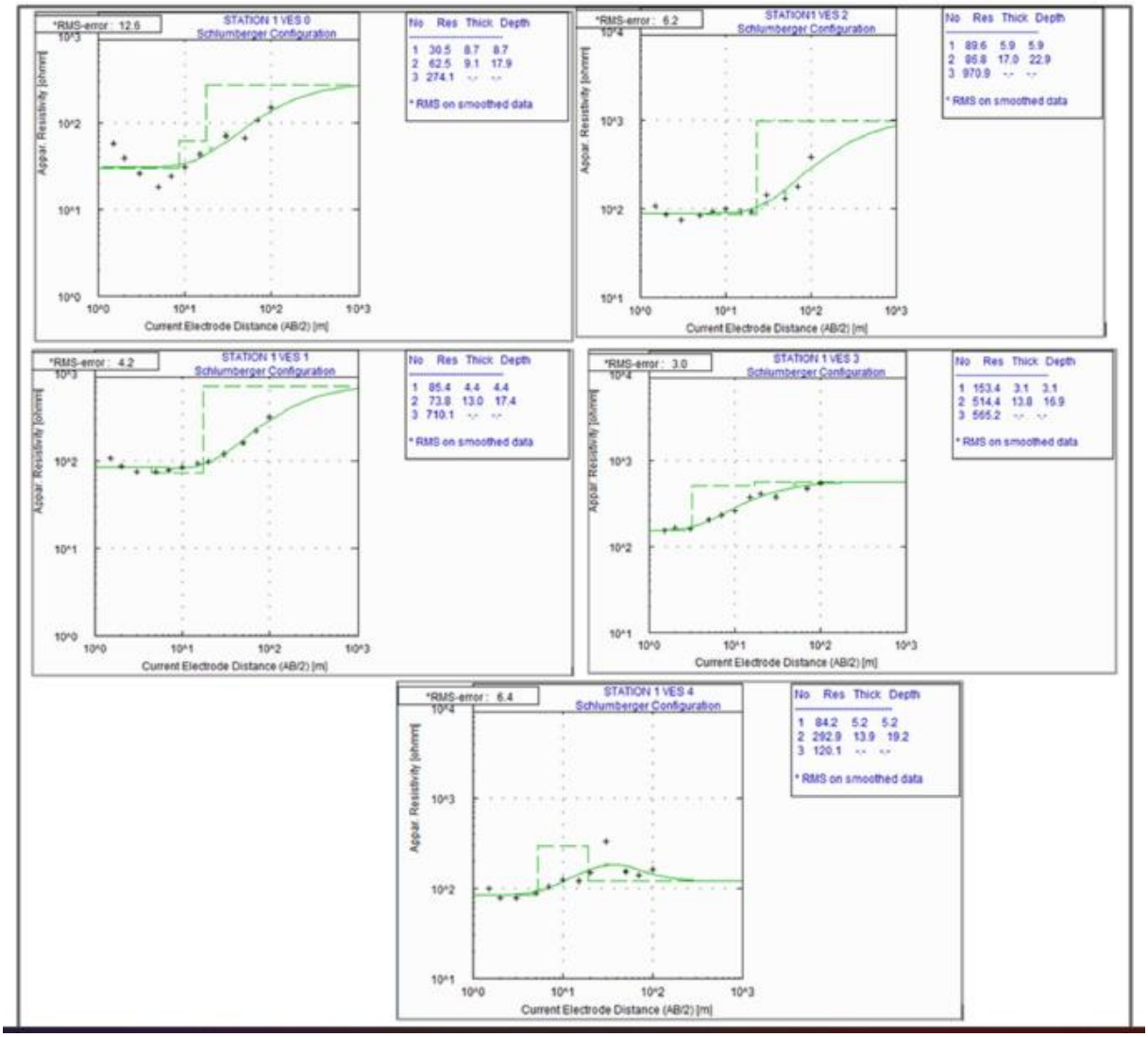

Figure 4.26: Site 1 Resistivity curves. The solid green line indicates modelled curve and the broken line represents the observed curve (Mpofu *et al.*, 2020).

The contribution of geophysics as tools for groundwater exploration was illustrated in this study, with the hydrogeological interpretation supported by the remote sensing data. Fractured zones were seen by low resistivity areas in the geophysical data and were determined to have high groundwater potential. Mpofu *et al.* (2020) recommended further study in Ndlambe using the magnetic and gravity methods.

4.2.16 Houtriver Gneiss groundwater assessment

An integrated geophysical and geological survey was conducted in Mamadila, Polokwane Municipality, Limpopo (Muchinigami *et al.*, 2021). The area is underlain by a crystalline basement of Houtriver gneiss. Geophysical surveys that were conducted were 1D ground magnetics which was used to identify potential water-controlling lateral heterogeneities such as dykes. This was followed by a frequency domain electromagnetic survey using the EM34 to identify points of potential interest. Figure 4.27 shows the magnetic and EM34 profiles for one of the lines with the potential groundwater anomaly indicated by an arrow. Vertical electrical sounding in the Schlumberger configuration was conducted to investigate changes in lithostratigraphy at specific anomalous areas (Muchinigami *et al.*,2021).

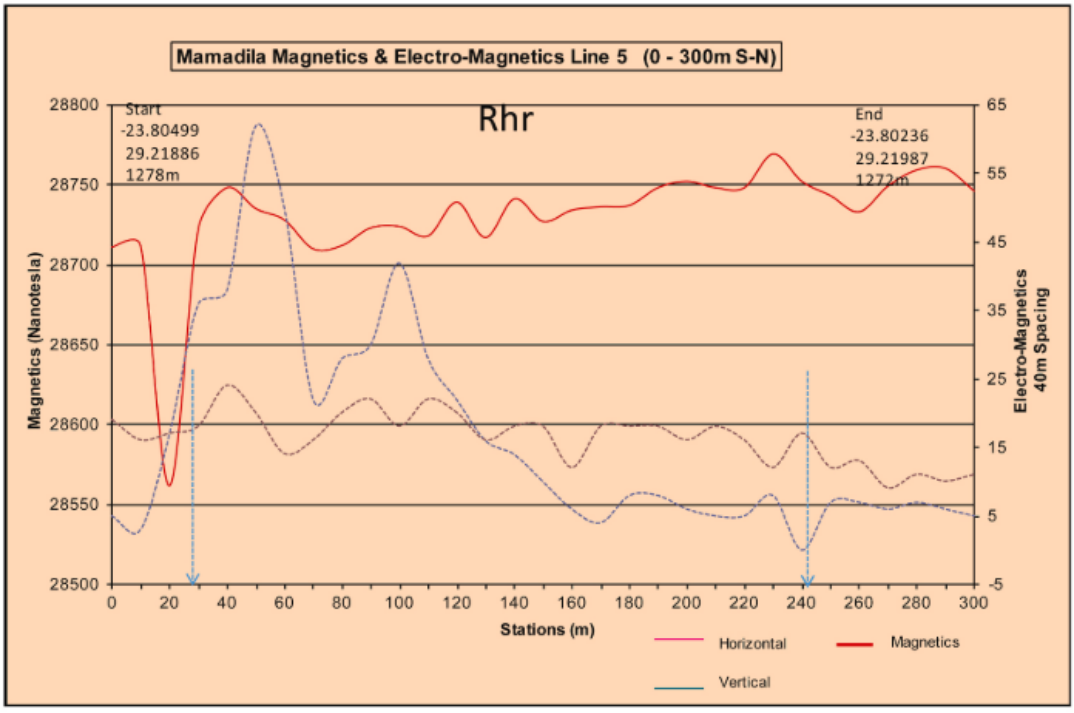

Figure 4.27: Magnetic susceptibility and vertical and horizontal FDEM results along line 5. Positions of anomalies highlighted (Muchinigami *et al.*, 2021)

Figure 4.28 shows the VES that was conducted at the anomalous site indicated in Figure 4.27. The VES showed the inferred depth of influence, and it was found that groundwater bearing rock is

fractured with resistivities <120 Ohm.m (Muchinigami et al., 2021). Distinct differences in the observed resistivity is attributed to groundwater occurrence in the rock. A total of 10 drilling sites were identified (Muchinigami *et al.*, 2021).

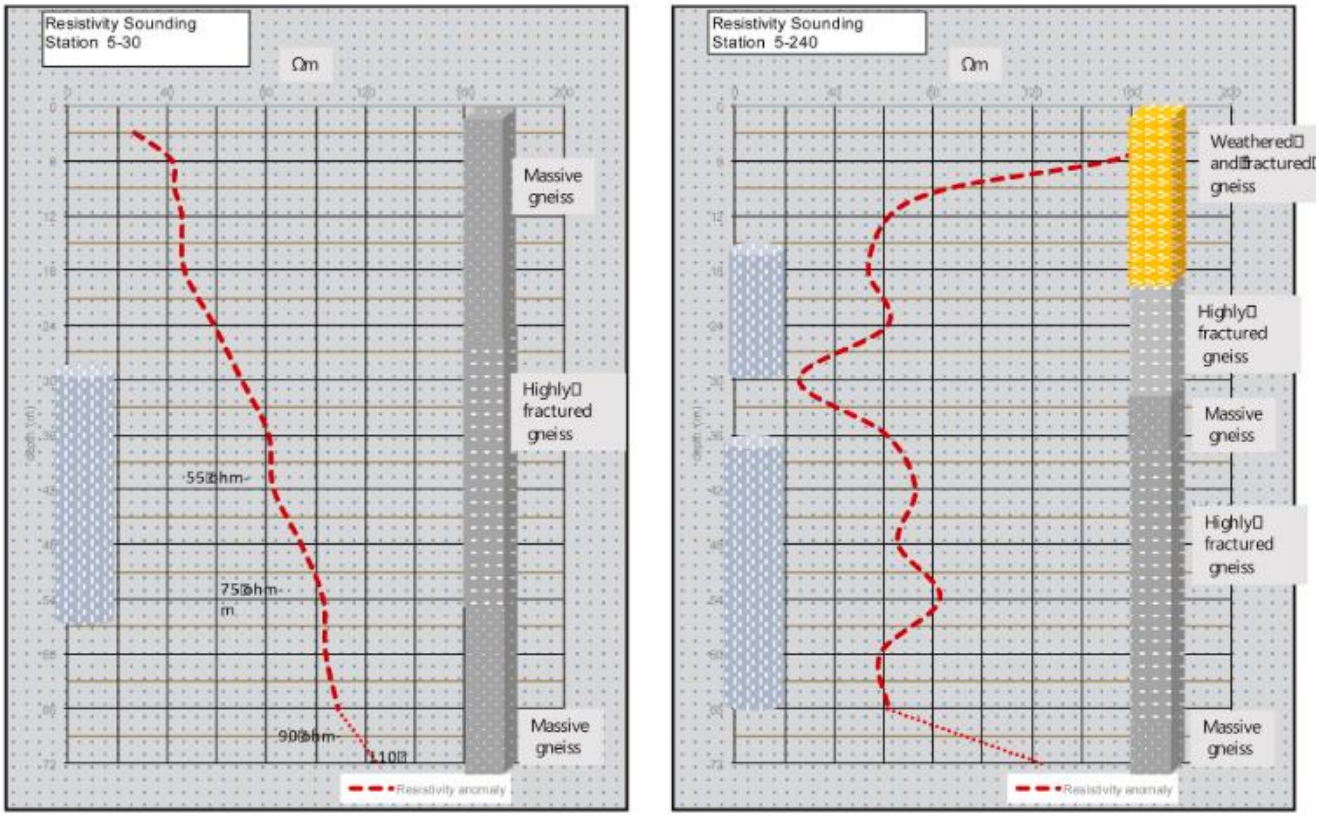

Figure 4.28: VES at 30 m and 240 m along line 5. Depth variation profile shown for reference (Muchinigami *et al.*, 2021)

The interpretation of the geophysical survey result combined with a geological analysis was used to infer potential borehole sites. The lithostratigraphic section constructed from borehole data showed that groundwater occurs in heterogenous multilayered formation, where groundwater occurrence is controlled by pegmatite lineaments, degree of weathering and dip of diabase dykes, amongst others. The approach used in the study was recommended for use in siting boreholes in the Houtriver Gneiss (Muchinigami *et al*., 2021).

4.2.17 Groundwater potential of a dyke in the North West

Van Wyk (2021) investigated the success of three geophysical equipment (ABEM Terrameter LS 2, EM34-3 and Magnetometer G5) in delineating a dolerite dyke. The study area was Modderfontein 3831P farm in the North West province underlain by the Malmani Subgroup dolomites, Timeball Hill Formation shales with subordinate sandstones and diabase intrusions all cut through by a dolerite dyke. Three traverses were taken for each of the geophysical surveys, which were conducted separately to avoid interference.

The 2D electrical resistivity tomography was conducted using the ABEM Terrameter LS 2. Figure 4.29 shows the apparent resistivity pseudosection for profile 1. Two anomalies encircled in black have low resistivities; anomaly 1) relates to an observed drainage channel, while anomaly 2) is interpreted to be a weathered zone. The higher resistivity anomalies are circled in red, with anomaly 3) expected to be the dolerite dyke.

The electromagnetic survey was conducted using the EM 34-3 with an intercoil spacing of 40 m for both horizontal (HD) and vertical (VD) dipoles because the dyke was expected at depths of ±30 m (Van Wyk, 2021). The data was processed in Surfer 14 to generate a contoured map of the VD and HD. Figure 4.30 shows the combined results of the HD for all three profiles as a contour map. A high conductivity zone (red shape) houses two smaller higher conductivity zones encircled in black and labelled 1) and 2). These zones are either deeper clay content or groundwater-bearing zones (Van Wyk, 2021).

A Proton Memory Magnetometer G5 was used to conduct the magnetic survey. The natural magnetic intensity was set to 28000 nT with 10 m station spacings. Figure 4.31 shows the magnetic intensity contour map for the site. A high-intensity anomaly encircled in red is likely the dolerite dyke, while the low magnetic intensity anomaly circled black is likely the same weathered zone observed in the resistivity pseudo section (Figure 4.29). The results obtained from the three surveys showed agreement and were successful in outlining a dolerite dyke (Van Wyk, 2021).

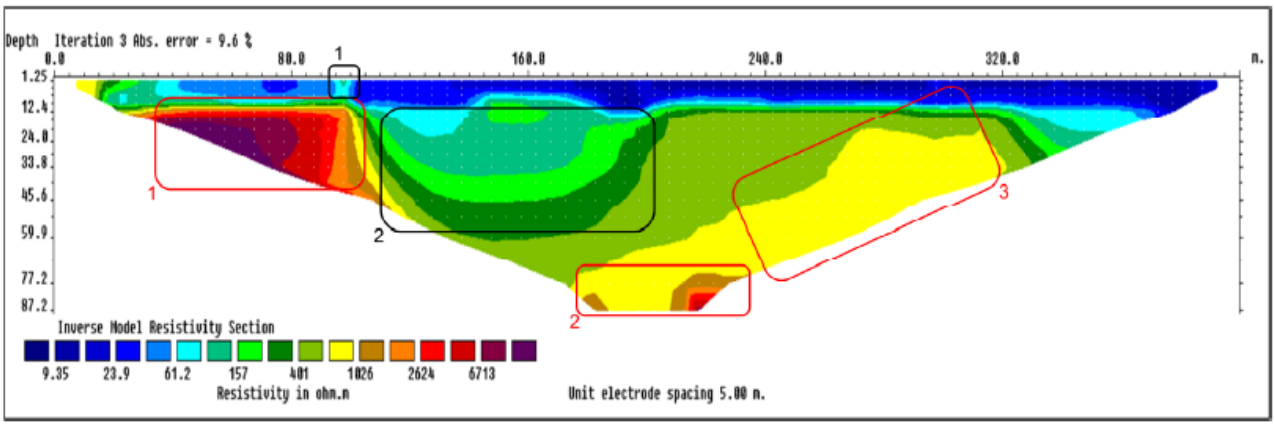

Figure 4.29: Resistivity pseudo section for profile 1 (Van Wyk, 2021).

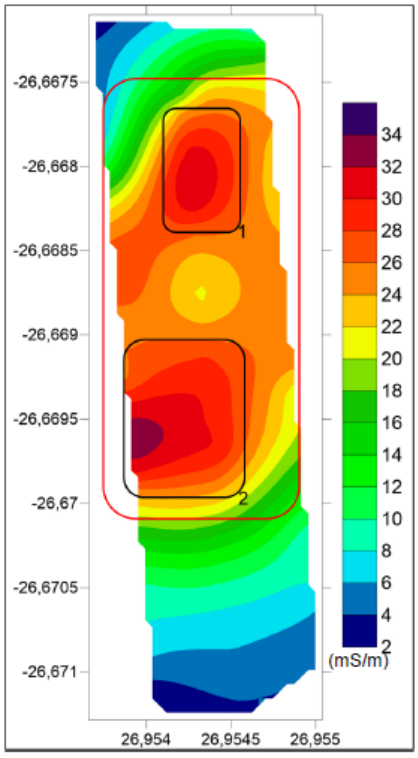

Figure 4.30: EM 34 HD interpolated results (Van Wyk, 2021).

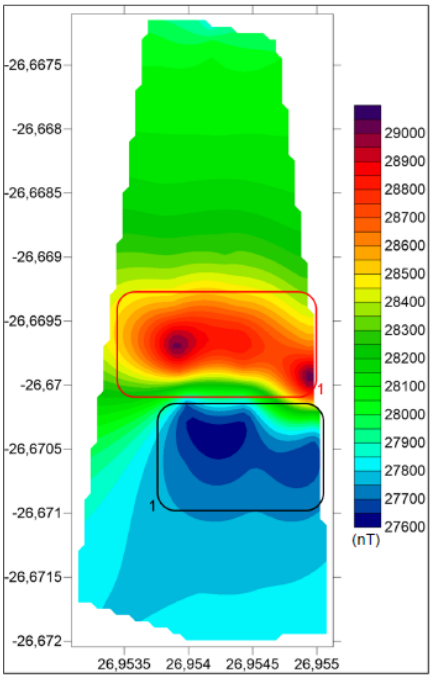

Figure 4.31: Magnetic intensity contour map (Van Wyk, 2021).

4.2.18 Groundwater potential in a fractured Karoo Aquifer

A study was undertaken to understand groundwater resources in Alice, Eastern Cape. The aim was to determine overburden thickness and depth to bedrock and to select subsurface aquifer zones for drilling (Adesola *et al.*, 2023). Alice is found within the Karoo Basin and is found within the Balfour Formation of the Beaufort Group. A ground magnetic survey was conducted using the G857 magnetometer, and data were collected from 8458 points (Adesola *et al.*, 2023). Two magnetometers

were used, with one used to measure diurnal variations. Base station readings were taken every 30 s with interline spacing kept at 20 m. The magnetic data were processed using the Oasis Montaj 9.10 software from Geosoft. Data enhancements were applied to the residual magnetic data to identify the edges of geological features. Magnetic depth slicing was conducted using GETECH GETGRID software.

The reduced to the pole (RTP), total horizontal derivative (THD), first vertical derivative, and analytical signal spatial maps were used to display the results. For example, the residual map (Figure 4.32) could not be accurately interpreted, so it was reduced to the pole and displayed as an RTP map (Figure 4.33), which showed a magnetic intensity of 21361.0 nT to 27735.7 nT. High magnetic intensity (possible dolerite dykes) can be seen in the NE and SW parts of the RTP map, while a pair of narrow low intensity anomalies can be seen in the center of the map.

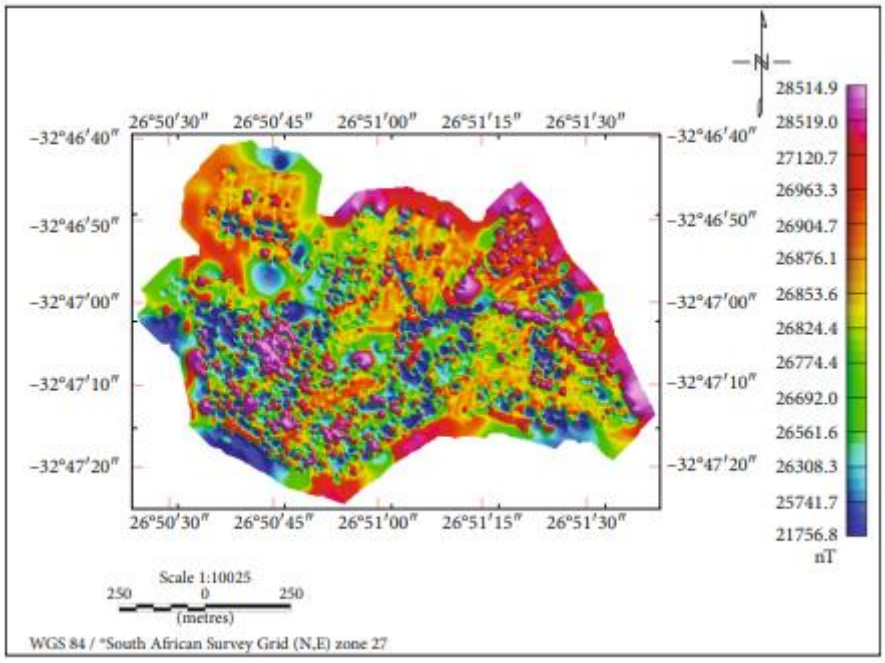

Figure 4.32: Residual magnetic map (Adesola *et al.*, 2023).

VES was also conducted in Alice using the ABEM Terrameter SAS 1000C in the Schlumberger array (Adesola *et al.*, 2023). Twenty-five soundings were completed. The partial curve matching technique was used to analyse the VES data using the WINRESIST software (geoelectric model) and the SURFER-10 software (geoelectric section). Four geoelectric layers could be identified from the VES data curves are the HA and HK types, whose representatives are shown in Figure 4.34. The third layer with resistivities between 136-352 Ohm.m and might be 9.9-172 m thick and 16.1-163 m deep is the possible aquifer (Adesola *et al.*, 2023). It comprises mudstone and sandstone. One geoelectric section that was generated along a line near what is called East Camp is shown in Figure 4.35. Adesola *et al.* (2023) showed that the magnetic and resistivity surveys are important tools in identifying zones that could potentially be groundwater bearing.

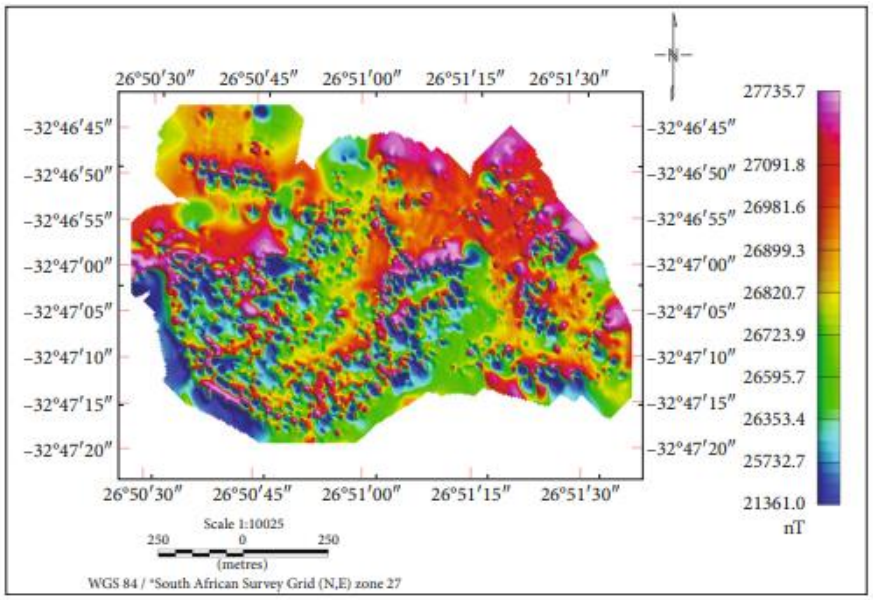

Figure 4.33: Reduced to the pole map (Adesola *et al.*, 2023).

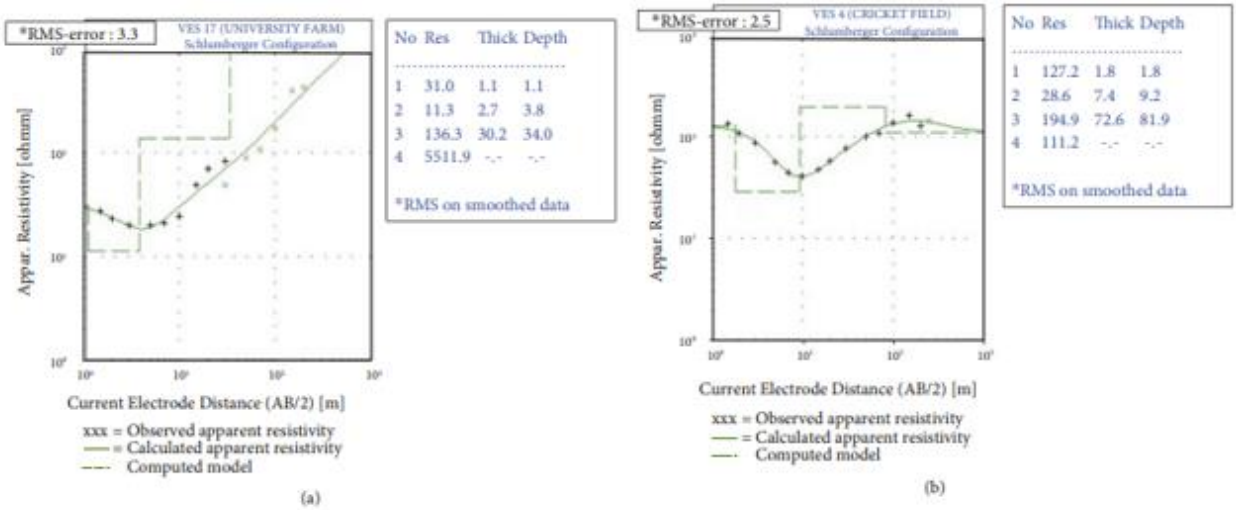

Figure 4.34: VES curves a) HA type b) HK type. Modified from (Adesola *et al.*, 2023).

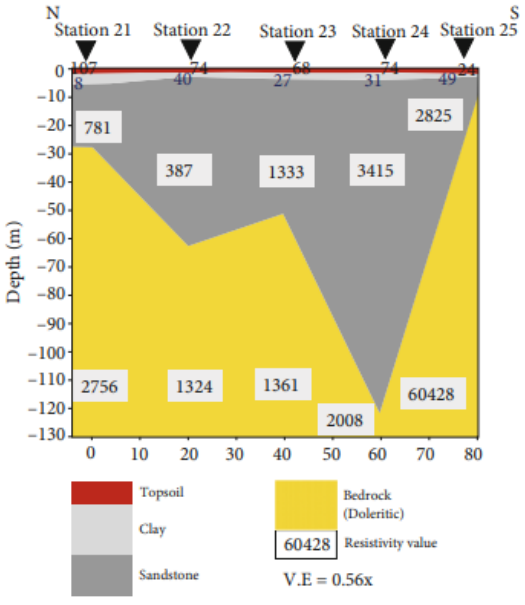

Figure 4.35: East camp geoelectrical section. Modified from (Adesola *et al.*, 2023).

4.2.19 Groundwater exploration in Bloemfontein using an unconventional technology

Gomo (2023) conducted two field tests using the ADMT 300S for groundwater exploration in Bloemfontein, which falls on the Karoo Supergroup (Beaufort Formation). The aim was to determine how well the equipment results could be explained by observations made during drilling and from lithology. Specific drilling locations were chosen by other geophysical means from prior surveys conducted by independent consultants. The electrical potential difference was measured at 5 m depth intervals up to 300 m, with 2 m spacing between measurement points (Gomo, 2023). Although the equipment does have a built-in ability to produce models of the electric potential difference, the raw data from the AMDT for the potential difference at a specific frequency was downloaded and plotted against depth (Gomo, 2023).

This data was compared to the lithological data collected during drilling. Figure 4.36 shows the depth profile obtained for Site 1, with lithology shown. The changes in lithology correspond to the observed change in the potential difference. Fresh dolerite was intersected at ~55 m and is reflected in the elevated electric potential difference of 0.08 mV (Gomo, 2023). The groundwater strike (shown by black broken lines in Figure 4.36) corresponded with low potential differences, such as 0.018 mV at 60 m in the saturated sandstone layers. The preliminary results obtained in this study show that the technology has some potential to be of use in groundwater exploration, although further study in more diverse settings is encouraged (Gomo, 2023).

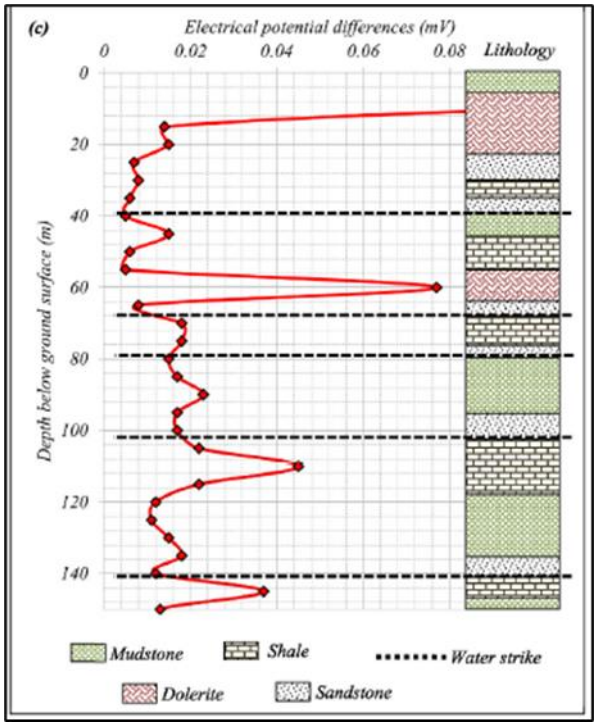

Figure 4.36: Electric potential difference and lithology at site 1. Modified from (Gomo, 2023).

4.2.20 Summary of publications

Table 4.1 shows a summary of published papers that relate to geophysical exploration in South Africa covered in the previous section. The title, method used and the broad geological region where the study was conducted are also shown. The papers are listed from oldest to youngest. It is noted that most of the studies summarised were published post-2010, which may correspond with increased focus on groundwater at the time, or it could be other materials were published as hard copies which were not accessible at the time of this study. The majority of the studies reviewed used more than one geophysical method of exploration, with the magnetic, electromagnetic and resistivity based methods consistently being the most popular. The Karoo and Limpopo Mobile Belt were settings most often encountered in this literature.

Table 4.1: Summary of publications dealing with geophysical groundwater exploration in South Africa.

Year	Title of publication	Author(s)	Geophysical Method(s)	Area (geology)
1955	Some Applications of Geophysical Prospecting in the Union of South Africa	Enslin	Resitivity, EM, magnetics	South Africa (region)
1975	Geophysical Exploration for Potable Groundwater Supplies in the Kalahari Gemsbok National Park	Martinelli	Resistivity	Kalahari
1989	Evaluation of the Applicability of Geophysical Methods for Groundwater Exploration in the Central Limpopo Metamorphic Belt, NW Transvaal	Du Toit	Resistivity, magnetics, EM	Limpopo Mobile Belt
1993	Geophysics Applied to Groundwater Exploration in the Kalahari Regions of Southern Africa	Botha and Vorster	TDEM, seismic reflection	Kalahari
2001	An Integrated Multidisciplinary Approach to Groundwater Exploration in the Nebo Granite, Northern Province	Botha *et al* .	Aeromagnetics, airborne radiometric, airborne EM, ground magnetic, ground EM	Nebo Granite, Bushveld Complex
2001	Integrated Geophysical Survey as Applied to Groundwater exploration	Fraser	Siesmic reflection, EM, resistivity	Tygerberg Formation, Malmesbury Group
2002	Groundwater Exploration In Geologically Complex And Problematic Terrain	Sami *et al.*	EM, magnetic, resistivity	Limpopo Mobile Belt, Bushveld Complex, Natal Metamorphic complex, Dwyka Group
2012	Time-lapse Resistivity and Geophysical Measurements at Dayspring Children's Village	Webb *et al* .	Aeromagnetics, airborne EM, resisitivity, gravity, seismic	Silverton Formation, Pretoria Group
2014	Regional Interpretation of Aeromagnetic Data for Groundwater Exploration in Capricorn District, Limpopo, South Africa	Sakala *et al* .	Aeromagnetics	Limpopo Mobile Belt

Table 4.1 (continued): Summary of publications dealing with geophysical groundwater exploration in South Africa.

Year	Title of publication	Author(s)	Geophysical Method(s)	Area (geology)
2016	Assessment of Groundwater Resource in the Tsineng Area, Northern Cape: A Geophysical Survey Perspective	Mokgatle	Airborne EM, gravity, EM, magnetics, resistivity	Ghaap Group, Griqualand West basin
2016	Magnetic and Electromagnetic Signatures around Polile Tshisa Hot Spring in the Northern Neotectonic Belt in the Eastern Cape Province, South Africa	Madi *et al* .	Magnetics, EM	Molteno Formation, Karoo
2017	Feasibility Plan for Groundwater Resource Development of the Malmani Dolomites within the Olifants River Water Supply System: Hydrogeological Exploratory Investigations Report	DWS	Magnetics, EM	Malmani Subgroup, Transvaal
2018	Ground Water Potential Zones Investigation Using Ground Magnetic Survey in South Africa	Ratshiedana *et al* .	Magnetics	Soutpansberg Group
2019	An Integrated Approach to Groundwater Exploration Using Remotely Sensed Imagery and Geophysical Techniques: A case study in the Archaen basement and Karoo sedimentary basins of Limpopo Province of South Africa	Magakane	Aeromagnetica, resistivity	Limpopo Mobile Belt, Soutpansberg Group, Karoo Supergroup
2020	Remote Sensing, Geological, and Geophysical Investigation in the Area of Ndlambe Municipality, Eastern Cape Province, South Africa: Implications for Groundwater Potential	Mpofu *et al* .	Resistivity	Cape fold belt
2021	Integration of Hydrogeophysical and Geological Investigations in Enhancing Groundwater Potential Assessment in Houtriver Gneiss Crystalline Basement Formation of South Africa	Muchinigami *et al* .	EM, magnetic, resistivity	Limpopo Mobile Belt

Table 4.1 (continued): Summary of publications dealing with geophysical groundwater exploration in South Africa.

Year	Title of publication	Author(s)	Geophysical Method(s)	Area (geology)
2021	Evaluation of the Magnetotelluric TC 150 Instrument for Geophysical Groundwater Exploration	Van Wyk	EM, magnetic, resistivity	Pretoria & Chunniespoort Groups, Transvaal
2023	Hydrological Evaluation of the Groundwater Potential in the Fractured Karoo Aquifer Using Magnetic and Electrical Resistivity Methods: Case Study of the Balfour Formation, Alice, South Africa	Adesola *et al* .	Magnetics, resistivity	Balfour Formation, Karoo
2023	Use of Electric Potential Difference in Audio Magnetotelluric (AMT) Geophysics for Groundwater Exploration	Gomo	Tellurics	Beaufort Group, Karoo

4.3 GROUNDWATER EXPLORATION IN THE KAROO SUPERGROUP

This section summarises consultant reports of geophysical exploration conducted in areas underlain by the Karoo Supergroup.

4.3.1 Case study 1: Matlakeng Ext.11 Pilot groundwater exploration program and groundwater resource assessment

Geovation (2021) was requested to undertake a pilot exploration study on the groundwater potential for the proposed Matlakeng Ext 11 Township and mixed-use development near Zastron, Free State. Its purpose was to determine groundwater potential and establish how much groundwater can contribute to the total water demand (Geovation, 2021). The site is underlain by the Molteno Formation mudstones and sandstones extensively intruded by dolerite dykes and sills. Joints, fractures, bedding planes, and weathered rocks are ideal for groundwater development in this area (Geovation, 2021).

The consultant acquired aeromagnetic data for the area to select potential targets for the ground geophysical survey. The magnetic method was then used as a reconnaissance tool to identify areas where further resistivity surveys were warranted. Figure 4.37 shows an aeromagnetic map generated for the area in question. According to Geovation (2021), the black broken line represents the mapped geological fault, while the broken pink line indicates the “magnetic” fault. A-A’, B-B’ and C-C’ represent proposed geophysical traverses for this project. The aeromagnetic map and geological map available for the area were combined to generate the geology and magnetic fault map in Figure 4.38.

The magnetic survey was conducted along the three proposed traverses with an additional fourth traverse D-D’ added. An additional investigation using three 2D ERT surveys was done where magnetic anomalies were detected. Figure 4.39 shows a satellite image with the positions of the magnetic and resistivity traverses illustrated. Six boreholes were proposed from the interpreted resistivity and magnetic data, while nine boreholes were eventually drilled. Three of the nine boreholes were pump tested, while others were backfilled. Figure 4.40, Figure 4.41, and Figure 4.42 show the magnetic and resistivity profiles along lines A and C. On the figures, “PBX” represents proposed borehole positions. Three boreholes were drilled around PB1 on line A. However, only one was tested. The successful boreholes on the site had were associated with dolerite intrusions and had yields of ~0.5 L/s.

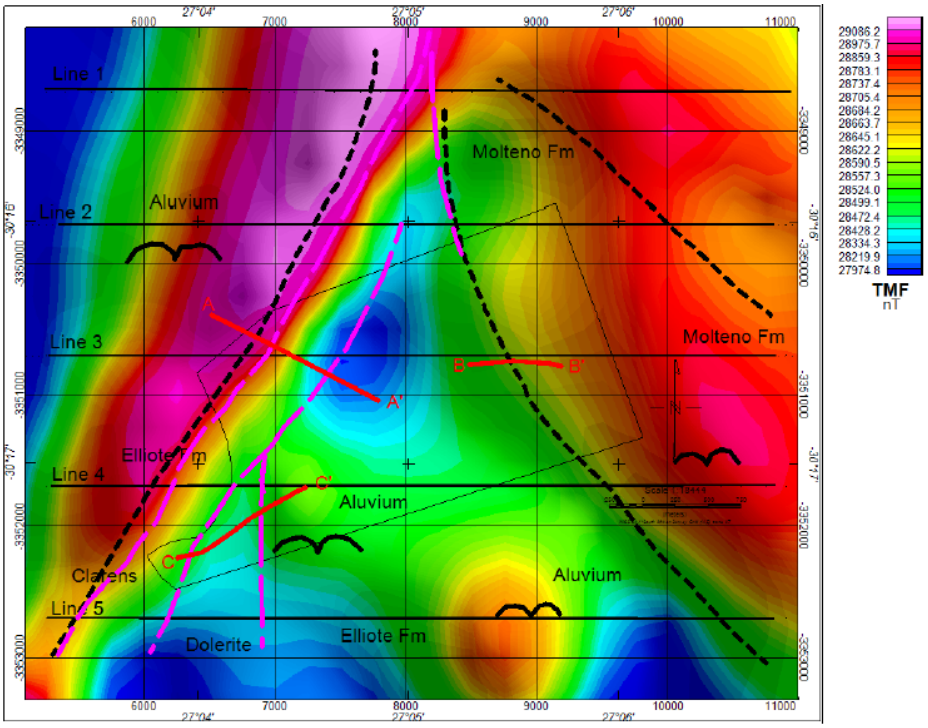

Figure 4.37: Aeromagnetic map for Matlakeng Extension 11 (Geovation, 2021).

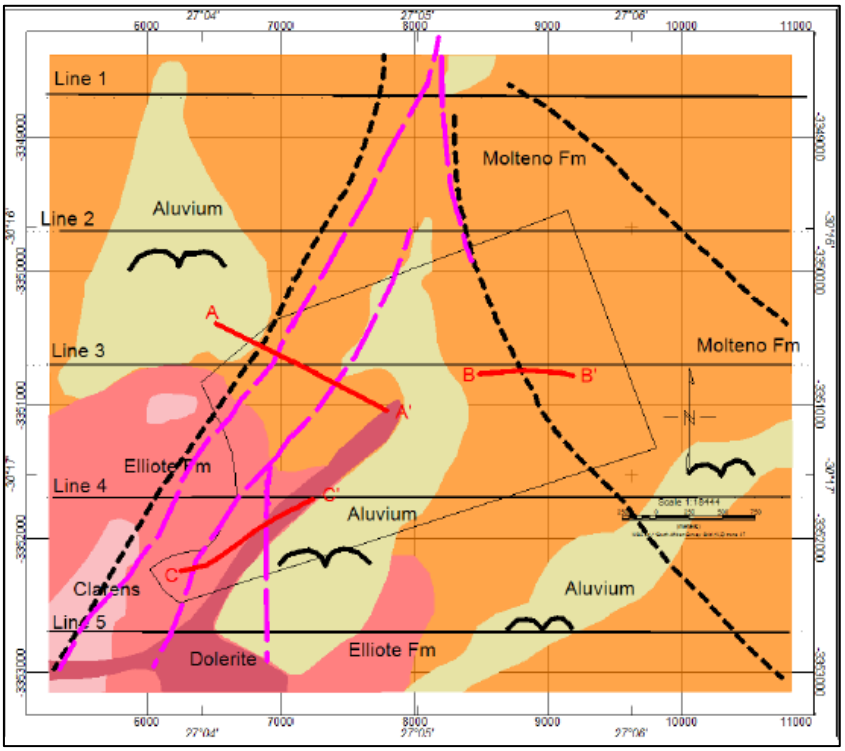

Figure 4.38: Geology, magnetic faults and proposed survey lines (Geovation, 2021).

Figure 4.39: Satellite image of the study area (Geovation, 2021).

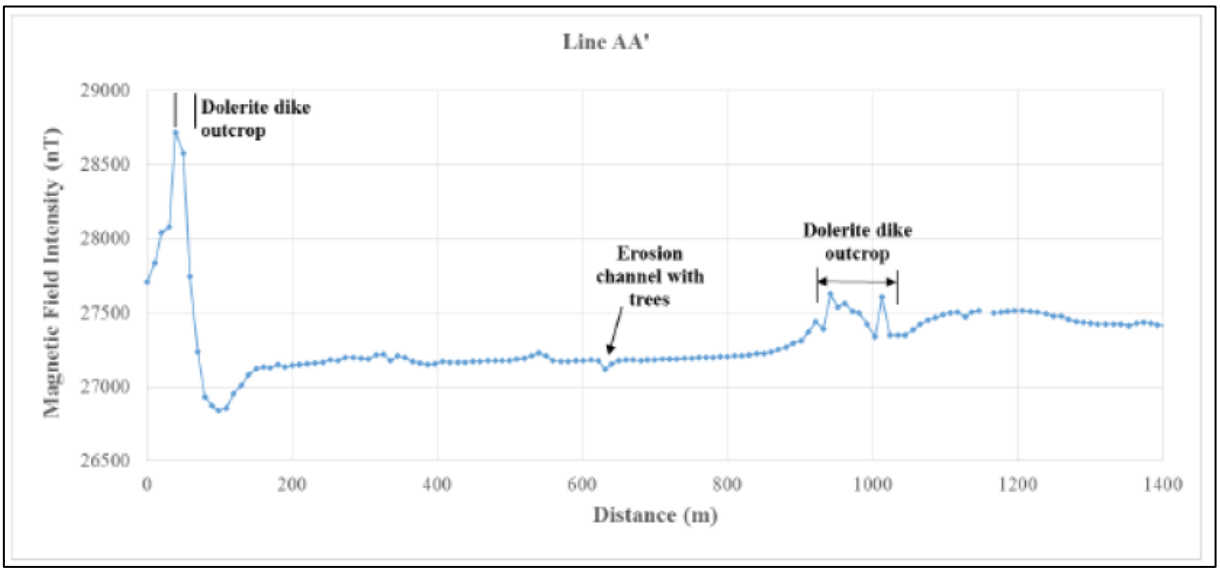

Figure 4.40: Magnetic Profile along line A (Geovation, 2021).

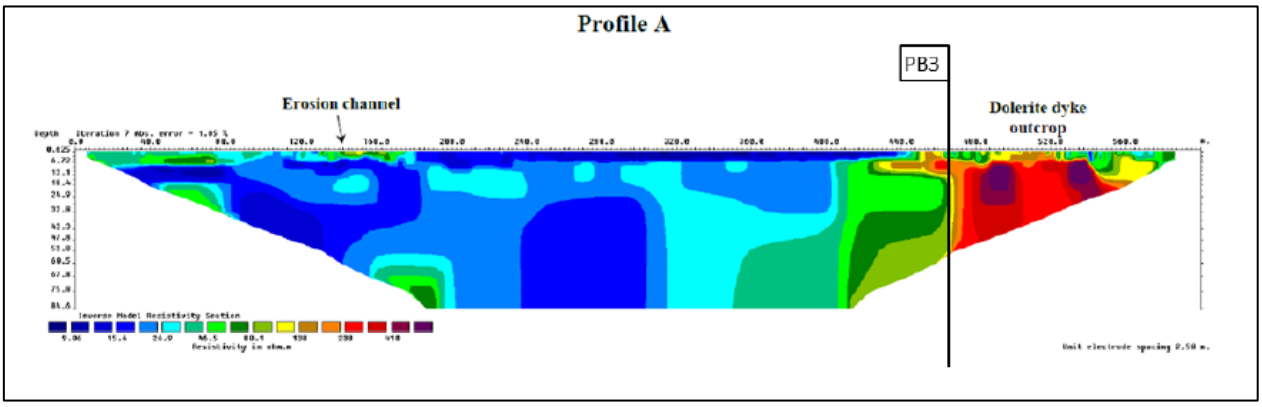

Figure 4.41: Modelled resistivity section across line A (Geovation, 2021).

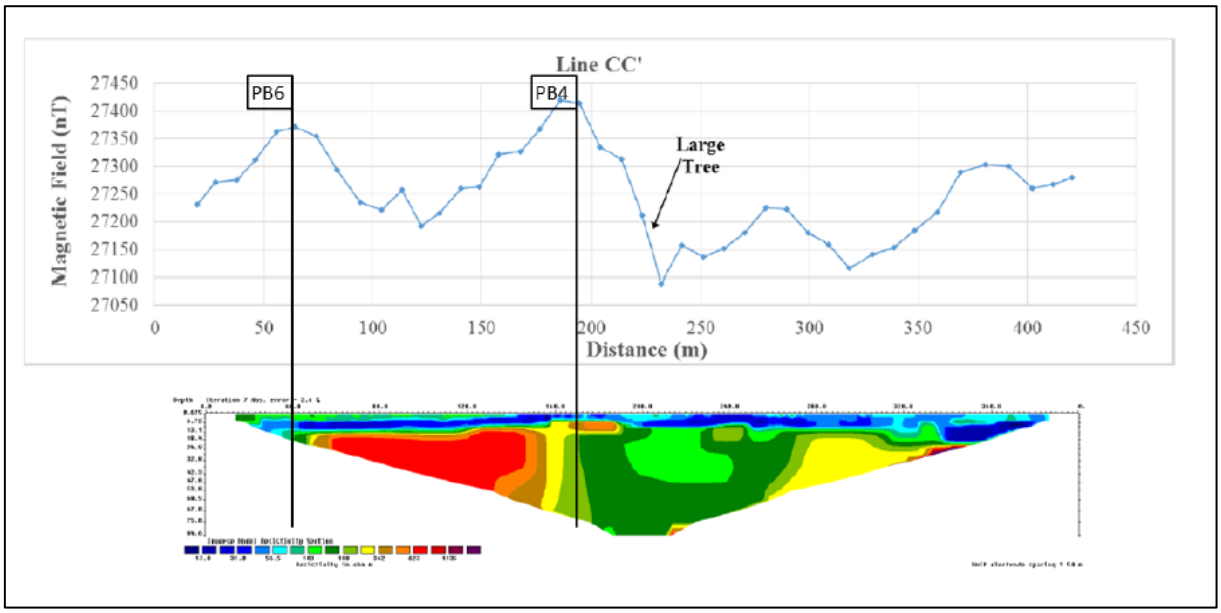

Figure 4.42: Magnetic profile and resistivity section across line C (Geovation, 2021).

4.3.2 Case study 2: Borehole siting in the Ubuntu Municipality

As part of a groundwater supply project, the consultant sited 16 boreholes in Victoria West, Richmond, Loxton, Hutchinson and Merriman. The area is underlain by the Adelaide Subgroup Teekloof Formation), which are mudstones, shales and minor sandstones. Dolerite dykes and sills are present, and unconsolidated alluvium and colluvium are on the surface (GHT Consulting, 2013).

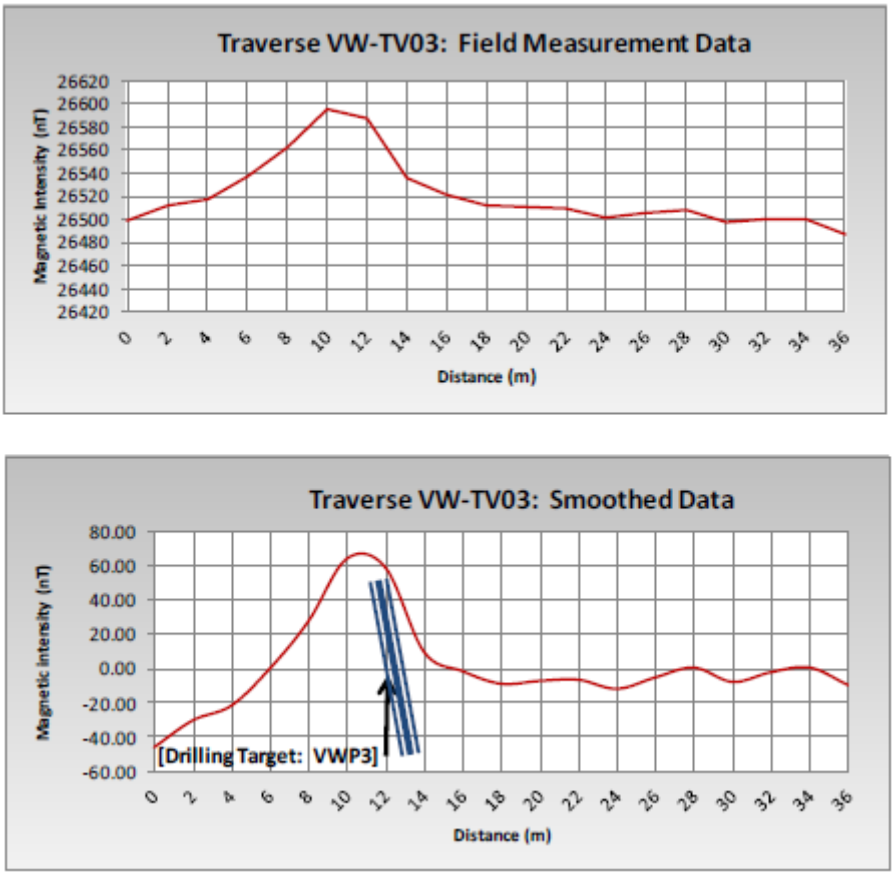

Figure 4.43: Victoria West magnetic profile (GHT Consulting, 2013).

The magnetic method was used to conduct the surveys as particular focus was placed on determining dolerite dyke position in the area. For the town of Victoria West, four lines were conducted with four drilling targets identified. The field and smoothed magnetic data for one of the traverses, VW-TV03, are shown in Figure 4.43. The profile was in a S-N direction with 2 m station spacing and was 36 m long. One drilling target was sited on the anomaly, associated with a potential dolerite dyke around station 12 (GHT Consulting, 2013). The borehole drilled on this position was drilled to 80 mbgl with water strike at 26 mbgl and 49 mbgl and a blow yield of 3200 L/h, but was abandoned due to low yield (GHT Consulting, 2013). Four more traverses were conducted for Loxton, with four targets identified. The remainder of the boreholes were sited based on geological observations and interpretations. A total of 16 boreholes were drilled for the project.

4.3.3 Case study 3: Haza Primary School

A borehole was sited at the Haza Primary School in the Umgungundlovu District in KwaZulu Natal. The area is underlain by the Adelaide Formation mudrock and minor sandstones. As part of the study, a geophysical survey was carried out using the PQWT-TC500 (African Groundwater, 2022a). According to Gomo (2023), the equipment is based on Audio Magnetotellurics (AMT) and exploits electric potential difference for groundwater exploration. A single traverse was then conducted and data collected at 1 m intervals along the line. A GPS was used to record the selected drilling position. Figure 4.44 shows the results obtained for the survey (station number against depth). The curve shows the potential difference detected which is then mapped.

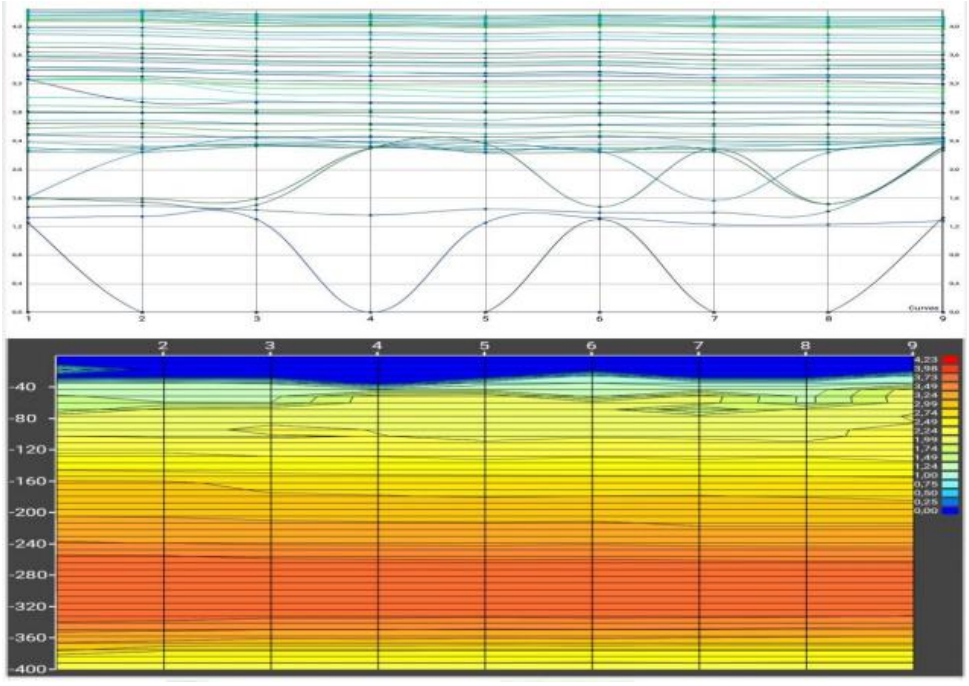

Figure 4.44: Haza PQWT results (African Groundwater, 2022a).

4.3.4 Case study 4: Nquthu Local Municipality

A project was undertaken in the Nquthu Local Municipality, KwaZulu Natal, to develop groundwater resources. The water supply of the four main reservoirs around the town was to be augmented (Engeolab, 2020). Nquthu is underlain by the sedimentary Vryheid Formation (Pv) in the west, with scattered remnants of the Pietermaritzburg Formation (Pp). In small sections in the south, there are scattered tillite and minor shales of the Dwyka (C-Pd). The Jurassic (Jd) dolerites cover most of the northern study area. The Masotcheni Formation (Qm), consisting of sandy clay, sand and gravel, covers drainage lines. The geology of the four sites is shown in Figure 4.45. Lineaments such as faults and dykes are seen on the map. Aquifers in the area are mainly classified as intergranular and fractured.

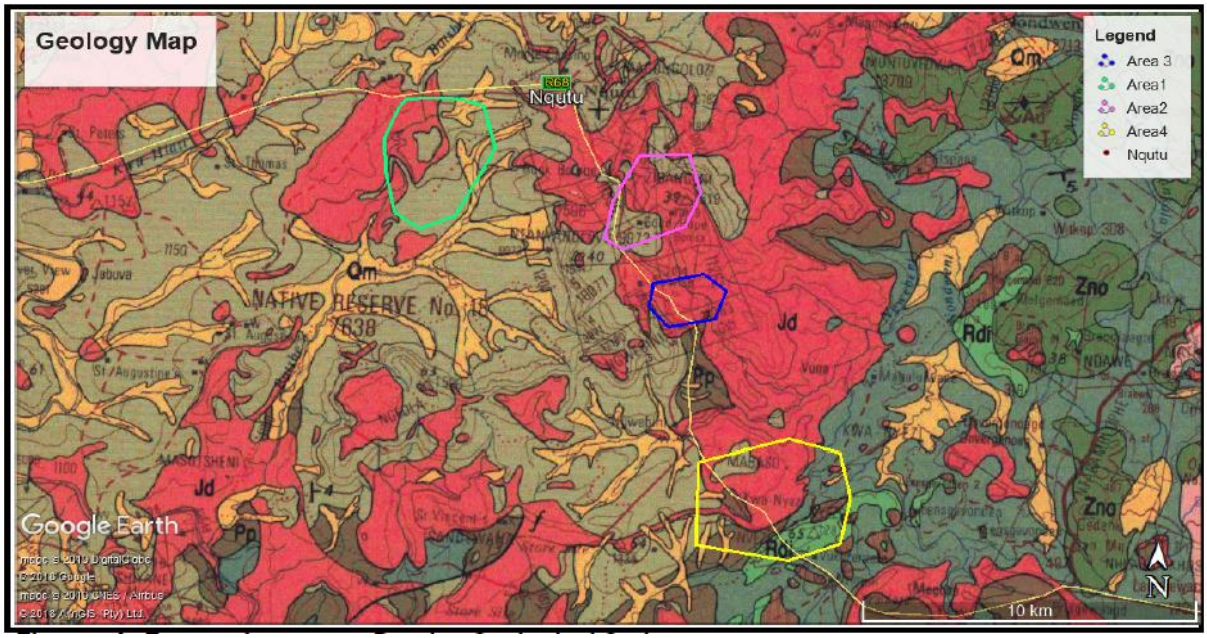

Figure 4.45: Nquthu regional geology with study locations (Engeolab, 2020).

As part of this project, geophysical surveys were undertaken to identify appropriate borehole locations. Remote sensing (ASTER, Landsat and Sentinel) was to identify potential zones of interest where the geophysical surveys were to be conducted, which were lineaments. The magnetic method (Geotron G5 proton magnetometer) and electromagnetic (Geonics EM34-3) methods, supplemented by a telluric receiver, were used for the survey (Engeolab, 2020). A 5 m station spacing was used, with an intercoil spacing of 20 m and 40 m for the EM survey in both the vertical and horizontal dipole orientations. Electrode spacing was kept at 5 m for the telluric receiver.

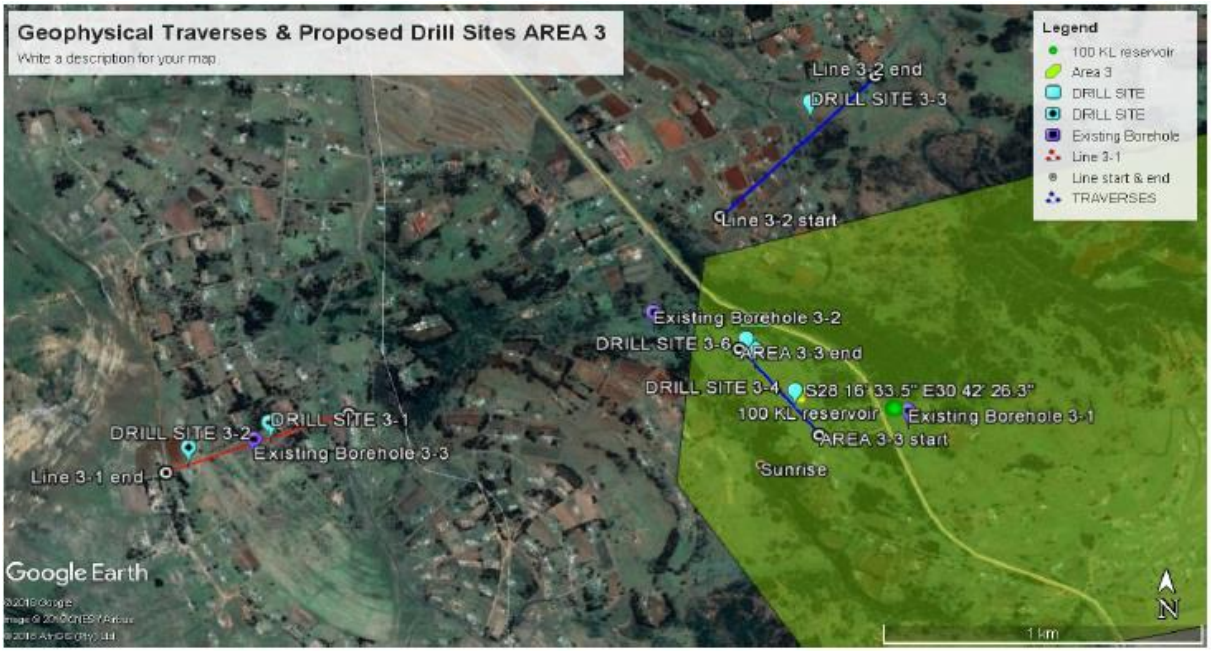

Figure 4.46: Area 3: Geophysical traverses and drilling locations (Engeolab, 2020).

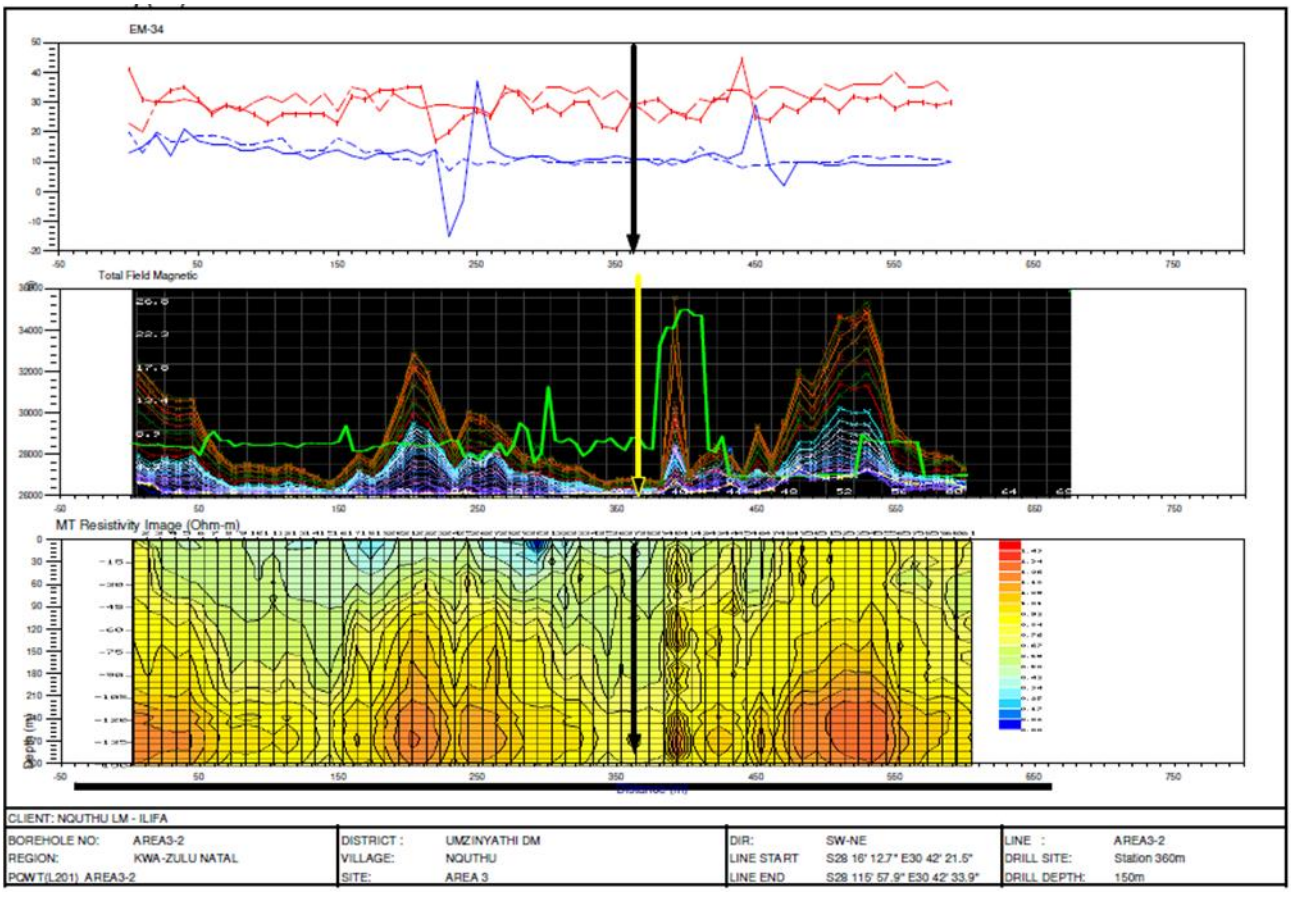

Figure 4.47: EM, Magnetic, Potential difference and mapped response of tellurics at Area 3: Line 2 (Engeolab, 2020).

Area 3 geophysical traverses and proposed drilling locations are shown in Figure 4.46. The EM apparent conductivity and magnetic profile, the potential difference curves and mapped response for line 2 in Area 3 are shown in Figure 4.47. The drilling location is proposed at 350 m along the traverse

to a proposed depth of 150 m. The position is indicated by an arrow on the various diagrams (Engeolab, 2020). The borehole drilled in that position had a final blow yield of 4000 L/h (Engeolab, 2020). The water strike was at the contact between the Vryheid shale and dolerite. Fifteen geophysical traverses were completed, and 16 possible borehole locations were identified (Engeolab, 2020).

4.4 GROUNDWATER EXPLORATION IN THE CAPE SUPERGROUP

In this section, geophysical prospecting from unpublished reports in the Cape Supergroup is summarised.

4.4.1 Case study 1: Farm 1, Hermanus

The study area is on an outcrop Cape Granites of the Cape Granite suite, which form the basement of the Cape Supergroup. It is for this reason that this study is also included here. The groundwater exploration was conducted by Cape Geophysics (2011) employing a 2D ERT survey. The traverse length was 800 m in a North-South direction. The kind of ERT device used was not specified. A fault zone, weathered zone and clay-rich zone were interpreted from the profile, and these are illustrated in the geoelectric model for the site. From this interpretation, two drill sites were identified, the drill site and an alternative site. The drill site had a blow yield of 4 L/s (Cape Geophysics, 2011). The geoelectric model generated for this traverse is shown in Figure 4.48.

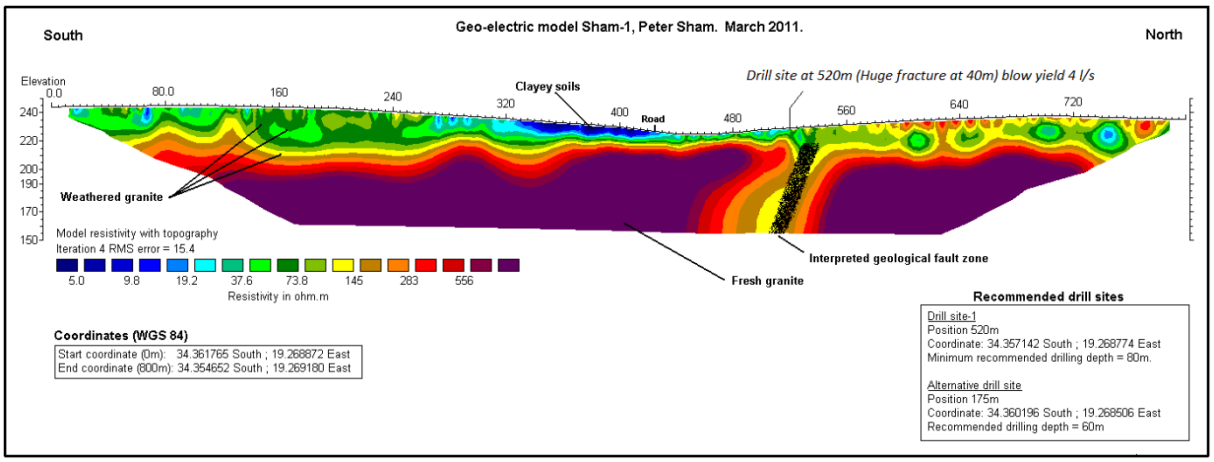

Figure 4.48: Geoelectric model for Farm 1 (Cape Geophysics, 2011).

4.4.2 Case study 2: Farm 2, Napier

2D ERT surveys were conducted on a farm by Cape Geophysics (2019b) in 2019 and 2015. One traverse in 2015 and six more in 2019, with traverse lengths of approximately 300 m. Due to a fault, the farm sits upon the TMG sandstones juxtaposed against the Bokkeveld shales. Specifically, these are the sandstones of the Skuwerberg Formation of the Nardouw Subgroup and the Gydo Formation

of the Ceres Subgroup. The strata in the area are overturned; therefore, different formations are encountered laterally, which is reflected in the geoelectrical models generated for the project. One of the models is shown in Figure 4.49. Four potential drill sites were identified mainly along interpreted fault zones on three of the six survey lines (Cape Geophysics, 2019b).

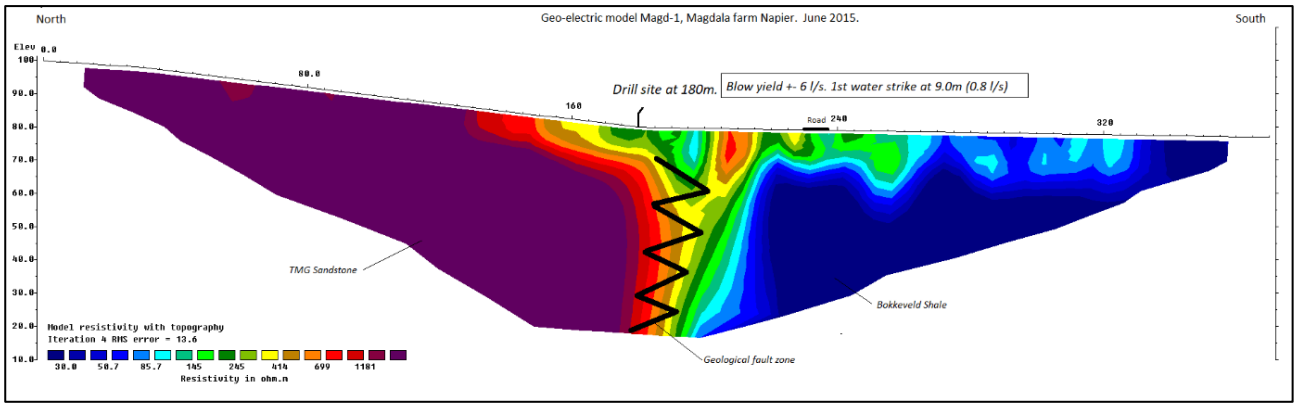

Figure 4.49: Geoelectrical model for Farm 2 (Cape Geophysics, 2019b).

4.4.3 Case study 3: Farm 3, Stanford

A geoelectric model was constructed from 2D ERT data collected in 2021 by Cape Geophysics (2021). The model provided in Figure 4.50 shows that one drill site was identified near an interpreted fault zone. The comments made by the consultant on the model show the importance of interpreting the results with local geology in mind. The area is overlain by Cenozoic sands of the Bredasdorp Formation and underlain by Skuwerberg Group sandstones and Cape weathered granites. The traverse length was 800 m while the blow yield was 1800 L/h (Cape Geophysics, 2021).

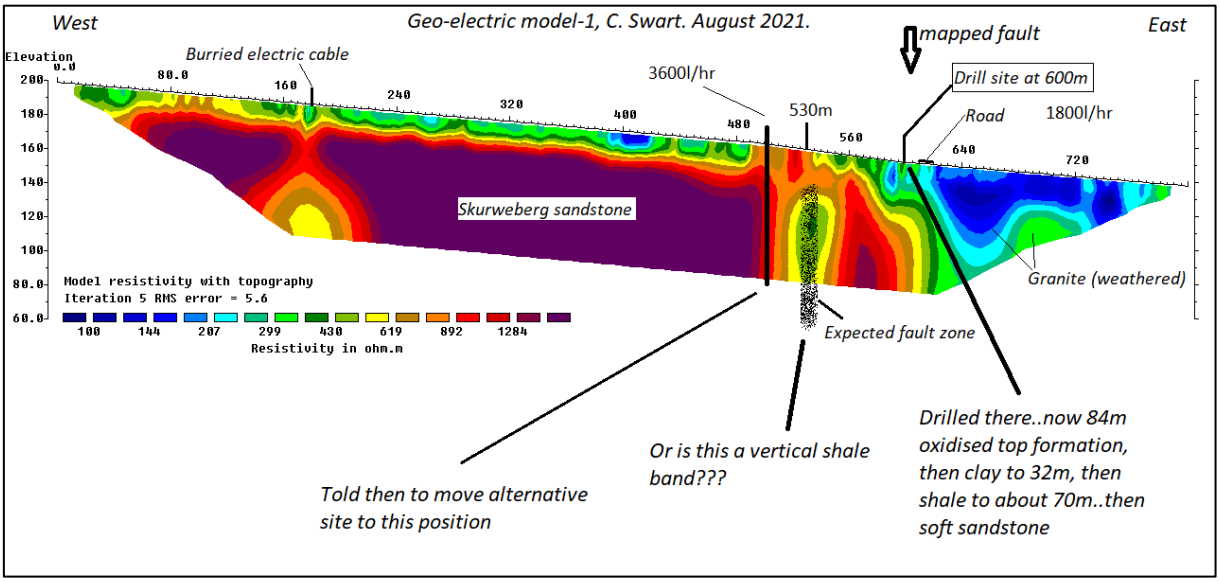

Figure 4.50: Geoelectric model for Farm 3 (Cape Geophysics, 2021).

4.4.4 Case study 4: Farm 4, Kleinmond

A 2D ERT survey was conducted on a farm near Kleinmond in April 2019 to site a borehole (Cape Geophysics, 2019c). The traverse length was 400 m in a SSE to NNW direction. The resistivity survey was conducted using the Wenner and Schlumberger electrode arrays, and the result from the two arrays were compared. The Bredasorp group sands underlie the area. The ERT survey resolved a fault that can be seen clearly on the geological map of the area. Figure 4.51 and Figure 4.52 show the geoelectric sections for the Schlumberger and Wenner arrays.

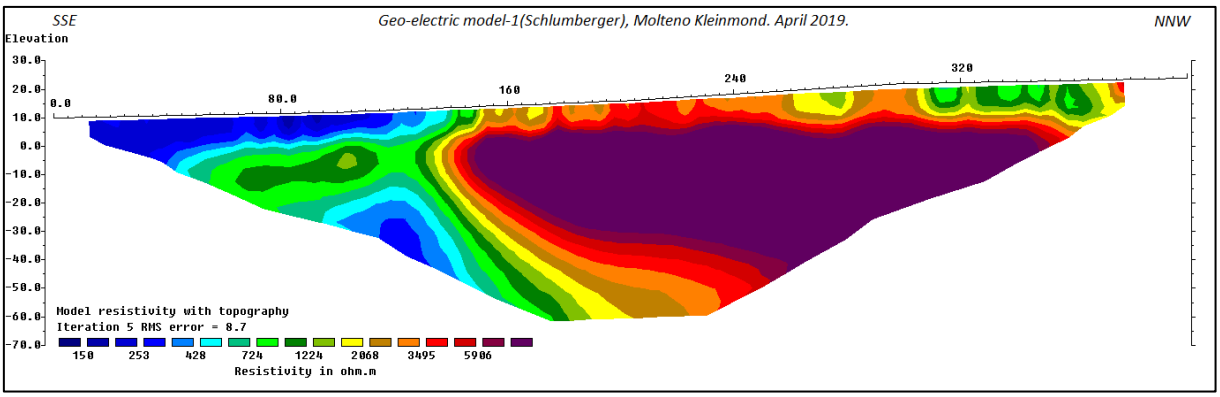

Figure 4.51: Farm 4 Geolectric model-Schlumberger Array (Cape Geophysics, 2019c).

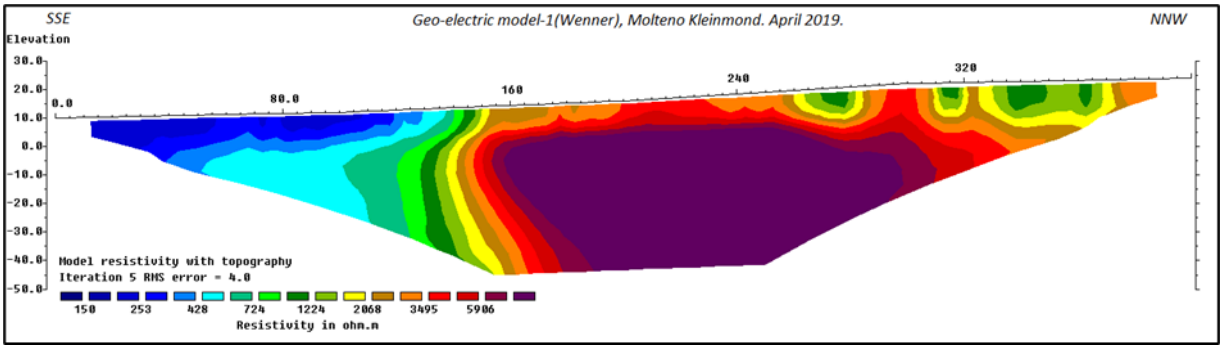

Figure 4.52: Farm 4 Geolectric Model- Wenner Array (Cape Geophysics, 2019c).

4.4.5 Case study 5: Farm 5, Southern Blooms

A geoelectric model was constructed from a 2D ERT survey conducted in 2019 by Cape Geophysics (2019a). The site had a preexisting borehole with a yield of 0.2 L/s. The traverse length was ~800 m in a SW-NE direction. A drill site was proposed at an interpreted fault zone. The area is underlain by TMG sandstones of the Skuwerberg Formation and overlain by the unconsolidated sands of the Bredasdorp Group. It must be noted that there is a stream in the vicinity of the site whose interaction with the aquifer is unknown. Figure 4.53 shows the geoelectric model generated from this survey. The interpretation of the lithology and proposed drill site position in the context of the modelled section are shown by labels in the figure. The drill site was at a possible fault or fracture zone (Cape Geophysics, 2019a).

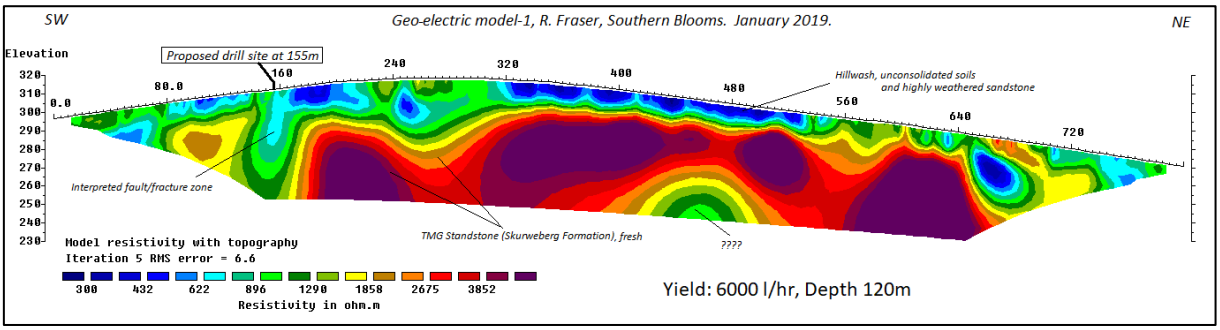

Figure 4.53: Farm 5 Geoelectric model (Cape Geophysics, 2019a).

4.4.6 Case study 6: Bakenshoogte, Botrivier

The geophysical survey was conducted on municipal land to identify a new drilling target for drinking water for the community in the area and the Bakenshoogte property (GEOSS, 2020). An unspecified number of boreholes were present before exploration. The area is underlain by Ceres subgroup lithologies, particularly the Voorsthoek formation mudstones, Gydo formation mudstones (which act as aquitards) and Gamka formation sandstones. The TMG Skuwerberg formation sandstones also occur in the area (GEOSS, 2020). A fault is present between the TMG and Bokkeveld group contact, which is ideal for groundwater development. Figure 4.54 shows the geology of the area with the drill target positions shown.

A resistivity (ERT) and an EM survey were conducted in the area. Two survey lines, one using each method, were made. A fault structure is present in the area, and two drilling targets were identified from the two surveys (GEOSS, 2020). These were chosen in joints on the fault and contact zone. The modelled resistivity section and conductivity from the EM survey are shown in Figure 4.55 and Figure 4.56, respectively. The fault is seen as a peak in the EM profile and a low resistivity zone in the resistivity model. In the images, *sandsteen*=sandstone, *verweerde sone*=weathered zone and *skalie rots*=shale.

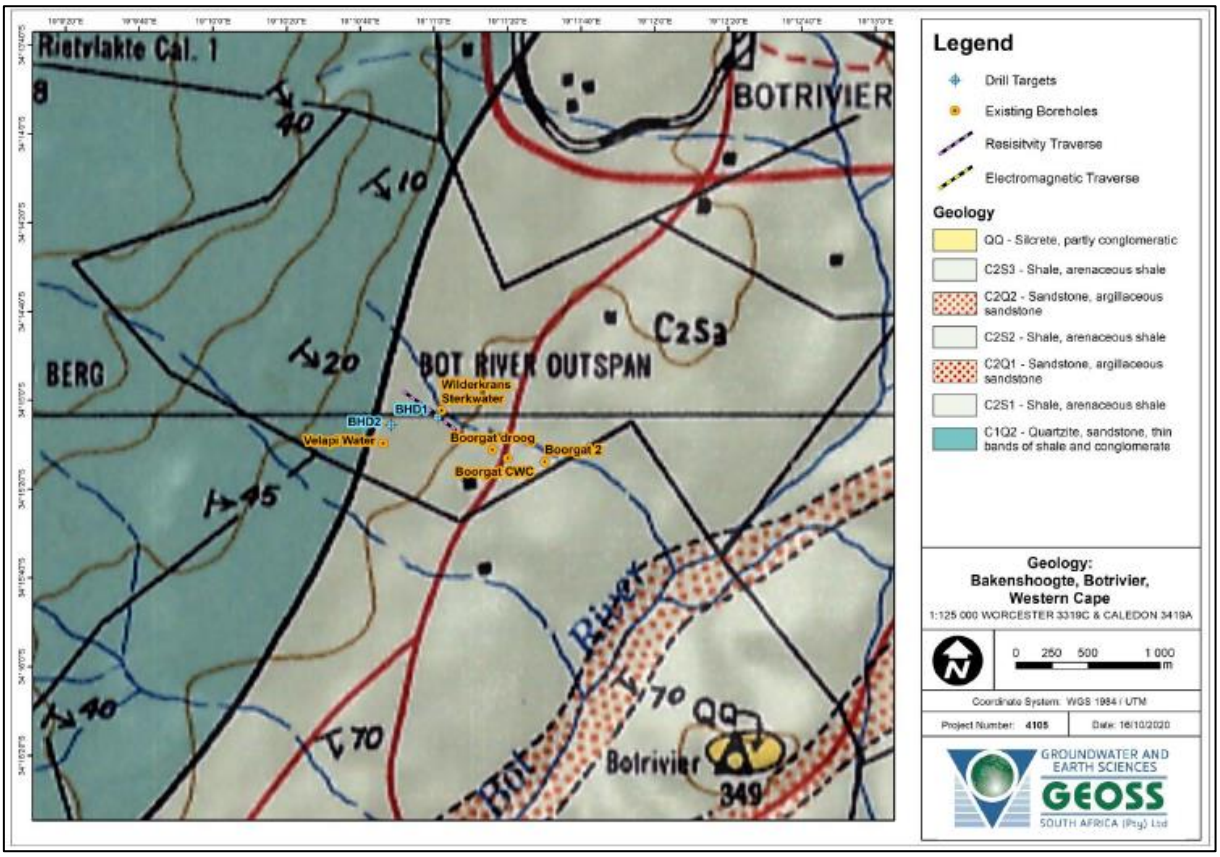

Figure 4.54: Geology of Bakenshoogte (GEOSS, 2020).

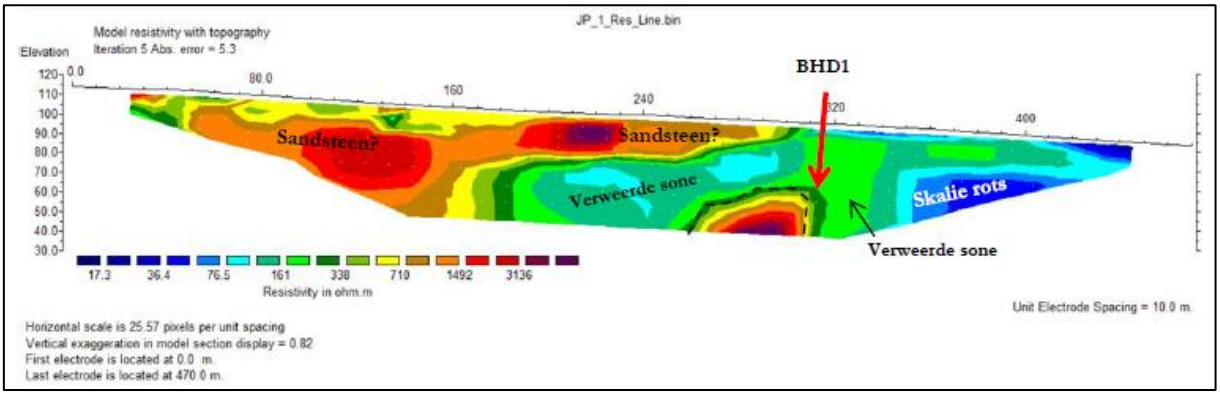

Figure 4.55: Geoelectric model (GEOSS, 2020).

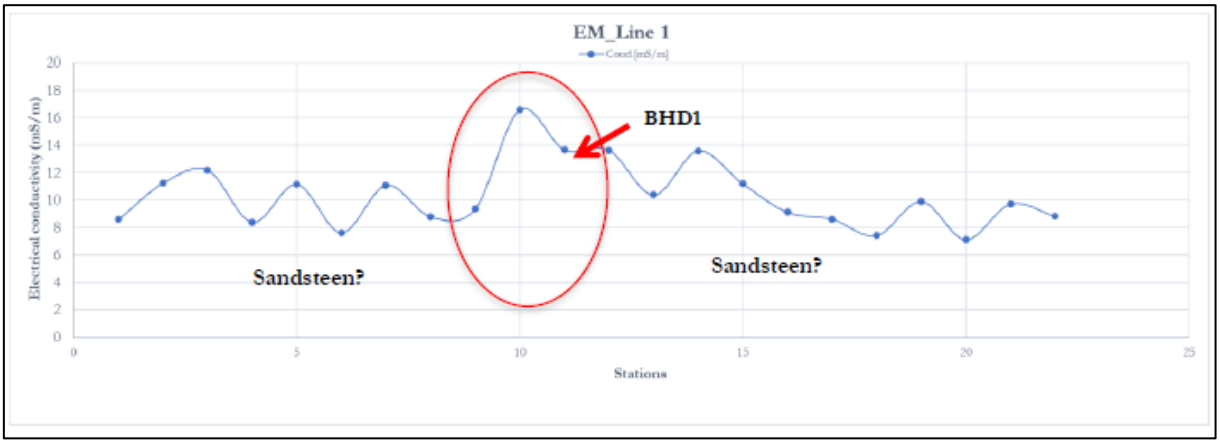

Figure 4.56: Modelled electromagnetic survey data (modified from GEOSS (2020)).

4.4.7 Case study 7: Klein Slangkop Private Estate, Cape Town

The area of interest is dominated by Peninsula formation quartzites of the TMG that form the erosion-resistant high-elevation Cape Peninsula mountain range. This Peninsula Formation forms the secondary fractured aquifer known as the Peninsula Aquifer. The Graaf Water Formation beneath it is an aquitard (Umvoto Africa, 2020). These are underlain by the Cape Peninsula Batholith of the Cape granite suit. The entire package is overlain by the wind-blown sands of the Sandveld group, which constitute a moderately to minor-yielding aquifer called the Noordhoek aquifer (an intergranular aquifer). Due to the proximity of the property to the sea, saline intrusion is a risk (Umvoto Africa, 2020).

Using two survey lines, a multielectrode resistivity survey was undertaken on the property (Umvoto Africa, 2020). Line 1 was orientated NW-SE 500 m long, and Line 2 was NE-SW and 300 m long. The aim of this survey conducted on 2 January 2020 was to determine:

- The thickness of the unconsolidated sediment (Sandveld Group),
- Presence of potentially groundwater-bearing fractures or fault zones in the property in conjunction with the LiDAR-based lineament mapping, and,
- Any saline intrusion as the property is located near the western coastline.

The resistivity lines' positions are shown in Figure 4.57. The red polygon in the figure is the estate boundary, while the green shows the common area where new boreholes are desired. The resistivity profiles produced across lines 1 and 2 were interpreted, and it was found that the unconsolidated sediment with lower resistivity (green to blue) was about 10-20 m thick (Umvoto Africa, 2020). A large potentially water-bearing fault was interpreted from the profiles. The fault was within the Peninsula Formation (Ope) and was targeted for drilling a potential abstraction borehole. No saline water was observed at depths of 50-60 mbgl (Umvoto Africa, 2020). Figure 4.58 a) and b) show the geoelectric models for lines 1 and 2, respectively. Red broken lines indicate possible fault or fracture zones in the Peninsula Formation, with black lines mark increasing resistivity beneath them. A single borehole was recommended to be drilled at fracture position in line one (Figure 4.58a) with two monitoring boreholes.

Figure 4.57: Position of the resistivity survey lines at Klein Slangkop (Umvoto Africa, 2020).

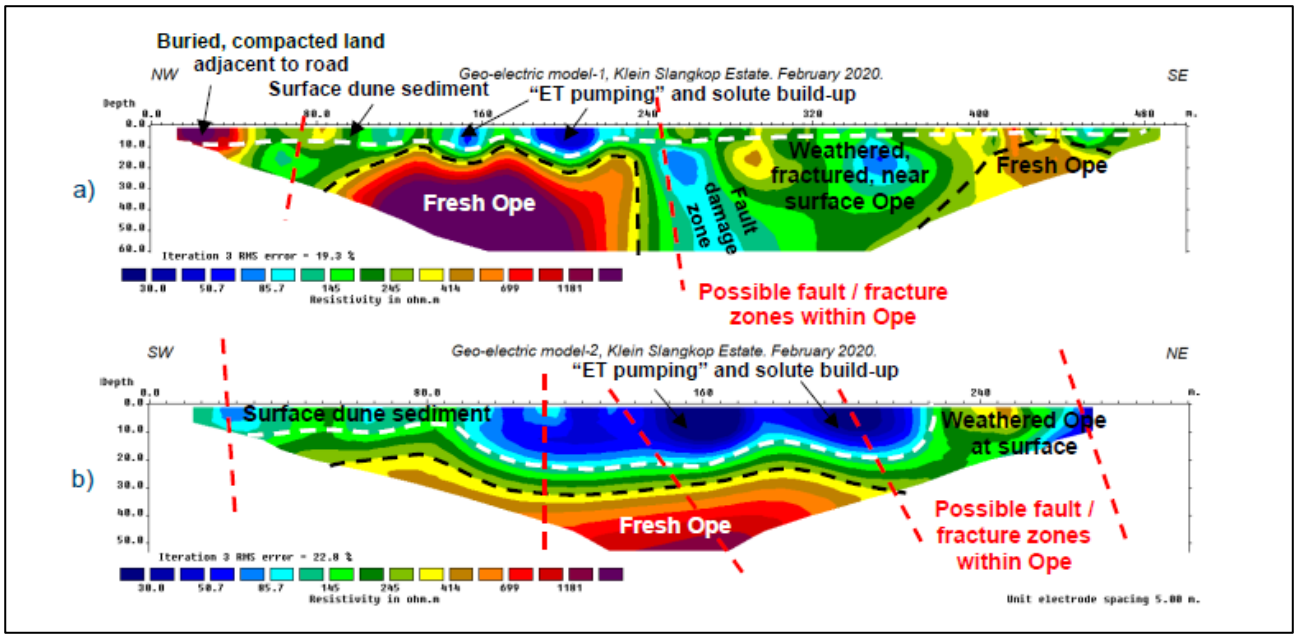

Figure 4.58: Modelled resistivity cross sections across a) Line 1 and b) Line 2 (Umvoto Africa, 2020).

4.4.8 Case study 8: Cape Fold Belt

Groundwater exploration was conducted in an area located in the Cape Fold Belt with thick vertical shale beds underlain by sandstone using the PQWT system. Figure 4.59 shows the recorded PQWT data. The investigation depth was 300 m, and there were 22 stations, 5 m apart. A borehole was drilled at station 16 (indicated with a red rectangle) where the data indicated low values for the electrical potential difference at depths of approximately 90 mbgl and 120 mbgl. Water was intersected at a depth of 70 mbgl with a yield of 2000 L/h. Additional water strikes occurred, and the final blow yield of the borehole was 8000 L/h (Rock Hounds, n.d.).

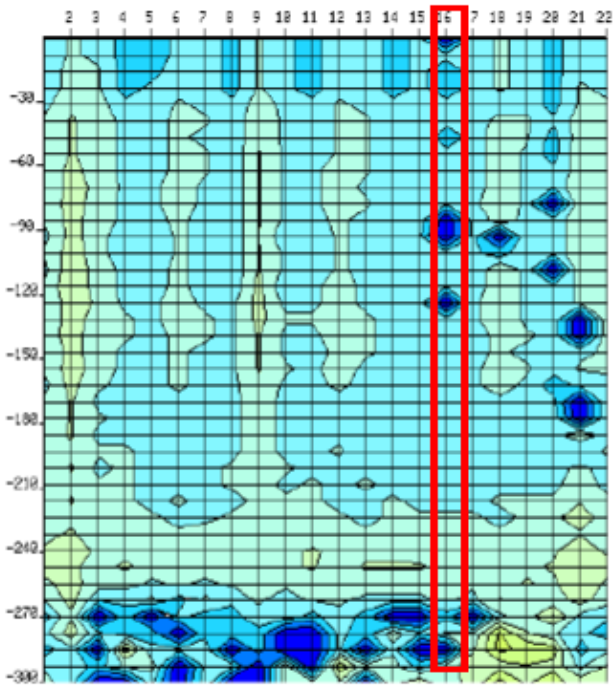

Figure 4.59: Mapped potential difference (Rock Hounds, n.d.).

4.5 GROUNDWATER EXPLORATION IN THE NAMAQUA-NATAL METAMORPHIC PROVINCE

A case study of geophysical prospecting conducted in the NNMP is presented.

4.5.1 Case study 1: Senzakahle Secondary School

Ground-based geophysics was conducted at Senzakahle Secondary School in Umgungundlovu District in KwaZulu Natal to site a borehole. The area is underlain by the Origibi Gorge granitoid intruded into the Natal Metamorphic Complex. The aquifer is medium to low yielding. The PQWT-TC500 groundwater detector was the method used to conduct the survey. The single traverse was selected from observation of geomorphology and data collected at 1 m intervals. Figure 4.60 shows the potential difference curves and a map generated from the survey (African Groundwater (Pty) Ltd, 2022b). A single borehole was drilled from the survey, 80 m with a blow yield of 2000 L/h

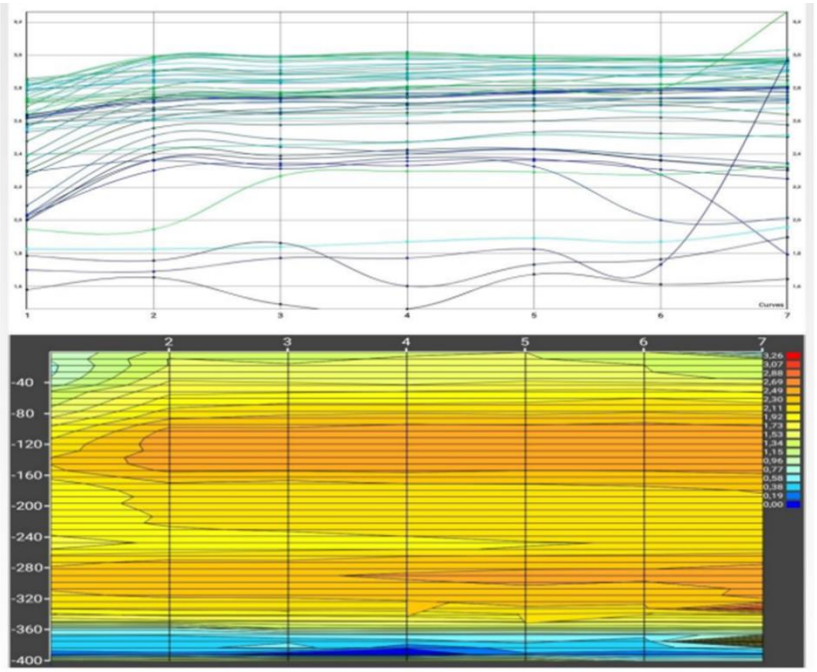

Figure 4.60: Senzakele PQWT Survey results (African Groundwater (Pty) Ltd, 2022b).

4.6 GROUNDWATER EXPLORATION IN THE BUSHVELD IGNEOUS COMPLEX

Groundwater exploration has been conducted extensively in the BIC, several case studies are presented here.

4.6.1 Case study 1: Rapotokwane Bulk Water Supply Groundwater exploration

The consultant was appointed to explore groundwater for the Rapotokwane village in Limpopo, and geophysics was conducted to aid borehole siting (Aurecon, 2014a). The study area sits on an outcrop of Nebo granite surrounded by Ecca Group shales, shaley sandstone, gritstone, sandstone, conglomerates and coal beds at the base and top. The Irrigasiie Formation is found northwest of the area, and the Clarens Formation fine-grained sandstones north of it. The aquifer is classified as a partly fractured and partly intergranular and fractured aquifer. Dolerite intrusions are not extensive, and groundwater favours fractures and joints developed locally along bedding planes, contacts, faults and shear zones (Aurecon, 2014a). The geology is shown in Figure 4.61.

Available aeromagnetic data for the area were interpreted structurally to identify potential groundwater exploration targets. Targets were chosen based on their potential for significant yields and accessibility of the site. The location of targets in relation to the village, existing infrastructure,

existing exploited boreholes and aquifers was also considered to avoid over-exploitation (Aurecon, 2014a).

The aeromagnetic data of 1 km flight line spacing were interpreted within a 15 km radius of the site. Total magnetic field intensity was then shown on a sun-shaded map. This data were overlain on available Council for Geoscience data because no high-resolution aeromagnetic data were available for the area. Lineaments were also identified from that data.

Three geophysical survey lines were conducted using the Geotron G5 proton magnetometer and ABEM Lund terrameter at a station and electrode spacing of 10 m. Three more traverses were conducted using the magnetometer and EM34-3 at a station spacing of 10 m and an intercoil spacing of 40 m. A total of seven survey lines (Figure 4.62) were explored, and eight drilling targets were identified and drilled (Figure 4.63). Only two boreholes, RP-BH2a and RP-BH3, from traverses D and X had a significant yield to justify pump testing (Aurecon, 2014a). Only a few selected results are discussed in this report.

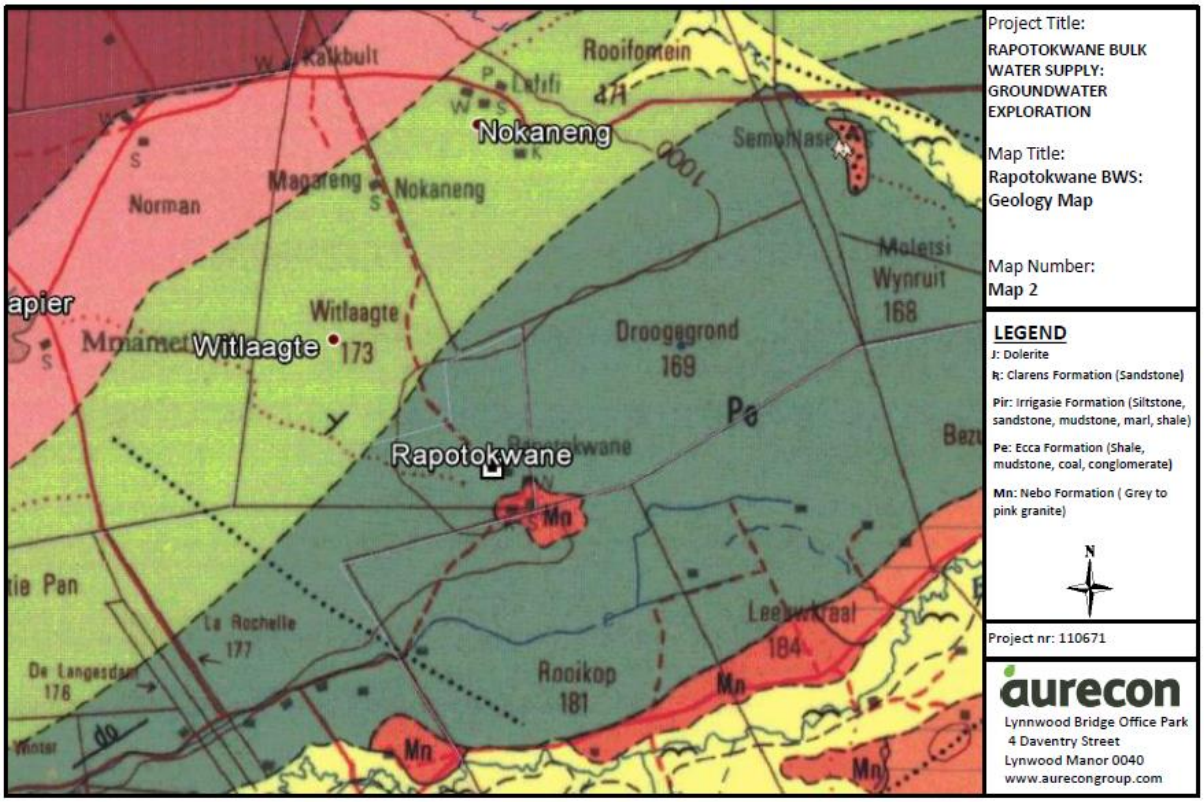

Figure 4.61: Rapotokwane geology map (Aurecon, 2014a).

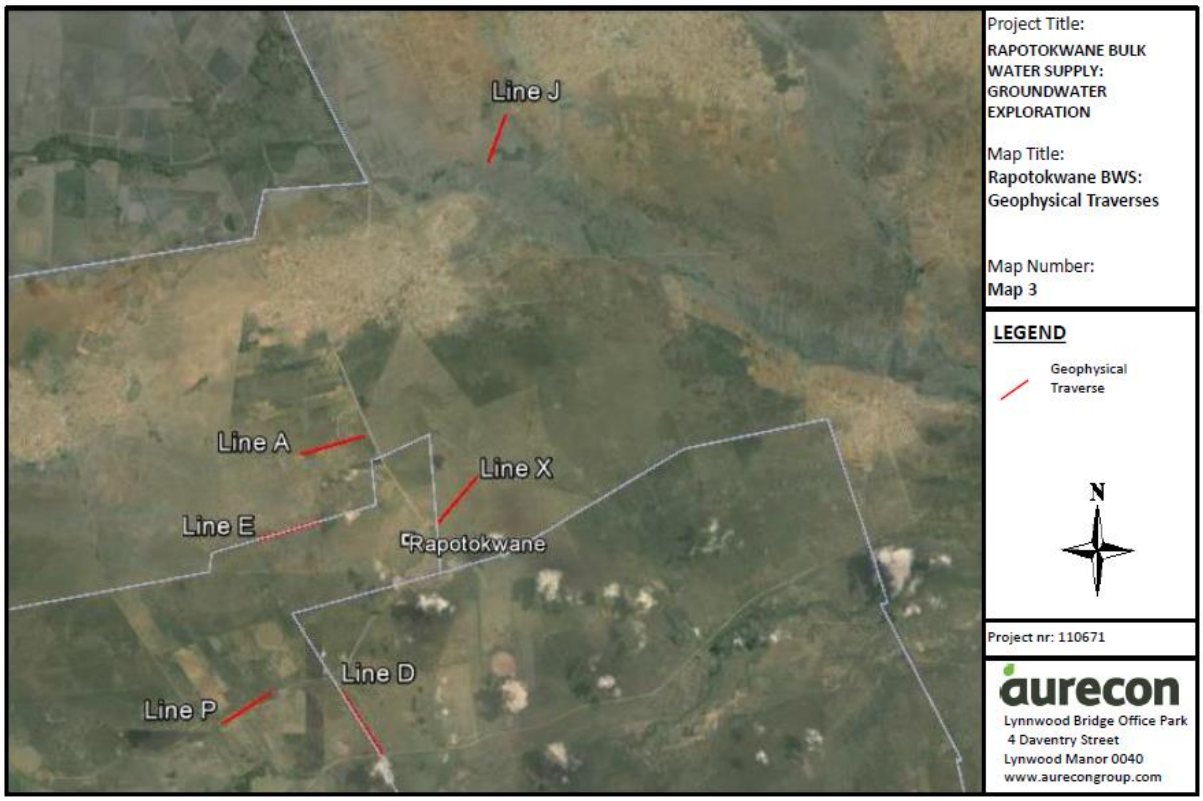

Figure 4.62: Geophysical survey lines (Aurecon, 2014a).

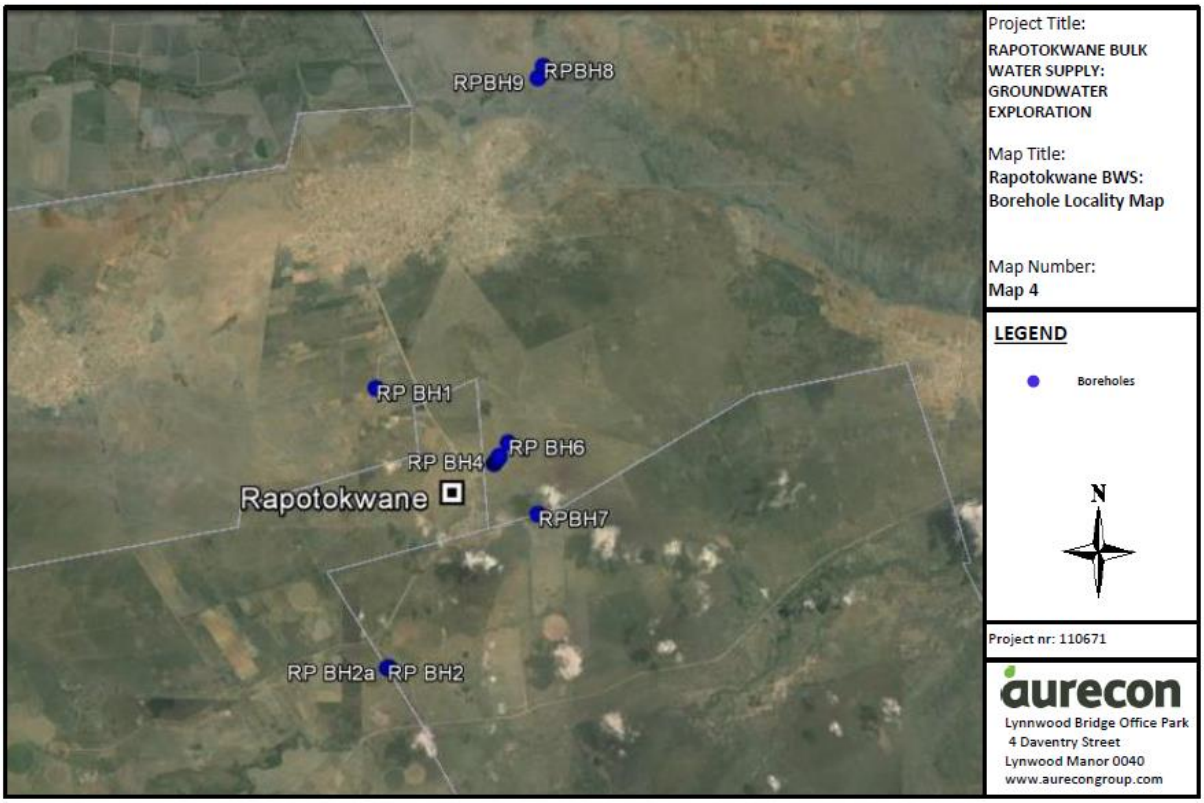

Figure 4.63: Borehole locality map (Aurecon, 2014a).

Figure 4.64 shows the magnetic profile produced along line 1 and the electrical conductivity obtained from the EM34-3. For the EM34-3, both the vertical and horizontal dipoles were used, with intercoil spacings of 20 m and 40 m. Results from another traverse (Line X) conducted using the resistivity

and electromagnetic methods are shown in Figure 4.66. Four boreholes were drilled from this traverse's interpretation, although only one RP-BH3 was successful. Figure 4.65 shows the magnetic profile of line A with the modelled resistivity at the bottom of the image. The position where a borehole was drilled along the profile and geoelectric model is indicated by a black arrow and corresponds to a spike in the magnetic profile and a zone of low resistivity adjacent to a high resistivity.

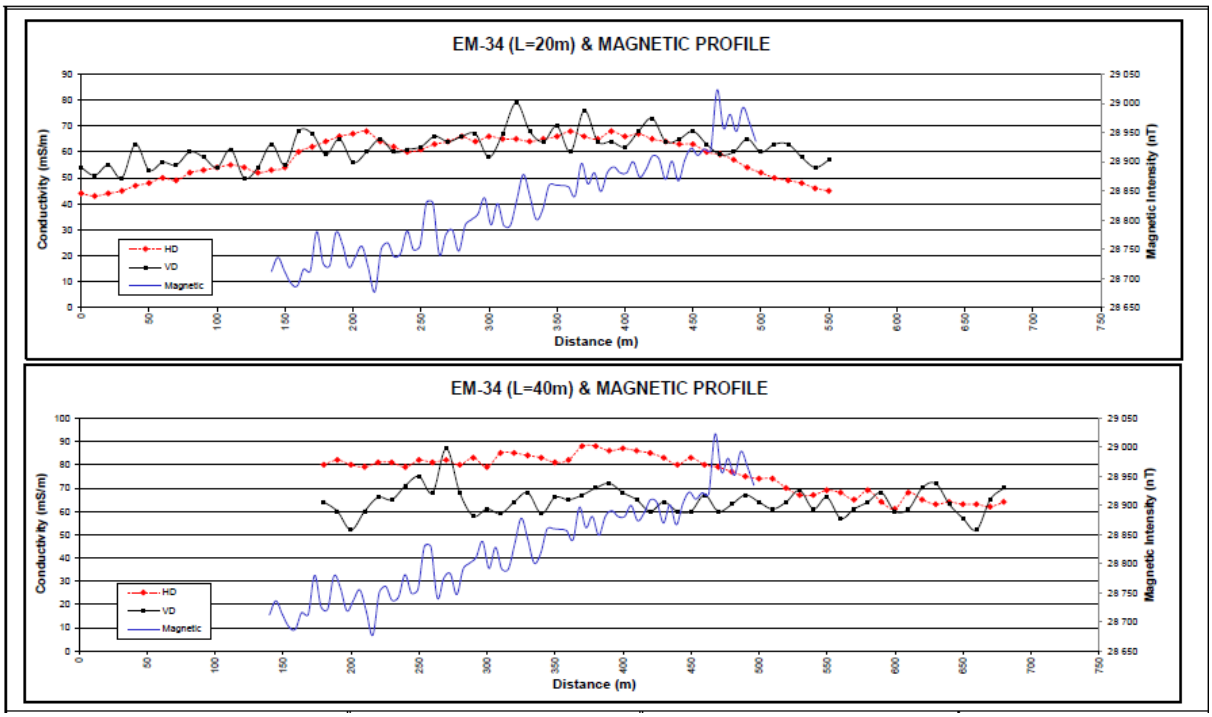

Figure 4.64: Conductivity and magnetic field intensity along line one (Aurecon, 2014a).

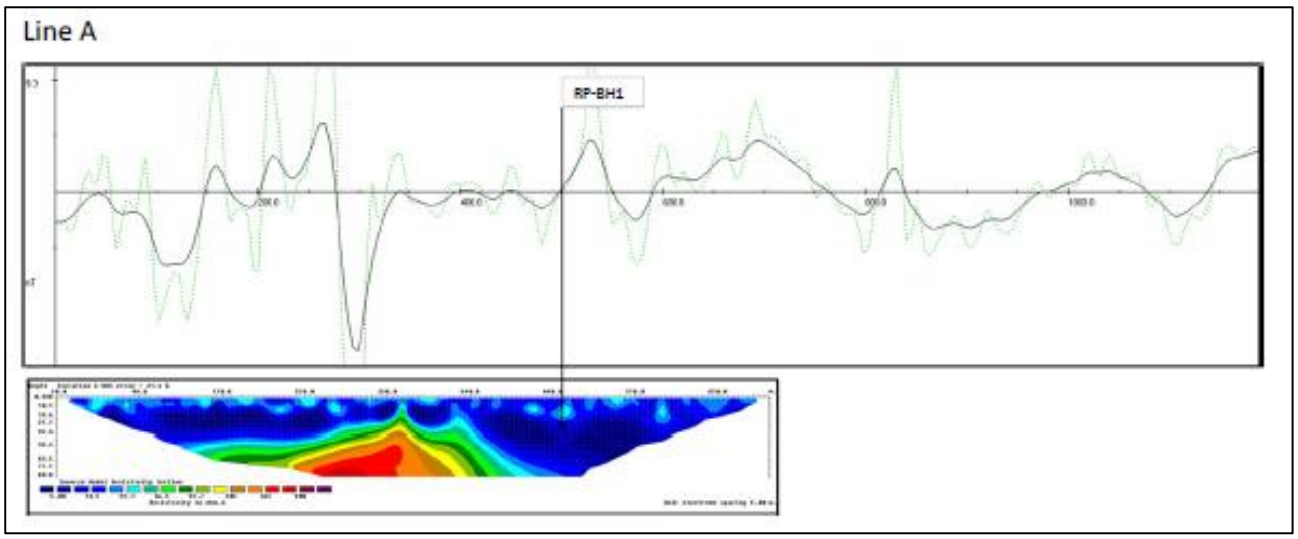

Figure 4.65: Line A magnetic field intensity and modelled resistivity section (Aurecon, 2014a).

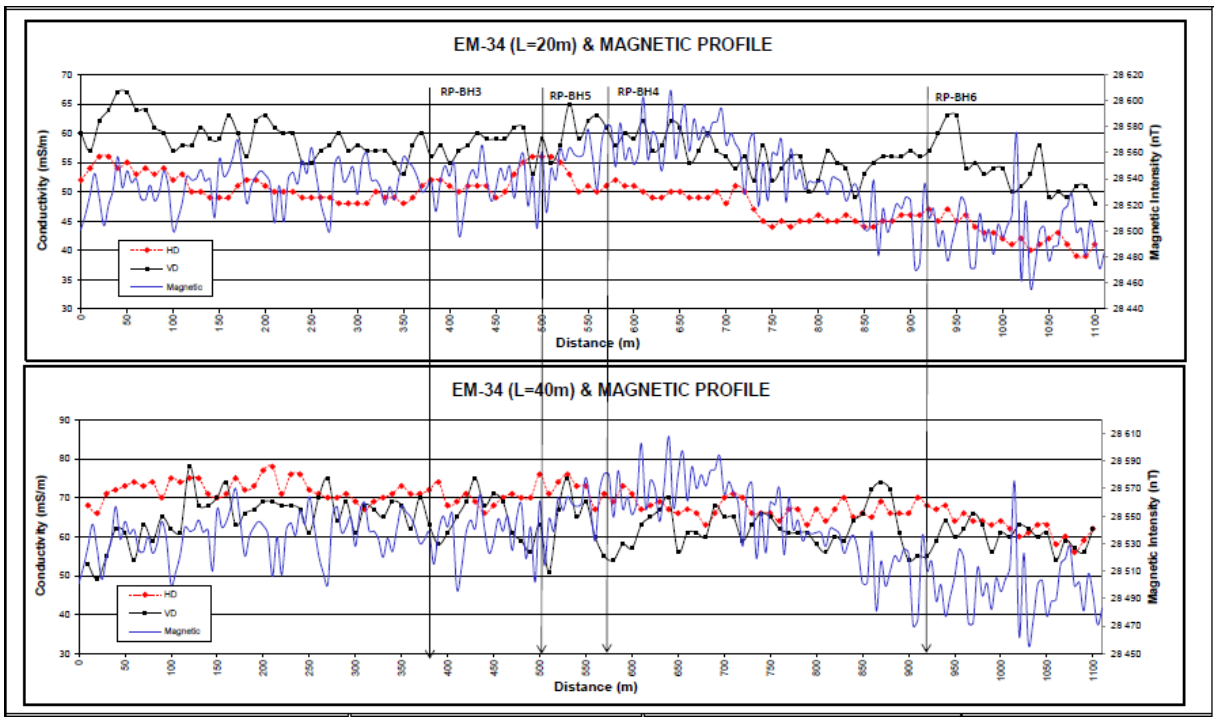

Figure 4.66: Line X conductivity and magnetic field intensity (Aurecon, 2014a).

4.6.2 Case study 2: Vingerkraal Village Water Supply- Groundwater Exploration

The consultant was appointed to explore groundwater for the Vingerkraal village and site boreholes through geophysics. Vingerkraal area is underlain by granophyric Bushveld granite. The village itself sits on a wedge of Magaliesberg quartzite from the Transvaal. The whole area is faulted upwards in a half-graben structure. There is a granophyre placer between the quartzite and the granite southwest of the Magaliesberg unit. The aquifer in this area is classified as intergranular and fractured. Figure 4.67 shows the geology of the area where the village is found.

Aeromagnetic data with 1 km flight line spacing were overlain with data acquired at a 200 m line spacing for increased accuracy of the identified potential geophysical targets. After interpreting the aeromagnetic data, a magnetic survey using the Geotron G5 proton magnetometer and an electromagnetic survey using the Geonics EM 34 were conducted (Aurecon, 2015). The station spacing employed for the surveys was 10 m, while intercoil spacing of 20 m and 40 m were used in the electromagnetic survey. Only five traverses (Figure 4.68) were surveyed, from which three boreholes were drilled. Modelled results for lines B, which produced the borehole with the highest blow yield (23500 L/h), and line H, which no borehole was drilled, are shown in Figure 4.69 and Figure 4.70. The EM34 surveys were conducted in both the vertical and horizontal dipole orientations. A black arrow along the profile in Figure 4.69 indicates the position of the borehole VK-BH3 which corresponds to an anomaly. Figure 4.71 shows the locality of the three boreholes which were

eventually drilled during this project. Only two out of three boreholes were successful. Borehole VK-BH1 was dry.

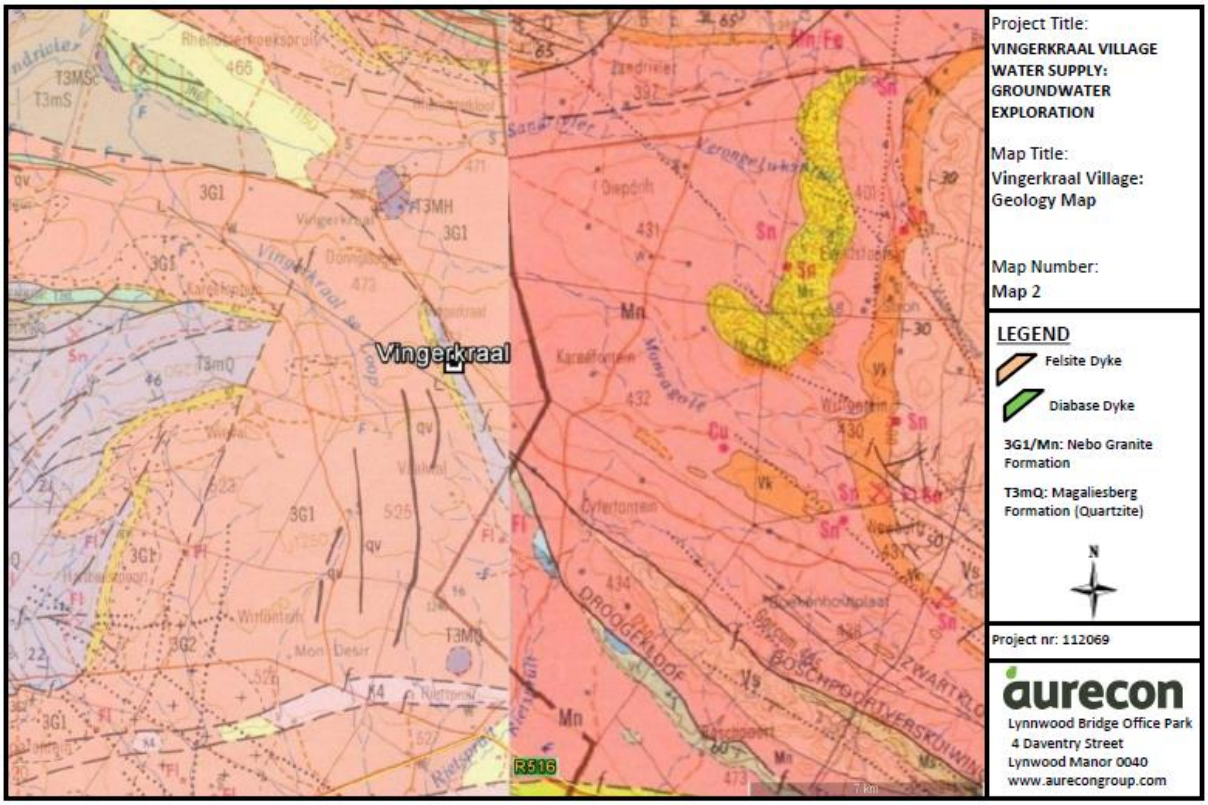

Figure 4.67: Vingerkraal regional geology (Aurecon, 2015).

Figure 4.68: Geophysical traverses at vingerkraal (Aurecon, 2015).

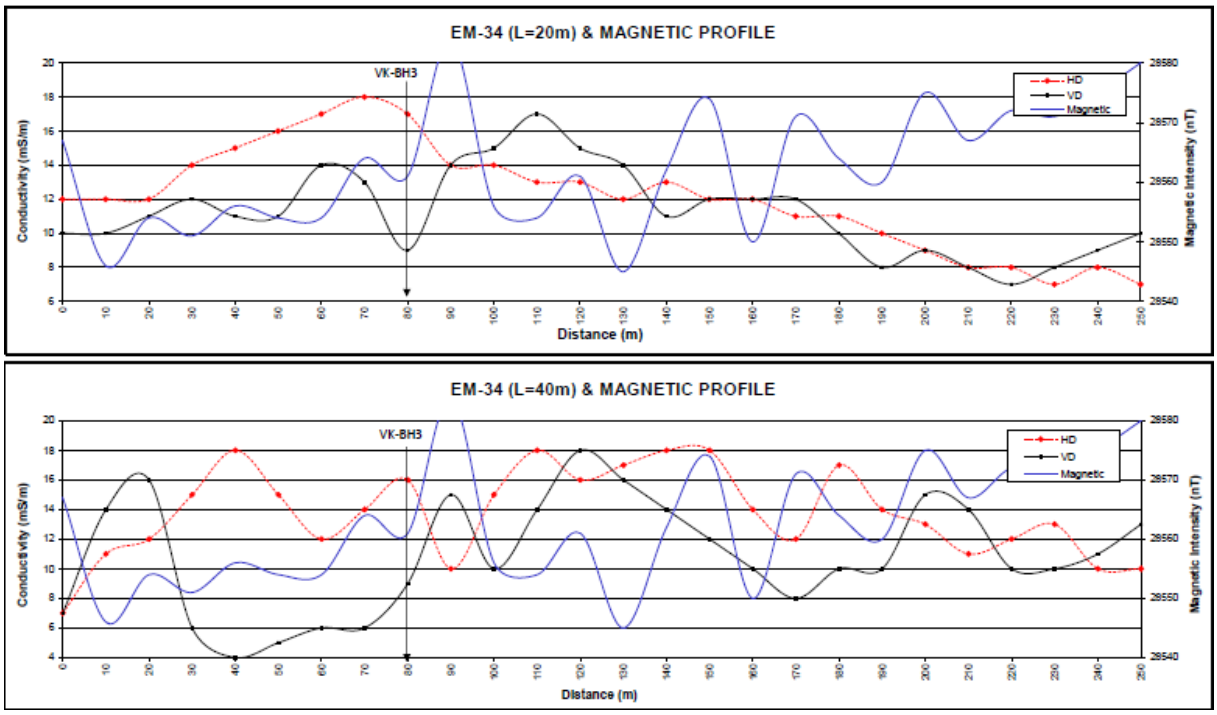

Figure 4.69: Conductivity and magnetic profile along line B, Vingerkraal (Aurecon, 2015).

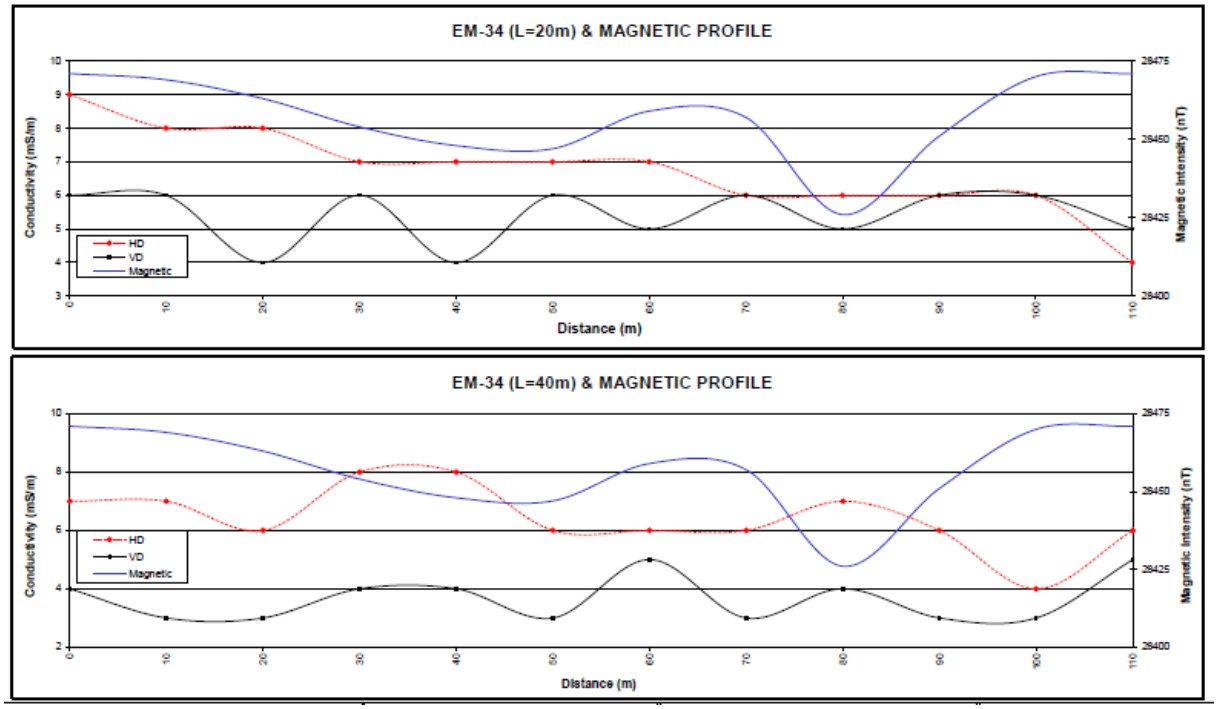

Figure 4.70: Conductivity and Magnetic profile along line H, Vingerkraal (Aurecon, 2015).

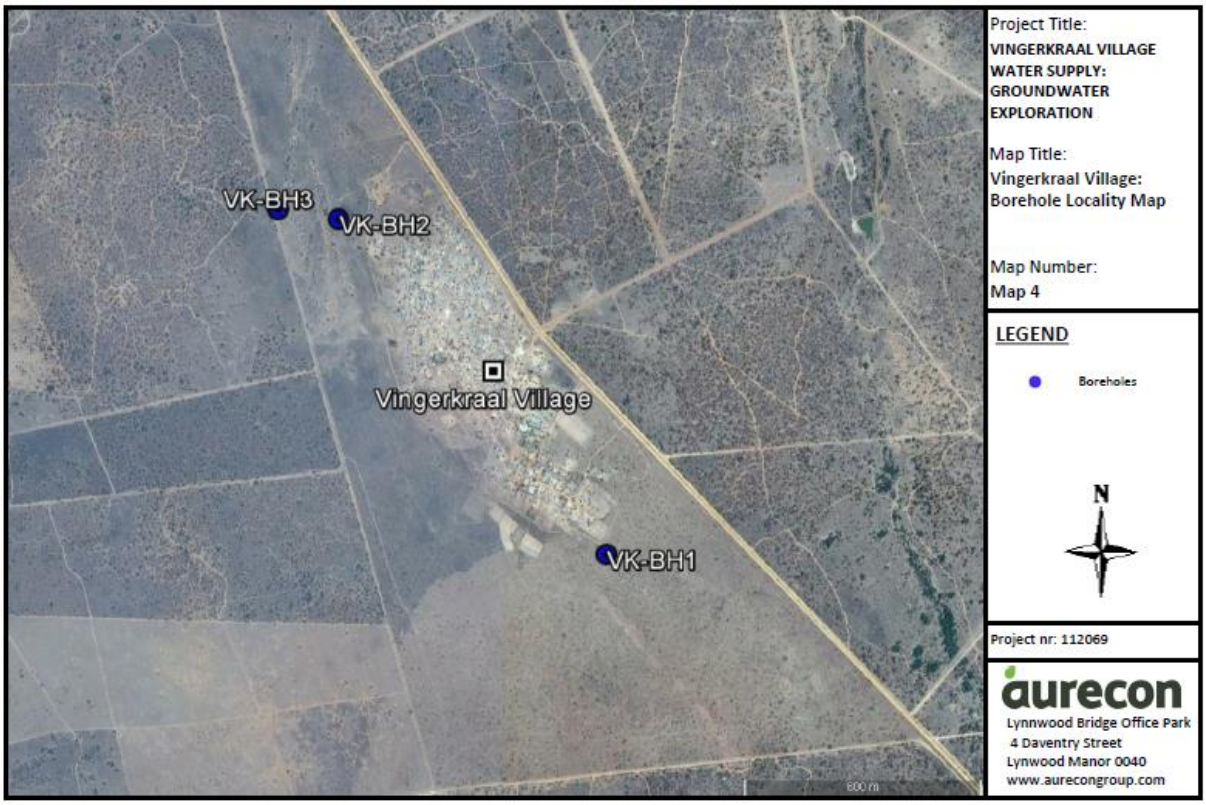

Figure 4.71: Borehole locality map, Vingerkraal (Aurecon, 2015).

4.6.3 Case study 3: Borehole siting at Legkraal

The consultant used a geophysical survey to site several boreholes near Legkraal in the North West Province as part of the Metsi Bophelo Boreholes Project. Undifferentiated surface deposits overlie the area with sub-outcrops of norite, gabbro-norite and anorthosite of the RLS northeast of the site. Syenite outcrops in the south. Groundwater occurs in faults and associated shear zones and intrusive dykes and contacts between lithological units (Aurecon, 2012a).

The consultant used a proton magnetometer and the Geonics EM34 to conduct the survey. 11 traverses were completed in March 2012 for the magnetic and electromagnetic methods. The station spacing was 10 m with an intercoil spacing of 40 m for the electromagnetic survey. Station spacing for the magnetic survey was set at 5m. The geophysical traverses and the borehole sites are shown in Figure 4.72. Four target anomalies were identified in interpreted weathered zones. Figure 4.73 and Figure 4.74 show the results obtained for LT1 and LT2 (Aurecon, 2012a). Traverse results from which the boreholes were drilled were not provided.

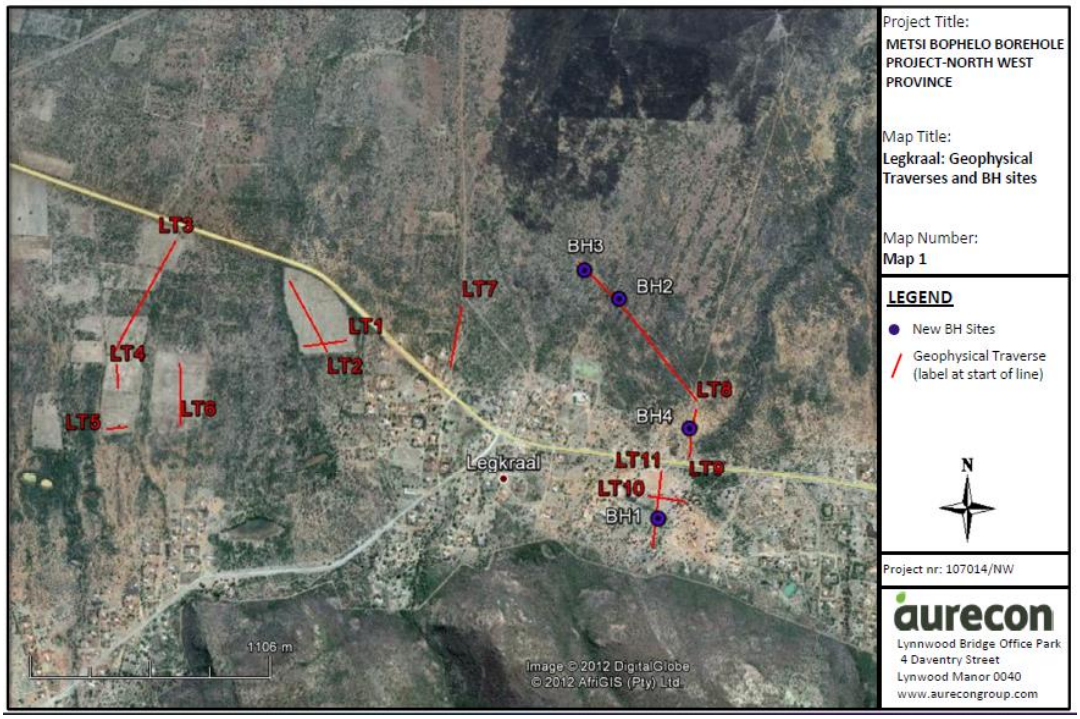

Figure 4.72: Geophysical traverses and borehole locations at Legkraal (Aurecon, 2012a).

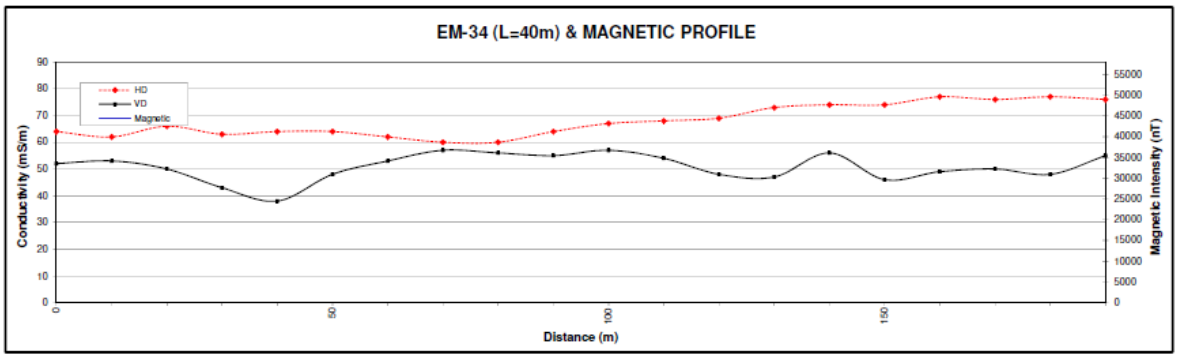

Figure 4.73: EM 34 results for traverse LT1 (Aurecon, 2012a).

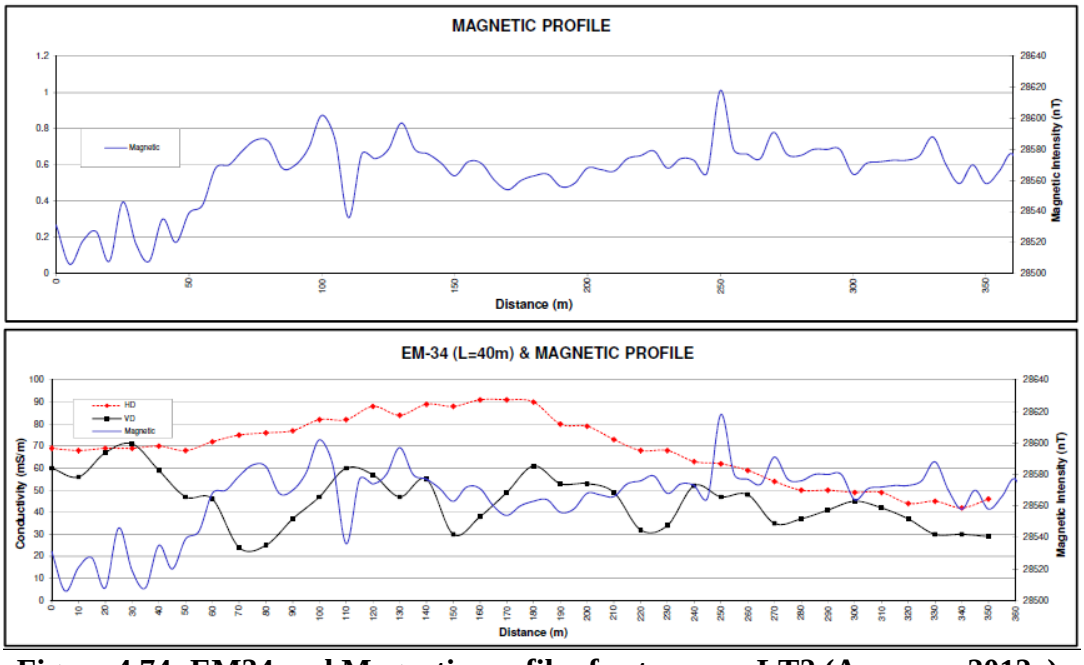

Figure 4.74: EM34 and Magnetic profiles for traverse LT2 (Aurecon, 2012a).

4.6.4 Case study 4: Groundwater Exploration for the Mabeleleng Water Supply Upgrade

The consultant conducted groundwater exploration near the Mabeleleng village in the North West province. A geophysical survey was used to site the two boreholes (Aurecon, 2012b). Undifferentiated surface deposits and the Rustenburg Layered Suite (Ruighoek pyroxenite) underlie the area. On a regional scale, E-W striking faults occur. Groundwater occurrence is associated with deeply weathered rock (Aurecon, 2012b). However, the rocks weather to a rich clay that tends to hinder groundwater recharge. Aquifers in the region are classified as fractured (Aurecon, 2012b).

When selecting geophysical targets, strata from a nearby mine were considered. The survey was conducted using the magnetic (proton magnetometer) and electromagnetic methods (Geonics EM34 ground conductivity meter). A station spacing of 10 m and intercoil spacings of 20 m and 40 m were used. Two traverses were conducted. Their locations and that of the boreholes drilled are shown in Figure 4.75. Line T1 was about 1.2 km long in a S-N direction, while T2 (600 m) was W-E (Aurecon, 2012b). The results obtained for the lines are shown in Figure 4.76 and Figure 4.77, respectively. The position of the borehole drilled from the survey, MBBH1, is indicated in Figure 4.76 and corresponded to a significant spike in the magnetic field intensity and a dip in the conductivity.

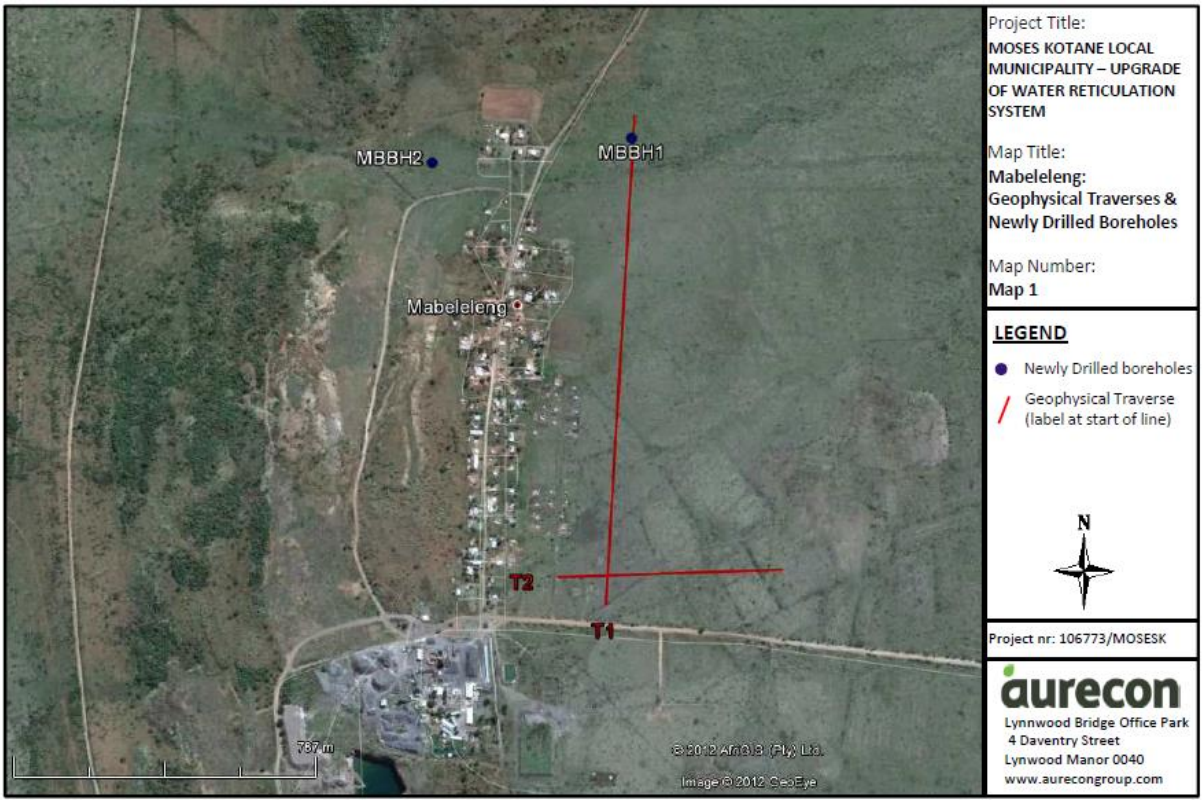

Figure 4.75: Geophysical traverses and drilled boreholes for Mabeleleng (Aurecon, 2012b).

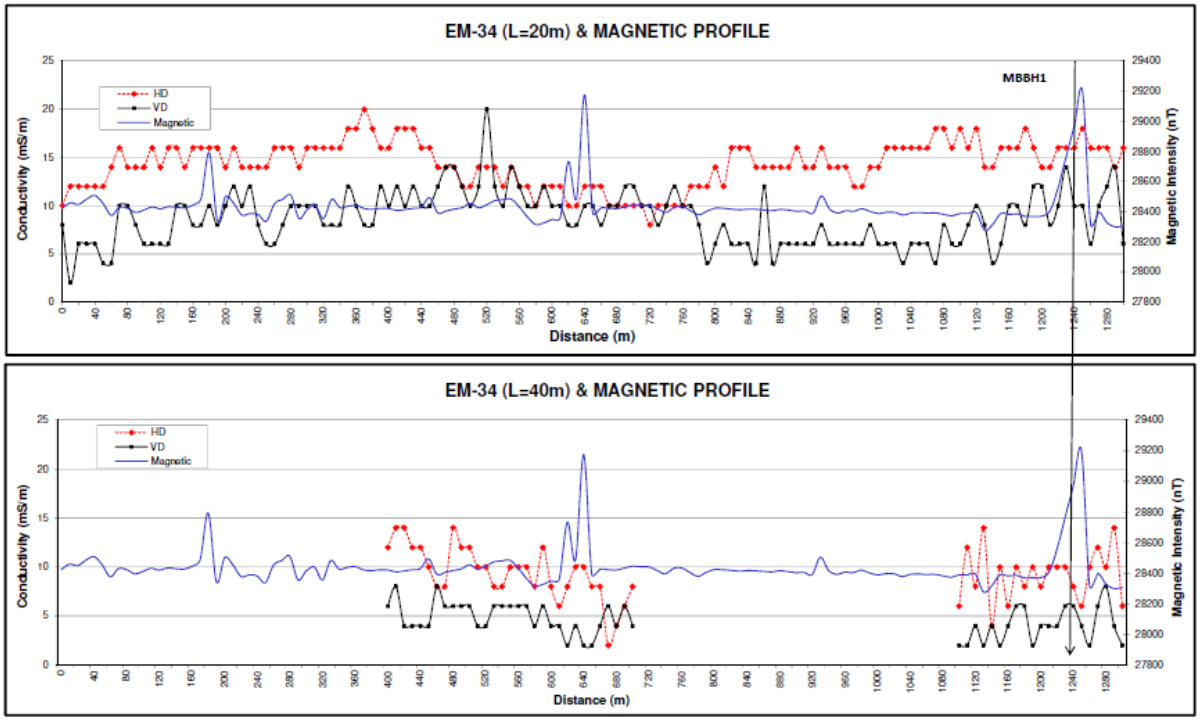

Figure 4.76: Line T1 EM34 and Magnetic profile (Aurecon, 2012b).

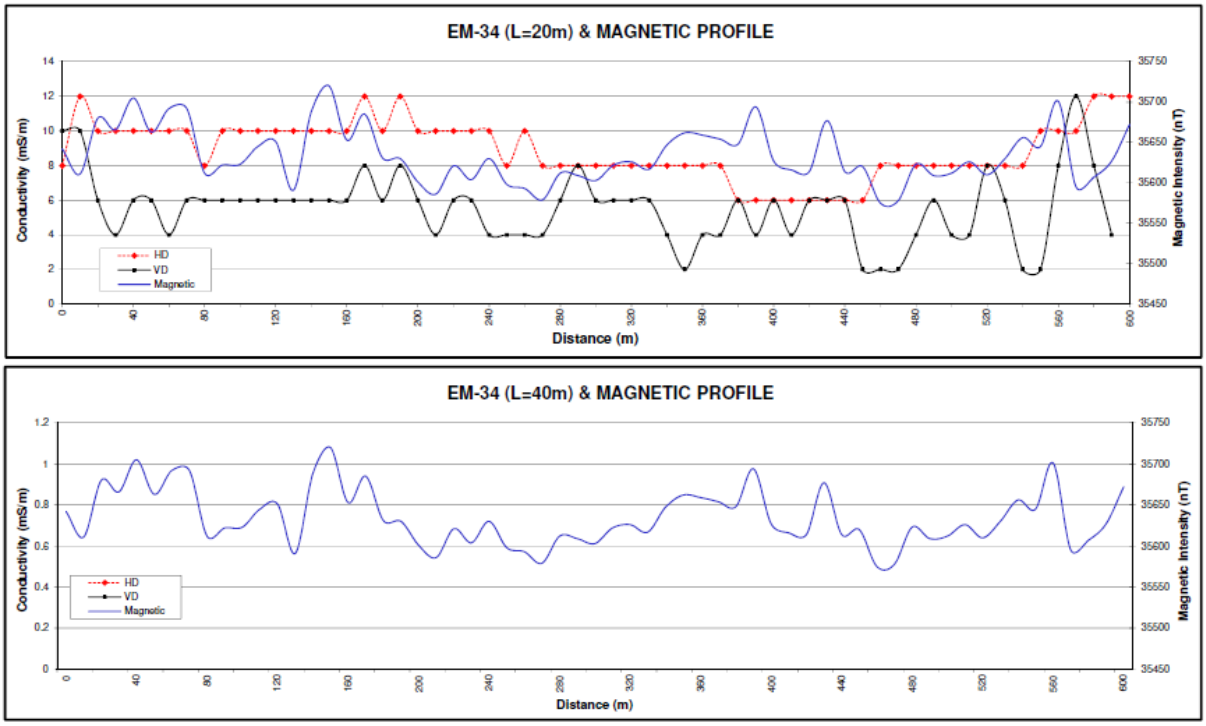

Figure 4.77: Line T2 EM34 and Magnetic profile (Aurecon, 2012b).

4.6.5 Case study 5: Groundwater Exploration for the Makgope Water Supply Upgrade

The consultant conducted groundwater exploration in the vicinity of Makgope in the North West for the Makgope water supply upgrade (Aurecon, 2012c). Undifferentiated surface deposits and the RLS Makgope pyroxenite, Groenfontein harzburgite and Kroondal norite underlie the area (Aurecon, 2012c). SE-NW striking faults occur regionally. Groundwater occurrence is associated with

weathered and fractured mafic rocks, although groundwater potential is generally considered low (Aurecon, 2012c). The magnetic (proton magnetometer) and the electromagnetic (Geonics EM34 ground conductivity meter) methods were used to conduct the survey (Aurecon, 2012c). Intercoil spacings were 20 m and 40 m, while station spacing was set at 10 m. A single traverse (Figure 4.78), 1200 m long N-S, was conducted. Two boreholes were drilled, one from an identified anomaly (Aurecon, 2012c). Figure 4.79 shows the results obtained from the survey. The magnetic field intensity shows a significant jump at around 60 m, which suggests interference in the survey caused by instrument failure.

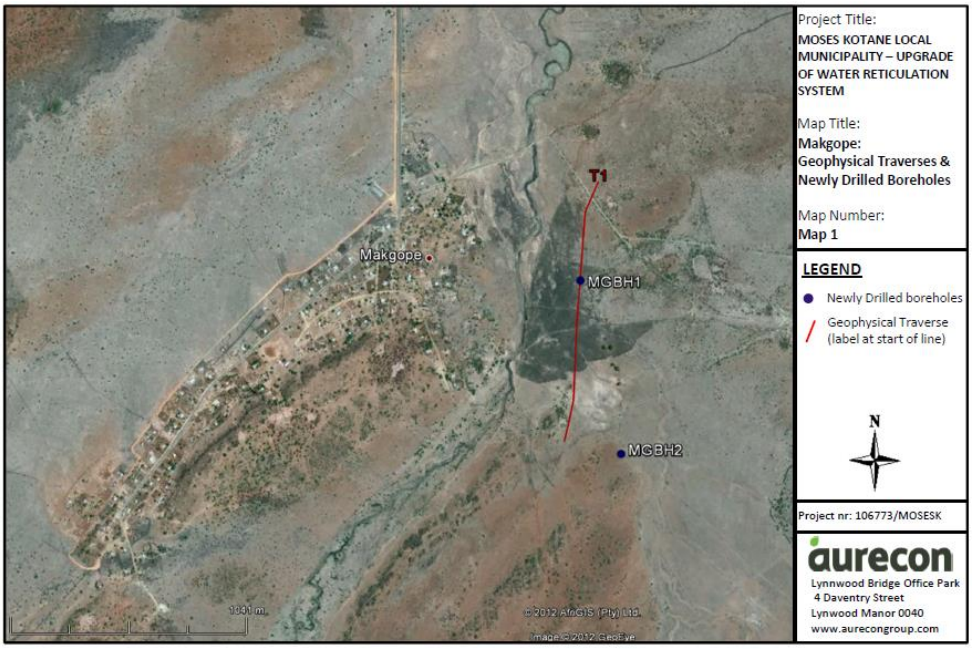

Figure 4.78: Geophysical survey line and borehole location for Makgope (Aurecon, 2012c).

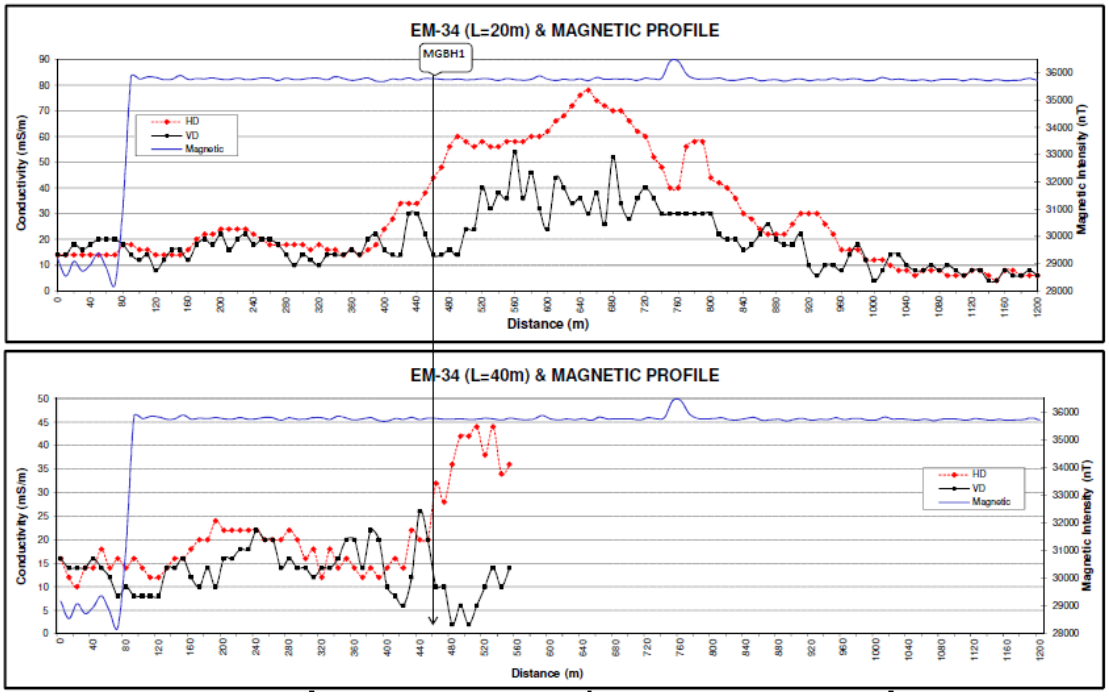

Figure 4.79: EM34 and Magnetic profile for line T1 (Aurecon, 2012c).

4.6.6 Case study 6: Groundwater Exploration for the Maologane Water Supply Upgrade

The consultant conducted groundwater exploration near Maologane in the North West as part of the Maologane water supply upgrade (Aurecon, 2012d). The area is characterised by undifferentiated surface deposits and the RLS, Pilanesberg Complex and Pretoria Group rocks. These are the Kroondal norite, Ruighoek pyroxenite (which may be chrome bearing), Sun City syenite and Magaliesberg quartzites (Aurecon, 2012d). Regionally, SE-NW and NE-SW striking faults are present.

Groundwater occurs in weathered and fractured mafic rocks. In the quartzites, groundwater occurs in fractures, faults and contacts with igneous rocks (Aurecon, 2012d). The groundwater potential of the area is low. The survey was conducted very close to the village, which was not favourable due to anthropogenic influences on the readings. A proton magnetometer and the Geonics EM34 were used for the survey. Three traverses were conducted with station spacing of 10 m and intercoil spacings of 20 m and 40 m, with two boreholes drilled. Figure 4.80 shows the geophysical traverses and the drilled borehole locations. Figure 4.81 shows the results obtained for traverse T3, which was 560 m long in the NE-SW direction. The location of the borehole MLBH1(dry) is indicated by an arrow (Aurecon, 2012d).

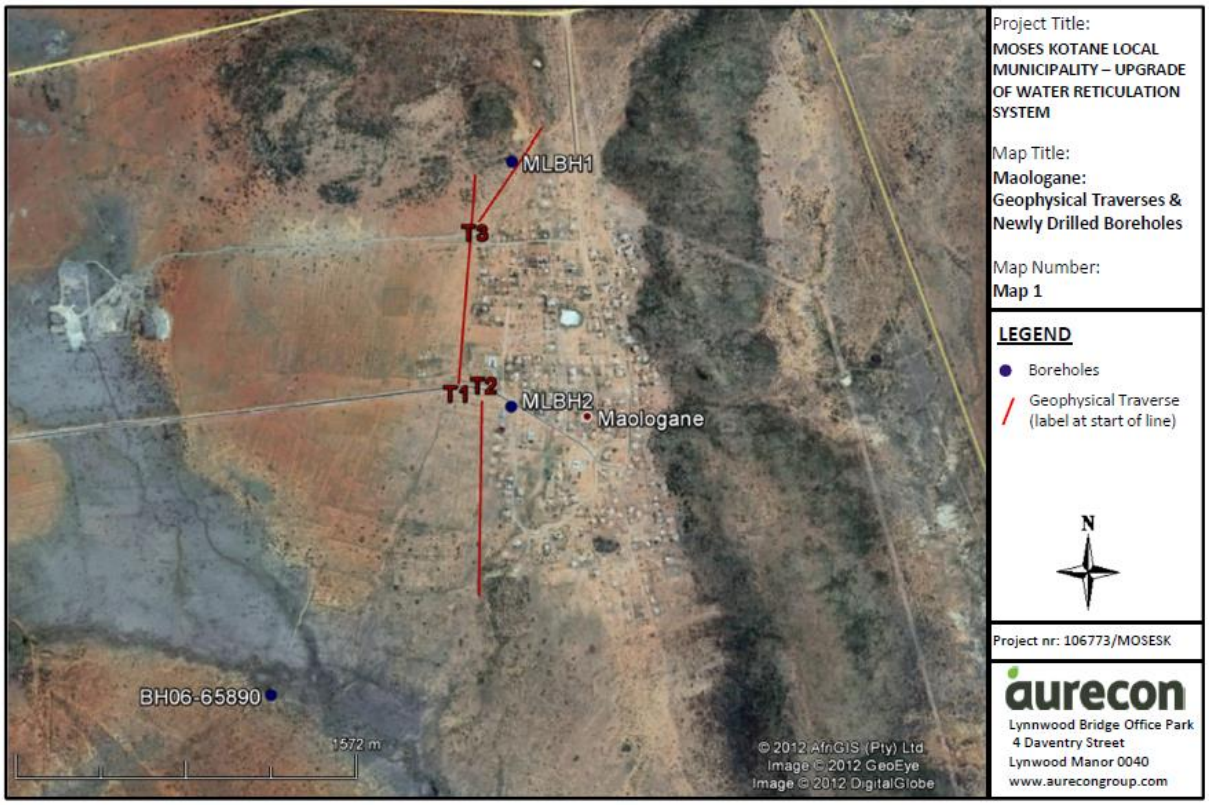

Figure 4.80: Geophysical traverses and boreholes at Maologane (Aurecon, 2012d).

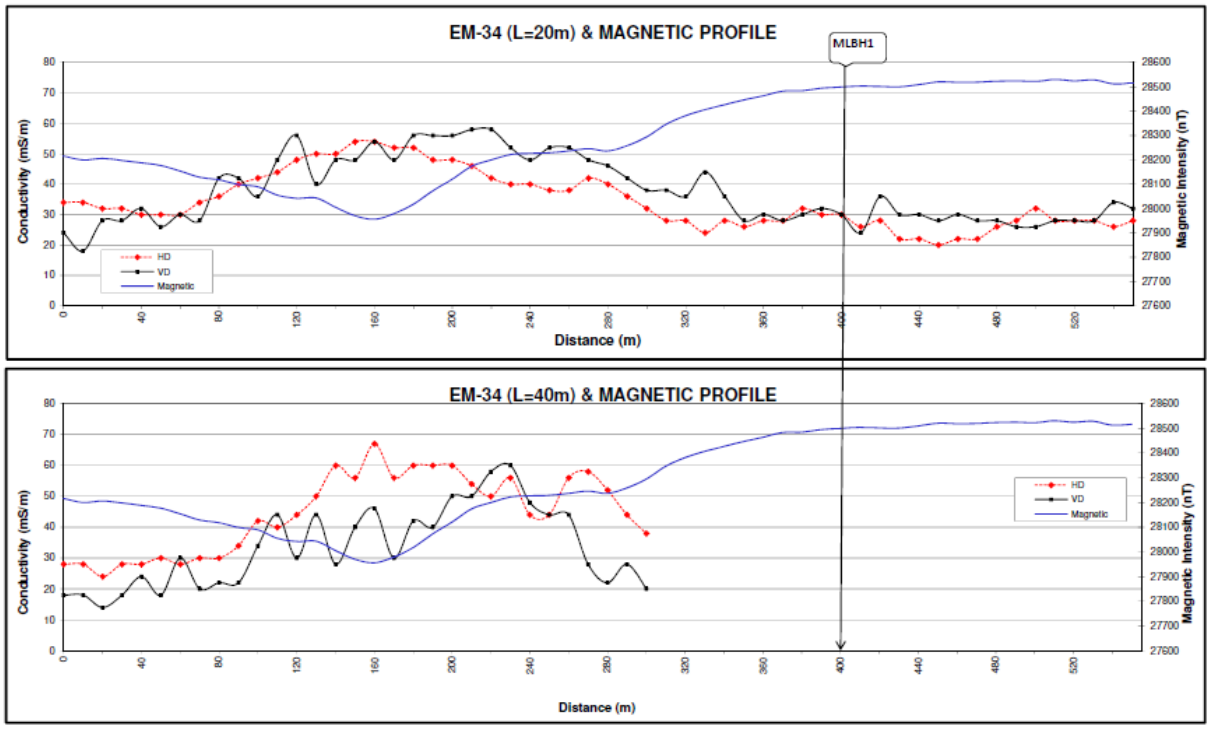

Figure 4.81: EM34 and Magnetic profile for line T3 (Aurecon, 2012d).

4.6.7 Case study 7: Borehole Siting at Ramoga

Boreholes were sited for Ramoga village in the North West province as part of the Metsi Bophelo Borehole Project. The geology of the area consists of Lebowa Granite Suite granites and Rashoop granophyres. Suboutcrops of RLS gabbro-norite and Bierkraal magnetite-gabbro in the NE of the site occur. There are NW-SE striking dolerite dykes in the area. Groundwater occurrence is associated with faults and their shear zones, intrusive dykes and lithological contacts (Aurecon, 2012e).

The geophysical survey was conducted using the Geonics EM34 and a proton magnetometer. The survey undertaken in March 2012 used seven geophysical traverses shown in Figure 4.82. Coil spacing was 40 m, with station spacing set at 10 m for the electromagnetic survey and 5 m for the magnetic survey. Four target anomalies were chosen at contacts (BH1 and BH4) or fractures (BH2 and BH3) (Aurecon, 2012e). Figure 4.83 shows the magnetic and EM34 profile for line RT1 which was SE-NW and 450 m long. The profile obtained for line RT5 is displayed in Figure 4.84; it was SE-NW and ~850 m long. Arrows indicate the proposed borehole positions.

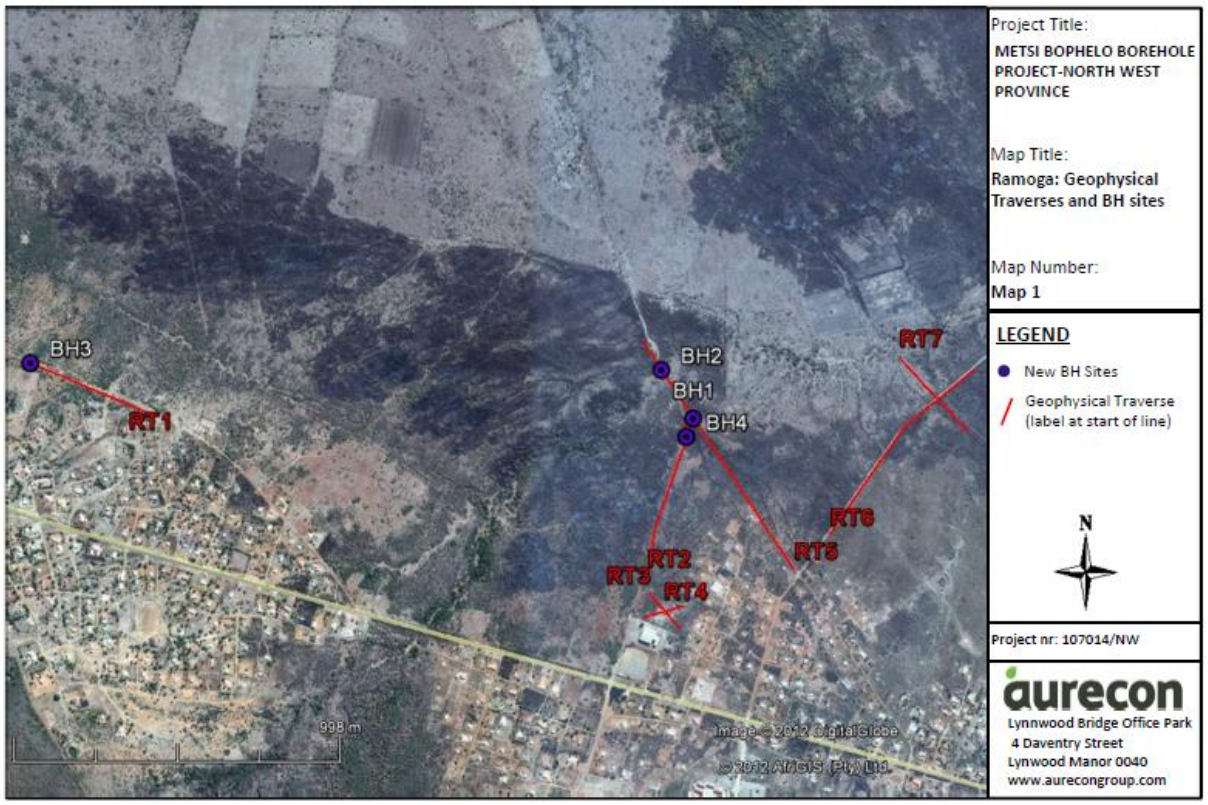

Figure 4.82: Geophysical traverses and proposed boreholes at Ramoga (Aurecon, 2012e).

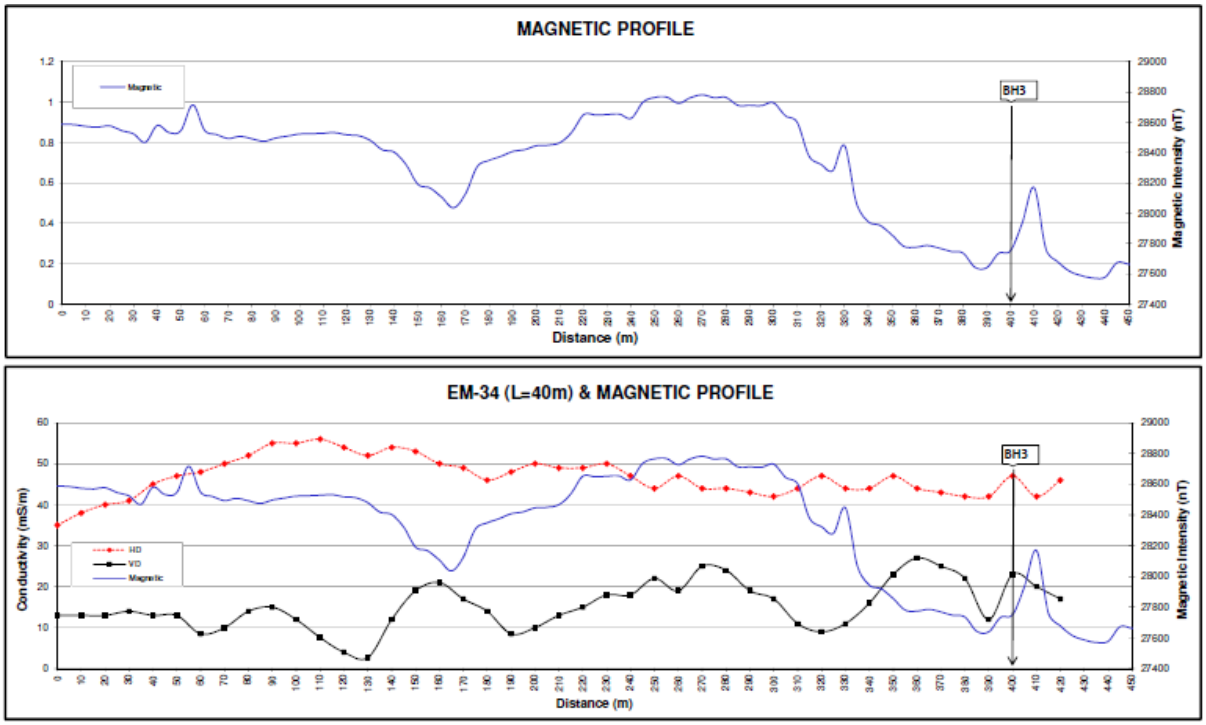

Figure 4.83: EM34 and Magnetic profile for line RT1 (Aurecon, 2012e).

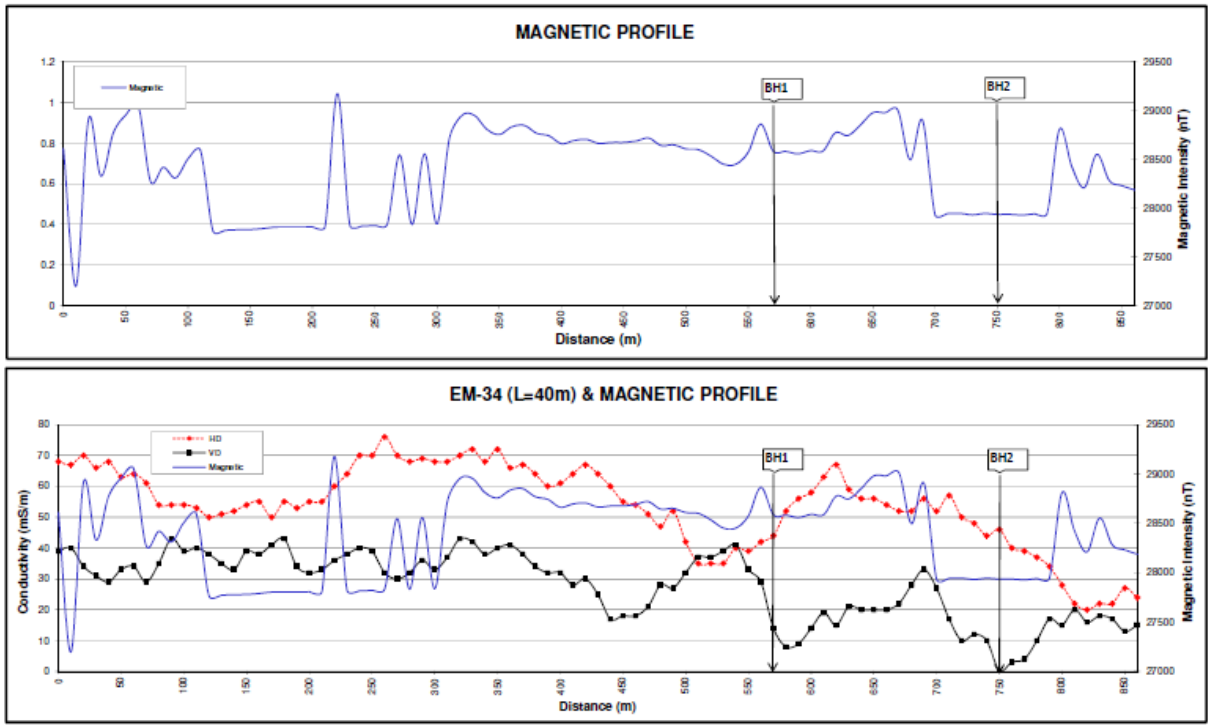

Figure 4.84: EM34 and Magnetic profile for line RT5 (Aurecon, 2012e).

4.7 GROUNDWATER EXPLORATION IN THE TRANSVAAL SUPERGROUP

The Transvaal hosts a particularly high-yielding karst aquifer in its dolomites. Case studies relating to exploration in the Transvaal Supergroup are summarised in this section.

4.7.1 Case study 1: Kameelzynkraal, Pretoria East Groundwater exploration

A client in Kameelzynkraal appointed the consultant to explore for groundwater and establish production boreholes. The Pretoria Group Silverton Formation underlies the site, and numerous dolerite dykes have intruded into these host rocks. This formation consists primarily of shales (which may be carbonaceous), hornfels and chert (Geovation, 2020).

For this project, high-resolution regional aeromagnetic data for the area were acquired to determine target areas. Following this, a ground magnetic survey was conducted using the Geotron G5 proton magnetometer to determine areas where further electromagnetic readings were needed (Geovation, 2020). The electromagnetics was conducted using the Geonics EM-34. The station spacing was 10 m with intercoil spacings of 20 m and 40 m with both vertical and horizontal dipoles adopted. The single survey line conducted for this study is shown in Figure 4.85. The red polygon indicates the property boundary for the client in question (Geovation, 2020).

The EM34 and magnetic profiles are shown in Figure 4.86. The intercoil spacing of 20 and 40 m profiles are presented separately. Four potential drilling targets (BH1-BH4) were identified from the interpreted data and are shown in Figure 4.87 (Geovation, 2020). These coincide with geological

contacts between different lithologies. Likely dolerite dykes in the case of boreholes 1, 2, and 4. These are places where there are significant spikes within the data (Geovation, 2020).

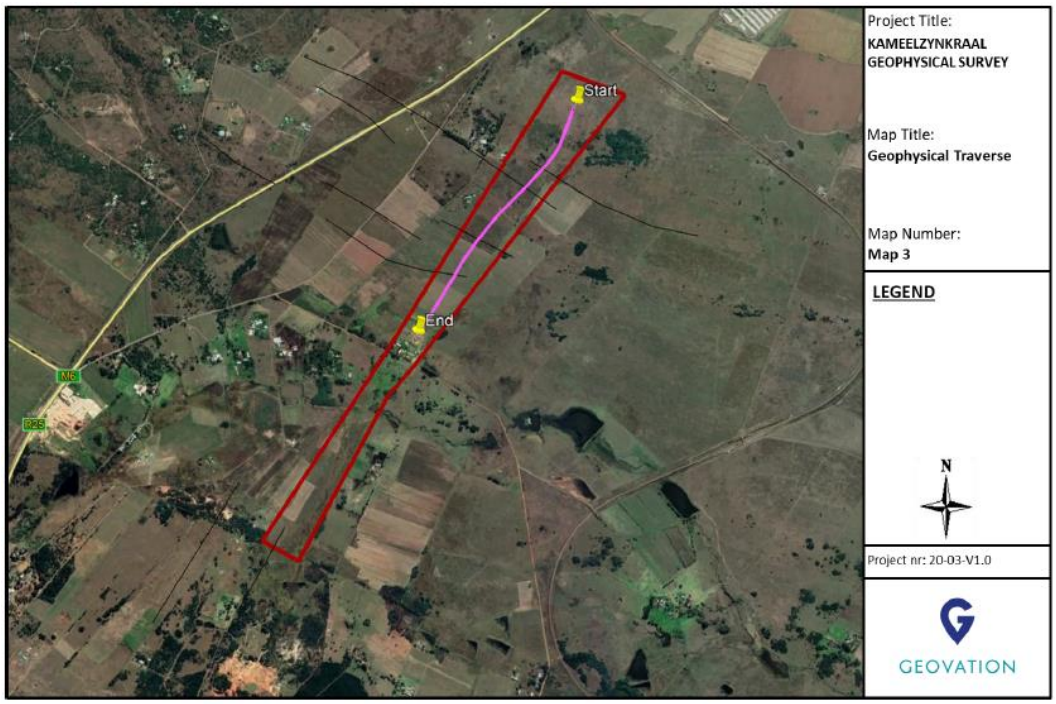

Figure 4.85: Geophysical survey line, Kameelzynkraal (Geovation, 2020).

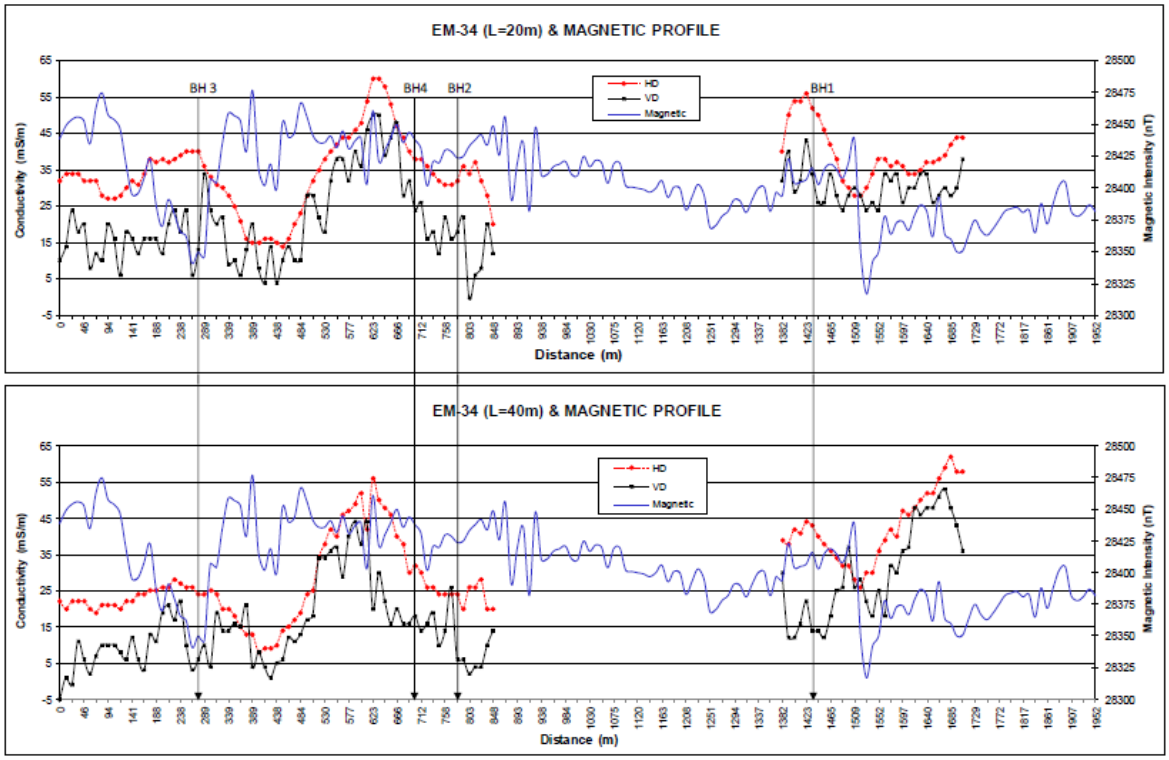

Figure 4.86: Conductivity and Magnetic Profile (Geovation, 2020).

Figure 4.87: Proposed drilling targets (Geovation, 2020).

4.7.2 Case study 2: Groundwater Exploration at Motswedi and Borakalo

The consultant conducted groundwater exploration near the villages of Motswedi and Borakolo in the North West province for the Metsi Bophelo Borehole Project. A ground geophysical survey was undertaken to site boreholes as part of the project (Aurecon, 2012f). The site is underlain by the Magaliesberg Formation orthoquartzites, shales, hornfels slate and minor dolomites from the Silverton Formation and diabase (Aurecon, 2012f). On a regional scale, several NW-SE striking faults occur. Upper beds are fractured, and lower beds are intergranular and fractured aquifers. Groundwater is associated with brecciated, shear or joint zones related to faults or the contacts of diabase sills with the country rock.

The electromagnetic (Geonics EM34 ground conductivity meter) and the magnetic (proton magnetometer) methods were used to conduct the survey. Intercoil spacing was 20 m and 40 m station spacing. Figure 4.88 shows the survey lines and newly drilled boreholes. The geophysical survey yielded no significant target anomalies. Thus, boreholes were drilled next to damaged or destroyed boreholes with usable historic yields (Aurecon, 2012f). Figure 4.89 and Figure 4.90 show results for two lines, BTR1 and GT1, respectively. The influence of cultural noise can be clearly seen on the GT1 profile.

Figure 4.88: Geophysical traverses and newly drilled boreholes: Motswedi and Borakolo (Aurecon, 2012f).

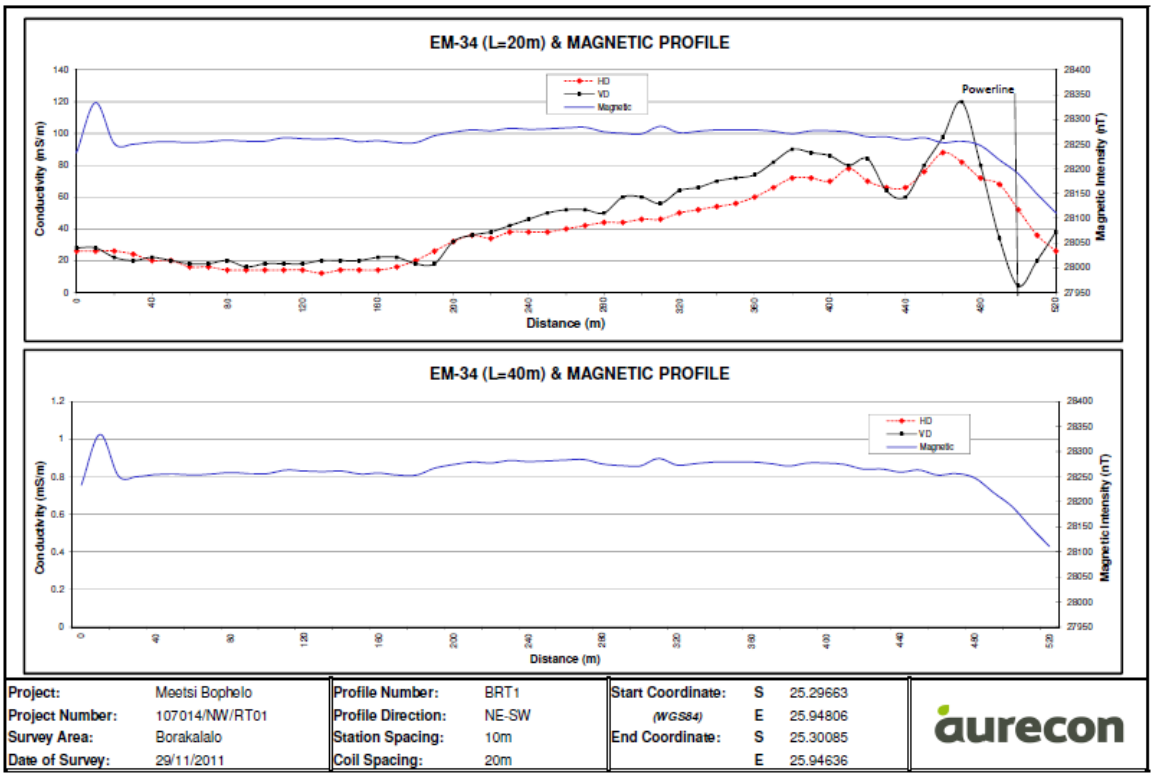

Figure 4.89: BRT1 EM34 and magnetic profile (Aurecon, 2012f).

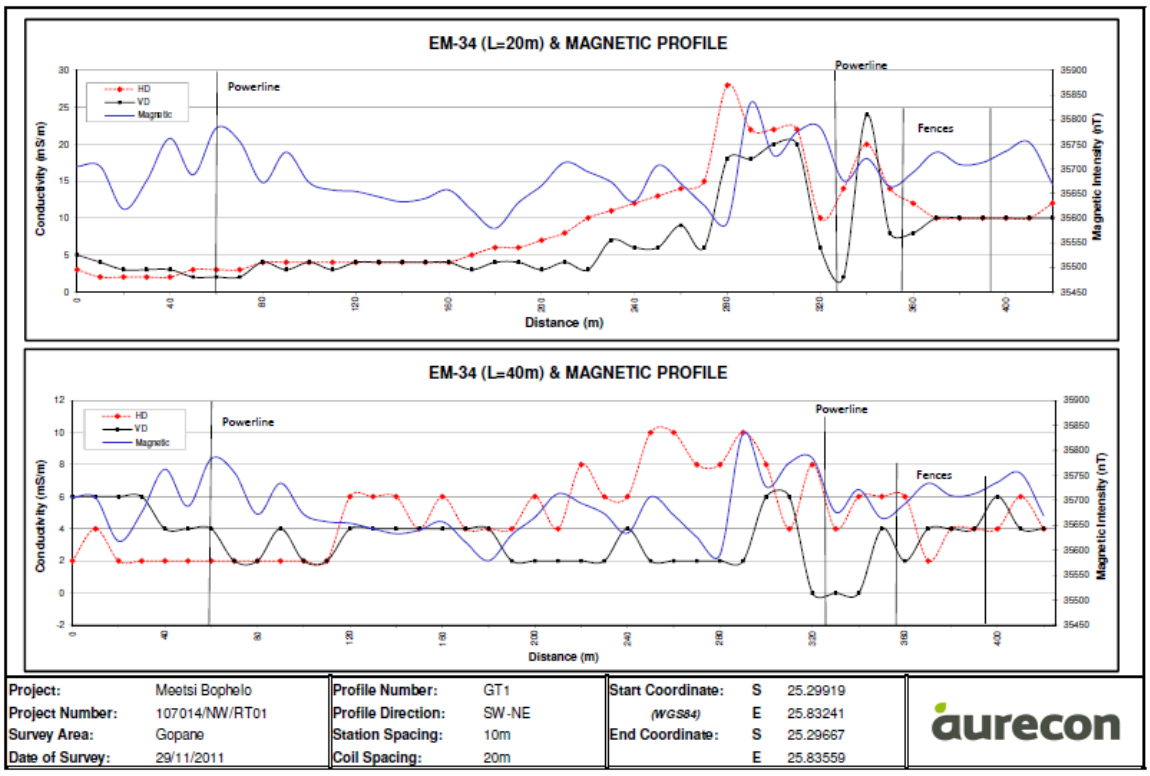

Figure 4.90: GT1 EM34 and magnetic profile (Aurecon, 2012f).

4.7.3 Case study 3: Borehole siting at Kameelboom

A ground geophysical survey was conducted to site boreholes near Kameelboon, North West, as part of the Metsi Bophelo Borehole Project. The area is underlain by undifferentiated surface deposits, Magaliesberg Formation quartzites and minor hornfels. RLS norites outcrops toward the southeast of the site. A NNW-SSE string syenite dykes are present in the area. Faults, shear zones and intrusive dykes are preferred for groundwater occurrence (Aurecon, 2012g).

The magnetic and electromagnetic methods were used for the project- a proton magnetometer and the Geonics EM34 ground conductivity meter, respectively. Four traverses were conducted in March 2012 with an intercoil spacing of 40 m and 10 m station spacing. Four target anomalies were identified for four potential boreholes which corresponded with possible syenite dykes. Figure 4.91 shows the traverses and prospective borehole locations, while Figure 4.92 shows results for KT4, and Figure 4.93 shows those of KT2. Potential boreholes were named in order of priority.

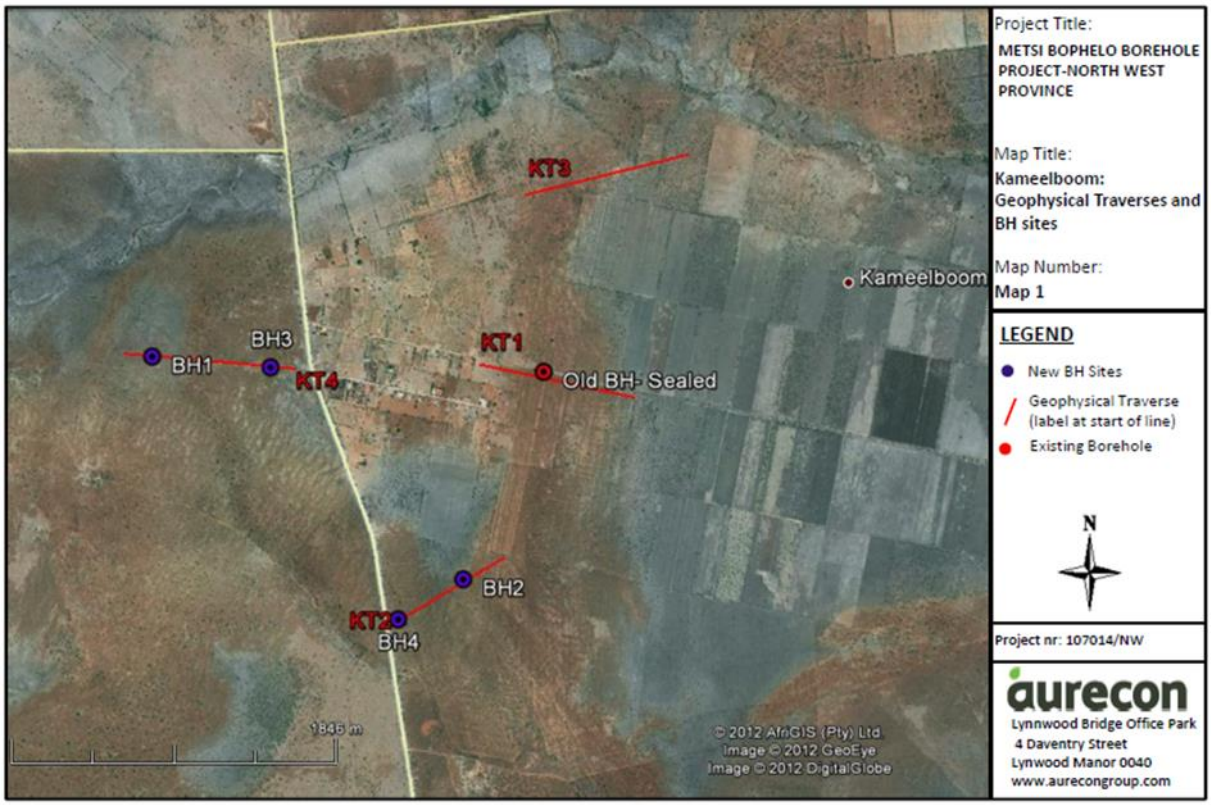

Figure 4.91: Geophysical traverses and borehole locations for Kameelboom (Aurecon, 2012g).

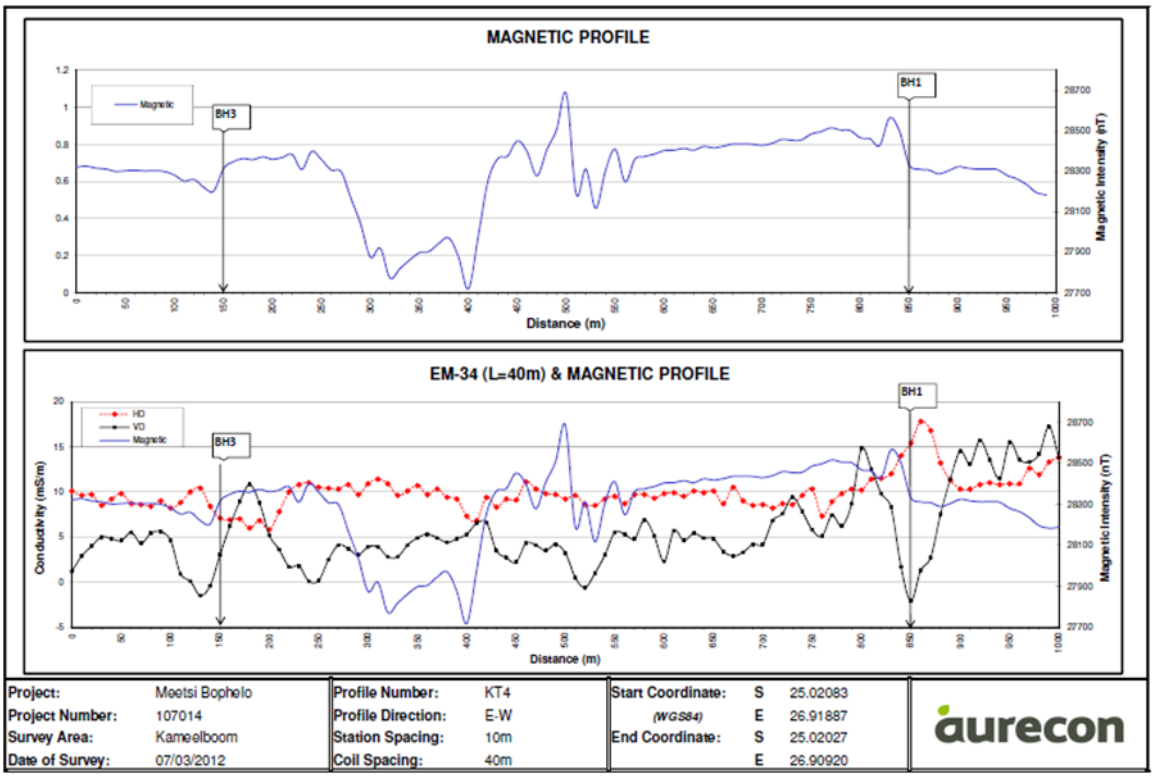

Figure 4.92: EM34 and Magnetic profile for line KT4 (Aurecon, 2012g).

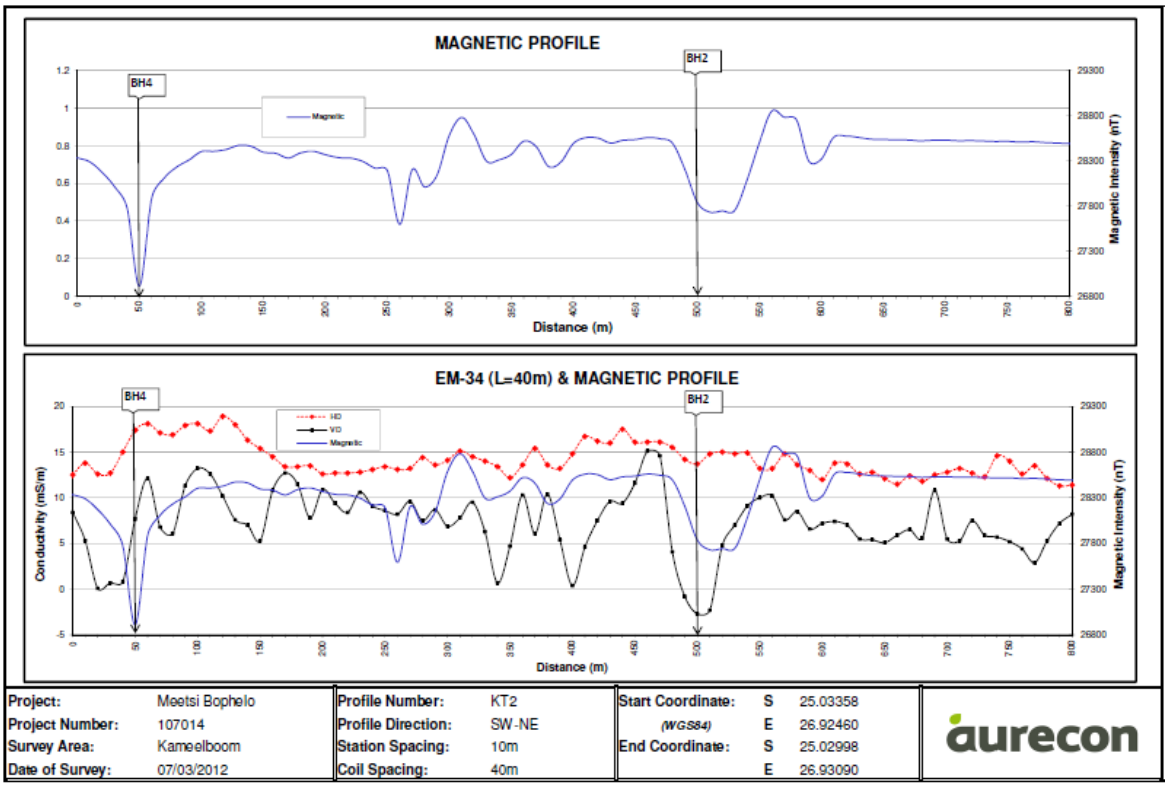

Figure 4.93: EM34 and Magnetic profile for line KT2 (Aurecon, 2012g).

4.7.4 Case study 4: Groundwater Exploration at Silwerkrans

Groundwater exploration was conducted in conjunction with the TCTA as part of the Metsi Bophelo Borehole Project (Aurecon, 2012h). The area is underlain by undifferentiated surface deposits and quartzites of the Daspoort Formation and Strubenkop Formation shales and slate. Regionally, NW-SE striking faults are present. Groundwater occurrence is associated with faults and related shear zones. Upper and lower contacts of intrusive dolerite sills with shale and quartzite horizons also favour groundwater occurrence. Upper beds are classified as intergranular and fractured, while lower beds are classified as fractured aquifers (Aurecon, 2012h).

A proton magnetometer and the Geonics EM34 were used to conduct the survey. Intercoil spacing was 20m, while station spacing was 10m with three survey lines. No significant anomalies were detected. Therefore, boreholes were drilled next to 3 damaged existing boreholes. The location of the boreholes and the geophysical traverses are shown in Figure 4.94. Figure 4.95 shows line SKT1 modelled results (Aurecon, 2012h).

Figure 4.94: Geophysical traverses and newly drilled boreholes: Silwerkrans (Aurecon, 2012h).

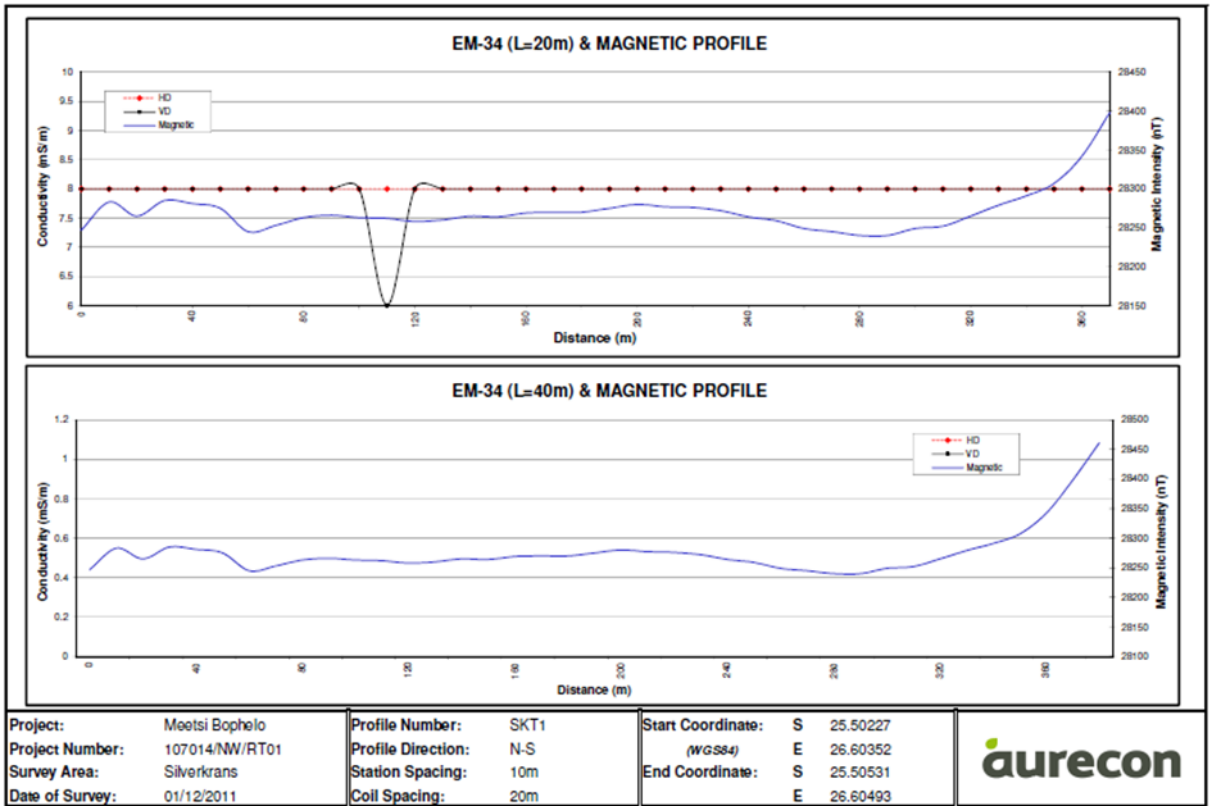

Figure 4.95: Line SKT1 EM34 and Magnetic profile (Aurecon, 2012h).

4.8 GROUNDWATER EXPLORATION IN THE VENTERSDORP SUPERGROUP

Groundwater exploration in areas underlain by rocks proper to the Ventersdorp Supergroup are scarce. This section summarises geophysical exploration for the region.

4.8.1 Case study 1: Ottosdal Bulk water supply Phase 2-Groundwater exploration

The consultant was appointed to conduct a groundwater exploration program as part of the Ottosdal Bulk water supply phase 2 for the town of Ottosdal in the North West province. An extra 120 L/s was required on Waagkraal 374 and 20 L/s on Witpoort 281, and exploration had a special focus on these farms (Aurecon, 2014b). The study area was ~80 km south of Litchenburg NW Province. Several lithological units underlie the area, the majority of which are andesitic, porphyritic and basaltic Ventersdorp Supergroup and Dominion Group lavas (Aurecon, 2014b). Ferruginous shale, BIFs quartzites and hornfels of the Hospital Hill formation are also present. The igneous lithologies overlie the sedimentary rock. The aquifer in this region is classified in part as a fractured aquifer and partly as an intergranular and fractured aquifer.

A geophysical survey was conducted as part of the project to site boreholes. Aeromagnetic data available for the Ottosdal region, collected at a flight line spacing of 200 m, were first reviewed, and total magnetic field data overlain on a topographic map of the area (Aurecon, 2014b). Priority areas for the ground geophysical survey were identified from this aeromagnetic data. Only areas where access was denied or where there would be infrastructural interference were excluded from the initial targets (Aurecon, 2014b). Figure 4.96 shows the proposed survey lines.

The initial traverses were conducted using the magnetic method (Geotron G5 proton magnetometer) and the electromagnetic (Geonics EM34-3) method at a station spacing of 10 m and 20 m intercoil spacing (Aurecon, 2014b). When deemed necessary, a follow-up was conducted using the EM34-3 at 40 m intercoil spacing. Resistivity imaging using the ABEM Lund Terrameter was also conducted, although no data for this survey were provided in the report. A total of 11 survey lines were made, 30 targets identified, and 13 boreholes drilled. Figure 4.97 shows the conductivity from the EM34-3 and the magnetic field intensity across Line A. The horizontal dipole and vertical dipole for the EM survey were both adopted, and the intercoil spacing of 40 m for this line was used at 0-400 m and 900-600 m (Aurecon, 2014b). Line F EM34 in Figure 4.98, however, did not require the use of the 40 m intercoil spacing. Borehole targets for both lines A and F (and other traverses) coincide with anomalies in the data. Borehole targets are indicated by arrows within the profiles. Figure 4.99 shows the location of boreholes drilled in this phase of the Ottosdal bulk water supply project (Aurecon, 2014b).

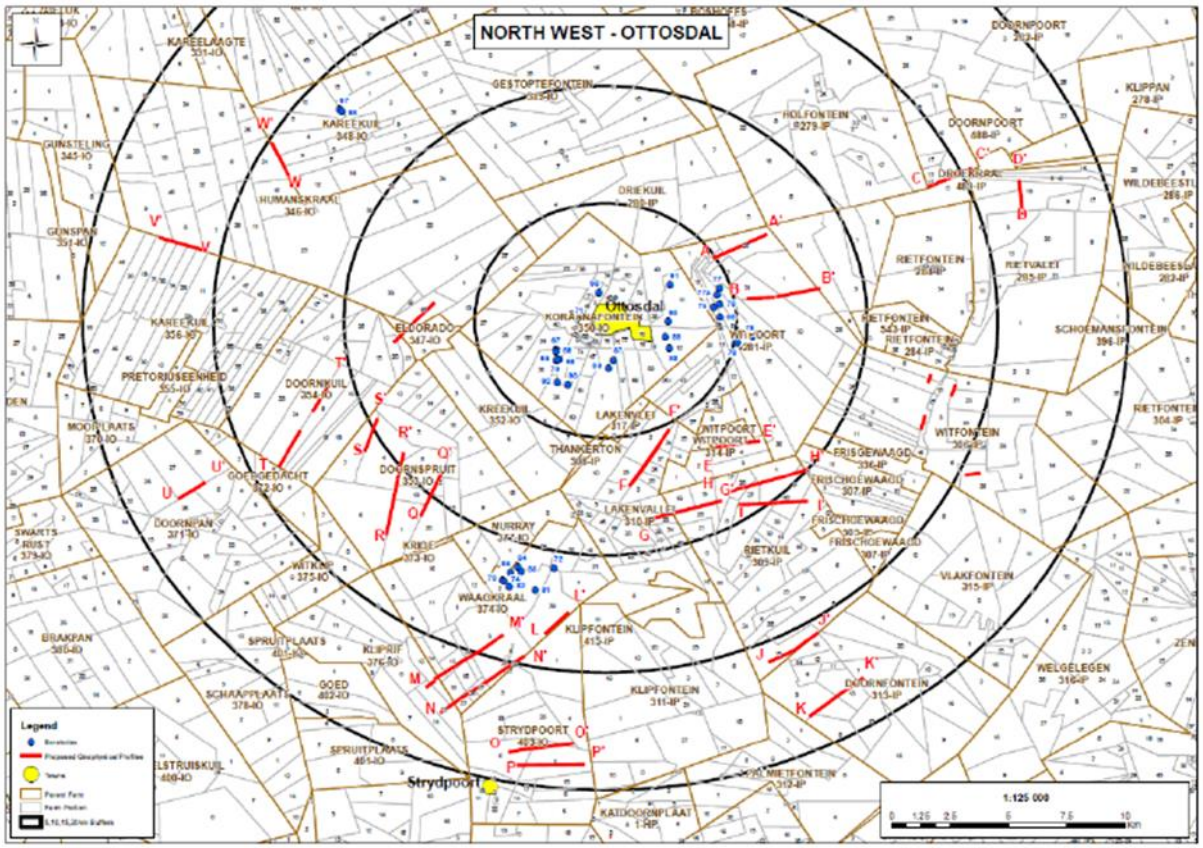

Figure 4.96: Proposed geophysical traverses (Aurecon, 2014b).

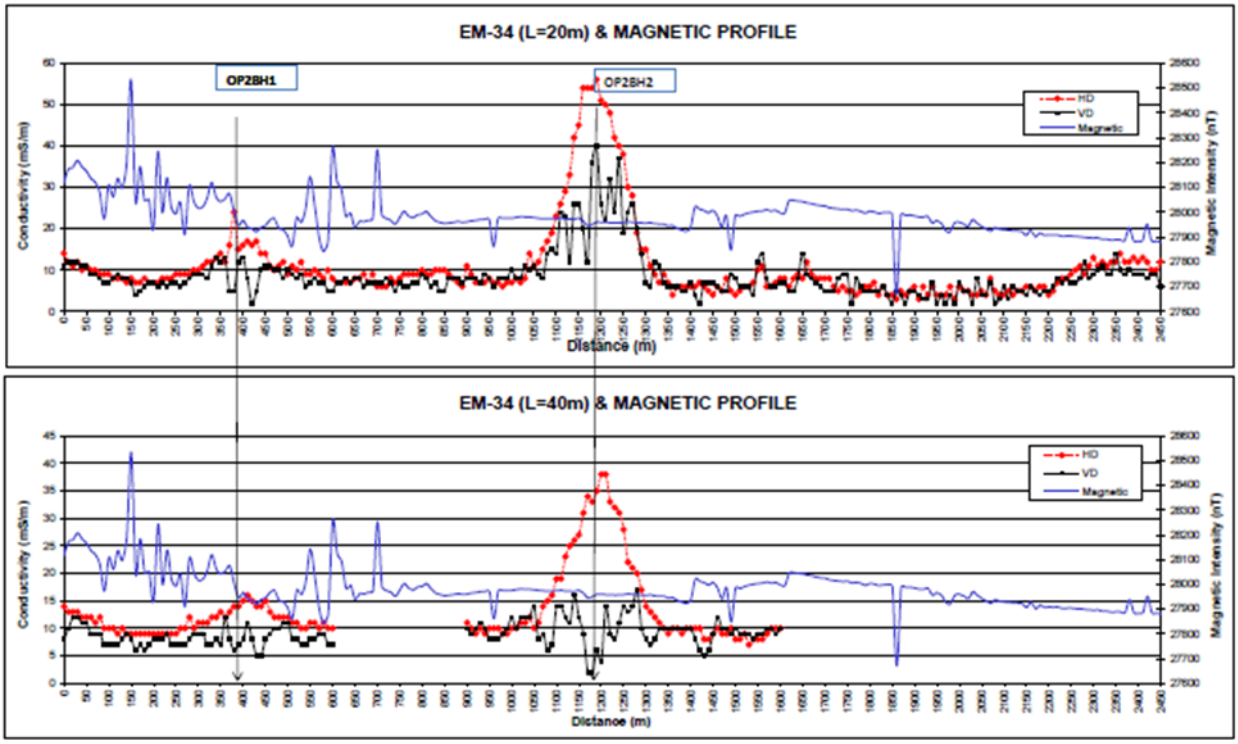

Figure 4.97: Conductivity and magnetic profile on Line A (Aurecon, 2014b).

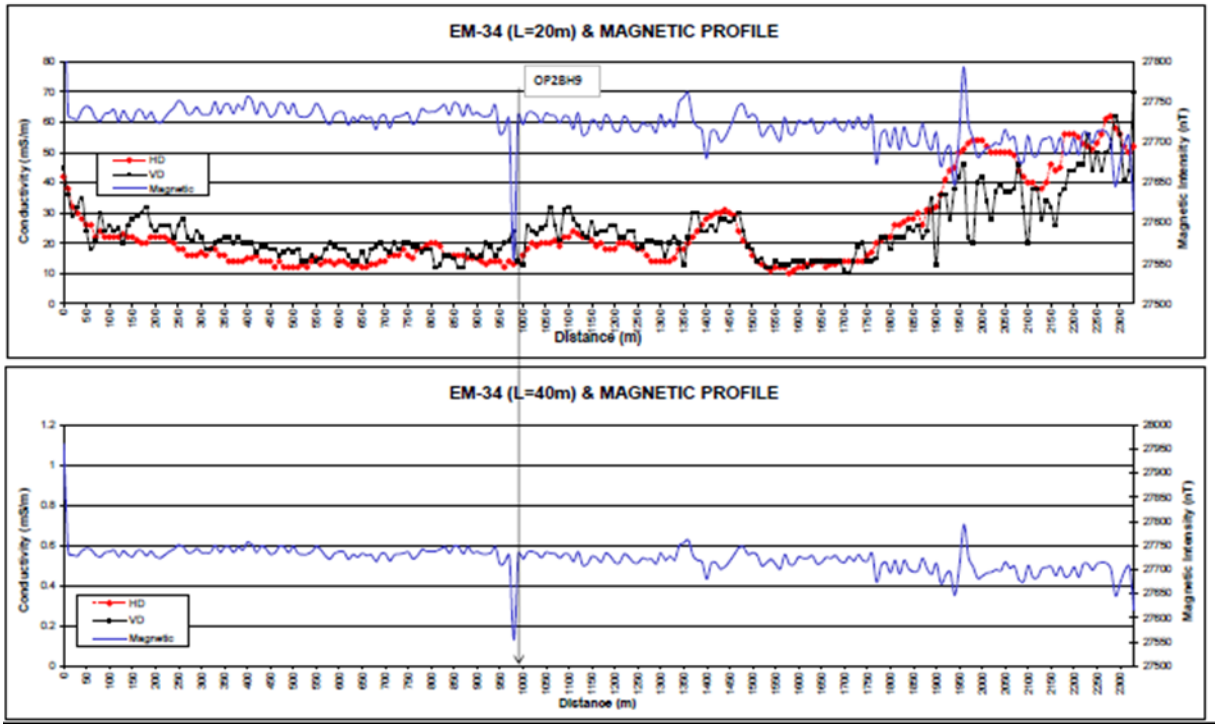

Figure 4.98: Conductivity and magnetic profile on Line F (Aurecon, 2014b).

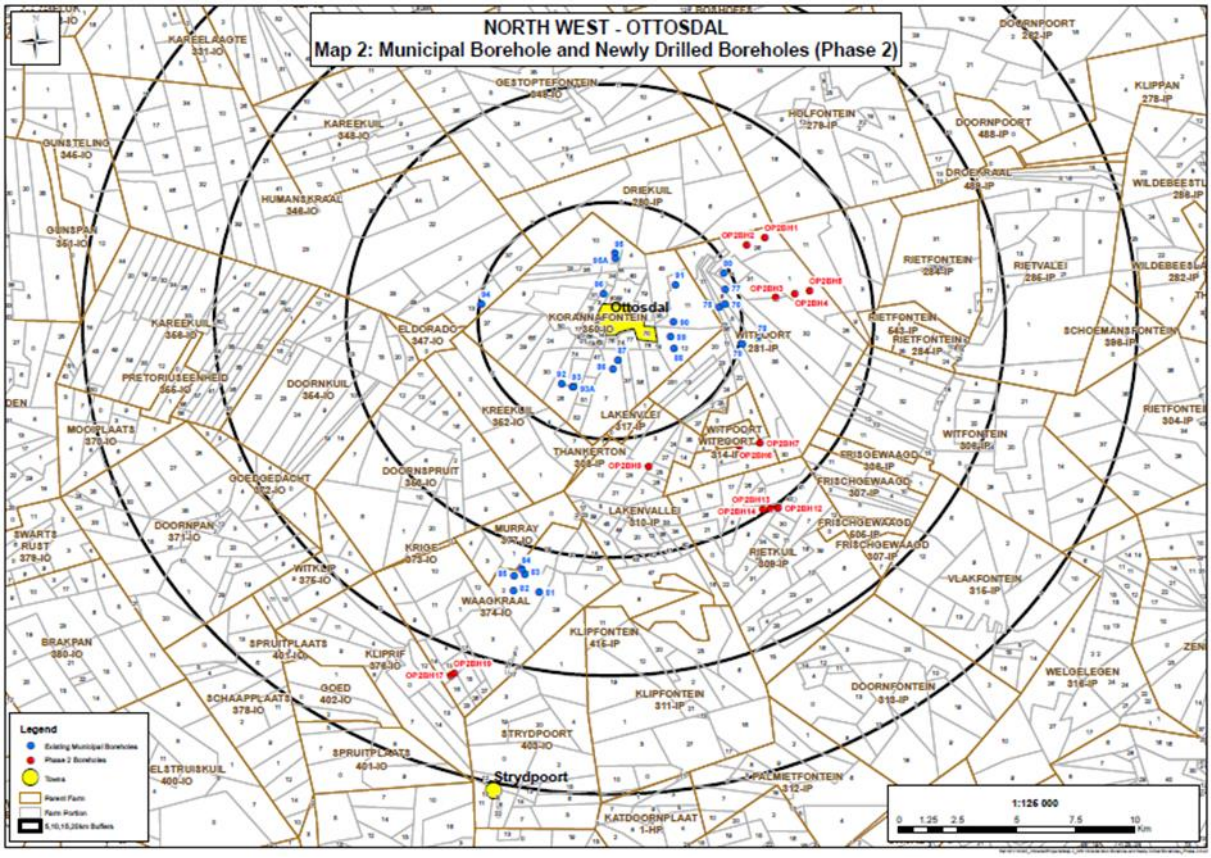

Figure 4.99: Existing municipal boreholes and newly drilled boreholes (Aurecon, 2014b).

4.9 GROUNDWATER EXPLORATION IN THE WITWATERSRAND SUPERGROUP

No unpublished case studies relating to the use of geophysics for groundwater exploration could be obtained at the time this study was conducted. This may be because of the unique nature of the areas underlain by this succession. According to Durrand (2012), the Witwatersrand pre-1886 was a farming community until the discovery of gold in the region. The extensive mining in the regions underlain by the assemblage saw a proliferation of several communities and urban centres on the Witwatersrand basin. Groundwater was a reliable source of water for the initial population that lived in the area. However, the rapid growth of the mining industry came with adverse effects, such as contamination of the groundwater in the region by mine and industrial effluent as well as sewage. The Witwatersrand is also overlain by the karst aquifers of the younger Transvaal that hold large volumes of water. This caused a need to pump millions of litres of water out of the mining voids which over time had consequences of ingress into the mine void and surface subsidence due to dewatering. The mining activities and the possible contamination of water thereof are likely deterrents to groundwater exploration in the area.

4.10 GROUNDWATER EXPLORATION IN THE BARBERTON SEQUENCE

Unfortunately, no case unpublished reports of geophysical groundwater exploration in the Barberton Sequence could be found during this research project. The Barberton (like the Witwatersrand) has been affected by mining, and so water quality concerns exist in the area. The Makhonjwa mountains in Barberton, which comprise 40% of the Barberton Greenstone Belt, are a UNESCO World Heritage Site (UNESCO, 2023). This status means the area is of special administration, which could hinder free exploration and exploitation of aquifers in the area.

4.11 GROUNDWATER EXPLORATION IN THE KALAHARI GROUP

Groundwater is a major source of freshwater in arid regions such as the Kalahari. In this section groundwater exploration conducted in the Kalahari Group is summarised.

4.11.1 Case study 1: Groundwater Exploration for the Madibogo water supply upgrade

The consultant was appointed to conduct groundwater exploration for the Madibogo groundwater supply upgrade. The area is mainly overlain by the sands of the Gordonia formation of the Kalahari Group. Banded iron formations, schists, dolomite, rhyolite and amphibolite are present east of

Madibogo. To the west and southwest, outcrops of undifferentiated Kraaipan Group greenstones are present (Aurecon, 2011, 2012i).

This study area falls on the fractured and intergranular and fractured aquifer types (van Dyk, 2000). Aeromagnetic data for the area were acquired, and priority areas for geophysical exploration were identified, which corresponded with lineaments observed in the aeromagnetic maps. The geophysical survey was conducted using the magnetic (Geotron G5 proton magnetometer), electromagnetic (Geonics EM34) and resistivity (ABEM Lund Terrameter) methods (Aurecon, 2011, 2012i). The station spacing used was 10 m, and a 20 m/40 m intercoil spacing for the EM34. In the first phase, seven traverses were conducted, from which ten boreholes were drilled, seven being successful (Aurecon, 2011). In the second, 18 survey lines were conducted with 25 boreholes drilled, 10 of which were successful (Aurecon, 2011, 2012i).

The aeromagnetic maps with geophysical exploration targets for the first and second phases of the project are shown in Figure 4.100 and Figure 4.101, with survey directions perpendicular to the strike of the chosen structures.

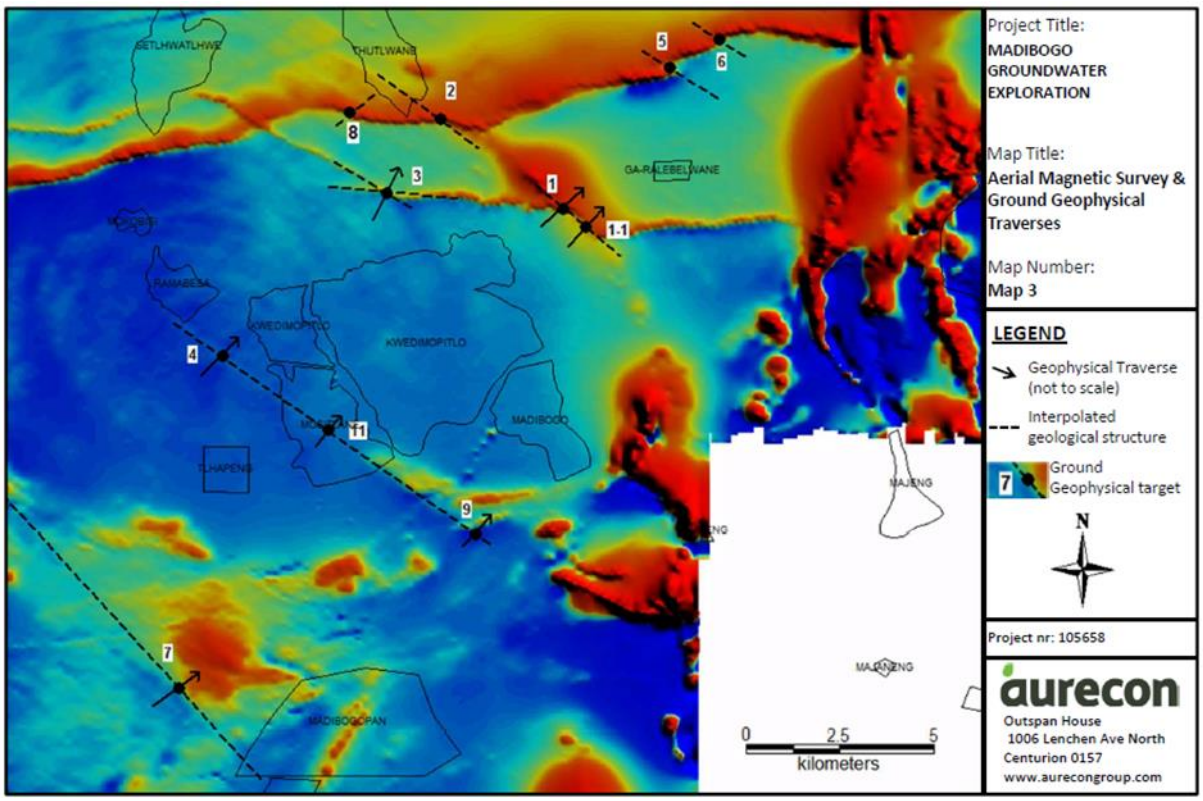

Figure 4.100: Phase 1 aerial magnetic survey and ground geophysical lines (Aurecon, 2011).

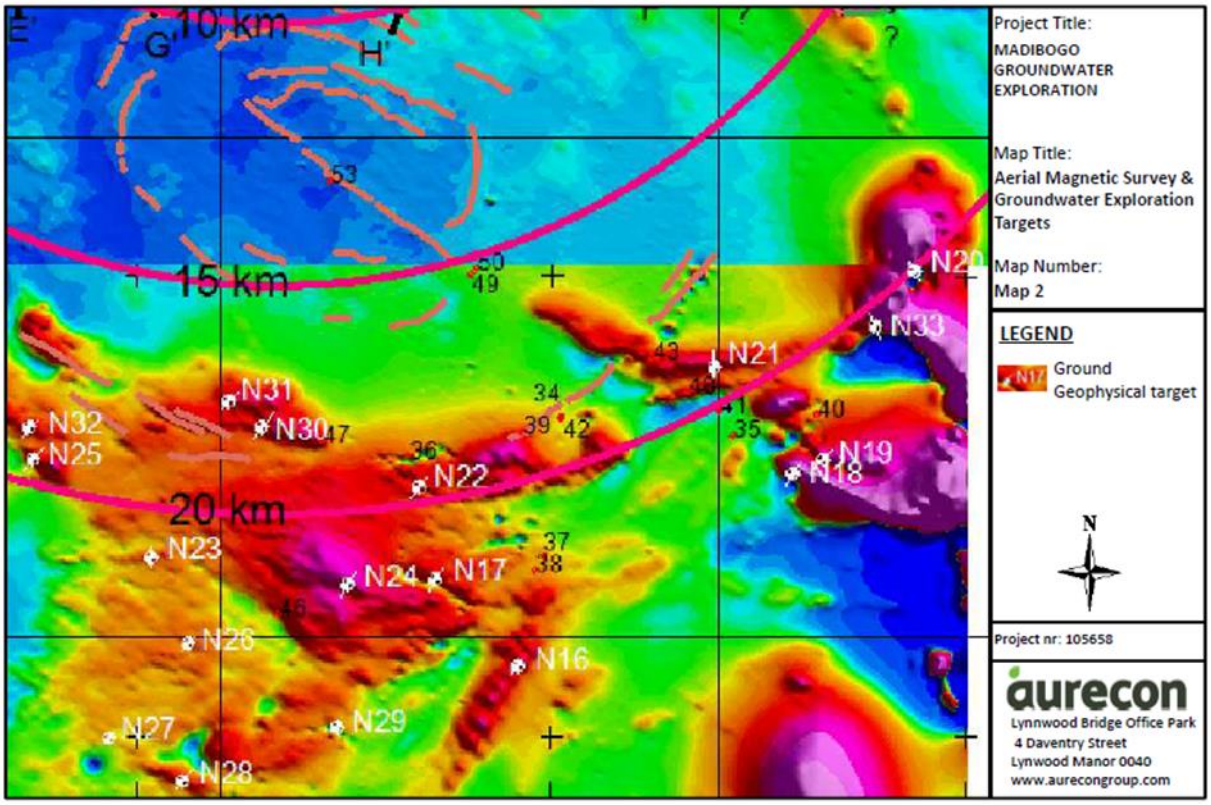

Figure 4.101: Phase 2 aerial magnetic survey and exploration targets (Aurecon, 2012i).

The conductivity and magnetic profiles from Phase 1 are shown in Figure 4.102 and Figure 4.103. In the second phase, additional resistivity surveys were conducted, which is reflected in Figure 4.104 and Figure 4.105. In both sets of results, drilling target positions are shown by arrows (Aurecon, 2011, 2012i). The newly drilled, and existing boreholes are shown on Figure 4.106.

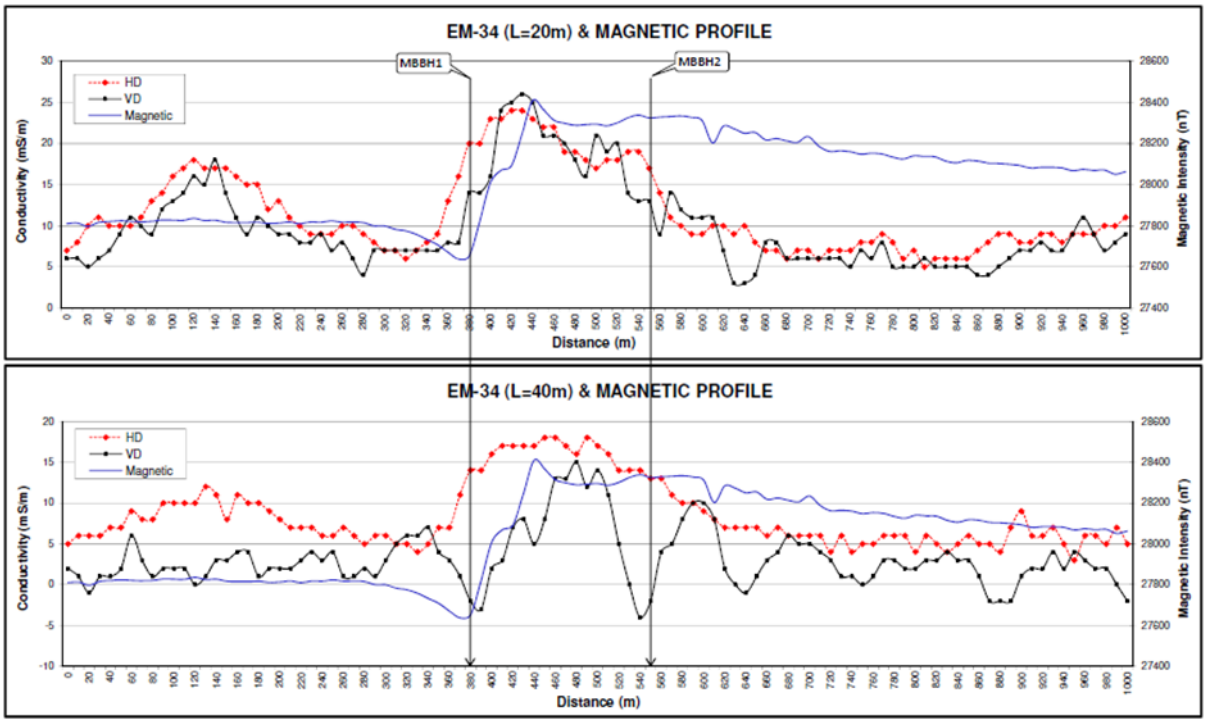

Figure 4.102: Phase 1 Line T1 (Aurecon, 2011).

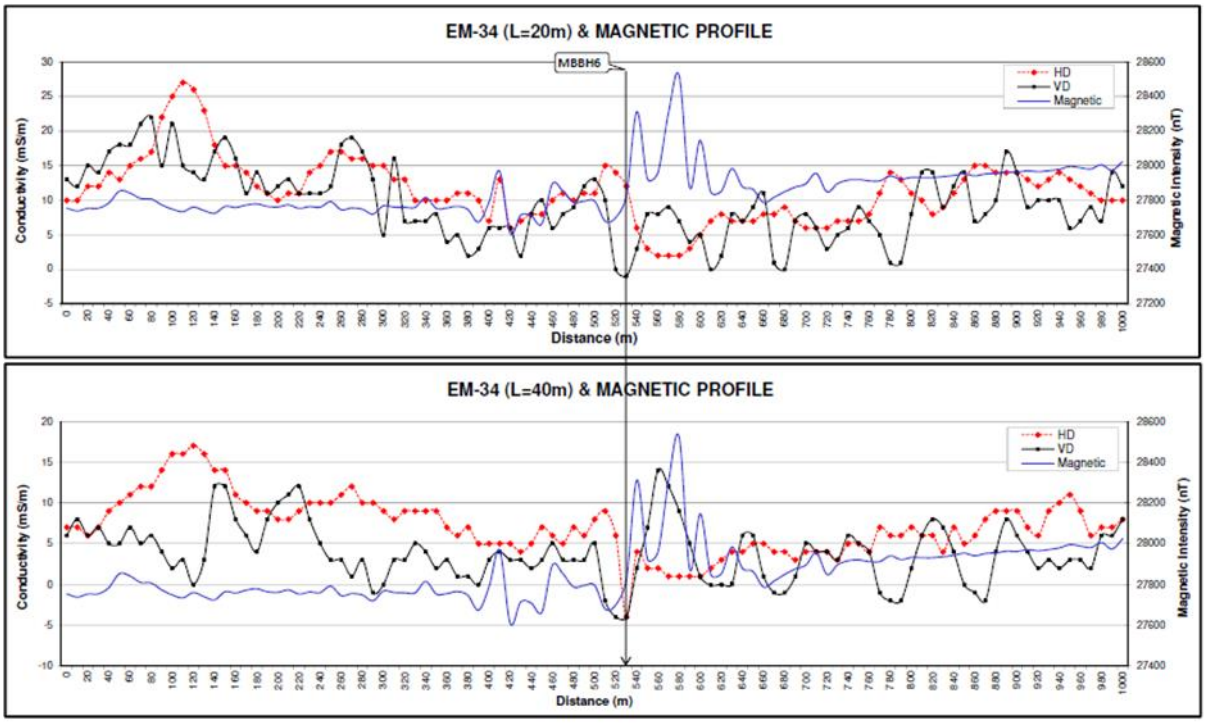

Figure 4.103: Phase 1 Line T7 (Aurecon, 2011).

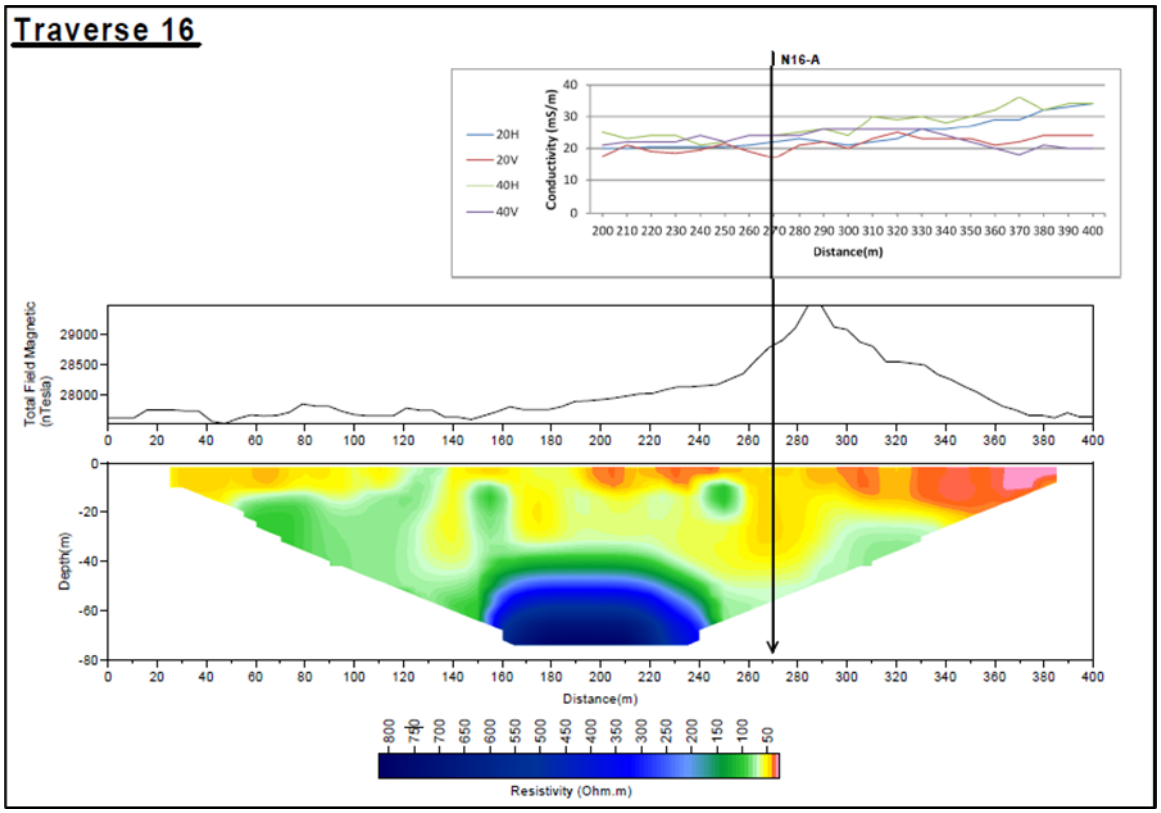

Figure 4.104: Phase 2 Traverse 16 (Aurecon, 2012i).

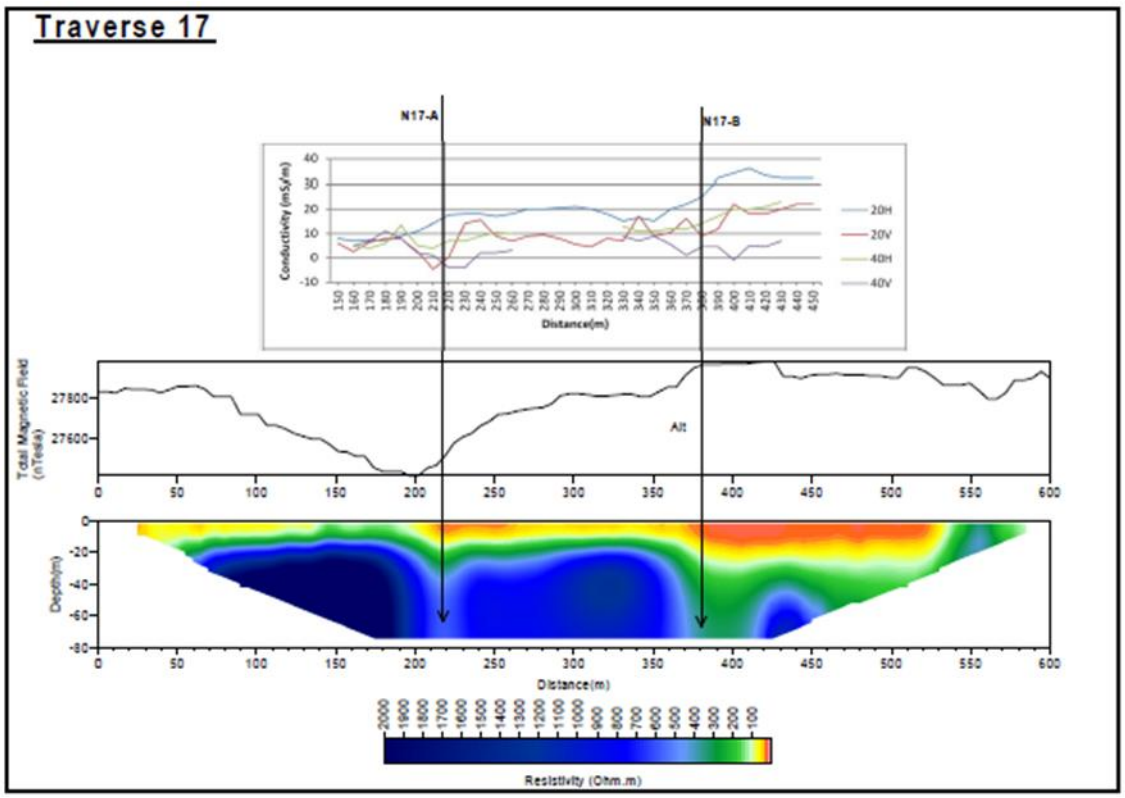

Figure 4.105: Phase 2 Traverse 17 (Aurecon, 2012i).

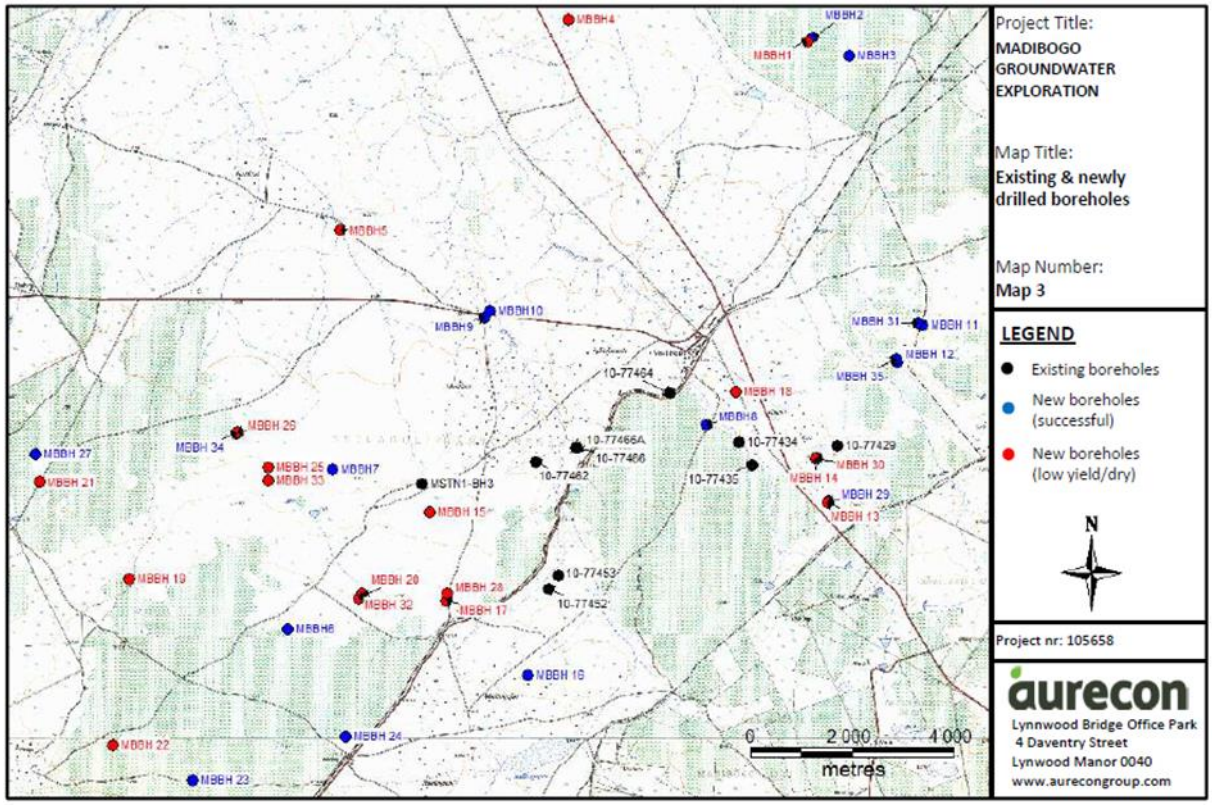

Figure 4.106: Phase 1 and 2 newly drilled and existing boreholes (Aurecon, 2012i).

4.11.2 Case study 2: Groundwater Exploration at Setlagole

The consultant was contracted to perform groundwater exploration for the village of Setlagole in the North West. The majority of the study area is underlain by aeolian sands of the Gordonia Formation,

with some outcrops of the Kraaipan Group granites, migmatite schist and amphibolite. The aquifer is, however, classified as an intergranular and fractured and fractured aquifer (Aurecon, 2012j).

A geophysical survey was conducted as part of the project to site boreholes. Priority geophysical targets were chosen from high-resolution aeromagnetic data for the area. Then, a ground geophysical survey was conducted using magnetic, electromagnetic and resistivity methods. The tools used were the Geotron G5 proton magnetometer, the Geonics EM-34 and the ABEM Lund terrameter for each survey method (Aurecon, 2012j).

Eight geophysical traverses were initially chosen, but the consultant added eight more with the extension of the project. At the end of the survey, 32 potential drilling targets were identified, while 30 boreholes were drilled. These were drilled on identified anomalies or next to damaged or destroyed boreholes with usable historical yield. Of the thirty drilled boreholes, 15 were successful and pump tested (Aurecon, 2012j). Figure 4.107 shows the ground geophysical survey lines; a small red dot shows the location of Setlagole. A 10 m station spacing was used, and for the EM survey, an intercoil spacing of 20 m and 40 m was used with the vertical and horizontal dipole orientation.

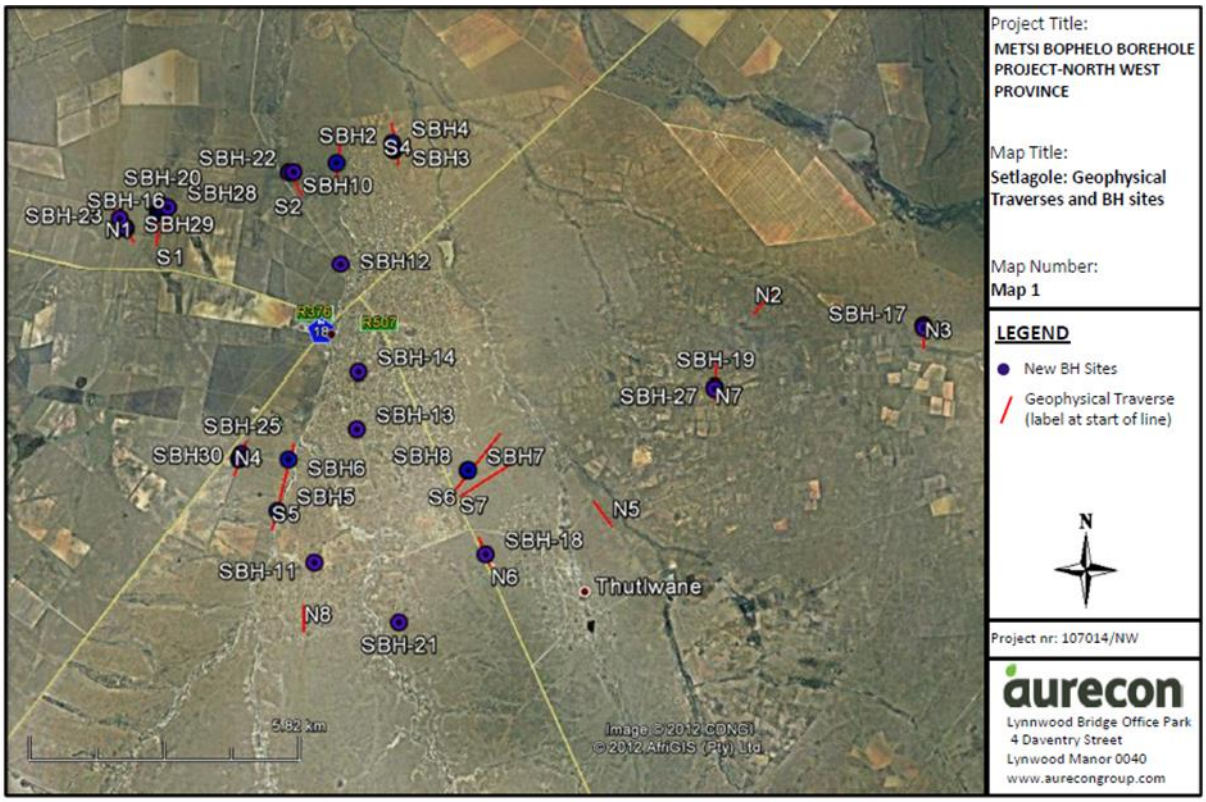

Figure 4.107: Geophysical traverses and borehole locations (Aurecon, 2012j).

Figure 4.108 shows the modelled results for line S6. For this traverse EM survey, only the 40 m intercoil spacing was used, and one borehole was sited. Traverse T7 results are shown in Figure 4.109, and two potential borehole targets were identified from this traverse, as shown by the arrows

(Aurecon, 2012j). These correspond to anomalies in the profiles and changes in resistivity seen in the resistivity model.

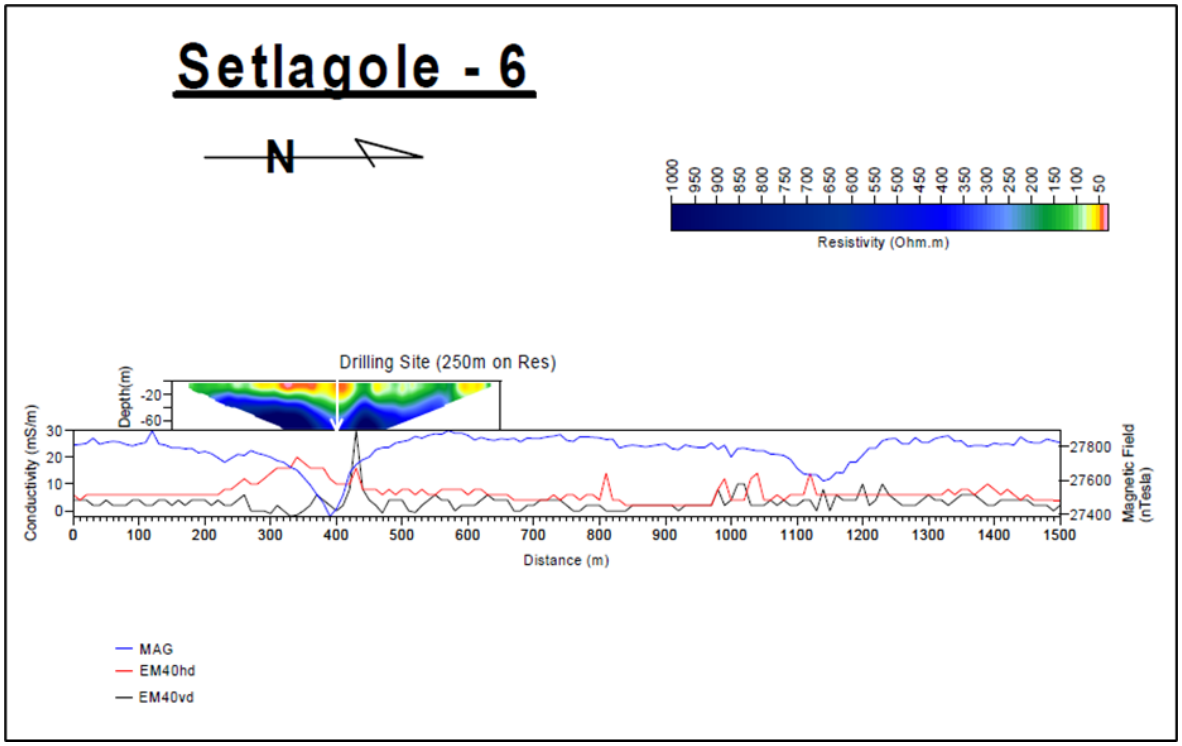

Figure 4.108: Line S6 modelled resistivity section, conductivity and magnetic profile (Aurecon, 2012j).

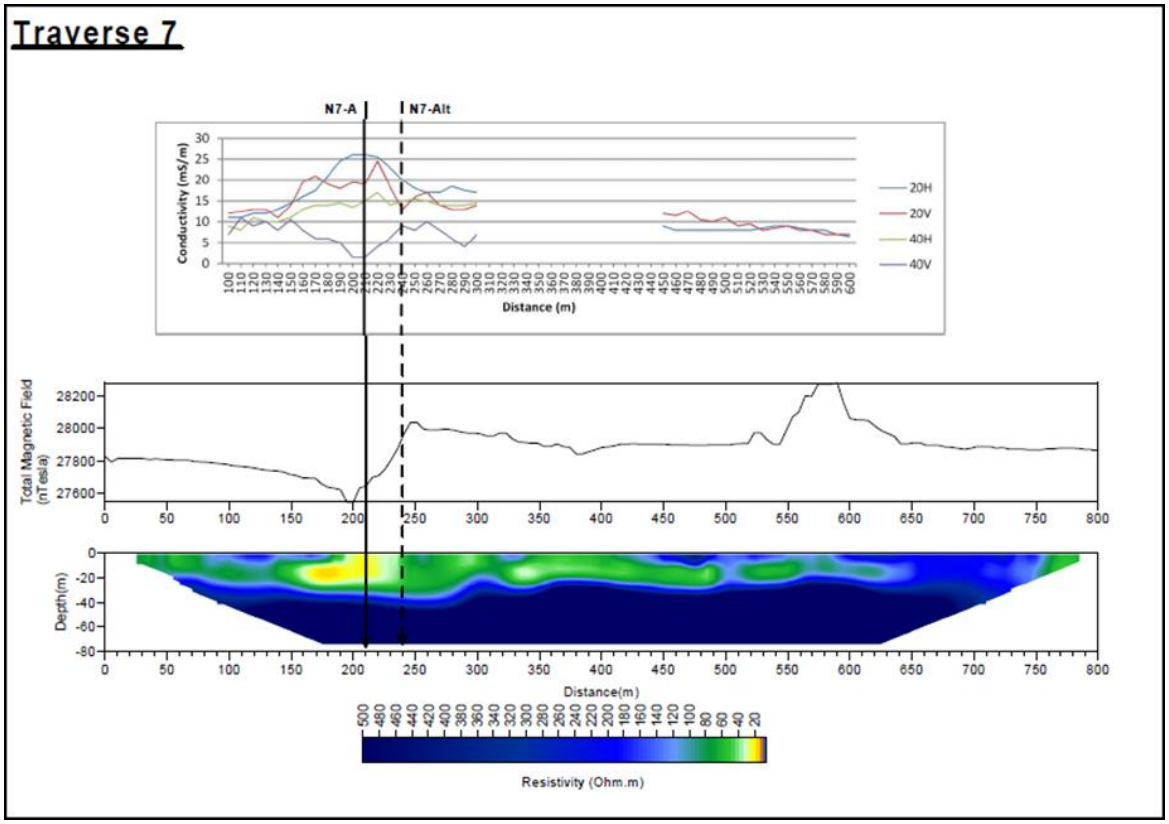

Figure 4.109: Line T7 modelled resistivity section, conductivity and magnetic profile (Aurecon, 2012j).

4.11.3 Case study 3: Groundwater Exploration at Ditloung

Boreholes were sited at Ditloung village in the North West province as part of the Metsi Bophelo Borehole Project (Aurecon, 2012k). The area is underlain by aeolian sands of the Kalahari, banded ironstone, schist, gneiss, granite, banded chert and jaspilite from the Kraaipan Group. Groundwater occurs in faults and associated shear zones. The area falls on an intergranular and fractured aquifer.

Magnetic and electromagnetic techniques were used to conduct the survey with a station spacing of 10 m with an intercoil spacing of 20 m. However, problems with accessibility at the anomaly locations led to the boreholes being drilled close to pre-existing boreholes (Aurecon, 2012k). The geophysical traverse and the borehole locations are shown in Figure 4.110, while Figure 4.111 shows the electromagnetic conductivity and magnetic intensity along line DT1.

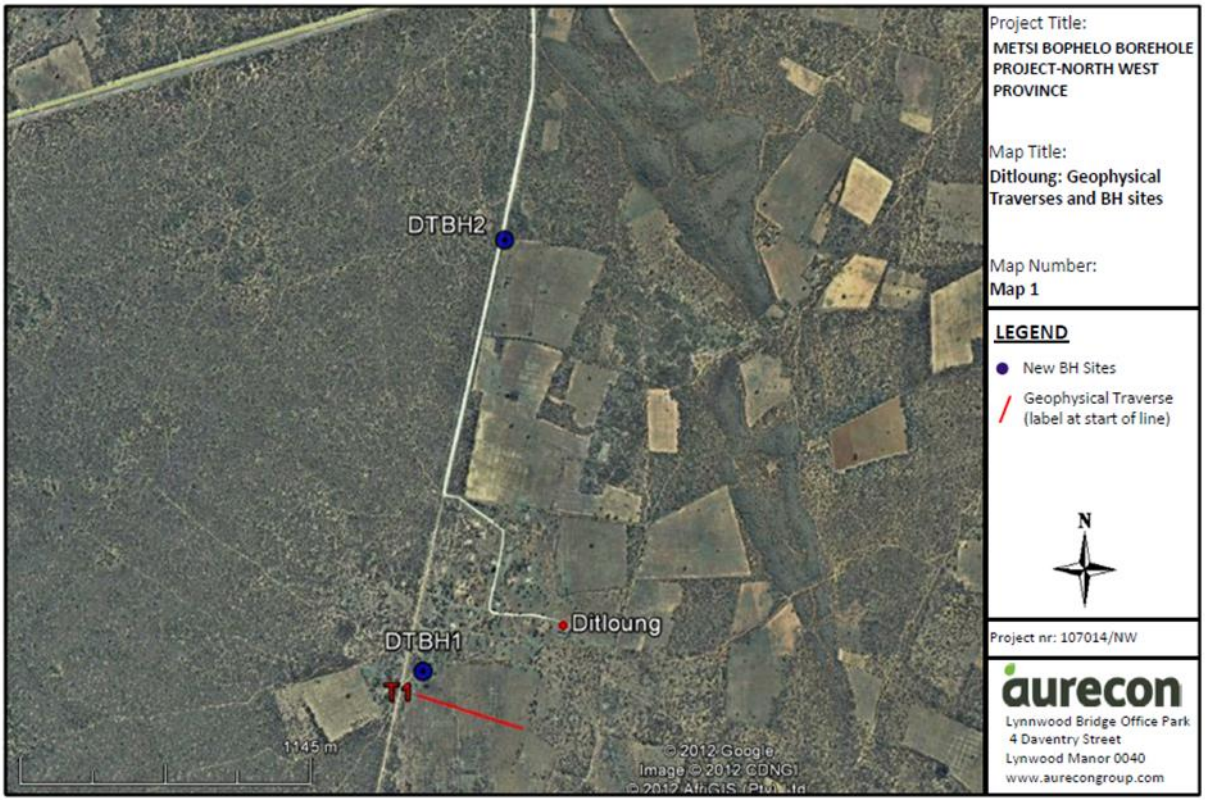

Figure 4.110: Geophysical traverses and borehole sites at Ditloung (Aurecon, 2012k).

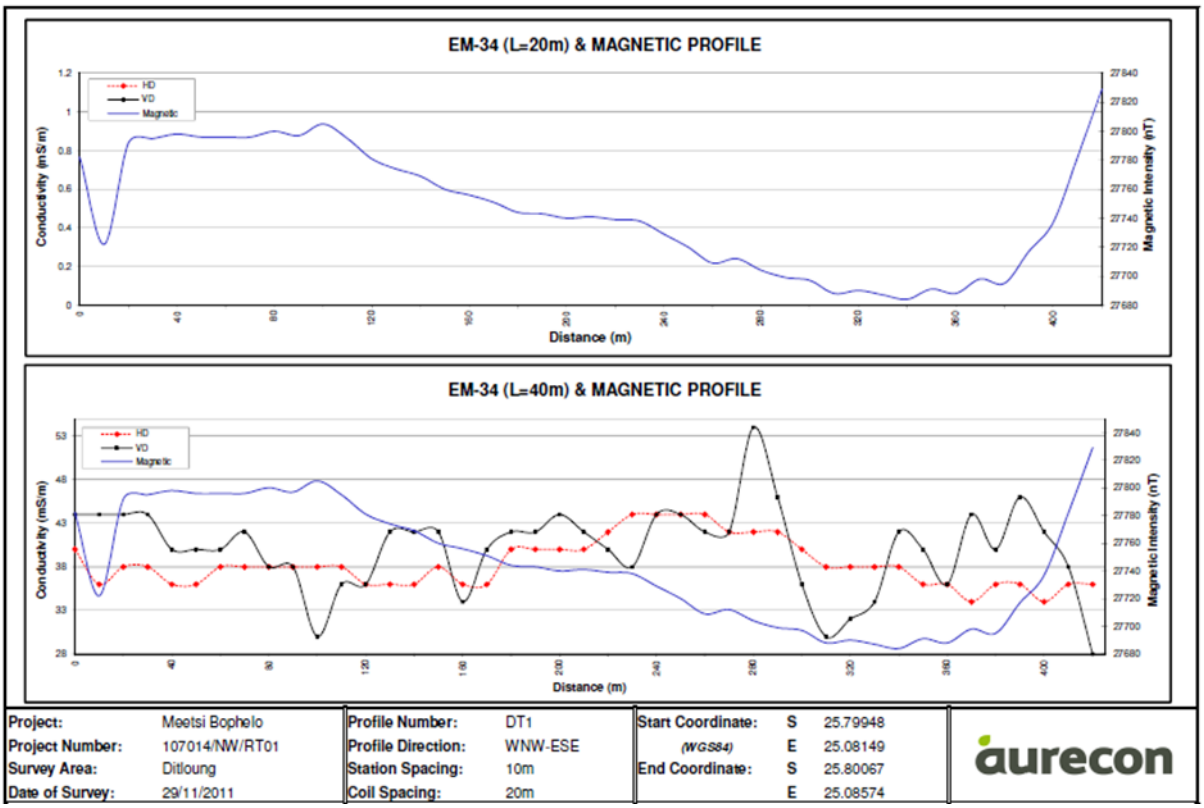

Figure 4.111: Line DT1 EM34 and Magnetic profile (Aurecon, 2012k).

4.11.4 Case study 4: Groundwater Exploration at Logageng

Groundwater exploration was conducted in the vicinity of Logageng in the North West province as part of the Metsi Bophelo Borehole Project. The area is underlain by the Gordonia formation sands, siliceous sandstones, pebble conglomerate, gritstone, and silcrete of the Kalahari Group. A river in the area exposed variegated jaspilite and chert and basic lava with interbedded banded ironstone, pillow lava, rhyolite and the greenschist of the Kraaipan Group. Tertiary age calcretes are common. The aquifer is classified as a fractured aquifer (Aurecon, 2012l).

A combination of the magnetic (proton magnetometer), resistivity (ABEM Lund Terrameter) and electromagnetic (Geonics EM34) methods was used for this project. The area has a thick sand cover, so it was recommended that DC resistivity and the Controlled Source Audio Magnetotellurics (Geometrics Stratagem) be used for future exploration. Eight boreholes were drilled, five of which were based on identified geophysical anomalies and the remainder were sited near existing vandalised boreholes. Three were successful. Figure 4.112 shows the location of the boreholes and traverses.

Figure 4.113 shows the modelled resistivity across traverses 2, 4, 7, and 9, with the conductivity and Magnetic profile across traverse 9 also shown. Borehole locations are indicated by arrows in the image. Borehole 9 was one of the successful boreholes (Aurecon, 2012l).

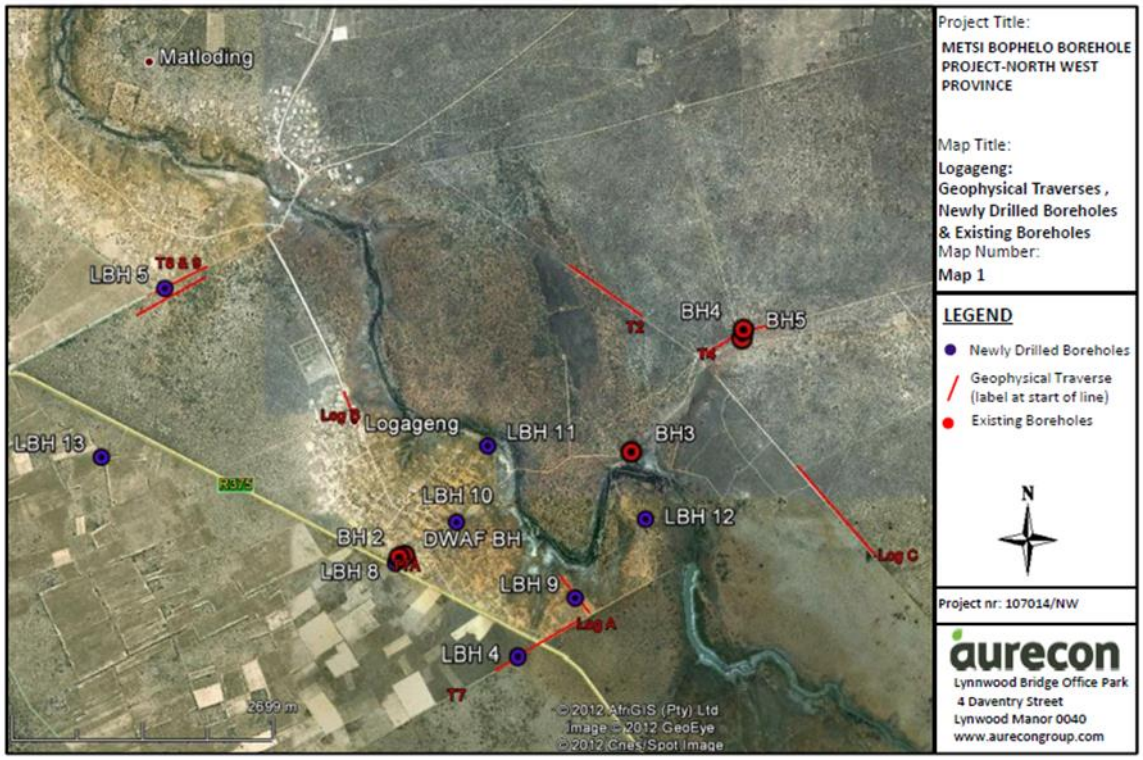

Figure 4.112: Geophysical traverses, new and preexisting boreholes for Logageng (Aurecon, 2012l).

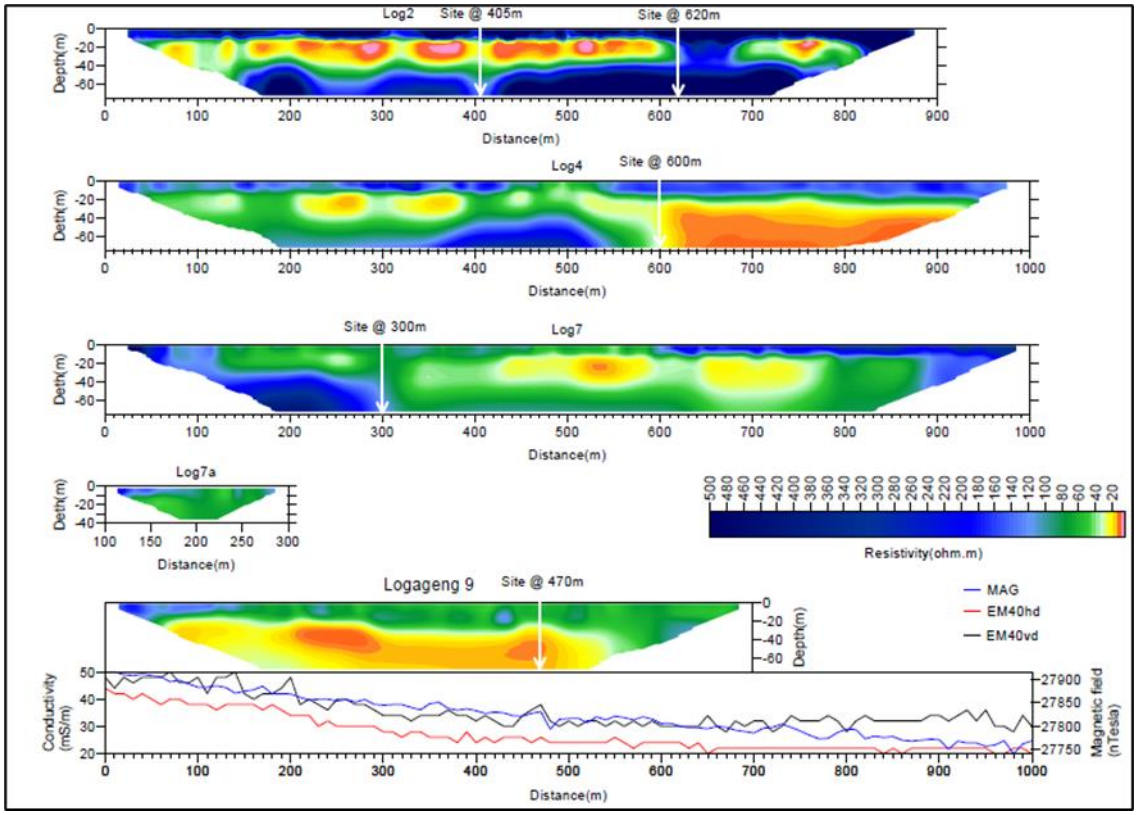

Figure 4.113: Modelled resistivity sections for lines 2, 4, 7, and 9. Conductivity and magnetic intensity across line 9 are also shown (Aurecon, 2012l).

4.12 DISCUSSION

It can be seen that the majority of case studies used more than one method of exploration, with methods being chosen depending on the availability of equipment and the environment in which the exploration was conducted. Structures that were typically targeted were weathered zones, fault and fracture zones, contacts between different lithologies, and dolerite dykes. These are typically regions with increased permeability and can influence the groundwater flow regime.

Aeromagnetic data was also used to determine features of interest in the form of lineaments (typically elongated regions of higher magnetic intensity) to plan the ground geophysical survey traverses and was used in this manner throughout all the specified geological regions. During the ground geophysical surveys, it is noted that the frequency domain electromagnetic (EM34) and magnetic methods were often used together and presented on the same profiles. The EM is able to detect narrow conductive structures such as faults, and weathered dykes are also conductive and can be seen in the EM data by anomalous changes in conductivity. The presence of magnetic bodies such as dolerite dykes is also seen as changes in the magnetic intensity as either positive or negative anomalies. These are then interpreted based on the local geology and structures to determine the features with higher groundwater potential that may produce the observed response.

Resistivity methods are able to determine the subsurface resistivity distribution. Vertical electrical sounding was used to show the vertical changes in resistivity. Curve matching techniques are then used for data interpretation to determine the best fit for the observed apparent resistivity data and to create a model of the resistivity of the ground. Lower resistivities may indicate areas with higher groundwater potential. However, most studies which employed resistivity used 2D ERT to give a model of the subsurface resistivity. This model clearly shows the changes in resistivity in the lateral and vertical directions and can clearly delineate weathered zones and faults. Weathered zones can be seen as areas of lower resistivity in the modelled sections, while faults or intrusive features can be seen as regions of contrasting resistivities juxtaposed against each other, which can inform groundwater exploration.

The resistivity method has a shortcoming in that different layer boundaries may not be clearly delineated. The resistivity, EM, and magnetic methods were used in all eight regions where case studies were conducted. This is because faults, fractures, weathered zones, and dolerite intrusions occur throughout the country. The few studies which used the seismic method (in areas underlain by the Kalahari Group, Cape and Transvaal Supergroups) were able to give a very clear image of the structure of the subsurface by showing the positions of faults, their orientation and depth of the weathered zone. These were also areas which had a thick cover of sand. In areas where cavities caused by dolomite dissolution exist (such as areas underlain by the Transvaal), the gravity method was

particularly useful. These cavities may be seen on residual gravity maps as areas with local gravity deficits. The unconventional methods were used in case studies conducted in the areas underlain by the NNMP, Karoo and Cape Supergroup. Potential difference pseudosections were then observed, and targets were chosen where there seemed to be a change in potential difference.

Twenty-nine unpublished consultant reports and 20 published papers were available to the author at the time this study was conducted. One published report (see Sami *et al.* 2002a; 2002b) was divided into four case studies because it was a very large project. Therefore, in these 51 case studies, geophysical methods were used 107 times. This figure does not include the number of times a single study used the method (traverses) but reflects the total number of times different methods appear in all the South African cases covered in this project. Figure 4.114 shows a bar chart representing the number of times the different geophysical methods were used for groundwater exploration.

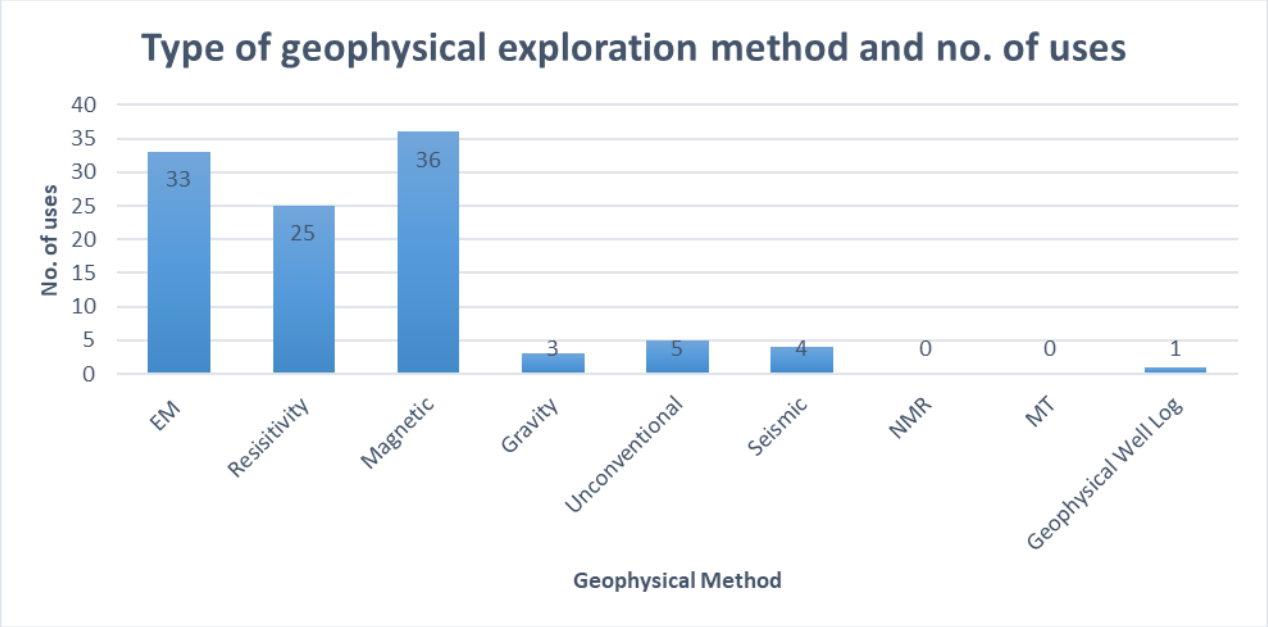

Figure 4.114: Comparison of number of uses for different geophysical methods

The magnetic method had the highest use, occurring 36 times, followed by the electromagnetic and resistivity methods, which appeared 33 and 25 times, respectively. This is also in line with the occurrence of the geophysical methods for groundwater exploration seen in the international case studies. These three methods have the longest history of use in the country, with the earliest paper reviewed here by Enslin (1955) detailing their use. Seeing that about 2/3 of South Africa's area is intruded by dykes, it is no wonder that majority of the papers included some form of magnetic exploration in their methodology. The frequency-domain electromagnetic EM34, proton precession magnetometer and the ABEM resistivity equipment were used most often (Figure 4.115). In the available pool of papers, magnetotelluric methods and magnetic resonance sounding were not encountered. Unconventional methods using "water detectors" were used five times. The case studies

also demonstrated that an understanding of local geology is necessary for the correct interpretation of obtained geophysical data.

Figure 4.115 A) ABEM Terrameter LS 2 set B) Geotron G5 Proton Memory Magnetometer C) Geonics EM34-3. Modified from (Guideline Geo, n.d; ASEG, n.d; Geomartix Earth Science Ltd, 2023)

CHAPTER 5:
CONCLUSIONS AND RECOMMENDATIONS

Although geophysical groundwater exploration has been used in South Africa for over 60 years, it is not well documented, and there is a dearth of written material relating to the subject in the country. From the literature, it can be seen that geophysical methods are numerous and are chosen based on a variety of factors such as the local geology and structural features as well as anthropogenic influences. In South Africa, groundwater occurrence is often associated with fractured and fault zones, weathering basins, contacts between different lithologies, and dolerite dykes and sills. These imply that the most appropriate (and readily accessible) geophysical methods for groundwater exploration in South Africa are the resistivity, electromagnetic and magnetic methods. It was found that these methods are by far the most commonly applied methods during groundwater prospecting in the country.

Resistivity is able to delineate weathering basins, which appear as regions of low resistivity in resistivity models generated from 2D ERT surveys. Magnetic methods can detect dolerite dykes, which appear in magnetic intensity profiles as spikes. Electromagnetic methods can detect thin conductive 2D structures such as faults as dips or peaks in conductivity profiles or as regions of higher conductivity in conductivity maps. These conditions occur in almost all the geological regions taken into consideration in this study, which is likely why these methods were the most preferred. Some areas, such as the Kalahari have high contact resistance, which can interfere with the efficacy of resistivity methods. Seismic methods were used in such areas to give detailed models of the subsurface from depth-velocity or depth-time sections. In areas such as the Transvaal, water-bearing cavities from dolomite dissolution were detected as regions with lower gravitational acceleration. The study also showed an increasing number of studies using new and unconventional methods for their exploration, which proponents prefer due to their ease of use and affordability.

Although geophysical groundwater prospecting is used in South Africa, the quality and detailing of reporting are variable. Some studies show detailed reports with sound methodologies, while others are unclear and can be described as anomaly hunting. It is recommended that the importance of relating geophysical data interpretation to the local geology during groundwater prospecting be emphasised. There is a wide range of methods available internationally, and more research must be conducted on their applicability in the country in the context of groundwater exploration. In particular, methods based on Nuclear Magnetic Resonance, which can detect water directly, must be adopted more often. The Transient Electromagnetic Method is also neglected as opposed to its counterpart, the Frequency Domain Electromagnetic Method. Its use can be expanded as it is suitable for deep investigations and can help in the selection of exploration targets in conductive regions.

Finally, the repository of geophysical survey reporting in groundwater exploration is very scant. Therefore, scholarly research must be conducted on geophysical groundwater exploration to build the body of knowledge relating to this subject. In this way, future researchers can numerically determine the "success" of each kind of method in the context of South Africa. This "success" which is often subjective must be predefined so that a guideline of which methods are most appropriate in which regions can be created.

REFERENCES

Abdel Zaher, M., Younis, A., Shaaban, H. and Mohamaden, M.I. 2021. Integration of geophysical methods for groundwater exploration : A case study of El Sheikh Marzouq area, Farafra Oasis, Egypt. The Egyptian Journal of Aquatic Research. 47:239–244. DOI: 10.1016/j.ejar.2021.03.001.

Abiye, T.A., Mengistu, H. and Demlie, M.B. 2011. Groundwater Resource in the Crystalline Rocks of the Johannesburg Area, South Africa. Journal of Water Resource and Protection. 3. DOI: 10.4236/jwarp.2011.34026.

Adesola, G.O., Gwavava, O. and Liu, K. 2023. Hydrological Evaluation of the Groundwater Potential in the Fractured Karoo Aquifer Using Magnetic and Electrical Resistivity Methods: Case Study of the Balfour Formation, Alice, South Africa. International Journal of Geophysics. 1–18. DOI: 10.1155/2023/1891759.

African Groundwater (Pty) Ltd. 2022. Siting of Borehole at Haza Primary School No. (2.2)5421. Pietermaritzburg. Available: https://www.dws.gov.za/ghreport/Home/View.aspx?Id=11224.

African Groundwater (Pty) Ltd. 2022. Geohydrological Report for Senzakahle Secondary School GH4372. Available: https://www.dws.gov.za/ghreport/Home/View.aspx?Id=11228.

Agangi, A., Hofmann, A., Eickmann, B. and Marin-Carbonne, J. 2019. Mesoarchaean Gold Mineralisation in the Barberton Greenstone Belt: A Review. In The Archaean Geology of the Kaapvaal Craton, Southern Africa. A. Kroner and A. Hofmann, Eds. Springer, Cham. 171–184. DOI: 10.1007/978-3-319-78652-0_7.

Agyemang, V.O. 2022. Groundwater Exploration by Magnetotelluric Method Within The Birimian Rocks of Mankessim, Ghana. Applied Water Science. 12(3):1–6. DOI: 10.1007/s13201-022-01576-9.

Aidu Energy Technology. 2023. ADMT 300SX. Available: http://www.aiduny.com/detail/503.html [2023, July 05].

Alexander, M. 2018. South Africa's Weather And Climate | South Africa Gateway. Available: https://southafrica-info.com/land/south-africa-weather-climate/ [2021, December 24].

Anhaeusser, C.R. 2014. Archaean Greenstone Belts And Associated Granitic Rocks - A review. Journal of African Earth Sciences. 100:684–732. DOI: 10.1016/j.jafrearsci.2014.07.019.

Anomohanran, O., Ofomola, M.O. and Okocha, F.O. 2017. Investigation Of Groundwater In Parts Of Ndokwa District In Nigeria Using Geophysical Logging And Electrical Resistivity Methods: Implications For Groundwater Exploration. Journal of African Earth Sciences. 129:108–116. DOI: 10.1016/j.jafrearsci.2016.12.008.

Anomohanran, O., Isioma, J., Ruth, O., Emekeme, E.I. and Oviri, M. 2021. Determination Of Groundwater Potential And Aquifer Hydraulic Characteristics In Agbor, Nigeria, Using Geo-Electric, Geophysical Well Logging And Pumping Test Techniques. Modeling Earth Systems and Environment. 7(3):1639–1649. DOI: 10.1007/s40808-020-00888-6.

ASEG. n.d. Geotron Model G5 Proton Memory Magnetometer. Available: https://www.aseg.org.au/sites/default/files/Geotron_G5_magnetometer.pdf [2023, November 17].

Arefayne, S.H. and Abdi, S. 2016. Groundwater Exploration for Water Well Site Locations Using Geophysical Survey Methods. Hydrology Current Research. 07(01):1–7. DOI: 10.4172/2157-7587.1000226.

Aurecon. 2011. Groundwater Exploration for The Madibogo Water Supply Upgrade 105658-V1.0-2011.

Aurecon. 2012a. Borehole Siting at Legkraal Doc No. 107014-LK-2012.

Aurecon. 2012b. Groundwater Exploration for the Mabeleleng Water Supply Upgrade Doc No. 106773-MAB-2012.

Aurecon. 2012c. Groundwater exploration for the Makgope Water Supply Upgrade Doc No. 106773-MAK-2012.

Aurecon. 2012d. Groundwater Exploration for the Maologane Water Supply Upgrade Doc No 106773-MAO-2012.

Aurecon. 2012e. Borehole Siting at Ramoga Doc No. 107014-RG-2012.

Aurecon. 2012f. Groundwater Exploration at Motswedi and Borakolo Doc No. 107014-MB-2012.

Aurecon. 2012g. Borehole siting at Kameelboom Doc No. 107014-KB-2012.

Aurecon. 2012h. Groundwater Exploration at Silwerkrans Doc No. 107014-SK-2012.

Aurecon. 2012i. Groundwater Exploration for the Madibogo Water Supply Upgrade Doc No. 105658-V1.0-2012.

Aurecon. 2012j. Groundwater Exploration at Setlagole Doc No. 107014-SET-212.

Aurecon. 2012k. Groundwater Exploration at Ditloung Doc No. 107014-DT-2012.

Aurecon. 2012l. Groundwater Exploration at Logageng Doc No. 107014-LOG-2012.

Aurecon. 2014a. Rapotokwane Bulk Water Supply Groundwater Exploration Doc. No.110671-RAP-2014.

Aurecon. 2014b. Ottosdal Bulk Water Supply Phase 2 Groundwater Exploration, 110297-OTT-2014.

Aurecon. 2015. Vingerkraal VILLAGE WATER SUPPLY : GROUNDWATER EXPLORATION 112069-VK-2015.

Balasubramanian, A. 2017. Methods of Groundwater Exploration. Mysore.

Baran, E. 2003. An Explanation of the 1:500 000 General Hydrogeological Map Kroonstad 2725. Pretoria: Department of Water Affairs and Forestry.

Barnard, H.C. 2000. An Explanation of the 1:500 000 General Hydrogeological map Johannesburg 2526. Pretoria: Department of Water Affairs and Forestry.

Basheer, A.A. and Alezabawy, A.K. 2020. Geophysical and hydrogeochemical investigations of Nubian sandstone aquifer, South East Sinai, Egypt: Evaluation of groundwater distribution and quality in arid region. Journal of African Earth Sciences. 169:103862. DOI: 10.1016/j.jafrearsci.2020.103862.

de Beer, C.H. 2002. The Stratigraphy, Lithology and Structure of the Table Mountain Group. In A Synthesis of the Hydrogeology of the Table Mountain Group-Formation of a Research Strategy. K. Pietersen and R. Parsons, Eds. Pretoria: Water Research Commission. 8–18.

Blake, D., Mlisa, A. and Hartnady, C. 2010. Large-Scale Quantification Of Aquifer Storage And Volumes From The Peninsula And Skurweberg Formations In The Southwestern Cape. Water SA. 36(2):177–184. DOI: 10.4314/wsa.v36i2.183727.

Booth, P.W.K. 2011. Stratigraphic, Structural, and Tectonic Enigmas Associated with the Cape Fold Belt: Challenges for Future Research. South African Journal of Geology. 114(3–4):235–248. DOI: 10.2113/gssajg.114.3-4.235.

Botha, F.S. and Van Rooy, J.L. 2001. Affordable Water Resource Development In The Northern Province, South Africa. Journal of African Earth Sciences. 33:687–692. DOI: 10.1016/s0899-5362(01)00093-8.

Botha, W. and Vorster, A. 1993. D046 Geophysics Applied to Groundwater Exploration in the Kalahari Regions of Southern Africa. In EAGE 55th Meeting and Technical Exhibition. 1–2.

Botha, J.F., Verwey, J.P., van der Voort, I., Vivier, J.J.P., Buys, J., Collision, W.P. and Loock, J.C. 1998. Karoo Aquifers: Their Geology, Geometry and Physical Properties. WRC Report No. 487/1/98. Water Research Commission.

Botha, W., Combrinck, M., Botha, F.S. and van Rooy, J.L. 2001. An Integrated Multidisciplinary Approach to Groundwater Exploration in the Nebo Granite, Northern Province. WRC Report No. 862/1/01

Branch, T., Ritter, O., Weckmann, U., Sachsenhofer, R.F. and Schilling, F. 2007. The Wliitehill Formation - A High Conductivity Marker Horizon In The Karoo Basin. South African Journal of Geology. 110:465–476.

Brandl, G., Cloete, M. and Anhaeusser, C.R. 2006. Archaean Greenstone Belts. In The Geology of South Africa. M.R. Johnson, C.R. Anhaeusser, and R.J. Thomas, Eds. Pretoria: Geological Society of South Africa and Council for Geoscience. 9–56. DOI: 10.1038/072346a0.

Bumby, A.J., Eriksson, P.G., Catuneanu, O., Nelson, D.R. and Rigby, M.J. 2012. Meso-Archaean and Palaeo-Proterozoic Sedimentary Sequence Stratigraphy of the Kaapvaal Craton. Marine and Petroleum Geology. 33(1):92–116. DOI: 10.1016/j.marpetgeo.2011.09.010.

Cape Geophysics. 2011. Granites Near Hermanus. Survey Results.

Cape Geophysics. 2019a. Table Mountain Sandstone Near Napier. Modelled Survey Results.

Cape Geophysics. 2019b. Sandstone Shale Contact Near Napier. Modelled Survey Results.

Cape Geophysics. 2019c. Shale Sandstone Faulted Contact Near Kleinmond. Modelled Survey Results.

Cape Geophysics. 2021. Sandstone Granite Contact Near Stanford. Modelled Survey Results.

Catuneanu, O. and Eriksson, P.G. 1999. The Sequence Stratigraphic Concept And The Precambrian Rock Record: An Example from the 2.7-2.1 Ga Transvaal Supergroup, Kaapvaal craton. Precambrian Research. 97:215–251. DOI: 10.1016/S0301-9268(99)00033-9.

Catuneanu, O., Hancox, P.J. and Rubidge, B.S. 1998. Reciprocal Flexural Behaviour And Contrasting Stratigraphies: A New Basin Development Model For The Karoo Retroarc Foreland System, South Africa. Basin Research. 10:417–439. DOI: 10.1046/j.1365-2117.1998.00078.x.

Catuneanu, O., Wopfner, H., Eriksson, P.G., Cairncross, B., Rubidge, B.S., Smith, R.M.H. and Hancox, P.J. 2005. The Karoo Basins Of South-Central Africa. Journal of African Earth Sciences. 43:211–253. DOI: 10.1016/j.jafrearsci.2005.07.007.

Cawthorn, R.G., Eales, H.V., Walraven, F., Uken, R. and Watkeys, M.K. 2006. The Bushveld Complex. In The Geology of South Africa. M.R. Johnson, C.R. Anhaeusser, and R.J. Thomas, Eds. Pretoria: Geological Society of South Africa and Council for Geoscience. 261–281.

Chandra, P.C. 2015. Groundwater Geophysics in Hard Rock. CRC Press/Balkema.

Chave, A.D. and Jones, A.G. 2012. Introduction to the Magnetotelluric Method. In The Magnetotelluric Method: Theory and practice. A.D. Chave and A.G. Jones, Eds. Cambridge. 1–18.

Chevallier, L., Goedhart, M. and Woodford, A.C. 2001. The Influences Of Dolerite Sill And Ring Complexes On The Occurrence Of Groundwater In Karoo Fractured Aquifers: A Morpho-Tectonic Approach. Water Research Commission. WRC Report No. 937/1/01

Christiansen, A.V., Auken, E. and Sorensen, K. 2009. The transient electromagnetic method. In Groundwater Geophysics: A tool for hydrogeologists. 2nd ed. R. Kirsch, Ed. Berlin: Springer Berlin Heidelberg.

Conrad, J., Nel, J. and Wentzel, J. 2004. The challenges and implications of assessing groundwater recharge: A case study - northern Sandveld, Western Cape, South Africa. Water SA. 3(5 (Special Edition)):75–81.

Cornell, D.H., Thomas, R.J., Moen, H.F.G., Reid, D.L. and Moore, J.M. 2006. The Namaqua-Natal Province. In The Geology of South Africa. M.R. Johnson and C.R. Anhaeusser, Eds. Pretoria: Geological Society of South Africa and Council for Geoscience. 325–379.

Dankert, B.T. and Hein, K.A.A. 2010. Evaluating The Structural Character And Tectonic History Of The Witwatersrand Basin. Precambrian Research. 177:1–22. DOI: 10.1016/j.precamres.2009.10.007.

Durand, J.F. 2012. The Impact Of Gold Mining On The Witwatersrand On The Rivers And Karst System Of Gauteng And North West Province, South Africa. Journal of African Earth Sciences. 68:24–43. DOI: 10.1016/J.JAFREARSCI.2012.03.013.

Du Toit, W.H. 1989. Evaluation of the Applicability of Geophysical Methods for Groundwater Exploration in the Central Limpopo Metamorphic Belt, NW Transvaal GH3648.

Du Toit, W.H. and van Lelyveld, M. 2014. An Explanation of the 1:500 000 General Hydrogeological Map Phalaborwa 2330. Pretoria: Department of Water Affairs.

Du Toit, W.H. and Sonnekus, C.J. 2014a. Explanation of the 1:500 000 Hydrogeological Map 2326 Polokwane. Pretoria: Department of Water Affairs.

Du Toit, W.H. and Sonnekus, C.J. 2014b. An Explanation of the 1:500 000 General Hydrogeological Map Nelspruit 2530. Pretoria: Department of Water Affairs.

DWS. 2011a. Cape Supergroup. Department of Water and Sanitation. Available: https://www.dws.gov.za/Groundwater/Groundwater_Dictionary/index.html?cape_supergroup.htm [2022, August 01].

DWS. 2011b. Namaqua-Natal Belt. Department of Water and Sanitation. Available: https://www.dws.gov.za/Groundwater/Groundwater_Dictionary/index.html?swaziland_and_namaqualand_seri.htm.

DWS. 2011c. Transvaal Supergroup. Department of Water and Sanitation. Available: https://www.dws.gov.za/Groundwater/Groundwater_Dictionary/index.html?transvaal_supergroup2.htm.

DWS. 2011d. Tertiary Deposits South Africa. Department of Water and Sanitation, Available: https://www.dws.gov.za/Groundwater/Groundwater_Dictionary/index.html?tertiary_deposits_south_africa.htm.

DWS. 2016. National Groundwater Strategy. Department of Water and Sanitation. Pretoria South Africa.

DWS. 2017. Feasibility Plan for Groundwater Resource Development of the Malmani Dolomites within the Olifants River Water Supply System: Hydrogeological Exploratory Investigations Report. 1st ed. D. Blake, L. Towers, and D. McGibbon, Eds. Umvoto Africa Pty (ltd) on behalf of Department of Water and Sanitation (DWS) Directorate: Water Resources Planning Systems (D:WRPS), Report No.: 04/B50/00/9016/3/1b.

DWS. 2018. National Water and Sanitation Master Plan: Volume 1: Call for Action; Version 10.1; Ready for the future and ahead of the curve. 3(October):72. Available: http://www.dwa.gov.za/National Water and Sanitation Master Plan/DocumentsReports.aspx.

Eales, H.V. and Cawthorn, R.G. 1996. The Bushveld Complex. Layered intrusions. 181–229.

Engeolab. 2020. Geohydrological Investigation Completion Report Phase-Nquthu Local Municipality Isandlawana, KwaZulu Natal. Project No. 18-LL3261.

Enslin, J.F. 1955. Some Applications of Geophysical Prospecting in the Union of South Africa. Geology of South Africa. xx(4):886–912.

Epuh, E.E., Okolie, C.J., Daramola, O.E., Ogunlade, F.S., Oyatayo, F.J., Akinnusi, S.A. and Emmanuel, E.O.I. 2020. An Integrated Lineament Extraction From Satellite Imagery And Gravity Anomaly Maps For Groundwater Exploration In The Gongola Basin. Remote Sensing Applications: Society and Environment. 20. DOI: 10.1016/j.rsase.2020.100346.

Eriksson, P.G., Condie, K.C., van der Westhuizen, W., van der Merwe, R., de Bruiyn, H., Nelson, D.R., Altermann, W. and Catuneanu, O. 2002. Late Archaean Superplume Events: a Kaapvaal – Pilbara perspective. Journal of Geodynamics. 34:207–247.

Ernstson, K. 2009. Magnetic, Geothermal And Radioactivity Methods. In Groundwater Geophysics: A Tool For Hydrogeologists. 2nd ed. R. Kirsch, Ed. Berlin, Heidelberg: Springer Berlin Heidelberg. DOI: 10.1007/978-3-540-88405-7_9.

Fourie, F.D. n.d. Geophysics For Geohydrologists. Unpublished lecture notes. The Institute for Groundwater Studies, the University of the Free State. Bloemfontein, South Africa.

Field, M., Stiefenhofer, J., Robey, J. and Kurszlaukis, S. 2008. Kimberlite-Hosted Diamond Deposits Of Southern Africa : A Review. Ore Geology Reviews. 34:33–75. DOI: 10.1016/j.oregeorev.2007.11.002.

Fitts, C. 2013. 1 - Groundwater: The Big Picture. In Groundwater Science. 2nd ed. Academic Press. 1–22. Available: https://doi.org/10.1016/B978-0-12-384705-8.00001-7.

Franchi, F. and Mapeo, R.B.M. 2019. Evolution of an Archaean Intracratonic Basin: A Review Of The Transvaal Supergroup Lithostratigraphy In Botswana. Earth-Science Reviews. 191:273–290. DOI: 10.1016/j.earscirev.2019.02.007.

Fraser, L. 2001. Integrated Geophysical Survey as Applied to Groundwater exploration. In 7th SAGA Biennial Technical Meeting and Exhibition. 1–4. DOI: https://doi.org/10.3997/2214-4609-pdb.143.11.4.

Friese, A., Swartz, H., Titus, R., Fielies, A., Davids, S. and Domoney, R. 2006. Geomechanical Modeling As A Tool For Groundwater Exploration Of Fractured Rock Aquifers In The Namaqualand Region, South Africa. WRC Report No 117/1/06. Preto: Water Research Commission.

Frimmel, H.E. 2019. The Witwatersrand Basin and Its Gold Deposits. In The Archaean Geology of the Kaapvaal Craton, Southern Africa. A. Kroner and A. Hofmann, Eds. Springer, Cham. 255–275. DOI: 10.1007/978-3-319-78652-0_10.

Gabriel, G. 2009. Microgravimetry. In Groundwater Geophysics: A Tool For Hydrogeologists. 2nd ed. R. Kirsch, Ed. Berlin: Springer Berlin Heidelberg.

Galland, O., Bertelsen, H.S., Eide, C.H., Guldstrand, F., Haug, T., Leanza, H.A., Mair, K. and Palma, O. 2018. Storage And Transport Of Magma In The Layered Crust-Formation Of Sills And Related Flat-Lying Intrusions. In Volcanic and Igneous Plumbing Systems: Understanding Magma Transport, Storage, and Evolution in the Earth's Crust. Elsevier Inc. 113–138. DOI: 10.1016/B978-0-12-809749-6.00005-4.

Geomatrix Earth Science Ltd. 2023. EM34-3 from Geonics. Available: https://www.geomatrix.co.uk/land-products/electromagnetic/em34-3/ [2023, May 10].

GEOSS. 2020. Hidrogeologiese Ondersoek Vir Verdere Grondwater Ontwikkeling Te Bakenshoogte, Botrivier, Wes Kaap Report No. 2020/09-28.

Geovation. 2020. Groundwater Exploration at Kameelzynkraal – Pretoria East 20-03-V1.0.

Geovation. 2021. Matlakeng Ext 11: Pilot Groundwater Exploration Program and Groundwater Resource Assessment 20-16.2.

GHT Consulting. 2013. Geohydrological Report Geophysical Siting, Percussion Drilling And Aquifer Test Pumping For The Towns Of Victoria West, Loxton, Richmond, Hutchinson and Merriman.

Gomo, M. 2023. Use Of Electric Potential Difference In Audio Magnetotelluric (AMT) Geophysics For Groundwater Exploration. Groundwater for Sustainable Development. 20(October 2022):100864. DOI: 10.1016/j.gsd.2022.100864.

Gomo, M. and Ligavha-Mbelengwa, L. 2020. Investigation Of Factors Influencing Groundwater Quality In A Typical Karoo Aquifer In Beaufort West Town Of South Africa. Environmental Earth Sciences. 79(196). DOI: https://doi.org/10.1007/s12665-020-08936-1.

Grab, S. 2015. Sandstone Landforms of the Karoo Basin: Naturally Sculpted Rock. In Landscapes and Landforms of South Africa. S. Grab and J. Knight, Eds. Springer, Cham. 11–21. DOI: 10.1007/978-3-319-03560-4_2.

Grab, S. and Knight, J. 2015a. The Drakensberg Escarpment: Mountain Processes at the Edge. In Landscapes and Landforms of South Africa. S. Grab and J. Knight, Eds. Springer, Cham. 1–55. DOI: https://doi.org/10.1007/978-3-319-03560-4_1.

Grab, S. and Knight, J. 2015b. Landscapes and Landforms of South Africa: An Overview. In Landscapes and Landforms of South Africa. S. Grab and J. Knight, Eds. Springer, Cham. 9. DOI: DOI 10.1007/978-3-319-03560-4_1.

Guideline Geo. n.d. ABEM Terrameter LS 2. Available: https://wwwguidelinegeoc.cdn.triggerfish.cloud/uploads/2016/09/ABEM-Terrameter-LS-2-TechSpec-231113-web.pdf [2023, November 17].

Hansma, J., Tohver, E., Schrank, C., Jourdan, F. and Adams, D. 2016. The Timing Of The Cape Orogeny : New 40 Ar / 39 Ar Age Constraints On Deformation And Cooling Of The Cape Fold Belt, South Africa. Gondwana Research. 32:122–137. DOI: 10.1016/j.gr.2015.02.005.

Hasan, M., Shang, Y., Jin, W. and Akhter, G. 2021. Joint Geophysical Prospecting For Groundwater Exploration In Weathered Terrains Of South Guangdong, China. Environmental Monitoring and Assessment. 193(11). DOI: 10.1007/s10661-021-09521-0.

Hill, M., Barker, F., Hunter, D. and Knight, R. 1996. Geochemical characteristics and origin of the Lebowa Granite Suite, Bushveld Complex. International Geology Review. 38(3):195–227. DOI: 10.1080/00206819709465331.

Humbert, F., de Kock, M., Lenhardt, N. and Altermann, W. 2019. Neoarchaean to Early Palaeoproterozoic Within-Plate Volcanism of the Kaapvaal Craton: Comparing the Ventersdorp Supergroup and the Ongeluk and Hekpoort Formations. In The Archaean Geology of the Kaapvaal Craton, Southern Africa. A. Kroner and A. Hofmann, Eds. (Regional Geology Reviews). Cham: Springer, Cham. 277–302. DOI: https://doi.org/10.1007/978-3-319-78652-0_11.

Inductive Coupling Effects - Instrumentation Tools. n.d. Available: https://instrumentationtools.com/inductive-coupling-effects/ [2022, January 29].

Johnson, M.R., Van Vuuren, C.J., Hegenberger, W.F., Key, R. and Shoko, U. 1996. Stratigraphy of the Karoo Supergroup in Southern Africa: An Overview. Journal of African Earth Sciences. 23(1):3–15. DOI: 10.1016/S0899-5362(96)00048-6.

Johnson, M.R., Van Vuuren, C.J., Visser, J.N.J., Cole, D.I., Wickens, H.D. V., Christie, A.D.M. and Roberts, D.L. 1997. Chapter 12 The Foreland Karoo Basin, South Africa. Sedimentary Basins of the World. 3:269–317. DOI: 10.1016/S1874-5997(97)80015-9.

Johnson, M.R., Van Vuuren, C.J., Visser, J.N.J., Wickens, H.V., Christie, A.D.M., Roberts, D.L. and Brandl, G. 2006. Sedimentary Rocks of the Karoo Supergroup. In The Geology of South Africa. M.R. Johnson, C.R. Anhaeusser, and R.J. Thomas, Eds. Pretoria: Geological Society of South Africa and Council for Geoscience. 461–499.

Jolayemi, O.O., Robb, L., Lenhardt, N. and Hughes, H.S.R. 2020. Different Melt Source Regions For The Volcanics Of The Bushveld Large Igneous Province: New Observations From MELTS Modelling Of The Palaeoproterozoic Rooiberg Group (South Africa). Journal of African Earth Sciences. 172:103999. DOI: 10.1016/j.jafrearsci.2020.103999.

Jones, A.Z. 2019. Electromagnetic Induction and Faraday's Law. Available: https://www.thoughtco.com/electromagnetic-induction-2699202 [2022, January 29].

Jonker, B. and Abiye, T. 2017. Groundwater Potential Of The Eastern Kalahari Region Of South Africa. South African Journal Of Geology. 120(3):385–402. DOI: 10.25131/gssajg.120.3.385.

Kearey, P., Brooks, M. and Hill, I. 2002. An Introduction to Geophysical Exploration. 3rd ed. Malden, MA: Blackwell Science.

King, G.M. 2002. Explanation of the 1:500 000 Hydrogeological Map Durban 2928. Pretoria: Department of Water Affairs and Forestry.

King, R.B., Danskin, W.R., Constable, S. and Maloney, J.M. 2022. Identification Of Fresh Submarine Groundwater Off The Coast Of San Diego, USA, Using Electromagnetic Methods. Hydrogeology Journal. 30(3):965–973. DOI: 10.1007/s10040-022-02463-y.

Kinnaird, J.A., Kruger, F.J. and Cawthorn, R.G. 2003. An Isotopic Study of Flourite Related to the Granites of the Bushveld Complex. Johannesburg: Economic Geology Research Institute (Incorporating the Hugh Allsopp Laboratory).

Kirsch, R. 2006. Groundwater Geophysics: A Tool For Hydrogeology. Springer Berlin Heidelberg. DOI: 10.5860/choice.44-1535.

Kirsch, R. and Ernstson, K. 2009. Geoelectric Methods. In Groundwater Geophysics: A Tool For Hydrogeology. 2nd ed. R. Kirsch, Ed. Berlin, Heidelberg: Springer Berlin Heidelberg. 85–117. DOI: 10.1007/978-3-540-88405-7_3.

Knight, J. 2019. The Making of the South African Landscape. In The Geography of South Africa: Contemporary Changes And New Directions. Springer, Cham. 7–14. DOI: https://doi.org/10.1007/978-3-319-94974-1_2.

Kröner, A., Hoffmann, J.E., Wong, J.M., Geng, H.-Y., Schneider, K.P., Xie, H., Yang, J.-H. and Nhleko, N. 2019. Archaean Crystalline Rocks of the Eastern Kaapvaal Craton. In The Archaean Geology of the Kaapvaal Craton, Southern Africa. A. Kroner and A. Hofmann, Eds. (Regional Geology Reviews). Springer, Cham. 1–32. DOI: 10.1007/978-3-319-78652-0_1.

Lee, S.C.H., Noh, K.A.M. and Zakariah, M.N.A. 2021. High-Resolution Electrical Resistivity Tomography And Seismic Refraction For Groundwater Exploration In Fracture Hard Rocks: A Case Study In Kanthan, Perak, Malaysia. Journal of Asian Earth Sciences. 218:104880. DOI: 10.1016/j.jseaes.2021.104880.

Lennard, C. 2019. Multiscale Drivers of the South African Weather and Climate. In The Geography of South Africa: Contemporary Changes And New Directions. J. Knight and C.M. Rogerson, Eds. Springer, Cham. 81–89. DOI: https://doi.org/10.1007/978-3-319-94974-1.

Leyland, R. 2015. Some Variations in South African Karoo Dolerites and their effect thereof on Aggregate Properties. In Engineering Geology for Society and Territory-Volume 5. G. Lollino, A. Manconi, F. Guzzetti, M. Culshaw, P. Bobrowsky, and F. Luino, Eds.

Lin, H. and Lin, L. 2019. A Typical Groundwater Storage Assessment in the Tugela Area, South Africa. Hydrogeology Journal. 27(3):827–840. DOI: 10.1007/s10040-018-1897-9.

Lourens, P.J.H. 2013. The Relation Between South African Geology And Geohydrology. Master's dissertation, University of the Free State, South Africa.

Maćkowski, T., Sowiżdżał, A. and Wachowicz-Pyzik, A. 2019. Seismic Methods in Geothermal Water Resource Exploration: Case Study from Łódź Trough, Central Part of Poland. *Geofluids*. 1–11. DOI: 10.1155/2019/3052806.

Madi, K., Nyabeze, P.K., Gwavava, O., Sekiba, M. and Zhao, B. 2016. Magnetic and Electromagnetic Signatures around Polile Tshisa Hot Spring in the Northern Neotectonic Belt in the Eastern Cape Province, South Africa. Acta Geophysica. 64(4):943–962. DOI: 10.1515/acgeo-2016-0001.

Magakane, R. 2019. An Integrated Approach To Groundwater Exploration Using Remotely Sensed Imagery And Geophysical Techniques: A Case Study In The Archean Basement And Karoo Sedimentary Basins Of Limpopo Province Of South Africa. Unpublished master's dissertation, University of Venda, South Africa.

Mariita, N.O. 2009. The Gravity Method. In Short Course IV on Exploration for Geothermal Resources. 1–9.

Martinelli, E. 1975. Geophysical Exploration for Potable Groundwater Supplies in the Kalahari Gemsbok National Park. Water SA. I(2):53–56.

Masilela, M. and Beckedahl, H. 2022. Karst Geomorphology And Related Environmental Problems In Southern Africa – A Review. Journal of African Earth Sciences. 196. DOI: 10.1016/j.jafrearsci.2022.104686.

McCarthy, T.S. 2006. The Witwatersrand Supergroup. In The Geology of South Africa. M.R. Johnson and C.R. Anhaeusser, Eds. Geological Society of South Africa and Council for Geoscience. 155–186.

McCarthy, T. and Rubigde, B. 2005. The Story Of Earth And Life: A Southern African Perspective On A 4.6 Billion Year Journey. Cape Town: Struik Publishers.

McCourt, S., Armstrong, R.A., Grantham, G.H. and Thomas, R.J. 2006. Geology And Evolution Of The Natal Belt, South Africa. Journal Of African Earth Sciences. 46:71–92. DOI: 10.1016/j.jafrearsci.2006.01.013.

Mekel, J.F.M. 1988. Photogeology. In General Geology. Boston, MA: Springer US. 638–650. DOI: 10.1007/0-387-30844-X_86.

Metwally, S.E.M., Elska, S.M., Zarif, F.M. and Saad, A.F. 2023. Applications Of Well Logging Techniques To Evaluate The Groundwater Aquifers Between Southwest Bane Sweif And West Asyoute Governorate, Upper Egypt. Kuwait Journal of Science. 50(1B):1–18.

Meyer, P.S. 2001. Explanation of the 1:500 000 Hydrogeological Map Cape Town 3317. Pretoria: Department of Water Affairs and Forestry.

Meyer, P.S. 2003. An Explanation of the 1:500 000 General Hydrogeological map Bloemfontein 2924. Pretoria: Department of Water Affairs and Forestry.

Miller, J.A., Dunford, A.J., Swana, K.A., Palcsu, L., Butler, M. and Clarke, C.E. 2017. Stable Isotope And Noble Gas Constraints On The Source And Residence Time Of Spring Water From The Table Mountain Group Aquifer, Paarl, South Africa And Implications For Large Scale Abstraction. Journal of Hydrology. 551:100–115. DOI: 10.1016/j.jhydrol.2017.05.036.

Milloy, S.F., Mclean, K. and Mcnamara, D.D. 2015. Comparing Borehole Televiewer Logs With Continuous Core: An Example From New Zealand. In Proceedings World Geothermal Congress 2015 Melbourne, Melbourne, Australia, 19-25 April 2015. 1–6. DOI: 10.13140/RG.2.1.2877.0805.

Miner, W.J., Adamson, J.K., Hasbrouck, J.C., Monforte, S.P. and Vera, M.R. 2022. Geophysical Reconnaissance Of The Western Basin Of The Plaine Du Nord Aquifer, Haiti. Hydrogeology Journal. 30(5):1417–1432. DOI: 10.1007/s10040-022-02490-9.

Mndaweni, S.S.E., Naicker, S. and Blake, D. 2019. Hydrostratigraphy of the Malmani Subgroup Dolomites Within The Northeastern Escarpment (Limpopo and Mpumalanga, South Africa). South African Journal of Geology. 122(3):283–298. DOI: 10.25131/sajg.122.0022.

Mokgatle, T. 2016. Assessment of Groundwater Resource in the Tsineng Area, Northern Cape: A Geophysical Survey Perspective. Master's dissertation, University of the Free State, South Africa.

Mokoena, P., Kanyerere, T. and van Bever Donker, J. 2020. Hydrogeochemical Characteristics And Evaluation Of Groundwater Quality For Domestic And Irrigation Purposes : A Case Study Of The Heuningnes Catchment, Western Cape Province, South Africa. SN Applied Sciences. 2:1–12. DOI: 10.1007/s42452-020-03339-0.

Mokoena, P., Manyama, K., van Bever Donker, J. and Kanyerere, T. 2021. Investigation Of Groundwater Salinity Using Geophysical And Geochemical Approaches: Heuningnes Catchment Coastal Aquifer. Western Cape Province, South Africa. Environmental Earth Sciences. 80. DOI: 10.1007/s12665-021-09507-8.

Moore, J.E. 2011. Field Hydrogeology: A Guide for Site Investigations and Report Preparation. 2nd ed. Boca Raton: CRC Press. DOI: 10.1201/b11056.

Moore, J.M., Tsikos, H. and Polteau, S. 2001. Deconstructing the Transvaal Supergroup, South Africa: Implications for Palaeoproterozoic palaeoclimate models. Journal of African Earth Sciences. 33(3–4):437–444. DOI: 10.1016/s0899-5362(01)00084-7.

Mpofu, M., Madi, K. and Gwavava, O. 2020. Remote Sensing, Geological, And Geophysical Investigation In The Area Of Ndlambe Municipality, Eastern Cape Province, South Africa: Implications For Groundwater Potential. Groundwater for Sustainable Development. 11:1–16. DOI: 10.1016/j.gsd.2020.100431.

Muchingami, I., Mkali, A., Vinqi, L., Pietersen, K., Xu, Y., Whitehead, R., Karsten, J. and Villholth, K. 2021. Integration Of Hydrogeophysical And Geological Investigations In Enhancing Groundwater Potential Assessment In Houtriver Gneiss Crystalline Basement Formation Of South Africa. Physics and Chemistry of the Earth. 123. DOI: 10.1016/j.pce.2021.103009.

Mukherjee, R., Latypov, R. and Balakrishna, A. 2017. An Intrusive Origin Of Some UG-1 Chromitite Layers In The Bushveld Igneous Complex, South Africa: Insights From Field Relationships. Ore Geology Reviews. 90:94–109. DOI: 10.1016/j.oregeorev.2017.03.008.

Murray, R., Baker, K., Ravenscroft, P., Musekiwa, C. and Dennis, R. 2012. A Groundwater-Planning Toolkit For The Main Karoo Basin: Identifying And Quantifying Groundwater-Development Options Incorporating The Concept Of Wellfield Yields And Aquifer Firm Yields. In Water SA International Conference on Groundwater. V. 38. 407–416. DOI: http://dx.doi.org/10.4314/wsa.v38i3.6.

Musa, A.A., Ben-Awuah, J., Saad, R. and Andriamihaja, S. 2017. Combined use of 2D Electrical Resistivity and Seismic Refraction in Hydrogeophysical Exploration. Petroleum and Coal. 59(1):1–9.

Muthamilselvan, A. 2021. Identification Of Suitable Sites For Open And Bore Well Using Ground Magnetic Survey. Journal of Groundwater Science and Engineering. 9(3):256–268. DOI: 10.19637/j.cnki.2305-7068.2021.03.008.

Mvandaba, V., Mwenge Kahinda, J.-M., Hobbs, P., Nzuza, P., Le Roux, A. and Arnold, K. 2019. Green Book. The Impact Of Climate Change On South Africa's Future Groundwater Availability. Pretoria: CSIR. Available: https://pta-gis-2-web1.csir.co.za/portal/apps/GBCascade/index.html?appid=73c7e05d7a1e4b0dbacc99b3709f7065.

Ndlovu, M.S., Demlie, M. and Butler, M. 2019. Hydrogeological setting and hydrogeochemical characteristics of the Durban metropolitan district, eastern South Africa. South African Journal of Geology. 122(3):299–316. DOI: 10.25131/sajg.122.0026.

Nel, M. 2017. Groundwater: The Myths, The Truths And The Basics. L. van Vuuren, Ed. Water Research Commission. SP 108/17

Odhiambo, B.D. 2016. The Place of Geobotany in Geology. International Journal of Geobotanical Research. 6:27–36. DOI: 10.5616/ijgr 160004.

Olatinsu, O.B. and Salawudeen, S.Y. 2021. Integrated Geophysical Investigation Of Groundwater Potential And Bedrock Structure In Precambrian Basement Rocks Of Ife, Southwest Nigeria. Groundwater for Sustainable Development. 14:100616. DOI: 10.1016/j.gsd.2021.100616.

Oosthuizen, A.C. and Richardson, S. 2011. Sinkholes And Subsidence In South Africa. Cape Town.

Pan, J., Lu, K., Wang, Z., Li, K. and Li, Z. 2021. Advantages of the Optimum Pulse Moment in Surface NMR and Application in Groundwater Exploration. Groundwater. 59(2):199–213. DOI: 10.1111/gwat.13046.

Partridge, T.C., Botha, G.A. and Haddon, I.G. 2006. Cenozoic Deposits Of The Interior. In Geology of South Africa. M.R. Johnson, C.R. Anhaeusser, and R.J. Thomas, Eds. Pretoria: Geological Society of South Africa and Council for Geoscience. 585–604.

Patra, H.P., Adhikari, S.K. and Kunar, S. 2016. Groundwater Prospecting and Management. (Springer Hydrogeology). Singapore: Springer Singapore. DOI: 10.1007/978-981-10-1148-1.

Peel, M.C., Finlayson, B.L. and MacMahon, T.A. 2007. Updated World Map of the Koppen-Geiger climate classification. Hydrology and Earth System Sciences. 11(5):1633–1644. DOI: https://doi.org/10.5194/hess-11-1633-2007.

Pietersen, K., Beekman, H.E. and Holland, M. 2011. South African Groundwater Governance Case Study. Water Research Commission. WRC Report No. KV 273/11

Polteau, S., Moore, J.M. and Tsikos, H. 2006. The geology and geochemistry of the Palaeoproterozoic Makganyene diamictite. Precambrian Research. 148:257–274. DOI: 10.1016/j.precamres.2006.05.003.

Pozdnyakova, L., Pozdnyakov, A., Zhang, R., 2001. Application of Geophysical Methods to Evaluate Hydrology and Soil Properties in Urban Areas. Urban Water 3, 205–216.

PQWT. n.d. PQWT S500 500M Water Detector. Available: https://www.pqwtdetector.com/PQWT-S500-500M-Water-Detector-pd6980618.html [2023, May 10].

Rabbel, W. 2009. Seismic Methods. In: Groundwater Geophysics. 2nd ed. R. Kirsch, Ed. Berlin, Heidelberg: Springer Berlin Heidelberg. DOI: 10.1007/978-3-540-88405-7_2.

Ratshiedana, P.E., Nwobodo-Anyadiegwa, N.E. & Kidoge, I. 2018. Ground Water Potential Zones Investigation Using Ground Magnetic Survey in South Africa. In Proceedings of the International Conference on Industrial Engineering and Operations Management. 1155–1164.

Reynolds, J.M. 1997. An Introduction to Applied and Environmental Geophysics. John Wiley and Sons, Inc., 605 Third Avenue, New York, USA.

Rock Hounds. n.d. Groundwater And Geotech Investigations By PQWT Telluric Receiver. Rock Hounds (Pty) Ltd. George, South Africa.

Rosewarne, P. and Weaver, J. 2002. Identification of Targets for Drilling in Table Mountain Group Aquifers. In A synthesis of the hydrogeology of the Table Mountain Group aquifers: Formation of a research strategy. WRC Report No TT 158/01. K. Pietersen and R. Parsons, Eds. 85–88.

Rubigde, B. and Hancox, J. 2002. The Karoo Supergroup. Rocks and Minerals. 77:54–59.

SACS. 1980. Stratigraphy of South Africa. In Lithostratigraphy of the Republic of South Africa, South West Africa/Namibia, and the Republics of Bophuthatswana, Transkei and Venda. L.E. Kent, Ed. Handbook Geological Survey of South Africa. 690.

Sakala, E., Tessema, A. and Nyabeze, P.K. 2014. Regional Interpretation Of Aeromagnetic Data For Groundwater Exploration In Capricorn District, Limpopo, South Africa. International Journal of Modelling and Simulation. 34(1):36–42. DOI: 10.2316/Journal.205.2014.1.205-5846.

Sami, K., Neumann, I., Gqiba, D., de Kock, G. and Grantham, G. 2002a. Status Groundwater Exploration in Geologically Complex and Problematic Terrain-Guidelines (Volume 1). Pretoria: Water Research Commission. WRC Report No. 966/1/02

Sami, K., Neumann, I., Gqiba, D., de Kock, G. and Grantham, G. 2002b. Groundwater Exploration in Geologically Complex And Problematic Terrain - Case Studies (Volume 2). Pretoria: Water Research Commission. WRC Report No. 966/2/02

Schluter, T. 2008. Geological Atlas of Africa: With Notes on Stratigraphy, Tectonics, Economic Geology, Geohazards, Geosites and Geoscientific Education of Each Country. 2nd ed. Springer-Verlag Berlin Heidelberg. DOI: 10.1007/978-3-540-76373-4.

Scoon, R.N. and Viljoen, M.J. 2019. Geoheritage of the Eastern Limb of the Bushveld Igneous Complex, South Africa: a Uniquely Exposed Layered Igneous Intrusion. Geoheritage. 11:1723–1748. DOI: 10.1007/s12371-019-00360-7.

Sedhuraman, M., Revathy, S.S. and Babu, S.S. 2014. Integration of Geology and Geomorphology for Groundwater Assessment using Remote Sensing and GIS Techniques. International Journal of Innovative Research in Science, Engineering and Technology. 3(3):10203–10211.

Shone, R.W. and Booth, P.W.K. 2005. The Cape Basin, South Africa: A Review. Journal of African Earth Sciences. 43:196–210. DOI: 10.1016/j.jafrearsci.2005.07.013.

Siemon, B. 2009. Electromagnetic methods: Frequency domain. In Groundwater Geophysics: A Tool for Hydrogeology. 2nd ed. R. Kirsch, Ed. Berlin: Springer Berlin Heidelberg.

Skursch, O., Tegner, C., Lesher, C.E. and Cawthorn, R.G. 2020. Two Expressions Of The Transition From Mafic Cumulates To Granitoids In The Bushveld Complex, South Africa: Examples From The Western And Eastern Limbs. Lithos. 372–373:105671. DOI: 10.1016/j.lithos.2020.105671.

Stats SA. 2023a. General Household Survey Report 2022. P0138(August). Available: https://www.statssa.gov.za/publications/P0318/P03182022.pdf.

Stats SA. 2023b. Statistics South Africa | Improving lives through data ecosystems. Available: https://www.statssa.gov.za/ [2023, November 13].

Tankard, A.J., Jackson, M.P.A., Erikssson, S.C., Hobday, D.K., Hunter, D.R. and Minter, W.E.L. 1982. Crustal Evolution of Southern Africa: 3.8 Billion Years of Earth History. Springer-Verlag New York. DOI: 10.1007/978-1-4613-8147-1.

Telford, W.M., Geldart, L.P. and Sheriff, R.E. 1990. Applied Geophysics. 2nd ed. Cambridge: Cambridge University Press.

Thomas, R.J., Agenbacht, A.L.D., Cornell, D.H. and Moore, J.M. 1994. The Late Kibaran of Southern Africa: Tectonic Evolution and Metallogeny. Ore Geology Reviews. 9:131–160.

Titus, R., Witthüser, K. and Walters, B. 2009. Groundwater and Mining in the Bushveld Complex. In Abstracts of the International Mine Water Conference. Pretoria. 178–184.

Umvoto Africa. 2020. Klein Slangkop Private Estate Groundwater Assessment. Report No. 864/03/01/2020

UNESCO. 2023. Barberton Makhonjwa Mountains - UNESCO World Heritage Centre. Available: https://whc.unesco.org/en/list/1575/ [2023, November 16].

Van Dyk, G. du T. 2000. Vryburg (2522). In 1:500 000 Hydrogeological Map Series of the Republic of South Africa. Department of Water Affairs and Forestry.

Van Tonder, G., Bardenhagen, I., Riemann, K., van Bosch, J., Dzanga, P. and Xu, Y. 2001. Manual On Pumping Test Analysis In Fractured-Rock Aquifers. Institute for Groundwater Studies on Behalf of Water Research Commission. Bloemfontein: University of the Free State

Van Wyk, T. 2021. Evaluation Of The Magnetotelluric TC 150 Instrument For Geophysical Groundwater Exploration. Unpublished master's dissertation. North West University, South Africa.

Valois, R., Vouillamoz, J.M., Lun, S. and Arnout, L. 2018. Mapping Groundwater Reserves In Northwestern Cambodia With The Combined Use Of Data From Lithologs And Time-Domain-Electromagnetic And Magnetic-Resonance Soundings. Hydrogeology Journal. 26(4):1187–1200. DOI: 10.1007/s10040-018-1726-1.

Vegter, J.R. 2006. Hydrogeology of Groundwater Region 26: Bushmanland. WRC Report No TT 285/06. Pretoria: Water Research Commission.

Webb, S.J., Ashwal, L.D. and Cawthorn, R.G. 2011a. Continuity Between Eastern And Western Bushveld Complex, South Africa, Confirmed By Xenoliths From Kimberlite. Contributions to Mineralogy and Petrology. 162:101–107. DOI: 10.1007/s00410-010-0586-z.

Webb, S.J., Ngobeni, D., Jones, M., Abiye, T., Devkurran, N., Goba, R., Ashwal, L.D. and Lee, M. 2011b. Hydrogeophysical Investigation For Groundwater At The Dayspring Children's Village, South Africa. Leading Edge. 30(4):434–440. DOI: 10.1190/1.3575291.

Webb, S.J., Ngobeni, D., Lee, S.A., Sepato, O., Jones, M., Abiye, T., Lee, M.D. and Pellerin, L. 2012. Time-Lapse Resistivity And Geophysical Measurements At Dayspring Children's Village. In Society of Exploration Geophysicists International Exposition and 82nd Annual Meeting 2012, SEG 2012. 974–978. DOI: 10.1190/segam2012-1353.1.

WHO. 2020. Water, Sanitation, Hygiene, And Waste Management For SARS-Cov-2, The Virus That Causes COVID-19. Interim Guidance. (29 July):1–11. Available: https://www.who.int/publications/i/item/water-sanitation-hygiene-and-waste-management-for-the-covid-19-virus-interim-guidance.

Woodford, A.C. and Chevallier, L. 2002. Hydrogeology of the Main Karoo Basin : Current Knowledge and Future Research Needs. Pretoria: Water Research Commission.

World Bank Climate Change Knowledge Portal. 2021. South Africa - Climatology | Climate Change Knowledge Portal. Available: https://climateknowledgeportal.worldbank.org/country/south-africa/climate-data-historical [2021, December 28].

Wright, C.Y., Kapwata, T., du Preez, D.J., Wernecke, B., Garland, R.M., Nkosi, V., Landman, W.A., and Dyson, L. 2021. Major Climate Change-Induced Risks To Human Health In South Africa. Environmental Research. 196 (September 2020):110973. DOI: 10.1016/j.envres.2021.110973.

Xu, Y., Lin, L. and Jia, H. 2009. Groundwater Flow Conceptualization and Storage Determination of the Table Mountain Group (TMG) Aquifers. WRC Report No. 1419/1/09. Water Research Commission.

Yaramanci, U. and Hertrich, M. 2009. Magnetic Resonance Sounding. In Groundwater Geophysics. 2nd ed. R. Kirsch, Ed. Berlin, Heidelberg: Springer Berlin Heidelberg. 253–273. DOI: 10.1007/978-3-540-88405-7_8.

Zohdy, A.A.R. 1989. A New Method For The Automatic Interpretation Of Schlumberger And Wenner Sounding Curves. Geophysics. 54(2):245–253. DOI: 10.1190/1.1442648

ABSTRACT

Groundwater is of prime importance to many communities in water-scarce South Africa. In some areas, groundwater is the sole source of fresh water. With the rapidly increasing population and increased climate variability due to climate change, the search for usable groundwater resources is of prime importance. There has been a plethora of methods used in groundwater prospecting, such as esoteric, geobotanical, geomorphological, geological and geophysical methods. Geophysical methods exploit contrasts in the physical properties of the Earth. When used with an understanding of local geological conditions, geophysical methods are able to characterise the subsurface hydrogeological conditions with the implication that drilling operations may be more successful. However, information on which methods are often employed for groundwater exploration and in which geological setting is scarce and often unpublished, which makes evaluation of such methods difficult. The present study aims to consolidate currently available information on which geophysical methods are currently used in South Africa, in which geological settings, the targets that are often the focus of groundwater prospecting, the expected geophysical response of such targets, and to give recommendations of which methods need to be employed more often. The study comprises a critical literature review and reports on geophysical groundwater exploration in nine geological regions of South Africa. These regions were chosen to be representative of different geological settings in the country, namely; the Kalahari Group, the Karoo Supergroup, the Cape Supergroup, the Bushveld Igneous Complex, the Namaqua Natal Metamorphic Province, the Transvaal Supergroup, the Ventersdorp Supergroup, the Witwatersrand Supergroup and the Barberton Supergroup. The results of the study show that contact zones, fractured zones, weathered rock, dolerite dykes and faults are often the most targeted features. These appear as anomalies in the recorded geophysical data that show the presence of contrasts between host rock and target and are interpreted based on local geology to determine features with groundwater potential and to site boreholes. Several case studies where geophysical exploration was conducted in South Africa showed that the magnetic, electromagnetic, and resistivity methods are the overwhelmingly preferred methods because of their relative ease of use and suitability to detect contrasts between targets and host rocks in most South African settings. It was also seen that unconventional water detectors are gaining prominence, and more studies need to be done to understand their mode of operation and accuracy. The study found relatively newer technologies, such as Nuclear Magnetic Resonance, are not often applied in South Africa and recommends that they be adopted and their applicability in the region be studied.

APPENDIX A

LETTER OF REQUEST

UNIVERSITY OF THE FREE STATE
UNIVERSITEIT VAN DIE VRYSTAAT
YUNIVESITHI YA FREISTATA

UFS·UV
NATURAL AND AGRICULTURAL SCIENCES
NATUUR- EN LANDBOUWETENSKAPPE
INSTITUTE FOR GROUNDWATER STUDIES (IGS)
INSTITUUT VIR GRONDWATERSTUDIES (IGS)

University of the Free State
P.O. Box 339, Bloemfontein, 9300
Tel: +27 51 401 2175
Fax: +27 51 447 3541

08 June 2022
Our Ref: L22.06.08

To whom it may concern,

Request for information on geophysical groundwater exploration projects

I am currently supervising a master's student, Libuseng Kolobe, who is doing research on the application of geophysical techniques for groundwater exploration in South Africa. The title of her dissertation is: "An appraisal of geophysical methods used for groundwater exploration in South Africa".

As the title indicates, the study will investigate which geophysical methods have been successfully used for groundwater exploration in different geological settings in South Africa. The study aims to describe the South African geology from a groundwater perspective with a focus on:

1) the types of groundwater targets associated with the different geologies,
2) the expected physical contrasts that could be exist between the groundwater targets and the host rock,
3) the geophysical methods that could be appropriate for groundwater exploration considering the physical contrasts,
4) the limitations of the different geophysical techniques (depth of investigation, resolution, sensitivity to noise, etc.), and,
5) case studies of groundwater exploration using different geophysical methods in the different geological environments.

It is for the case studies that we would be very grateful if you could assist us with examples (reports, data) of groundwater exploration investigations that you have done using geophysical methods. If the studies were done for a client and confidentiality applies, we will remove all references to your company, the client and the site location, and only discuss the results in general terms. On the other hand, if you would like to make this information available for marketing purposes, we would gladly include it in the dissertation and any publications that may result from the research.

We thank you in advance for any assistance.

Please feel free to contact me if you have any queries.

Yours sincerely,

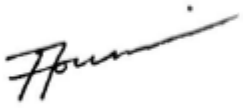

FD Fourie
Associate Professor
Institute for Groundwater Studies
Tel : 051 401 9576
Cell: 082 322 0501